FIRE SIMULATION COST REDUCTION FOR IMPROVED SAFETY AND RESPONSE FOR UNDERGROUND SPACES

Ali Haghighat

Dissertation submitted to the faculty of Virginia Polytechnic Institute & State University in partial fulfillment of the requirements for the degree of

Doctor of Philosophy
In
Mining Engineering

Kramer D. Luxbacher, Chair
Brian Y. Lattimer
Nino S. Ripepi
Steven J. Schafrik

September 15, 2017
Blacksburg, VA

Keywords: Fire Simulation Cost Reduction, Fire in Underground Space Environments, Multiscale Methodology, Reduced Order Model (ROM), Proper Orthogonal Decomposition (POD), Road Tunnel Fire, Mine Fire, Tenability Analysis

FIRE SIMULATION COST REDUCTION FOR IMPROVED SAFETY AND RESPONSE FOR UNDERGROUND SPACES

Ali Haghighat

ACADEMIC ABSTRACT

Over the past century, great strides have been made in the advancement of mine fire knowledge since the 1909 Cherry Mine Fire Disaster, one of the worst in U.S. history. However, fire hazards remain omnipresent in underground coal mines in the U.S. and around the world. A precise fire numerical analysis (simulation) before any fire events can give a broad view of the emergency scenarios, leading to improved emergency response, and better health and safety outcomes. However, the simulation cost of precise large complex dynamical systems such as fire in underground mines makes practical and even theoretical application challenging. This work details a novel methodology to reduce fire and airflow simulation costs in order to make simulation of complex systems around fire and mine ventilation systems viable. This study will examine the development of a Reduced Order Model (ROM) to predict the flow field of an underground mine geometry using proper orthogonal decomposition (POD) to reduce the airflow simulation cost in a nonlinear model. ROM proves to be an effective tool for approximating several possible solutions near a known solution, resulting in significant time savings over calculating full solutions and suitable for ensemble calculations. In addition, a novel iterative methodology was developed based on the physics of the fluid structure, turbulent kinetic energy (TKE) of the dynamical system, and the vortex dynamics to determine the interface boundary in multiscale (3D-1D) fire simulations of underground space environments. The proposed methodology was demonstrated to be a useful technique for the determination of near and far fire fields, and could be applied across a broad range of flow simulations and mine geometries. Moreover, this research develops a methodology to analyze the tenable limits in a methane fire event in an underground coal mine for bare-faced miners, mine rescue teams, and fire brigade teams in order to improve safety and training of personnel trained to fight fires. The outcomes of this research are specific to mining although the methods outlined might have broader impacts on the other fields such as tunneling and underground spaces technology, HVAC, and fire protection engineering industries.

FIRE SIMULATION COST REDUCTION FOR IMPROVED SAFETY AND RESPONSE FOR UNDERGROUND SPACES

Ali Haghighat

GENERAL AUDIENCE ABSTRACT

With the rapid advancement of technology, the mine fire knowledge has progressed significantly. Atmospheric monitoring and early sensing of heating has improved; the numerical analysis has been expedited with the usage of supercomputers, and more regulations and standards have been set to increase health and safety of miners. In spite of advancements in these areas, fire hazards remain a critical hazard in underground mines. Developing an emergency plan for the safe escape and for fighting the fire is one of the most important issues during a fire event in underground space environments such as mines. A precise fire numerical analysis (simulation) before any fire events can give a broad view of the emergency situation that leads to improving the health and safety issues in the mining industry. Unfortunately, the precise simulation of the large complex dynamical system such as a fire in underground spaces is costly. This work details a cutting edge approach to reduce the fire and airflow simulation costs in order to make simulation of complex systems around fire and mine ventilation systems viable. The main focus of this proposal is to develop novel methodologies to decrease the time of the fire and airflow simulations. The developed methodologies prove to be useful techniques for the reduction of fire simulation and airflow simulation costs. In addition, this study will examine the development of a comprehensive methodology to analyze the tenable limits in a fire event in an underground coal mine in order to improve safety and training of personnel trained to fight fires. These simulations, applied to training, will result in more efficient evacuations (e.g., the decision to leave can be made quickly and with less delay), as well as safe and effective firefighting under certain situations. The target of this research is specific to mining industry although the methods outlined might have broader impacts on the other fields such as tunneling and underground spaces technology, HVAC, and fire protection engineering industries. Therefore, this research may have an immense contribution on the improvement of health and safety associated with firefighting.

ACKNOWLEDGEMENTS

First and foremost, I would like to express my sincere gratitude to my advisor, Dr. Kray Luxbacher, for all the support and guidance she has given over the course of my graduate career. I truly appreciate all of the time and effort she has used to help me throughout this experience. She has been both a mentor and a true friend to me throughout my career as a graduate student.

I wish to thank Dr. Brian Lattimer who has shared his knowledge of fire dynamics above and beyond what was needed of him. I would also like to express my sincere gratitude to Dr. Steven Schafrik for providing a technical support on the high performance computer that was utilized for my numerical research studies. I would like to further extend my appreciation to Dr. Nino Ripepi for his encouragement and support.

I would like to show my appreciation to the National Institute for Occupational Safety and Health (NIOSH) for providing the funding of my research and education.

Finally, I would like to express my deepest appreciation to my family and friends for supporting me through this experience. My abundant thankfulness to my brother Mohammad and his wife Maryam, and my sister Mahsa for guidance and advice that I undertake graduate study. Finally I would like to express my thanks to my mother Mahnaz, Mahroo, and Mahdis for keeping me grounded.

I would like to dedicate this dissertation to my family, especially my mom, for her understanding, encouragement, and full emotional support of my graduate study. In addition I also would like to dedicate this dissertation to the memory of my father, Karim.

This research was developed under Contract No. 200-2014-59669, awarded by the National Institute for Occupational Safety and Health (NIOSH). The findings and conclusions in this report are those of the authors and do not reflect the official policies of the Department of Health and Human Services; nor does mention of trade names, commercial practices, or organizations imply endorsement by the U.S. Government.

TABLE OF CONTENTS

LIST OF FIGURES

Page

LIST OF TABLES

Page

1. Introduction

1.1. Introduction

Fires in underground coal mines, in the U.S. and around the world, have contributed significantly to fatalities and casualties in mines. Most recently, the Soma coal mine fire in Turkey in 2014 claimed 301 lives (Lowen, 2015). Therefore, there is a crucial need to have a robust fire safety plan of the occupants and the emergency response layout. Early simulation in consideration of possible fire events, applied to training, is critical for safe and efficient escape and firefighting that leads to improving the health and safety issues in the mining industry. Unfortunately, the simulation and control of large complex dynamical systems such as the fire in underground space environments can make unmanageably large demands on computational resources, creating a need for efficient model utilization. The proposed research provides a novel approach to reduce the fire and airflow simulations cost in order to improve the health and safety in the underground space environments such as underground mines. The target of this research is specific to mining although the methods outlined might have broader impacts on the other fields such as tunneling and underground spaces technology, HVAC, and fire protection engineering industries. The main objectives of this research study are summarized as follows:

1. To determine the most probable fire locations in U.S. underground coal mines according to a risk analysis based on MSHA accident data.
2. To develop a smoke layer depth, and smoke transport study for a methane fire event at a coal mine working face in order to provide a knowledge to begin assessing tenability requirements for firefighters and barefaced miners during a fire incident at the working faces in underground coal mines.
3. To develop an approach to analyze the tenable limits in a methane fire event a coal mine working face for barefaced miners, fire brigades, and mine rescue teams.
4. To develop computationally efficient reduced-order models (ROMs) to reduce the airflow simulation cost for high resolution areas of a mine (working face).
5. To develop a sensitivity study of the ROM with respect to various inlet velocity boundary conditions for examining the results near the known solution.

6. To develop a statistical analysis on the computational fluid dynamics (CFD) data of the road tunnel fire simulations in order to determine the critical parameters in the analysis of road tunnel fires.
7. To develop a novel methodology for selection of interface boundary in the multiscale (3D-1D) fire simulations in transportation tunnels.
8. To apply the developed novel approach on underground mine fire simulations for expanding an algorithm for determination of interface boundary for multiscale fire simulations of all kinds of fire events in underground mines.

The first three objectives are presented as manuscripts in chapters 3, 4, and 5. In chapter 6, work toward objectives four and five are presented. Finally, objectives six, seven, and eight are presented in chapters 7, 8, and 9, respectively.

In chapter 2, an overview of fire research in the mining industry and tunnel fires are provided and the limitations and gaps are discussed. The literature review has drawn on background information from categories of USBM fire research history, experimental studies of tunnel fires, fire simulation research projects, and international standards for fire prevention and control in tunneling and underground coal mines to allow a full understanding of the new material developed in the subsequent chapters. It has also demonstrated that different studies have been carried out on analysis of fire events in underground mines or tunnels. This chapter demonstrates that CFD numerical analysis is the useful tool for precise studies near fire field. However, for the huge domains such as underground mine environments, because of lower computational requirements, network modeling software (1D models) is commonly used for fire analysis. It is noteworthy that network modeling approaches (1D) cannot analyze the characteristics of complex three-dimensional (3D) flow regions typically encountered close to the fire. The other numerical approach is introduced as the multiscale approach which can be utilized to couple a CFD solver with a network model, with the intention of decreasing the cost of simulation without losing the accuracy. This approach still can be expensive because of CFD analysis for near fire field. This literature review was carried out to allow a better understanding of a proposed novel approach which decreases the cost of simulation drastically in the subsequent chapters and also has implications for increasing the health and safety in the

mining industry. With the use of this approach, the results precision will still be maintained. Finally, the literature review shows the fundamental math which is utilized for developing the proposed novel approach in the subsequent chapters.

In chapter 3, a risk analysis of mine fires for all U.S. underground coal mines from 2000–2012 was completed to identify locations that have a high risk for fire incidents. The data for this analysis was extracted from the Mine Safety and Health Administration's (MSHA) mine fire accident reports database. After identifying fire incidents from this database, a risk matrix was developed for underground locations that showed a significant propensity for fire incidents. This matrix associates the hazards and risks with the severity and frequency of their consequences at each location. These significant mine areas will be the concentration of future studies regarding fire simulation, fire and airflow simulation cost reduction, and mitigation methodologies.

In chapter 4, a numerical study was conducted to investigate the effects of different levels of damage to the ventilation curtain on the ventilation flow into the CM area during a methane fire event at a working face. Smoke can limit visibility to the degree that it is difficult for personnel to even approach the fire, and if they do approach it may still be nearly impossible to assess the magnitude and involvement. The main focus of this study was to provide knowledge to begin assessing tenability requirements for firefighters and barefaced miners during a fire incident at the working faces in underground coal mines. In addition, this study was carried out to develop an understanding of conditions that result from several scenarios to train and prepare personnel, and rescue teams.

In chapter 5, a study was carried out to develop an approach to analyze the tenable limits in a fire event in an underground coal mine for bare-faced miners, mine rescue teams, and fire brigade teams in order to improve safety and training of personnel trained to fight fires. The source of the combustion products analysis and the exposure effect were considered to assess the potential for harm to mine personnel, mine rescue teams, or fire brigades during a firefighting operation, taking into account their training and personal protective equipment during 5 and 15 minutes exposure. The temperature, visibility, radiation, and concentration of combustion products based on different auxiliary

ventilation damage assumptions following an ignition at the working face were investigated.

In chapter 6, the use of full order computational fluid dynamics (CFD) models using FLUENT and separate reduced order models (ROMs) for providing detailed high fidelity ventilation flow predictions was investigated. The focus of this research was to develop ROMs for reduction of airflow simulation cost at a working face for an underground mine. A ROM was produced to predict the flow field of a complex tunnel geometry (Continuous Miner (CM) working face) using proper orthogonal decomposition (POD) to reduce the simulation cost in the nonlinear model. A full order CFD model was developed using Fluent for ventilation at the continuous miner face, and a comprehensive study was conducted to assess the model accuracy and convergence. CFD model results were then used to construct a ROM using proper orthogonal decomposition (POD) with the method of snapshots, and ROM predictions were compared to the full order CFD model. A sensitivity study of the ROM with respect to various inlet velocity boundary conditions was utilized to examine the results near the known solution.

In chapter 7, a statistical analysis on the computational fluid dynamics (CFD) data of the road tunnel fire simulations was developed in order to determine the significant parameters that can affect the fluid characteristic in underground space environments. This study was crucial further study on the reduction of fire simulation cost. The developed statistical analysis was applied to the tunnels with 73.73 m^2 and 119.8 m^2 cross sections and 960 m in length. The selected fluid characteristics (response variables) were the average temperature, the average density, the average viscosity, and the average velocity. The impact of tunnel dimension, inlet air velocity, HRR, and the physical fire size (fire perimeter) on the fluid characteristics downstream of the fire source were quantified. The prediction of the designed statistical models were assessed; then the significant parameter effect and the parameter interactive effects on different response variables were determined individually. Next, the effect of computational domain length on the selection of the significant parameters downstream of the fire source was analyzed.

In chapter 8, a study was carried out to develop a novel methodology to select the interface boundary between the 3D CFD model and a 1D model in the multiscale simulation of vehicle fire events in a transportation tunnel. A detailed fluid dynamics analysis was utilized to determine the interface boundary between CFD and 1D models during vehicle fire events in a road tunnel. The effect of changes in heat release rate (HRR) and air velocity on the selection of an interface boundary was investigated. An indirect coupling strategy was utilized to couple CFD models to 1D models at the selected interface boundary; then, the coupled models results were compared to the full CFD model results. The findings were utilized to recommend a novel iterative methodology for the selection of interface boundary in multiscale fire simulations in the road tunnels and more complex geometries such as mines.

Finally, in chapter 9, the developed methodology in chapter 8 was utilized to determine the interface boundary between CFD model (near fire field) and 1D model (far field) of the fire simulations at a coal mine working face in steady state condition. The impact of velocity changes, HRR changes, and the ventilation curtain position on the selection of interface boundary to decompose the model into 3D and 1D subdomains were investigated. The indirect coupling strategy was utilized to couple CFD models to the 1D models at the selected interface boundary. An algorithm based on the physics of the fluid structure, Turbulent Kinetic Energy (TKE) of the dynamical system, and the vortex dynamics was developed for the selection of 3D-1D interface boundary for all types underground mine fire multiscale simulations. The developed approach can be utilized to determine the interface boundary of multiscale simulation of different types of fire (e.g., longwall fires, electrical installation, gob fires, belt fires, etc.) in underground mines or more complex computational domain.

1.2. Research Impacts

The proposed research will have several impacts on mining, tunneling, and fire protection engineering industries.

1.2.1. Frontier Expansion

There has been a limited amount of research in the area of multiscale (CFD-network) fire modeling in tunneling while there is no solid multiscale fire modeling in the mining industry. In addition, there is no research in applications of ROM on CFD of airflow simulations in underground mines. Moreover, research on the determination of CFD-network interface boundaries for methane fire incidents at the working face of a mine has not been investigated. Furthermore, there is a lack of information on the tenability analysis in mining engineering industry. The proposed research provided a novel approach to select the interface boundary for multiscale fire simulations for underground space environments based on the physics of the fluid structure which it results in the reduction of fire simulation cost for huge computational domains. This research study developed an approach to analyze the tenable limits for bare-faced miners, mine rescue teams, and fire brigade teams in a fire event. Moreover, a ROM for reduction of airflow simulation cost at a working face for an underground mine was developed.

1.2.2. Practical application in mining industry

The solutions in the proposed research can all be implemented and fully executed on a mine working face fires and entries model. This research has been focused on the reduction of numerical modeling cost and also can be applied on to other 3D simulator softwares which solve problems numerically via finite difference, finite volume, or finite elements. In addition, this study was carried out to develop an approach to analyzing the tenability limits during a fire incident in underground mines for miners and all kinds of rescue teams. The outcomes of this research can be utilized to design the emergency response layout, to develop evacuation plans, and to improve fire safety in underground space environments.

1.2.3. Practical application in tunneling

The solutions in the proposed research can all be implemented and fully executed in fire tunnel models. This study can decrease the cost of simulation (time and number of processors for numerical analysis) for fire study in the tunneling industry. Therefore, the

efficiency of health and safety assessments can be improved under the proposed approach with running different simulations before any fire incident.

1.2.4. Expansion of Research and Educational Infrastructure

The fire science and engineering body of knowledge for mining is improved by translating common tools (i.e., ANSYS Fluent®, Fire Dynamics Simulator (FDS), tenability analysis, and Reduced Order Model (ROM), and MATLAB coding) to mining.

1.2.5. Educational Uses

The results from the proposed research can be extremely helpful for engineering scholars and students to grasp an understanding of proper CFD simulations, network modeling, and reducing the order of numerical models for decreasing the simulation cost. Moreover, this research can be a foundation for tenability analysis in underground mine fire incidents to improve the mine rescue or fire brigade teams' safety and performance. The outcome of this research can be utilized in all area of numerical modeling with the following purposes:

- Reduction of airflow simulation cost of underground mines based on POD
- Reduction of fire simulation cost in tunneling and underground space environments such as underground mines
- Fire safety plan and emergency response layout improvement
- Improved understanding of fire scenarios for firefighters, mine rescue teams, and fire brigades for tenability analysis
- Determination of numerical analysis domain for numerical fire analysis of underground space environments.

1.3. Bibliography

Lowen, M., (2015). Turkey mine disaster: raw anger in Soma a year on. News article, BBC news. http://www.bbc.com/news/world-europe-32709431

2. Review of Fire Research Study for Underground Space Environments

The following review paper will be submitted to a mining specific journal. It was entirely written by Ali Haghighat with editorial input from Dr. Kray Luxbacher and may be compressed to meet journal requirements.

2.1. Abstract

With the rapid advancement of technology, mine fire knowledge has progressed significantly. The experimental equipment has been improved; numerical analysis has been expedited with the usage of supercomputers; and more regulations and standards have been set to improve health and safety of miners. In spite of advancements in these areas, fire hazards remain a considerable concern in mines all around the world. Different tunnel fire research outcomes have been used in the advancement of fire knowledge in the mining industry. Therefore, not only fire research projects in the mining industry but also fire studies in tunnels have contributed to improving the knowledge in various areas such as fire prevention, fire protection, and technology. This literature review provides an overview of fire research achievements in the mining industry and also tunnel fires studies in the United States and all around the world as well as identification of research gaps. This literature review has also demonstrated the codes and standards for fire prevention and control in mines and tunnels for different groups of workers such as barefaced miners, mine brigade, mine rescue teams, and firefighters. However, the focus of this literature review is more on numerical analysis of fire in tunneling and underground mines and various mathematical approaches to decrease the simulation costs.

2.2. Experimental Fire Research

Fire experiments can be classified by type to different areas such as fire plumes, pool fires, air and gas movement, growing fire, flame spread, compartment fire, smoke detection, sprinklers, mist system, suppression system, combustion model, soot deposition and etc. Additionally, they can also be classified by the locations. Before the 1960s, most of the fire research projects were focused on three main areas which are associated with the fire safety in mine tunnels. These three main areas are coal (on the coalface, in sacks, coal dust explosion, coal properties, etc.), wooden structures (wooden supports for the mine

tunnel ceiling), and conveyor belts (Carvel et al., 2005). However, later fire research, such as fire in tunnels, drew research focus.

2.2.1. Mine Fires Experimental Research

By briefly glancing over mine fire research projects in the United State, it is evident that most of the studies were carried out or funded by the U.S. Bureau of Mines (NIOSH). Keenan, explained that because of the Cherry Mine fire in Illinois in 1909, the U.S. Bureau of Mines (USBM) was established. During that incident, 259 miners lost their lives (Keenan, 1963). It is noteworthy that the U.S. Bureau of Mines (NIOSH) has been playing a key role in the improvement of the knowledge in fire research in the mining industry in different aspects such as experimental, numerical, or computational analysis. According to the number of fatalities and non-fatal incidents in underground and surface mines from the past to present, these fire research projects have had an immense impact in the improvement of health and safety in the mining industry. Smith and Thimons summarized the highlights of the Bureau of Mines and NIOSH fire research from 1910 to 2010 (Smith et al., 2010). This study showed that the rate of injuries and fatalities decreased dramatically because of the major advances in mine fire safety. However, the hazards will continue to evolve because of deeper and gassier mining operations. An early interest in fire research was in spontaneous heating during coal storage. Particularly in the heating of government buildings and powering naval vessels, which required huge amounts of coal to be stockpiled. Therefore, the spontaneous combustion prevention research area pulled the focus of different researchers because of economic reasons (Smith et al., 2010).

Rice (1912) described the causes of coal mine fires in the early years. That study showed the causes of early coal mine fires were from different potential sources such as the careless handling of open lights, improper fuel storage practices, the use of long-flame explosives, short circuits in electrical equipment, the lighting of accumulations of gas, and spontaneous heating. He proposed some precautions to decrease the probability of fire hazards in coal mines and also suggested some techniques to fight the fire in underground coal mines (Rice, 1912).

One of the turning points of USBM in terms of fire research happened in 1929 when a flammability laboratory was set up. The main area of research at that time was, in the determination of the inflammable limits of methane and the distillation products of coal in the air (Smith et al., 2010).

In the 1930's, some improvements were achieved in the use of ventilation for elimination of gas accumulation hazards. In the post-war years research was conducted on the influence of materials and methods for quenching coal mine fires (Howarth et al., 1949). Additionally, a new study was carried out on the cause, behavior, and control of mine fires in 1936. The USBM worked on data collection of the fire products such as gas composition. And also in that decade, a study was conducted on the mechanism of flame propagation in an entire mine (Godbert et al., 1936).

In the 1940's, a part of USBM research was allocated to gas-indicating devices for the Navy, which consequently, contributed to improvements in mine fire detection. Furthermore, the diesel equipment development in underground mines with the intention of eliminating electrical hazards of trolley lines was carried out in 1947 by the USBM. In 1951, the use of a permissible diesel locomotive for underground was approved. Basically, the fundamental research on combustion, fluid dynamics, kinetics, and thermodynamics were initiated in 1948 and continued up to the end of the fifties by the USBM. Most of the research areas were on mechanisms of ignition, propagation, and stabilization of flame and flame quenching (Smith et al., 2010).

In the fifties, many studies were focused on various areas such as an investigation of fire resistance of conveyor belting. Additionally, some research projects were carried out to investigate the fire characteristics of the electrical cables and hydraulic fluid. These studies were carried out to determine the associated hazards. One of the most important outcomes of that decade was a schedule of acceptance requirements for fire resistant conveyor belting which it was designed by the Bureau of mines (Smith et al., 2010).

In the early 1960's, most of USBM's fire experiments were focused on coal mine fire control techniques, the influence of different fire extinguishing agents and their

applications on simulated mining machines (Mitchell et al., 1961). Moreover, USBM had a significant contribution to the space program in the 1960's, with research areas related to fire extinguishment on spaceships. Also, some studies were carried out on the characteristics of various rocket propellants and their combinations in terms of flammability. They conducted a research to investigate the fire behavior in oxygen-rich environments which illustrated that the treatment which was used for flame proofing space fabrics, had an immense impact on the flammability of the material (Kutcha et al., 1969).

In the 1970's, research on the detection, control, and extinguishment of mine fires and explosions was continued at a faster pace. In 1971, most research projects were concentrated on detection and suppression systems or sealing. Those extensive research projects led to the in-mine detection and suppression systems which are still used today. Because of Sunshine Mine fire at a silver mine in 1972, the number of research projects on fire prevention in metal-nonmetal mines increased (Smith et al., 2010). As Greuer explained, the first generation of submicron smoke and metal oxide detectors were developed in that decade. Moreover, the MFIRE mine ventilation code was one of the products of this research (Greuer 1977).

Fire research in the 1980's was on improvement of fire test standards for mine combustibles, such as plastic fluid containers, ventilation ducting, and polyurethane sealants (Egan, 1990). The Lake Lynn Laboratory (LLL), a dedicated federal research laboratory, began its operation in 1980 (Triesbsch et al., 1990). However, the fire gallery was constructed in 1984 for full-scale flammability testing of mine conveyor belting and other research (Lazzara et al., 1989). Different patents were licensed on a sensitive smoke detector for underground mines by the USBM in that decade, and the validation of the MFIRE ventilation code for toxic fume spread was also carried out (Smith et al., 2010).

In the 1990's the main part of fire research was focused on the prevention, detection, and suppression of mine fires (Conti, 1994). A computer program for the assessment of spontaneous combustion risk of an underground mining operation was developed in 1995 by the USBM (Smith et al., 1995).

In the 2000's, fire research was focused more on reducing the hazards of underground coal mine fires by applying advanced technology in various areas such as conveyor belt materials, suppression systems, and air monitoring systems (Smith et al, 2010). Moreover, a project using Computational Fluid Dynamics (CFD) for preventing, detecting, and suppressing spontaneous heating in mines, especially in gob areas, was conducted (Yuan et al., 2007). Additionally, the National Personal Protective Technology Laboratory (NPPTL) was established by NIOSH in 2001. The main mission of the lab is to prevent and reduce occupational disease, non-fatal and fatal injury for workers who rely on personal protective technologies such as miners and firefighters. Trevits (2009) explained the main causes of U.S. mine fires which were divided into five main areas of flame cutting and welding operations, frictional heating and ignitions, electrical shorts, mobile equipment malfunctions, and spontaneous combustion (Trevits et al., 2009).

2.2.2. Tunnel Fires Experimental Research

After the 1960's, fire in public transportation tunnels began to receive more attention. Studies in this area were conducted to improve the health and safety in road and railroad tunnels during fire incidents and early experiments included better understanding of fire dynamics. A series of fire experiments were carried out in an abandoned railway tunnel in Switzerland in 1965 to obtain a better understanding of fire phenomena in accident is involving a fuel tanker. The effect of different ventilation systems such as natural, longitudinal, and semi-transverse ventilation systems were considered to investigate different parameters including visibility, air temperature, CO and O_2 concentrations, and air velocity. In that study, maximum temperatures were achieved within 1 to 2 minutes from ignition (Haerter, 1994). Moreover, some fire experiments were done in an abandoned railway tunnel near West Meon, Hampshire by the Fire Research Station, in the UK in the early 1970s with the intention of determining the smoke-layer depth. The vehicle fire experiment was carried out in a tunnel with dimensions of 480 m x 8 m x 6 m as the length, width, and height respectively. The researchers determined that smoke layer was above the head height and the smoke laden layer depth in the thickest part was about 3 m (Heselden, 1978). Also, some tunnel fire experiments were carried out in Glasgow in 1970 to investigate the smoke-layer depth. A burner was set as a kerosene fuel

tray with dimensions of 1.2 m x 1.2 m, and the produced Heat Release Rate (HRR) for each tray in that experiment was about 2 MW. A railway tunnel with the dimension of 620 m long x 7.6 m wide x 5.2 m high was considered for the investigation of smoke layer depth. The thickest smoke laden layer was measured at about 3-4 m after 10 minutes for the highest HRR. The cooler layer air was observed with smoke after the fire started. The speed of smoke movement was measured by about 1-1.5 m/s (Heselden et al., 1970).

Thirty fire experiments were carried also out in Austria in the early 1970's for a better understanding of fire behavior in tunnels. Different pool fire sizes were utilized in a 390 m long railway tunnel. The temperature at the tunnel ceiling was measured over 1200^{O} C. However, the tunnel lining was not destroyed by the fire. Moreover, the ventilation fan characteristics in considered transverse ventilation system were recommended for both intake and exhaust fans (Pucher, 1994). This lead to recommend more robust ventilation systems and safer fire safety plans.

In 1980, 16 full-scale fire tests in a 700m-long fire gallery and 8 experiments in a road tunnel were conducted by the Japanese Public Works Research Institute (PWRI). Most of their studies were on the effect of sprinklers on smoke density and ventilation velocity influence on the heat release rate (HRR). Different petrol pool fires in different sizes, passenger cars, and buses were utilized in those experiments. It is evident that the smoke stratification (thermal layering) was prevented partially by longitudinal air velocity at 1 m/s, and there is no thermal layering with the use of 2 m/s as the longitudinal velocity. However with the increase of the longitudinal air velocity, the HRR of vehicle fires increased. It is noteworthy that the sprinklers did not extinguish car, bus, nor the pool fires totally, but the HRR reduced by the usage of sprinklers (Mizutani et al., 1982).

One of the largest tunnel fire tests was carried out in a tunnel in Norway by teams of fire researchers from different countries including Austria, Finland, France, Germany, Italy, Norway, Sweden, Switzerland, and the UK from 1990 to 1992. The test series was referred to as the EUREKA 'Firetun' test series. A railway tunnel in Germany and a small tunnel in Finland were utilized for wooden crib fire tests (Carvel et al., 2005). This study was carried out to provide information in different areas such as fire phenomena,

contaminant analysis, escape, rescue and fire-fighting possibilities, and influence of the surrounding structure on the fire. It was evident that the amount of damage to tunnel lining and vehicles depend on the vehicle type. The highest temperatures during vehicle fires were recorded at 900^{O} C. Moreover, the ventilation conditions had an immense impact on burning patterns and fire growth. Controlled ventilation was recommended for effective smoke management (Haack, 1995; Steinert, 1994; Ingason, 1995; Blume, 1995; Bahadir et al., 1995; Malhotra, 1995). As part of the EUREKA test series, researchers in France worked on heptane pool fire tests in their fire gallery. The main purpose of these experiments was calibration of their HRR measuring apparatus. The other objective of those series of tests was comparison of the Norway tunnel fire results with their own fire tests results (Marlair et al., 1993).

The other research area which pulled the focus of researchers in 1997 was cable fires. A series of cable fire tests were carried out in a tunnel to investigate the use of water mist systems for suppression of cable fires in New Zealand. In addition, the performance of different commercial systems was examined. In those series tests, 4 different water mist systems were tested. It was evident that 2 of them were met the performance requirements (Mawhinney et al., 1999).

From 1998 to 1999, a series of fire tests were performed in a fire gallery in the UK. The main goal of that research was to test the performance of the onboard fire suppression system (OFSS) to use on Heavy Goods Vehicles (HGV) - carrying trains in the Channel Tunnel. In that experiment, it was evident that the damage to the facilities was reduced with the use of OFSS (Grant et al., 1999).

Three pool fire experiments and a number of non-fire ventilation tests were done in the Mont Blanc Tunnel in Italy after the Mont Blanc fire disaster in 1999, to evaluate the performance of the ventilation system and fire and smoke behavior during a disaster. It was evident that smoke progressed by about 700-900 m from the fire source and it was limited if the ventilation was controlled according to pool fire tests 2 and 3. In addition, a good stratification was observed (Brousse et al., 2001). It is noteworthy that the experiments were carried out without the use of any vehicle in the tunnel. Therefore, the stratification

and smoke progress would be different with the presence of vehicles in the tunnel. Additionally, a series of 26 fire experiments were performed in the 2nd Benelux tunnel in Netherlands, in order to investigate the spread of smoke and heat, the influence of sprinklers, fire detectors effects and their performance, and the impact of ventilation fire size from 1999 to 2001. Poor visibility was observed at 100-200 m from the fire source while the tenability limits for toxic gases were not exceeded. In addition, because of poor visibility the escape route signs were not readable. It was recommended to set the signs at a lower level (Carvel et al., 2005).

Moreover, some experiments were carried out in Norway in 2003 to investigate five main goals such as the fire development in the heavy good vehicle (HGV) cargo loads, fire spread between vehicles, and production of toxic gasses, firefighting, and temperature development at the tunnel ceiling. In that experiment, it was evident that the temperature can reach to 1300^{O} C in HGV tunnel fire (Lonnermark et al., 2003; Ingason et al., 2003).

Furthermore, there was a full-scale fire test in the San Pedro de Anes Tunnel Safety Test (TST) Facility in Asturias, Spain in 2006 (Mawhinney et al., 2006). Trelles and Mawhinney utilized that experiments for the simulation of a series of full-scale fire suppression models with FDS version 4.0. (Trelles et al., 2010).

Some tunnel fire experiments were also carried out in the United States. The largest tunnel fire test series in terms of actual scale was the Memorial Tunnel Fire Ventilation Test Program (MTFVTP). About 98 pool fire tests were carried out ranging in size from 10 MW to 100 MW in an 850 m long two-lane road tunnel in West Virginia. The main objectives of that study were to obtain a comprehensive database in temperature and smoke movement from full-scale fire ventilation tests and also to determine the effect of ventilation system on the smoke spread and tunnel heat. One of the main achievements of these series of fire tests was that the longitudinal ventilation was able to control the smoke spread for fires up to 100 MW. The critical velocity was measured at about 2.5- 3 m/s. Therefore, this amount of velocity was sufficient to prevent back layering of smoke of 100 MW fire. Furthermore, the tenability limits for visibility reached the limits for temperature (Carvel et al, 2005). The project cost in excess of US $40 million while the EUREKA

‘Firetun’ test series cost about US $10 million (PIARK, 1999; Carvel et al., 2005). In addition, a qualitative analysis was carried out on a truck fire within a tunnel in order to analyze the spread of the toxic gasses and their concentrations within the tunnels during the fire event by Piergoirgio and others (Piergoirgio et al., 2002).

McGrattan and his colleague modeled the Howard Street Tunnel fire in Baltimore, which happened in 2001, using the Fire Dynamics Simulator (FDS). Numerous fire experiments were conducted in a decommissioned highway tunnel in West Virginia for validation of models in that study and included consideration of a 50 MW fire. The tunnel length is 2,650 m (8,700 ft, 1.65 mi) long. The compared results showed that the model results were favorable. That research was carried out with the intention of quantifying the peak gas and surface temperatures. One of the most important considerations in the fire analysis was the heat absorption by the tunnel wall. According to the results calculation, the temperature of the smoke exiting the tunnel at both ends was close to the ambient temperature (McGrattan et al., 2006).

Edwards and his colleagues conducted diesel-fuel fire experiments on the determination of critical air velocity which it plays a key role in the prevention of smoke rollback. The experiments were carried out in the facility of the National Institute for Occupational Safety and Health (NIOSH). In that study, the fire intensity varied from 50 to 300 kW by altering the size of the fuel tray area. FDS was utilized for simulation of the model to determine the critical air velocity for smoke reversal in a tunnel as a function of the fire intensity, and their results compared favorably with experimental results. In the simulation, a 50 m (164 ft) length of tunnel section was utilized with the fire located 30 m (100 ft) downwind from the entrance. Consistent with the data of experiments and simulation, it was evident that the critical velocity for hampering of a smoke layer upwind is proportional to the fire intensity to the 0.3 power. In that experiment, the fire intensities varied from 50 to 300 kW in a tunnel with the dimension of 2 m (6.6 ft) height and 2.9 m (9.5 ft) width (Edwards et al, 2005). Also, the CFD results showed that the effect of fuel type and the ambient temperature were inconsequential in the value of critical air velocity. Moreover, the critical velocity is smaller when we have inclined tunnel in comparison with

the horizontal tunnel for prevention of roll back during the fire events. It was determined that the ventilation velocity is a non-linear function of the inclined angle of the tunnel (Hwang et al., 2005).

Another combustible source of fire which must be considered is timber sets which are common to be used for roof support in the underground mines. Warner conducted an experiment on the effect of timber set spacing on fire propagation in a ventilated timbered roadway. A tunnel with length, width, and height of 53, 4.57, and 1.83 m, respectively, was considered for the fire spread experiment along the timber sets (Warner, 1975). The results of that research were utilized for validation of different timber fire simulations (Edwards and Hwang, 2006).

Edwards and his colleague used conveyor belt experiment results collected by Lazzara and his colleagues in 1987 for CFD simulation of conveyor belt fire spread (Lazzara et al., 1987; Edwards et al., 2006). The CFD study of flame spread along a conveyor belt showed good agreement with measurements of Lazzara and Perzak for air speeds less than 2 m/s (Edwards et al., 2006). Most of the studies on flame spread over horizontal combustible surfaces have been focused on the theoretical analysis and laboratory-scale experiments while large-scale experimental studies in that area are limited (Yuan et al., 2014). To clarify this issue one can be referred to research which was done on turbulent flame spread over large-scale horizontal polymethylmethacrylate (PMMA) surfaces (Apte et al., 1991).

Additionally, The NIOSH conducted research on determination of fire resistance capability of wider belts for use in underground coal mines. In that research, six different types of 183-cm- (72-in.)-wide conveyor belting was evaluated for fire resistance under large-scale test conditions. Full-scale fire experiments were conducted in the NIOSH Fire Suppression Facility (FSF) and the results were compared to the results of the belt evaluation laboratory test (BELT). In general, consistent with the data of experiment, it was evident that the BELT shows a reasonable correlation of the fire resistance characteristics of wider conveyor belting under full-scale fire conditions (Rowland et al., 2011). Besides, the other experiment was a large-scale conveyor belt fire. Then the CFD

model was validated based upon the flame spread results over a conveyor belt in the large-scale tunnel. Consistent with the data of CFD results, it was shown that the CFD results on maximum heat release rate, the maximum smoke temperature at the outlet, and maximum CO concentration at the exit were in good agreement with the large-scale test results (Yuan et al., 2014).

Harris worked on the determination of the heat flux from a tunnel fire with FDS when the rates of water varied (Harris, 2010). In that study, the experiments results on burning tests for shielded and unshielded standard plastic goods under various conditions of spray which were carried out by Arvidson, were utilized (Arvidson, 2010).

Consistent with the data of experimental fire studies, it is evident that tunnel fire experiments have played key roles in a better understanding of tunnel fire phenomena which contributed to improving tunnel fire prevention, protection knowledge, and technology. Because of the similar geometry, the outcomes of tunnel fire studies can contribute to mine fire research in different areas. These experiments can be helpful for the study of fire in the mine in terms of numerical, experimental, and computational studies. This literature review on tunnel fire and mine fire experiments can be utilized in the validation of tunnels and mines fire simulations. Moreover, consistent with the information of NFPA® 502, it is evident that the tenability limits are proposed as standards for road tunnels according to the experimental studies. However, there are no standards in terms of tenability limits for miners or mine rescue teams in NFPA® 120. Hence, this previous research can be leveraged to determine best practices in the underground mine in emergency situations.

2.3. Numerical and Computational Fire Research

Over the past two decades, numerical analysis of systems such as ventilation in underground mines, fire behavior, dust and Diesel Particular Matter (DPM) propagation, and explosion has been the focus of different researchers in mine ventilation. Two common numerical analysis approaches for mine fires investigations are Computation Fluid Dynamics (CFD) modeling of tunnel fires and network modeling.

Numerous CFD modeling studies have been utilized in different ventilation areas such as airflow behavior in the mine or mine ventilation ducting systems, improvement of auxiliary ventilation, spontaneous combustion in longwall gob areas, methane control in different areas of the mine, dust and DPM control, and mine fires and explosions.

For instance, Herdeen and Sullivan utilized CFD for investigation of airflow behavior in the mines (Herdeen et al., 1993). Also, there is CFD research in terms of investigation of dust distribution in longwall face, methane dispersion in different parts of the mine, longwall ventilation and validation, diesel particular exhaust from mining machine in room and pillar mines, gas control in a room-and-pillar coal mine, inertization in longwall gob areas, dust behavior in underground tunnels, and the effect of an air curtain for dust control at a longwall shearer (Srinivasa et al., 1993; Canoo, 2004; Tomata et al., 1999; Wala et al., 2003, Zheng et al., 2008; Sasmito et al., 2012; Ren et al., 2009; Torano et al., 2011; Wang et al., 2011). Moreover, some research was allocated to the air losses calculation in the ventilation system of a mine according to different methods of traditional and CFD (Diego et al., 2010).

On account of different fatal and non-fatal incidents in the mines in the United States which are caused by fire and explosion, these areas have attracted numerous researchers to utilize CFD for improvement of health and safety. NIOSH has conducted extensive research on different fire areas using CFD. Research on fire spread along combustibles was done by Edwards and Hwang (2006); in this research, a computational fluid dynamics (CFD) software FDS version 2 was applied to investigate the rate of fire propagation and compared to Douglas Fire timber results. Furthermore, the research results showed good agreement on the dependence of flame spread along a conveyor belt upon air speed in comparison with measurements of Lazzara and Perzak (1987). In that study, the rate of flame spread was evaluated for different areas in the mine such as the ribs and roof of a coal mine entry; timber sets; and a conveyor belt (Edwards et al., 2006). For the coal fire spread, the temperature dependent specific heat and thermal conductivity of coal and coke values reported by Merrick were utilized in the simulation (Merrick, 1983). The density of coal and coke were used as 1,330 kg /m3, 850 kg /m3, respectively which was

reported by Lee and his colleagues (Lee et al., 1977). The amount of 31,300 kJ /kg was set as the heat of combustion for the coal-based upon a bituminous coal (Flynn, 1949). Two different variables (209 kJ /kg and 1,300 kJ /kg) were considered as the heat of pyrolysis, Hp based upon two values which were suggested on different research projects respectively (Mahajan et al, 1976; Hertzberg et al., 1988). The pyrolysis temperature of the coal was set 525^{o} C based upon Hertzberg study (Hertzberg et al., 1988). These parameters can be utilized for mine fire modeling studies. Furthermore, they worked on the simulation of floor-level fires in a ventilated tunnel to investigate the correlation of smoke reversal length and tunnel ventilation. The results from the associated research showed the minimum amount of ventilation that should be provided, allowing for an evacuation path (clear and free from smoke and hot gasses path) from the fire source. The reported ventilation current should be proportional to the one-third power of the fire intensity according to the CFD results (Hwang et al., 2001).

In addition, some research projects were allocated to the initiation and fire spread characterization along the surfaces of a conveyor belt mounted in a ventilated full-scale experimental fire test gallery. These studies were carried out numerically and experimentally, and the simulation results were in agreement with the experimental results. A novel discrete particle-based model was proposed to represent the physical presence, combustion and flame spread along the conveyor belt surface (Lowndes et al., 2007). In addition, some studies were allocated to the validation of different CFD simulations. For instance, Cochard worked on the validation of Fire Dynamics Simulator (version 2.0). In that study, he compared the model results with a full-scale tunnel fire experiment which was conducted as part of the Massachusetts Highway Department Memorial Tunnel Fire Ventilation Test Program (Cochard, 2003).

Also, CFD modeling of spontaneous combustion in different areas of mines, especially gob areas, were studied. For example, Yuan and Smith, conducted research to investigate the spontaneous heating of coals in longwall gob areas with different apparent activation energies and reaction surface areas. In other research, they investigated the effects of coal properties on the spontaneous combustion in longwall gob areas using CFD

(Yuan et al., 2007; Yuan et al., 2008). Thy also conducted a study to simulate the spontaneous heating in a large-scale coal chamber with a forced ventilation system for investigation of the effects of airflow rate and order of reaction on the spontaneous heating process. That study showed the simulation results were in good agreement with the USBM test results (Yuan et al., 2009).

Moreover research projects were conducted to investigate the spontaneous coal combustion in a gob area. Li conducted research on a numerical model for flow field of irregular patterns of a gob with multiple points of leaking air. A CFD software (G3), was utilized to investigate the effect of leaking points on spontaneous combustion (Li, 2008). Taraba and Michalec (2011) conducted research on the effect of longwall face advance rate on the spontaneous heating process in the gob area. They utilized FLUENT to investigate the oxidation process of coal in the gob area. (Taraba et al., 2011). Also, Taraba et al. 2014, utilized a CFD software to investigate the effect of wind on the spontaneous heating of coal stockpiles (Taraba et al., 2013). Furthermore, they studied control of methane and spontaneous combustion (Tauziede et al., 1993; Ren et al., 2000).

Woodburn and Britter (1996), worked on sensitivity studies of computational fluid dynamics (CFD) simulations of a fire in a tunnel. FLOW3D was utilized for the simulation of models. The models were simulated experimental fire in a tunnel which was carried out in Buxton, UK. Two areas of a tunnel (the area around the fire and the area downstream of the fire) were selected for simulations. In part I, it was concluded that the simulation of conditions within the fire area required precise specification of velocity and heat initial and boundary conditions. There was good agreement between the simulation and experimental results (Woodburn et al., 1996). The main objective of that research was, quantifying the uncertainties in the simulation of a tunnel fire and comparing experimental results of tunnel fire to the simulation results (Woodburn et al., 1996).

Weisenpacher, Halada, and Glasa 2011 utilized parallel processing of Fire Dynamics Simulator (FDS) for the simulation of smoke transfer of a road tunnel fire. This study showed that precise results can be achieved, with the use of the parallel version of FDS (Weisenpacher et al., 2011).

In addition, a study was conducted by the department of fire protection engineering in China, simulating of smoke spread in a subway platform with the use of two different CFD softwares (FLUENT and FDS). Consistent with the results of the simulations compared to the experimental results, it was evident that the results from FDS software better corresponded with measured results than these of ANSYS Fluent for the temperature of middle platform, the roof temperature, and the smoke layer thickness. However, it was suggested that ANSYS Fluent is more convenient than the FDS (Binbin, 2011).

According to the reviewed literature, it is evident that the CFD is a useful tool to study fire behavior for the near field while it is not efficient for far field. Fire specifications and conditions near the fire area can be vital information for design of emergency planning in firefighting missions for fire brigade or mine rescue teams. Therefore, a precise fire numerical analysis before any fire events can give a broad view of the emergency situation, allowing for improved fire prevention, firefighting, and evacuation. One of the main gaps in the mining industry is the definition of near and far fields. There is no study to distinguish the near field from far fields. By determination of near and far fields, the domain of fire studies via different numerical methods such as CFD or network modeling will be defined.

The other approach to simulate fire events in mines or tunnels is network modeling. During the past two decades, two network modeling softwares have been commonly used for underground mine fires simulations. One of these is MFIRE which was developed by the USBM in the 1980s. This software is now maintained by NIOSH (Laage et al., 1995). The other is Ventgraph™ which it was developed by the Strata Mechanics Research Institute of the Polish Academy of Sciences in 1988. Recently, some software were introduced for the analysis of fire in underground mines such as VentFIRE™. This module is a part of Ventsim Visual program. Brake (2013) described modeling of three fire scenarios in underground hard rock mines using VentFIRE™ and he described the assumptions and the methodology to design and analyze the fire results. A study was carried out to simulate a fire event in the MS&T Experimental Mine future layout using VentFIRE™ software in order to investigate the amount of toxicity in the mine. The fastest and safest design to mitigate the hazard in that specific mine were proposed by Haghighat

and Gillies. The fire source was set as a burning Bobcat vehicle and the effect of the use of two different kinds of tires were investigated (Haghighat et al., 2015). This study has shown that the simulated fire scenarios can be utilized for improvement of mine fire safety plans and the emergency response layout. Additionally, a study was carried out to investigate the potential impacts of mine fires at a Freeport-McMoRan underground mine in Indonesia. Ventsim Visual program was utilized for the fire simulation scenarios (Brake et al., 2015).

A study was carried out on providing information for setting up an emergency min ventilation scheme and simulating fire using the MFIRE. An MFIRE numerical model was presented to simulate fires in underground facilities in Taiwan. A laboratory test was conducted in a small physical tunnel network to verify MFIRE. The results from that research showed that the ‘‘push– pull’’ ventilation model can have an immense impact on exhaust fire products (Cheng et al., 2001). However, this program has its own limitations: the complete mixing of airstreams and uniform distribution of contaminants are assumed as the airways are 1D. Moreover, no smoke layering is considered in the simulation code. Also, the impact of combustible ore, such a coal added fuel to the fire is underestimated, and the localized thermodynamics of the fire and associated chemical reactions are overlooked. Finally, improper input for time step increment can lead to the divergence in solution (Fox et al., 2015).

The other study was a mine fire simulation in Ventgraph™ software, preplanning of escape scenarios and general interaction with rescue responses, which was carried out by Gillies and Wu in 2004. The research project into mine fires was funded by the Australian Coal Association Research Program. One of the main objectives of this research was the introduction of Ventgraph to the Australian mining industry. This study showed that the diagonal branches could be useful during firefighting or mine rescue operations, for redirecting the fresh air to areas where it is needed (Gillies et al., 2004). And also, they undertook the other research on simulation of mine fire to gain a better understanding of how inertisation approaches can interact with complex ventilation system during a substantial fire. In that research, Ventgraph™ was utilized for simulation of mine fire (Gillies et al., 2009). Validation studies on Ventgraph™ were performed using data

gathered from a real mine fire (Wala et al., 1995). The application of fire simulation to Australian mines was examined in that study (Wu et al., 2004). The other primary research area was smoke rollback. Zhou and Smith worked on the development of an equation to predict the occurrence of smoke rollback and calculate the smoke rollback distance. They incorporated the equation into a mine fire simulation program (MFIRE 3.0). Hence, the improved MFIRE 3.0 is able to determine the smoke rollback in a fire entry to provide early warning for smoke rollback. In addition, it can also be used to verify the effectiveness of smoke rollback control efforts (Zhou et al., 2012). Stewart and his colleagues worked on the integration of rollback effect into the VentFire™ and the results comparison with the empirical methods (Stewart et al., 2015). However, the length of rollback in that software should be assigned by the simulator manually. So, there is no precise rollback phenomenon that is calculated numerically with the use of that software.

The integration of mine CFD and network models can considerably advance understanding of fires and their effects on mining systems because at present the boundary conditions for the CFD are either assumed or approximated, with little reference to their interaction with the rest of the mine network (Hansen et al., 2010). The coupled model is referred to as a multiscale methodology. It is noteworthy that there isn't any study to couple the CFD and network modeling together for simulation of fire in mines. This approach can be beneficial to decrease the simulation cost. And also the simulation results accuracy will be saved.

There are some studies which have been carried out on the coupling of CFD and network modeling in tunnels. Colella and his colleagues developed a novel methodology to couple CFD and 1D models of tunnel ventilation systems. The proposed method can provide precise results while reducing computational cost. With the usage of this approach, the complexity of full CFD models of flow in tunnels and the inaccuracies of simplified 1D models can be avoided (Colella et al., 2009). They also addressed simulation of tunnel ventilation flows during fires. In that study, a simple 1D network approach was utilized to model tunnel regions where the flow is fully developed (far field), and a CFD representation was used where flow conditions require 3D resolution (near field). Different fire sizes

ranging from 10 MW to 100 MW were investigated with varying velocities. Both direct and indirect coupling strategies were used and compared for steady state conditions. In addition, the grid sensitivity on the location of the 1D-3D interface boundaries was investigated and the interface boundaries locations were determined. Consistent with the research data, it is evident that the accuracy of the multiscale model is high when compared to the full CFD solution (Colella et al., 2011). Also, the multiscale approach was utilized to study the transient flow interaction between a growing fire and ramping-up ventilation scenarios. The time required to reach critical velocity conditions to remove rollback was investigated. The results from the multiscale approach showed that the required computing time decreased by 40 times without any loss of accuracy compare to the full CFD model (Colella et al., 2011). In addition, some numerical research was carried out on the coupling of multizone models with CFD for building airflow and contaminant transport (Wang et al., 2008). There are many approaches for coupling the CFD and network model of building energy (heat).

The literature review on fire numerical analysis has shown that the modeling of mine fires requires an understanding of fire chemistry, fire dynamics, and thermodynamic. The network modeling software is designed to provide a prediction of heat and fire products transfer over the gigantic areas such as entire mine, which extends kilometers in size. To permit this type of prediction, the physics of the airflow and heat transfer are simplified by treating sections of the mine as nodes where the conditions are spatially uniform. This type of numerical analysis has its own advantages and disadvantages. One of the most important advantages of network modeling software is that the computation is so fast. However, network models do not show us the precise physics and conditions near the fire source. In network modeling software, some natural phenomenon are overlooked because of 1D numerical analysis. To clarify this issue one can refer to the VentFIRE™ program which assumes that a fire is ‘throttled’ with insufficient oxygen when a fire produces zero net airflow, while, in reality, a bidirectional flow pattern may be established where fuel rich / oxygen deficient hot air travels in one direction away from the fire near the roof, while the cooler layer of fresh air travels to the fire compartment at floor level in the other direction (like a methane fire at a dead end working mine face). In addition,

VentFIRE™ is not able to simulate the chemistry of fire (Ventsim manual, 2014). Furthermore, the rollback should be assigned for a determined distance by the simulator. However, the rollback depends on different parameters such as fire intensity, the slope of the airways, and the critical air velocity. Also, an analysis of fire behavior at a working face with a curtain in MFIRE software is impossible (because of limitation in designing the airways).

More detailed types of predictions can be generated using computational fluid dynamics (CFD), which provide a solution to the Navier-Stokes equations. These partial differential equations are well-suited to model fire, but the size of the region predicted using CFD must be reduced dramatically (meters in length) to provide a solution in a reasonable timeframe. There is an increased need to create low dimensional, high fidelity, surrogate models that capture the dynamics of the system at a much lower computational cost. This technique is referred to as reduced order modeling (ROM). There has been limited research in the area of fire simulation cost reduction. As previously explained, a useful approach can be coupling of CFD and network modeling. The other approach can be reduced order modeling of CFD models.

In general, some gaps were observed in terms of reduction of simulation cost for fire simulation in mines. There has been limited amount of research in the area of multiscale (CFD-network modeling) fire modeling in tunneling while there is no multiscale fire modeling (CFD-network modeling) in the mining industry. In addition, there is no research in the implication of ROM on CFD fire simulations or the multiscale methodology (CFD-network modeling) for fire simulation. Moreover, research on the determination of CFD-network modeling interface boundaries for fire incidents at a mine working face has not been investigated. Various numerical fire analyses such as CFD fire studies or network modeling fire studies can be determined when the near and far field were determined.

2.3.1. Fire Dynamics Simulator (FDS)

Fire Dynamics Simulator (FDS), is a computational fluid dynamics (CFD) model of fire-driven fluid flow. FDS is a numerical solver of the Navier-Stokes equations appropriate for low-speed (Ma < 0.3), thermally-driven flow with an emphasis on smoke

and heat transport from fires. The formulation of the equations and the numerical algorithm are described elaborately in the FDS Technical Reference Guide (McGrattan et al., 2014). The result of an FDS simulation is displayed with a separate visualization program which is called Smokeview.

The time-dependent partial differential equations for conservation of mass, momentum and energy are solved on a 3-D grid covering the entire domain. The governing equations are approximated using second-order accurate finite differences on a collection of uniformly spaced three-dimensional grids (McGrattan et al., 2014).

FDS uses an explicit predictor-corrector finite differences algorithm to solve the Navier-Stokes equations on a rectilinear grid. As in reality, FDS is sensitive to its boundary conditions. All materials in the computation require accurate thermal material properties specification. All modes of heat transfer are included in FDS. Conduction and convection are handled in traditional ways, within the confines of the numerical grid and the simplified Navierstokes equations (Panchakarla et al., 2009). The turbulence model (Germano et al., 1991; Moin et al., 1991), the wall model (Werner Wengle (Werner et al., 1991)), and the scalar transport scheme (Superbee, (Roe, 1986); Charm (Zhou, 1995)) were improved in FDS Version 6.

The transport equations for density, mass fraction of species Y_α, and momentum u_i, are shown in equations (2-1), (2-2), and (2-3) respectively.

$$\frac{\partial \rho}{\partial t} = -\frac{\partial \rho\, u_i}{\partial\, x_i} + \dot{m}_b^m \tag{2-1}$$

$$\frac{\partial \rho\, Y_\alpha}{\partial t} = -\frac{\partial\, F_{\alpha,i}}{\partial\, x_i} + \dot{m}_\alpha^m + \dot{m}_{b,\alpha}^m \tag{2-2}$$

$$\frac{\partial\, u_i}{\partial t} = -\left(F_{u,i} + \frac{\partial \mathcal{H}}{\partial\, x_i} \right) \tag{2-3}$$

where $\mathcal{H}$ is the pseudo pressure which can be calculated according to equation (2-4).

$$\mathcal{H} = \frac{p}{\rho} - K \tag{2-4}$$

In equation (2-4), p is the fluctuating hydrodynamic pressure and K is the kinetic energy per unit mass. The equation of state and energy equations are combined with conservation of mass to provide a constraint on the velocity divergence which was explained by Bell as shown in equation (2-5) (Bell, 2004). Taking the divergence of the momentum equation provides an elliptic constraint on the pseudo-pressure.

$$\nabla.\,\mathrm{u} = \frac{1}{\rho}\left(\dot{m}_{\mathrm{b}}^{m} - \frac{D\rho}{Dt} \right) \tag{2-5}$$

The momentum equation has been modified with the intention of getting an extremely fast direct solution algorithm as shown in equation (2-6). Hence, the Poisson equation for $\mathcal{H}$ is separable.

$$\frac{\partial^2 \mathcal{H}}{\partial x_i \partial x_i} = -\left(\frac{\partial F_{\mathrm{u,i}}}{\partial x_i} + \frac{\partial(\nabla.\mathrm{u})}{\partial t} \right) \tag{2-6}$$

2.4. International Standards for Fire Prevention and Control in Coal Mines

Generally, there are three groups of people that could be expected to respond to fires in underground coal mines: bare-faced mine personnel, fire brigade teams, and mine rescue teams. All underground coal miners in the US are trained in firefighting and operators are required to provide firefighting equipment including rock dust, fire hose and waterlines, and fire extinguishers, in addition to regulated automatic fire suppression systems at key locations (US 30 CFR §75.1100-1106). Miners attempting to escape a mine with an active fire are encouraged to don self-contained self-rescuers (SCSRs) as soon as they suspect the atmosphere is compromised; however, most SCSRs commonly used in mines are not approved for firefighting. So, for regular mine personnel, tenability for firefighting is considered for barefaced miners while tenability for escape would be considered for miners under standard escape SCSRs (i.e., US 42 CFR §84, Subpart H). Fire brigade teams and mine rescue teams have similar equipment as surface fire fighters, including fire resistant clothing and rebreathers. Fire brigade teams tend to have training that is more specialized

for fire related emergencies while mine rescue teams are trained more broadly in mine emergency response.

Mine fire response varies tremendously and is complicated by the underground coal mine environment. Small fires are typically extinguished quickly by barefaced personnel. Large and involved fires would seem to call for immediate evacuation of barefaced personnel (and the donning of SCSRs); however, in the underground coal mine environment, the risk of a catastrophic methane-dust explosion during an escape is considerable, and the deployment of mine rescue teams and fire brigades can be time consuming. The decision to attempt an escape is difficult given that an explosive atmosphere could be developing and that escape routes can be several miles long. Crews must make such decisions within minutes of fire discovery.

It is instructive first to describe the personnel who would be expected to fight fires as well as their standard PPE. US law requires that mine personnel are trained in firefighting, suitable firefighting materials are available, and fire and evacuation drills are regularly held (US 30 CFR §75.1100). Mine personnel performing their regular jobs are expected to have SCSRs, hard hats, safety glasses, boots with metatarsal protection, hearing protection, lights, and gloves; select personnel will also have hand held gas detectors (oxygen [O_2], methane [CH_4], and carbon monoxide [CO]). Further, every mine shall have available a group of miners specifically trained in mine rescue and firefighting (US 30 CFR §75.1103-9(e), §75.1502). These teams must be able to deploy to the mine site within one hour (US 30 CFR §49.12), and would be likely to have self-contained breathing apparatus (SCBA) appropriate for fire, light duty fire resistant clothing and heavy duty turnout gear, as well as access to ventilation materials and firefighting materials. Their training in search and rescue and firefighting is more extensive than that of other mine personnel.

Personnel who intend to escape a mine emergency will typically don an SCSR if they suspect the mine atmosphere is compromised, and proceed to secondary or primary escapeways where they have the benefit of powered vehicles or life lines to assist in escape. Additionally, they have access to refuge chambers and SCSR caches. Surface firefighting

and rescue personnel (e.g., municipal or private) are usually available only for transport and treatment of victims as they are brought out of a U.S. mine, because hazards associated with fire in underground mines are particularly specialized. The toxic products can be distributed in the whole parts of mine during a mine fire. So the asphyxiating gasses can be created and spread in a short period of time. "In underground mines, an unplanned fire not extinguished within 10 minutes of discovery; in surface mines and surface areas of underground mines, an unplanned fire not extinguished within 30 minutes of discovery" (US 30 CFR §50.2).

According to MSHA, "in an underground environment, if miners attempt to fight a fire for 30 minutes and are unsuccessful, the fire will probably become uncontrollable. The requirement to report all underground fires not extinguished within 10 minutes of discovery will address those fires requiring activation of the fire-fighting plan and evacuation of miners. The revised reporting requirement will result in earlier fire-fighting plan activation as miners will notify supervisors more quickly who, in turn, can call in firefighting crews and allow miners to safely escape" (US 30 CFR §50.2). According to US law, for avoiding the explosion, the methane concentration should be less than 3% or greater than 20% and the oxygen concentration should be less than 10% in sealed areas (NIOSH, 2011) while in other countries, the regulation of permissible methane concentration is slightly lower such as 1% in Germany, 1.25% in the UK, 2% in France, and 2.5% in Spain (Noack, 1998). Numerous legislations and regulations should be studied for improvement of health and safety in underground mines. This standard and codes review can be helpful for determination of tenable limits for miners, mine rescue, and fire brigade teams.

2.5. Conclusion

The literature review has drawn on background information from categories of USBM fire research history, experimental studies of tunnel fires, fire simulation research projects, and standards for fire prevention and control in underground coal mines to allow a full understanding of the new material developed in the subsequent chapters. It has also demonstrated that different studies have been carried out on analysis of fire events in underground mines or tunnels but still there are some gaps in numerical analysis. CFD

numerical analysis is proven to be a useful tool for precise studies near fire field. However, for the huge domains such as underground mine environments, because of low computational requirements, network modeling software (1D models) can be an efficient tool for fire analysis at the far field. However, network modeling approach (1D) cannot analyze the characteristics of complex three-dimensional (3D) flow regions typically encountered close to the fire. The multiscale model can be utilized to couples a CFD model with a network model, with the intention of decreasing the simulation cost without losing the accuracy. This approach still can be expensive because of CFD analysis for near fire field. This literature review was carried out to allow a better understanding of a proposed novel approach which causes to decrease the cost of simulation drastically in the subsequent chapters. With the use of this approach, the results precision still will be saved. Finally, the literature review shows the fundamental math which was utilized for developing the proposed novel approach in the subsequent chapters. This literature review can be utilized in proposed research which it will determine the dependent parameters for selection of different numerical approaches in mine fire studies. These approaches can be CFD, network modeling, multiscale methodology, and ROM application on CFD fire simulations. Fire simulation, in concert with reasonable tenability guidelines, can be used to train miners as to when approaching fire barefaced is appropriate and when evacuation is the best option. These simulations, applied to training will result in more efficient evacuations (e.g., the decision to leave can be made quickly and with less delay), as well as safe and effective firefighting under certain situations. Also, it is clear that while U.S. regulation provides for firefighting training and equipment for all mine personnel, provision of basic firefighting PPE and a limited number of SCBAs could allow for immediate control of fires that could not otherwise be approached by barefaced personnel.

2.6. Acknowledgements

This research was developed under Contract No. 200-2014-59669, awarded by the National Institute for Occupational Safety and Health (NIOSH). The findings and conclusions in this report are those of the authors and do not reflect the official policies of

the Department of Health and Human Services; nor does mention of trade names, commercial practices, or organizations imply endorsement by the U.S. Government.

2.7. Bibliography

ANSYS, Inc., ANSYS FLUENT Theory Guide Help. ANSYS Workbench 14.5, ANSYS, Inc, 2013.

Apte, V. B., Bilger, R. W., Green, A. R., Quintiere, J. G., (1991). "Wind aided turbulent flame spread and burning over large scale horizontal PMMA surfaces". Combustion and flame, 85, 169-184

Arvidson. M., (2010). Large-Scale Water Spray and Water Mist Fire Suppression System Tests. In Proceedings of the Fourth International Symposium on Tunnel Safety and Security, pages 283–296.

Atkinson. (1992). Convective Heat Transfer from Fire Gases, 19, 217–245.

Bahadir, M., Wichmann, H., Zelinski, V., Lorenz, W., (1995). Organic pollutants during fire accidents in traffic tunnels. Proceeding of the International Conference on Fire Protection in Traffic Tunnels, Dresden, Germany, 12-13 September, 46-54.

Babrauskas, V., (1979). Technical Note 1103. National Bureau of Standards, Washington.

Beard, A., Carvel, R., (2005). The Handbook of Tunnel Fire Safety, Thomas Telford Ltd., London, (536pp., £85.00, Hardbound, ISBN: 0727731688)

Bell, J. B., (2004). AMR for low Mach number reacting flow, Paper LBNL-54351.

Berenson, P. J., Robertson, W. G., (1972). In Bioastronautics Data Book, Biotechnology, Virginia.

Binbin, W., (2011). Comparative Research on FLUENT and FDS's Numerical Simulation of Smoke Spread in Subway Platform Fire. Procedia Engineering 26, 1065 – 1075.

Blume, G., (1995). Temperature distribution and spread of toxic gases: effects on escape and rescue procedures. Proceeding of the International Conference on Fire Protection in Traffic Tunnels, Dresden, Germany, 12-13 September, pp. 56-65.

Brake, D. J., (2013). Fire Modelling in Underground Mines using Ventsim Visual VentFIRE Software, Australian Mine Ventilation Conference / Adelaide, SA, Australia.

Brake, R., Hatt, A., Sani, R., (2015). Modeling and simulation of multiple underground mine fire scenarios at Freeport Indonesia. In: Proceeding of the 15th North American Mine Ventilation Symposium, Blacksburg, VA, pp. 537–545.

Brani D. M, Black W. Z., (1992). "Two-zone model for a single-room fire". Fire Safety Journal, Vol. 19, Nos. 2-3, pp. 189—216.

Brousse, B., Voeltzel, A., le Botlan, Y., Ruffin, E., (2001). Ventilation and fire tests in the Mont-Blanc tunnel to better understand the catastrophic fire of the 24 March 1999.

Proceedins of the 3rd International Conference o Tunnel Fires and escape from tunnels, Washington, DC, 9-11 October, pp. 211-222.

Canoo, B., (2004). STAR-CD digs miners out of trouble. CD Adapco Dynamics, Fall 2004, 27–28.

Chatterjee, A., An introduction to the proper orthogonal decomposition. Current science, 78(7):808-817, 2000.

Cheng L.H., Ueng T.H. and Liu C.W., (2001). "Simulation of ventilation and fire in the underground facilities", Fire Safety Journal, 36, 597-619.

Cochard, S., Validation of Fire Dynamics Simulator (Version 2.0) Freeware. Tunnel Management International Journal, 6(4), December 2003.

Code of Federal Regulations. Part 30, Subsection 50.2 (6), January 28, 2016, http://www.msha.gov/30cfr/50.2.htm.

Code of federal regulations. CFR, Title 30. Part 75. Mandatory safety standards-underground coal mines. Subpart D- ventilation. §75.311. Main mine fan operation. March 3, 2016. http://www.ecfr.gov/cgi-bin/text-idx?SID=ff66c31275a19355f4ae7579f1814c34&mc=true&node=se30.1.75_1311&rgn=div8

Code of federal regulations. CFR, Title 30. Part 49. Mine rescue teams. Subpart B- Mine rescue teams for underground coal mines. §49.16. Equipment and maintenance requirements. March 3, 2016. http://www.ecfr.gov/cgi-bin/text-idx?SID=3359afc232ee55925c46b747d3be43d5&mc=true&node=se30.1.49_116&rgn=div8

Code of federal regulations. CFR, Title 29.Subpart Z- Toxic and hazardous substances. 29 CFR 1915.1000 - Air contaminants. March 3, 2016. http://www.ecfr.gov/cgi-bin/text-

idx?SID=6c1b832c4ec1d849f1eb1cbb21f51f95&node=pt29.7.1915&rgn=div5#se29.7.1915_ 11000.

Colella, F., Rein, G., Borchiellini, R., Carvel, R., Torero, J. L., Verda, V., (2009). "Calculation and design of tunnel ventilation systems using a two scale modelling approach". Building and Environment Journal. 44. 2357-2367.

Colella, F., Rein, G., Borchiellini, R., Torero, J. L., (2011). "A Novel Multiscale Methodology for Simulating Tunnel Ventilation Flows During Fires". Fire Technology. ISSN:0015-2684. ppp. 221 - 253.

Colella, F., Rein, G., Verda, V., Borchiellini, R., (2011). "Multiscale modeling of transient flows from fire and ventilation in lng tunnels". Computer & Fluids. 51. pp. 16–29.

Conti, R. S. 1994. Fire Fighting Resources and Fire Preparedness for Underground Coal Mines. U.S. Bureau of Mines, Information Circular 9410

Creedy, D. P., Clarke, R. D. C., (1992). Minimising Firedamp Risks on High Production Coalfaces: Computational Modelling Approach, Proceedings of an In ternational Symposium: Safety, Hygiene and Health in Mining, Harrogate, Doncaster: The Institution of Mining Engineers, pp192-203.

Delichatsios, M., (2004). Tenability conditions and filling times for fires in large spaces. Fire safety Journal 39. 643-662.

De Rosa, M. (2004). Analyses of mobile equipment fires for all U.S. surface and underground coal and metal/nonmetal mining categories, 1990-1999. National Institute for Occupational Safety and Health, IC 9467. DHHS (NIOSH) Publication No. 2004-105.

Diego, I., Torno, S., Toran˜o, J., Mene´ndez, M., Gent, M., (2010). A practical use of CFD for ventilation of underground works. Tunnelling and Underground Space Technology 26 (2011) 189–200.

Edwards, J. C., Hwang, C., C. (2006). CFD Modeling of Fire Spread along Combustibles in a Mine Entry. In Proceedings of the Society for Mining, Metallurgy and Exploration (SME) Annual Meeting, March 27-29, St. Louis, Missouri, preprint 06-027.

Edwards, J. C.; Franks, R. A., Friel, G. F., Yuan, L. (2005). Experimental and Modeling Investigation of the Effect of Ventilation on Smoke Rollback in a Mine Entry. In

Proceedings of the SME Annual Meeting, pages 1–6. Society for Mining, Metallurgy and Exploration.

Egan, M. R. 1990. Summary of Combustion Products From Mine Materials: Their Relevance to Mine Fire Detection. U.S. Bureau of Mines, Information Circular 9272.

Elman, H. C., Silvester, D. J., and Wathen, A. J., Finite elements and fast iterative solvers: with applications in incompressible fluid dynamics. Oxford University Press, 2014.

Enright, C., Ferrier, R. L., (2015). "Mine Rescue Manual: a Comprehensive Guide for Mine Rescue Team Members", Society for Mining, Metallurgy and Exploration Inc. eBook, ISBN: 978-0-87335-405-9

Federal Register. Rules and Regulations, Volume 71, Number 236, December 8, 2006, pp. 71429-71455. http://www.msha.gov/REGS/FEDREG/FINAL/2006finl/06-9608.asp

Fischhoff, B., Slovic, P., Lichtenstein, S., Read, S., Coombs, B., 1978. How safe is safe enough? A psychometric study of attitudes towards technological risks and benefits. Policy Sciences 9, 127–152.

Floyd, P., Nwaogu, T.A., Salado, R., George, C., 2006. Establishing a comparative inventory of approaches and methods used by enforcement authorities for the assessment of the safety of consumer products covered by the Directive 2001/95/EC on general product safety and identification of best practices. Final Report Prepared for DG/SANCO, European Commission by Risk & Policy Analysts Limited, United Kingdom

Flynn, G.J., (1949). "Average Heating Values of American Coals by Rank and by States", U.S. Bureau of Mines Information Circular 7538, (1949) 11 pages

Fox, J., Bowling, J., Schafrik, S., (2015). Principle roles of mine fire simulation in mine management and emergency planning. In: Proceeding of the 15th North American Mine Ventilation Symposium, Blacksburg, VA, pp. 493–499.

Fridolf, K., Andrée, K., Nilsson, D., Frantzich, H., (2013). The impact of smoke on walking speed. Fire and Materials.

Fridolf, K., (2014). Walking speed as function of extinction coefficient. Personal communication, Jan. 10.

Friel, G. F., Yuan, L., Edwards, J. C., Franks, R. A. (2006). Fire-generated smoke rollback through crosscut from return to intake – experimental and CFD study. Proceedings of the 11th U.S./North American Mine Ventilation Symposium, University Park, Pennsylvania, June 5-7, 2006. Mutmansky JM, Ramani RV. eds., London, U.K.: Taylor & Francis Group, 2006 Jun; 483-489

Germano, M., Piomelli, U., Moin, P., Cabot, W., (1991). A dynamic subgrid-scale eddy viscosity model, Phys. Fluids A, 3(7), 1760-1765.

Gillies, S., Wu, H. W., (2004). Case studies from simulating mine fires in coal mines and their effects on mine ventilation systems. Coal Operators' Conference, University of Wollongong & the Australasian Institute of Mining and Metallurgy, 111-125.

Gillies, S., Wu, H. W., (2009). FIRE SIMULATION SOFTWARE ASSISTING INERTISATION OF UNDERGROUND MINE WORKINGS. Presentation at Underground Methods Conference, Krakow, Poland, September.

Godbert, A. L., and Greenwald, H. P., 1936. Laboratory Studies of the Inflammability of Coal Dusts: Effect of Fineness of Coal and Inert Dusts on the Imflammability of Coal Dusts. Washington, D.C.: U.S. Bureau of Mines, Bulletin 389.

Grayson R.L , Kinilakodi, H. and Kecojevic, V. (2009), Pilot sample risk analysis for underground coal mine fires and explosions using MSHA citation data, Department of Energy and Mineral Engineering, The Pennsylvania State University, University Park, PA, USA. Safety Science 47, 1371–1378. <http://www.elsevier.com/locate/ssci>.

Grant, G., Southwood, P., (1999). Development of an onboard fire suppression system for Euro tunnel HGV shuttle trains. Proceedings of Interflam '99, Edinburgh, pp. 651-662

Greuer, R. E., 1977. Study of Mine Fires and Mine Ventilation. Part I, Computer Simulation of Ventilation Systems under the Influence of Mine Fires. U.S. Department of the Interior, Bureau of Mines, Contract No. S0241032, OFR 115(1)-78, NTIS No. PB288231.

Gülder Ö. L., Intasopa, G., Joo, H. I., Mandatori, P. M., Bento, D. S., Vaillancourt, M. E., (2011). Unified behaviour of maximum soot yields of methane, ethane and propane laminar diffusion flames at high pressures. Combustion and Flame 158, 2037–2044.

Haack, A., (1995). Introduction to the EUREKA project/BMBF research project 'Fire protection in underground transportation facilities'. Proceeding of the International

Conference on Fire Protection in Traffic Tunnels, Dresden, Germany, 12-13 September, pp. 6-18.

Haerter, A. (1994). Fire tests in the Ofenegg Tunnel in 1965. Proceedings of the International Conference on Fires in Tunnels, Boras, Sweden, 10-11 October, pp. 195-214.

Haghighat, A., Gillies, S., (2015). Fire behavior analysis of a mine future plan. In: Proceeding of the 15th North American Mine Ventilation Symposium, Blacksburg, VA, pp. 509–518.

Haghighat, A., Luxbacher, K., Lattimer, B., (2016). Simulation of a methane fire event at a coal mine working face with consideration of ventilation of ventilation curtain damage. SME Annual Meeting, Phoenix, Arizona.

Harris. K. J., (2010). Water Application Rates for Fixed Fire Fighting Systems in Road Tunnels. In Proceedings of the Fourth International Symposium on Tunnel Safety and Security, pages 351–362.

Hay, A., Borggaard, J. T., and Pelletier, D., (2009). Local improvements to reduced-order models using sensitivity analysis of the proper orthogonal decomposition, 629, 41–72. http://doi.org/10.1017/s0022112009006363.

He, Y., Fernando, A., Luo, M., (1998). "Determination of interface height from measured parameter profile in enclosure fire experiment"

Hertzberg, M., Zlochower, I.A., Edwards, J. C., (1988). "Coal Particle Pyrolysis Mechanisms and Temperatures" USBM RI 9169, 39 pages

Heselden, A. J. M., Hinkley, P. L. (1970). Smoke travel in shopping Malls: Experiments in Cooperation with Glasgow Fire Brigade. Part 1. Join Fire Research Organization, Fire Research Note NO. 832.

Heselden, A. J. M., (1978). Studies of fire and smoke behaviour relevant to tunnels. Proceedings of the 2nd International Symposium on Aerodynamics and Ventilation of Vehicles Tunnels, Cambridge, UK, 23-25 March 1976. BHRA Fluid Engineeering. Also Published as BRE Paper CP66/78.

Hinze, M., Volkwein. S., (2005). Proper orthogonal decomposition surrogate models for nonlinear dynamical systems: Error estimates and suboptimal control. In Dimension Reduction of Large-Scale Systems, pages 261–306. Springer, 2005.

Howarth, H. C., Nagy, J., and Hartmann, I. (1949). Experiments on the Control of Coal Mine Fires. Proc. 39th Annual Convention, Mine Inspectors' Inst. America, June, 1949.

Hwang, C. C., Edwards, J. C., (2005). The critical ventilation velocity in tunnel fires – a computer simulation. Fire Safety Journal, 40:213–244.

Hwang, C. C., Edwards, J. C., (2001). CFD MODELING OF SMOKE REVERSAL. Proceedings of The International Conference on Engineered Fire Protection Design, Applying Fire Science to Fire Protection Problems, San Francisco, CA, and June 11-15.

Ingason, H., (1995). Findings concerning the rate of heat release. Proceeding of the International Conference on Fire Protection in Traffic Tunnels, Dresden, Germany, 12-13 September, pp. 94-103.

Ingason, H., Lonnermark, A., (2003). Large scale fire tests in the Runehamer tunnel: heat release rate. Proceedings of the International Conference on Catastrophic Tunnel Fires, Boras, Sweden, 20-21 November. pp. 81-92.

Ingason, H., (2005). TG2.2– Target criteria. UPTUN Report WP2– task Group 2.

Ingason, H., Li, Y. Z., Lönnermark. A., (2015). "Tunnel Fire Dynamics". eBook, ISBN 978-1-4939-2198-0.

ISO (2004) Estimation of the lethal toxic potency of fire effluents. International Organization for Standardization, ISO 13344, Second edition.

Jin, T., (1978). Visibility through smoke. Journal of Fire & Flamability. 9:135–157.

Jin, T., Yamada, T., (1985). Irritating Effects of Fire Smoke on Visibility. Fire Science and Technology 5 (1):79-89.

Johnson G. A., Forshey, D. R., (1975). Automatic fire protection systems for large haulage vehicles: prototype development and in-mine testing. Minneapolis, MN: U.S. Department of the Interior, Bureau of Mines, Twin Cities Research Center, IC 8683. NTIS No. PB 246 704.

Jones, W. W., Peacock, R. D., Forney G. P., Reneke, P. A., Portier, R., (1993). "CFAST-the Consolidated Model of Fire Growth and Smoke Transport". NIST Technical Note 1299, Building and Fire Research Laboratory, National Institute of Standards and Technology, Gaithersburg, MD 20899-0001, USA.

Kaplan, S., Garrick, B.J., (1981). On the quantitative definition of risk. Risk Analysis 1, 11–27.

Keenan, C. M., (1963). Historical Documentation of Major Coal-Mine Disasters in the United States Not Classified as Explosions of Gas or Dust: 1846–1962. Washington, D.C.: U.S. Bureau of Mines, Bulletin 616.

Keski-Rahkonen, O., Holmjund, C., Loikkanen, P., Ludvigsen, H., Mikkola, E., (1986). Two full scale pilot fire experiments in a tunnel. Valtion Teknillinen Tutkimuskeskus (VTT) Technical Research Center of Finland, Research report 453.

Keski-Rahkonen, O. (1994). Tunnel fire tests in Finland. Proceeding of thee International Conference on Fires in Tunnels, Boras, Sweden, 10-11 October, pp. 222-237.

Kim, H. K., Lönnermark, A., Ingason, H., (2010). Effective Firefighting Operations in Road Tunnels. SP Technical Research Institute of Sweden. SP Report. ISBN 978-91-86319-46-5. ISSN 0284-5172. Borås.

Kocsis, K. C., (2009). New ventilation design criteria for underground metal mines based upon the "Life-Cycle' airflow demand schedule. PhD dissertation, the faculty of graduate studies, mining engineering, The University of British Columbia, Vancouver, Canada, August 2009.

Kuchta, J. M., Furno, A. L., and Martindill G. H., (1969). Flammability of Fabrics and Other Materials in OxygenEnriched Atmospheres: Ignition Temperature and Flame Spread Rates. Fire Technology, v. 5.

Kunikane, Y., Kawabata, N., Takekuni, K., Shimoda, A., (2002). A heat release rate onduced by gasoline pool fire in a large-cross-ssection tunnel. Proceedins of the 4th International Conference on tunnell fires, Basel, Switzerland, 2-4 December, pp.387-396.

Kunisch, K., Volkwein, S., Galerkin, S., (2002). Proper orthogonal decomposition methods for a general equation in fluid dynamics. SIAM Journal on Numerical analysis, 40(2):492–515, 2002.

Laage, L., Greuer, R., Pomroy, W., (1995). MFIRE User's Manual Version 2.20, 110 p (United States Bureau of Mines).

Layton, W., Introduction to the numerical analysis of incompressible viscous flows, volume 6. Siam, 2008.

Lazzara, C. P., Perzak, F.J., (1987). Effect of Ventilation on Conveyor Belt Fires, Symposium on Safety in Coal Mining, Paper 7.5, Pretoria, South Africa, Oct.

Lazzara, C. P. and Perzak, F. J. (1989). Conveyor Belt Flammability Tests: Comparison of Large-Scale Gallery and Laboratory-Scale Tunnel Results. Proc. 23 Int. Conf. of Safety in Mines Research Institutes, Washington, D.C.

Lee, C. K., Singer, J. M., and Chaiken R. F., (1977). "Coal Pyrolysis at Fire Level Heat Flux" Combustion Science and Technology, vol. 16, pp.205-213.

Li, Z. (2008). CFD simulation of spontaneous coal combustion in irregular patterns of goaf with multiple points of leaking air. Journal of China University of Mining and Technology, 18(4), 504–515. http://doi.org/10.1016/S1006-1266(08)60284-9

Lonnermark, A., Ingason, H., (2003). Large scale fire tests in the Runehamer tunnel: gas temperature and radiation. Proceedings of the International Conference on Catastrophic Tunnel Fires, Boras, Sweden, 20-21 November. pp. 81-92.

Lowndes I. S., Silvester S. A., Giddings, G., Pickering, S., Hassan, A. and Lester, E., (2007). "The computational modelling of flame spread along a conveyor belt", Fire Safety Journal, 42, 5167.

Luzik, S. J., (1996). "MSHA develops new fire-resistant check curtains". www.msha.gov/S&HINFO/TECHRPT/MINEWSTE/FIRESCC.pdf.

Mahajan, O. P., Tomita, A., Walker. P., L. (1976). "Differential Scanning Calorimetry Studies on Coal. 1. Pyrolysis in an inert atmosphere" Fuel, vol. 55, no.1, pp.63-69.

Malhotra, H. L., (1995). Goos vehicle fire test in a tunnel. Proceedings of the 2nd International Conference on Safety in Road and Rail Tunnels, Granada, Spain, pp. 237-244.

Marlair, G., Cwiklinski, C., (1993). Large-scale testing in the INERIS fire gallery: a major tool for both assessment and scaling-up of industrial fires involving chemicals. Proceedings of an industrial fires workshop, Apeldoorn, Netherlands, Proceedings EUR 15340 EN, pp. 303-309

Mawhinney J. R., Soja, E., Gillepsie, R., (1999). Mercury energy CBD tunnel project, New Zealand-performance based fire testing of a water mist suppression system. Proceedings of Interflam '99, Edinburgh, pp.663-673.

Mawhinney, J. R., Ingason, H. (2006) Full-scale fire testing of suppressed heavy goods vehicle fires in road tunnels—San Pedro de Anes Tests. Client Report HAI 5022-010-2 for Marioff Corporation Oy, Helsinki, Finland, August 2006

McDonald, L. B., Pomroy, W. H., (1980). A statistical analysis of coal mine fire incidents in the United States from 1950 to 1977. Minneapolis, MN: U.S. Department of the Interior, Bureau of Mines, Twin Cities Research Center, IC 8830. NTIS No. PB 81-148371

McGrattan, K. B., Hamins, A., (2006). Numerical Simulation of the Howard Street Tunnel Fire. Fire Technology, 42, 273–281, 2006

McGrattan, K., Hostikka, S., McDermott, R., Floyd, J., Weinschenk, C., Overholt, k., (2014). Fire Dynamics Simulator, Technical Reference Guide, Volume 1: Mathematical Model. National Institute of Standards and Technology, Gaithersburg, Maryland, USA, and VTT Technical Research Centre of Finland, Espoo, Finland, sixth edition, September 2014.

McPherson, M. J., (1993). Subsurface ventilation engineering, First edition, CHAPMAN & HALL. Ventilation Network Analysis, Chapter 7, 1993.

Merrick, D., (1983). "Mathematical Models of the Thermal Decomposition of Coal: 2. Specific Heats and Heats of Reaction" Fuel, vol. 62, no. 5, pp.540-546.

Merrick, D., (1983). "Mathematical Models of the Thermal Decomposition of Coal: 4. Heat Transfer and Temperature Profiles in a CokeOven Charge" Fuel, vol. 62, no. 5, pp.553-561.

Mitchell, D. W., Murphy, E. M., Nagy, J., and Christofel, F. P., (1961). Practical Aspects of Controlling an Underground Fire on a Mining Machine. U.S. Bureau of Mines, Report of Investigation 5846.

Mitchell, D. W., (1990). "Mine fires: prevention, detection, fighting". Maclean Hunter Publishing Co. DN: 622.82

Mizutani, T., Horiuchi, K., Akiyama, K. (1982). Experimental study of tunnel fires. Journal of the Japan Road Association, pp. 24-28.

Moin, P., Squires, K., Cabot, W., Lee, S., (1991). A dynamic subgrid-scale model for compressible turbulence and scalar transport, Phys. Fluids A, 3(11), 2746-2757.

Monaghan, W. D, Brune, J. F, Smith, A. C, (2005). Determining the root causes of flame cutting and welding fires in underground U.S. coal mines, Pittsburgh, National Institute for Occupational Safety and Health

MSHA, 2008a. Part 50 – Notification, Investigation, Reports and Records of Accidents, Injuries, Illnesses, Employment, and Coal Production in Mines. <http://www.msha.gov/30cfr/50.0.htm>.

MSHA, 2008b. MSHA's Data Retrieval System. <http://www.msha.gov/drs/drshome.htm>.

Mulholland, G. Janssens, M., Yusa, S., Twilley, W., Babrauskas, V., (1991). The Effect of Oxygen Concentration on CO and Smoke Produced by Flames. International association for fire safety science. Fire safety science proceeding, 3rd international symposium, Edinburgh, Scotland, pp. 585-594.

Mulholland, G., (1995). SFPE Handbook of Fire Protection Engineering, second edition, Section 2/ Chapter 15, (eds: P DiNenno, C Beyler, R Custer and W Walton) (National Fire Protection Association).

National Institute for Occupational Safety and Health, 2008a. NIOSH Mining Webpage, <http://www.cdc. gov/niosh/mining/topics/topicpage19.htm>, April 8.

National Cooperative Highway Research Program (NCHRP) Synthesis 415. (2011). Design fires in road tunnels. A synthesis of highway practice. Project 20-05, Topic 41-05. ISSN 0547-5570. ISBN 978-0-309-14330-1. Library of Congress Control No. 2010943183.

National Institute for Occupational Safety and Health (NIOSH) Mining Division. Use of CFD Modeling to Study Inert Gas Injection into a Sealed Mine Area. <http://www.cdc.gov/niosh/mining/pubs/pdfs/uocmt.pdf> (accessed March 2011).

NFPA® 502. Standard for Road Tunnels, Bridges, and Other Limited Access Highways. 2011 Edition. ISBN: 978-161665095-7.

Nilsen, A. R., Lindvik, P. A., Log, T., (2001). Full-scale fire testing in sub sea public road tunnels. Proceedings of the 9th International Interflam Conference, Edinburgh, Scotland, 17-19 September, pp. 913-924.

Noack, K., (1998). Control of gas emissions in underground coal mines. International Journal of Coal Geology 35, 57–82.

Panchakarla, S., Lilley, D. G., (2009) "The Fire Dynamics Simulator Code for Structural Fires". 47th AIAA Aerospace Sciences Meeting Including The New Horizons Forum and Aerospace Exposition 5 - 8 January 2009, Orlando, Florida.

Perard, M., (1992). Organization of fire trials in an operated road tunnel. Proceedings of the 1st International Conference on Safetyin Road and Rail Tunnels. Basel, Switzerland, 23-25 November. pp.161-170.

Perard, M., Brousse, B., (1994). Full size tests before opening two French tunnels. Proceedings of the 8th International Symposium on Aerodynamics and Ventilation of Vehicle Tunnels. Liverpool, 6-8 July, pp.383-408.

PIARK, (1999). Fire and smoke control in tunnels. The world Road Association (PIARC/AIPCR). report No. 05.05.B.

Piergiorgio, A., Giuseppe, D., Dino, F., Zappellini, G., Ferrari, A., (2001). CFD simulations of a truck fire in the underground Gran Sasso National Laboratory. In Proceedings of the 5th Italian Conference on Chemical and Process Engineering, volume 5 of AIDIC Conference Series. Associazione Italiana Di Ingegneria Chimica (AIDIC), Elsevier, May 2002. Papers presented at ICeaP-5, Florence, Italy, May 20-23, 2001

Pomroy, W. H., Bickel, K. L., (1980). Automatic fire protection systems for surface mining equipment. Minneapolis, MN: U.S. Department of the Interior, Bureau of Mines, Twin Cities Research Center, IC8832. NTIS No. PB 81-156937.

Pomroy, W. H., Carigiet, A. M., (1995). Analysis of underground coal mine fire incidents in the United States from 1978 through 1992. Minneapolis, MN: U.S. Department of the Interior, Bureau of Mines, Twin Cities Research Center, IC9426. NTIS No. PB 95-253720.

Prosser, B., and Ruckman, R. (2010). Conducting a fire modeling study, 13th United States/North American Mine Ventilation Symposium, pp.365–370.

Pucher, K., (1994). Fire tests in Zwenberg Tunnel (Austria). Proceedings of the International Conference on Fires in Tunnels, Boras, Sweden, 10-11 October. Pp.187-194.

Purser, D. A., (2008). Assessment of Hazards to Occupants from Smoke, Toxic Gases, and Heat. The SFPE Handbook of Fire Protection Engineering, 4th ed. edn. Quincy: National Fire Protection Association. 2–96 –2–193.

Ren, T. X., Edwards, J. S., (2000). Three-Dimensional CFD Modelling of Methane Flow Through Permeable Strata Around A Longwall Face, Trans. Institution of Mining and Metallurgy, Mining, Industry Section A, Vol 109, January-April.

Rice, G. S. (1912). Mine Fires, a Preliminary Study. Washington, D.C.: U.S. Bureau of Mines, Technical Paper 24.

Roache, P. J., (1994). "Perspective: A method for uniform reporting of grid refinement studies", Journal of Fluids Engineering, Vol. 116, No. 3, pp. 405–413, 1994.

Roache, P. J., (1998). Verification and Validation in Computational Science and Engineering, Hermosa Publishers, 1998.

Roe, P. L., (1986). Characteristics-based schemes for the Euler equations, Ann. Rev. Fluid Mech., 18, 337.

Rowland, J. H., Smith, A., C. (2011). Flammability of wider conveyor belts using large scale fire tests. Transactions of Society for mining, Metallurgy, and Exploration, 330, 345-349.

Sasmito, A. P., Birgersson, E., Ly, H. C., and Mujumdar, A. S. (2012). Some approaches to improve ventilation system in underground coal mines environment – A computational fluid dynamic study. Tunnelling and Underground Space Technology, 34, 82–95. http://doi.org/10.1016/j.tust.2012.09.006.

Shih, T. H., Liou, W. W., Shabbir, A, Yang, Z. And Zhu. J, (1995). A New Eddy-Viscosity Model for High Reynolds Number Turbulent Flows - Model Development and Validation. Computers Fluids, 24(3):227-238, 1995.

Simms, D. L., Hinkley, P. L., (1963). Fire Research Special Report No. 3, Her Majesty's Stationary Office, London.

Singer, J. M., Tye, R. P., (1979). "Thermal, mechanical, and physical properties of selected bituminous coals and cokes". Bureau of Mines Report of Investigations. Dept. of Interior, Bureau of Mines. Washington, D.C., USA.

Smith, A. C., Rumancik, W. P., and Lazzara, C. P., (1995). SPONCOM - A Computer Program for the Prediction of the Spontaneous Combustion Potential of an Underground Coal Mine. Proc. 26th Int.Conf. On Safety in Mines Research Institutes.v. 4. Katowice, Poland

Smith, A. C., Thimons, E. D. (2010). A summary of U. S. Mine fire research, 2010 SME Annual Meeting and Exhibit, February 28 - March 3, Phoenix, Arizona. Littleton, CO: Society for Mining, Metallurgy, and Exploration, Inc., 2010; :1-15. http://www.cdc.gov/niosh/mining/works/coversheet690.html

Srinivasa, R. B., Baafi, E. Y., Aziz, N. I., Singh, R. N., (1993). Three dimensional modeling of air velocities and dust control techniques in a longwall face. In: Proceeding of the 6th US Mine Ventilation Symposium, SME, Littleton, pp. 287–292.

Steinert, C., (1994). Smoke and heat production in tunnel fires, Proceednigs of the International Conference on Fiires in Tunnels, Boras, Sweden, 10-11 October, pp. 123-137.

Stewart, C. M., Aminossadati, S. M., Kizil, M. S., (2015). Underground Fire Rollback Simulation in Large Scale Ventilation Models. The 15th North American Mine Ventilation Symposium.pp.519-527.

Taraba, B., and Michalec, Z. (2011). Effect of longwall face advance rate on spontaneous heating process in the gob area – CFD modelling. Fuel, 90(8), 2790–2797. http://doi.org/10.1016/j.fuel.2011.03.033

Taraba, B., and Michalec, Z., Michalcova, V., Blejchar, T., Bojko, M., Kozubkova, M., (2013). CFD simulations of the effect of wind on the spontaneous heating of coal stockpiles. Fuel 118 (2014) 107–112.

Tauziede, C., Mouilleau, Y., Bouet, R., (1993). Modelling of Gas Flows in the Goaf of Retreating Faces. Paper Presented at the 25th International Conference on Safety in Mines Research Institutes Pretoria, SA.

Tomata, S., Uchino, K., Inoue, M., (1999). Methane concentration at heading faces with auxiliary ventilation. In: Proceeding of the 8th US Mine Ventilation Symposium, SME, Littleton, pp. 187–192.

Torano, J., Torno, S., Menendez, M., Gent, M., (2011). Auxiliary ventilation in mining roadways driven with roadheaders: validated CFD modeling of dust behaviour. Tunnelling and Underground Space Technology 26, 201–210.

Trelles, J., Mawhinney, J. R., (2010). CFD Investigation of Large Scale Pallet Stack Fires in Tunnels Protected by Water Mist Systems. JournalofFireProtectionEngineering,20(3):149–198,August.

Trevits, M. A., Yuan, L., Smith, A. C., Thimons, E. D., (2009). NIOSH MINE FIRE RESEARCH IN THE UNITED STATES. Proceedings of the Ninth International Mine Ventilation Congress, New Delhi, India, November 10-13, 2009. Panigrahi DC, ed., New Delhi, India: Oxford & IBH Publishing Co. Pvt. Ltd., 2009; 1:357-366. http://www.cdc.gov/niosh/mining/works/coversheet1531.html.

Triesbsch, G. and Sapko, M. J., (1990). Lake Lynn Laboratory: A State-of-the-Art Mining Research Laboratory. Proc. Int. Symp. On Unique Underground Structures, Denver, CO.

Van Duijne, F. H., Van Aken, D., Schouten, E. G., (2008). Considerations in developing complete and quantified methods for risk assessment. ScienceDirect. Safety Science 46, 245–254.

Wala, A. M., Dziurzynski, W., Tracz, J., Wooton, D., (1995). Validation Study of the Mine Fire Simulation Model. In Proceedings 7th US Mine Vent. Symp. (ed: A M Wala) pp.199-206 (Society of Mining Engineers: Littleton, Colorado)

Wala, A., Jacob, J., Brown, J., Huang, G., (2003). New approaches to mine-face ventilation. Mining Engineering 55 (3), 25–30.

Wang, L., Chen, Q., (2008). "Applications of a Coupled Multizone-CFD Model to Calculate Airflow and Contaminant Dispersion in Built Environments for Emergency Management". HVAC&R Research. Vol 14. Number 6. pp. 925-939.

Wang, P., Feng, T., Liu, R., (2011). Numerical simulation of dust distribution at a fully mechanized face under the isolation effect of an air curtain. Mining Science and Technology (China) 21, 65–69.

Warner, B. L., (1975). "Evaluation of Potential Fire Hazard Caused by Exposed Timber in Mine Passageways" USBM Contract Final Report, Contract No. H0144068.

Weisenpacher, P., Halada, L., Glasa, J., (2011). Computer simulation of fire in a tunnel using parallel version of FDS. 7th Mediterranean combustion symposium. Chia Laguna, Cagliari, Sardinia, Italy, September 11-15,

Werner, H., Wengle, H., (1991). Large-eddy simulation of turbulent flow over and around a cube in a plate channel, In 8th Symposium on Turbulent Shear Flows, 155-168.

Widzyk-Capehart, E., Watson, B., Agnew gold mine expansion mine ventilation evaluation using ventsim. The 7th international mine ventilation congress. 2001.

Woodburn, P. J., Britter, R. E. (1996). CFD Simulations o f a tunnel fire-Part I. Fire Safety Journal 26, 35-62.

Woodburn, P. J., Britter, R. E. (1996). CFD Simulations o f a tunnel fire-Part II. Fire Safety Journal 26, 63-90.

Wu, H. W., Gillies, A. D. S., Wala, A. M., (2004). Case studies from application of numerical simulation software to examining the effects of fires on mine ventilation systems, in Proceedings 10th US Mine Vent. Symp., (ed: R Ganguli and S Bandopadhyhy) pp 445-455 (Balkema, The Netherlands).

Yuan, L., and Smith, A. C. (2007). Computational Fluid Dynamics Modeling of Spontaneous Heating in Longwall Gob Areas. Trans Soc Min Metal Explor 2007 Dec; 322:37-44

Yuan, L., Smith, A. C., (2008). Numerical study on effects of coal properties on spontaneous heating in longwall gob areas. Fuel, 87(15-16), 3409–3419. http://doi.org/10.1016/j.fuel.2008.05.015

Yuan, L., Smith, A. C., (2009). CFD modeling of spontaneous heating in a large-scale coal chamber. Journal of Loss Prevention in the Process Industries, 22(4), 426–433.

Yuan, L., Mainiero, R. J., Rowland, J. H., Thomas, R. A. T., Smith, A. C. S., (2014). Numerical and experimental study on flame spread over conveyor belts in a large-scale tunnel. Journal of Loss Prevention in the Process Industries, Volume 30, July 2014, Pages 55–62.

Zheng, Y., Tien, J. C., (2008). DPM dispersion study using CFD for underground metal/ nonmetal mines. In: Proceeding of the 12th North American Mine Ventilation Symposium 2008, pp. 487–493.

Zheng, Y., (2011). Diesel particulate matter dispersion analysis in underground metal/nonmetal mines using computational fluid dynamics. PhD dissertation, 125. Missouri University of Science and & Technology. USA, 2011.

Zhou, G., (1995). Numerical simulations of physical discontinuities in single and multi-fluid flows for arbitrary Mach numbers, PhD Thesis, Chalmers University of Technology, Goteborg, Sweden.

Zhou, L., Smith, A. C., (2012). Improvement of a mine fire simulation program - incorporation of smoke rollback into MFIRE 3.0. Journal of Fire Sciences. ISSN:0734-9041. pp. 29-39.

3. Risk Assessment of Fire Incidents in U.S. Underground Coal Mines from 2000 to 2012

The following paper will be submitted to the 17th North American Mine Ventilation Symposium (NAMVS). It was entirely written by Ali Haghighat with editorial input from Dr. Kray Luxbacher and Dr. Edmond Jong may be compressed to meet the peer reviewed conference.

3.1. Abstract

A risk analysis of mine fires for all U.S. underground coal mines from 2000–2012 was completed to identify locations that have a high risk for fire incidents. The data for this analysis was extracted from the Mine Safety and Health Administration (MSHA) mine fire accident reports database. After identifying fire incidents from this database, a risk matrix was developed for underground locations that showed a significant propensity for fire incidents. This matrix associates the hazards and risks with the severity and frequency of their consequences at each location. These significant mine areas will be the concentration of future studies in fire behavior, suppression techniques, and simulation methodologies.

3.2. Introduction

Fires in underground mines pose significant hazards to personnel because of inherent restrictions to movement and limitations to egress routes. Despite improvements, mine fires remain serious hazards in underground coal mine. In order to better mitigate the risks from fire hazards in the modern underground mining environment, a better understanding of where fire events occur must be gained. The following paper presents an investigation on the number of fatal and non-fatal incidents in underground coal mines fires from 2000 to 2012. Three phases of risk assessment, risk identification, estimation, and evaluation, were applied to the recorded fire events from the MSHA incident database that occurred during this time period. Using this process, a fire hazard was first defined. This definition was then used to identify any incidents that had occurred as a result of the defined hazards. The seriousness of the injuries and damages were finally quantified for each incident though an estimate of severity and frequency and then aggregated according to underground location (ISO, 1999; Van Duijne, 2008). Using this approach, locations prone

to incidents resulting from fire hazards were first identified. The risk for the occurrence a fire incident in general was then estimated for each of the identified locations. The results of this assessment will be used to improve fire simulation techniques for the identified, high risk underground locations.

3.3. Risk Identification

A risk for this assessment was defined as any single occurrence of a fire initiated by the ignition of gas, dust, or electricity. Each recorded occurrence of such an event in the MSHA incident database was counted as a single fire incident. Both non-fatal incidents that were reportable but did not result in a fatality, and fatal incidents that fell into the aforementioned criteria were counted. Incidents in the MSHA database that were already classified as "generic" were not considered. The remaining incidents were then totaled and aggregated according to the underground location in which they occurred. In previous studies, a number of locations, which are listed in Table 3.1, were highlighted as high fire hazard areas (McDonald et al., 1980; Pomroy et al., 1995; De Rosa, 2004). These locations were used to group the fire incidents extracted from the MSHA incident database. The compiled number of non-fatal and fatal underground coal fire incidents from 2000 to 2012 are displayed in Table 3.1.

Table 3.1. Total number of recorded fatal and non-fatal fire incidents from 2000 to 2012 in underground coal mines

Fire Location	Non-fatal incident	Fatal incident
Flame cutting/welding areas	25	0
Gobline/sealed/abandoned/coal pit areas	10	1
Belt entry/feeder/slope/portal branch areas	43	1
Longwall panel/headgate/main return/Bleeder	160	1
Haulage/track rails	0	0
Power station/rectifier areas	3	0
Generator/transformer/fan/breaker/pump areas	5	0
Charging station	2	0
Mining face/intersection/crosscut areas	304	0
Maintenance areas	6	0
Mobile equipment working areas	15	0
Unknown	3	0

As can be seen in Table 3.1, three fatal incidents were classified as resulting from a fire hazard. These events were the Upper Big Branch explosion in 2010, the Aracoma Alma Mine Fire in 2006, and the Willow Creek Mine Explosion in 2005. These events were counted as fire incidents because the products of a fire were the ultimate cause of the fatalities. In contrast, the fatalities Sago Mine, Darby No. 1 Mine, and Jim Walters Resources Mine events that occurred in 2006 resulted from the products of an explosion rather than a fire. Although the aforementioned large mine events resulted in multiple fatalities by fire, they were each counted as a single incident based on the criteria introduced earlier in this section. The severity of these events will, however, be taken into consideration when generating the risk matrix.

The locations displayed in Table 3.1 that encompassed the highest number of total incidents were consolidated into four general areas to simplify data processing. The consolidated locations are the "Active Face," which includes the mining face, intersections, crosscut areas, longwall panels, headgates, main returns, and bleeders, the "Electrical Installation," which includes power stations, rectifier areas, generators, transformers, fan, breakers, pump areas, and charging stations, the "Belt Area," which includes belt entries, feeders, slopes and, portal branch areas, and the "Gob and Sealed Area," which includes the gobline, sealed, abandoned, and coal pit areas. The remaining locations such as maintenance areas, flame cutting or welding areas, etc., were categorized as "Other." The total number of non-fatal and fatal incidents in terms of the four consolidated locations are shown in Table 3.2.

Table 3.2. Total number of recorded non-fatal and fatal incidents from 2000 to 2012 by consolidated location

Fire Location	Non-Fatal Incidents	Fatal Incidents
Active Face	464	1
Gob and Sealed Area	10	1
Electrical installation	10	0
Belt Areas	43	1
Other	49	0

3.4. Risk Estimation

Risk analyses can either be qualitative or quantitative in nature. Qualitative risk analyses are subjective because of their dependence on human judgment. In contrast, quantitative risk analyses are more objective because they use historical data to identify the occurrences of major hazard-related incidents (Joy et al., 2007). As such, a quantitative risk estimation was performed on the processed fire incident data introduced in the previous section. The purpose of the risk estimation was to assign severity and frequency scores to the extracted fire incidents, which will be later used to generate the risk matrix. The criteria used for assigning severity and frequency values to the incident data are shown in Tables 3.3 and 3.4, respectively. Based on these criteria, scores were first assigned to each recorded incident. These scores across all fire incident types were then averaged by location (i.e., Active Face, Gob and Sealed Areas, Electrical Installation, Belt Areas, and Other) across the 13-year data assessment period. The resulting aggregated scores, which are shown in Table 3.5, shows the severity and frequency of any fire incident that occurred at the indicated location.

Table 3.3. Criteria used for the assignment of severity scores

Injuries-Damages Criteria	Value
• Death of one or more people • Permanent disability • Irreparable and extensive damage to materials • Production losses that affect forecasted results • Stop operations affecting the company's image	Critical 1.0
• Injuries with temporary disability on one or more person • Reparable and partial damage to materials • Production losses requiring special plans to recover	High 0.6-0.9
• Non-disabling injuries • Damage to materials not affecting production process • Minimum production losses. May be recovered within a short time	Moderate 0.2-0.5
• Almost no losses	Low 0.1

Table 3.4. Criteria used for the assignment of frequency scores

Criteria to estimate frequency	Name	Value	Frequency Score
Incident occurred more than 10 times per year	Frequent	Critical	1.0
Incident occurred between 3 to 10 times per year	Occasional	High	0.4-0.9
Incident occurred once or twice per year	Uncommon	Moderate	0.2-0.3
No recorded incidents	Remote	Low	0.1

Table 3.5. The average severity of consequence frequency scoring from 2000 to 2012

Criteria	Active face	Gob and sealed area	Electrical installation	Belt area	Other
Severity	0.4	0.4	0.3	0.6	0.4
Frequency	1	0.2	0.2	0.4	0.4

3.5. Risk Matrix

A risk matrix, which is shown in Figure 3.1, was generated using the locations, severity scores, and frequency scores estimated in the previous section. The green, yellow, orange, and red areas express areas of low, moderate, high, and very high risks, respectively. Each color coded area was defined by equally dividing the frequency and severity regions into four equal sections (i.e., 0-0.25 is low, 0.25-0.50 is moderate, 0.50-0.75 is high, and 0.75-1.00 is very high).

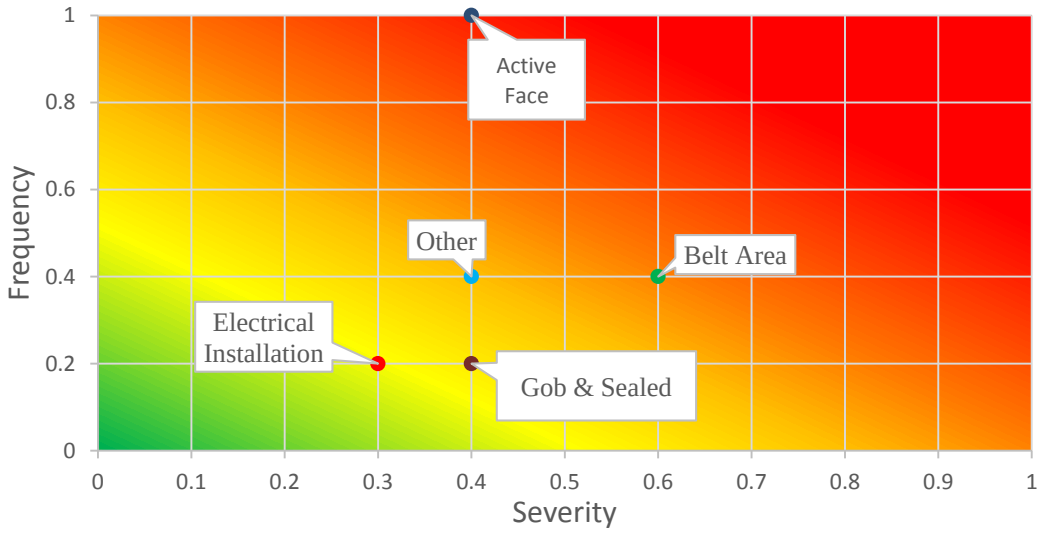

Figure 3.1. Risk matrix for underground locations that exhibited high numbers of total fire incidents from 2000 to 2012

As can be seen in Figure 3.1, the "Active Face" is a very high risk area for fire incidents and thus should receive the highest level of consideration for future studies. Despite the moderate average severity for the active face during this time period, this location was categorized as a very high risk because of its very high average incident frequency. In contrast, the "Belt Area" was categorized as a high risk area because of high average severity. The remaining categorized areas are at moderate risk for fire incidents. The "Other" fire incident category is also a high risk area. As such, further assessments should be completed on the different sub-locations of the "Other" group. Such an investigation is, however, beyond the scope of the current discussion. This risk matrix does not consider unreported incidents, which can potentially affect the placement of the categorized locations in the risk matrix.

3.6. Conclusion

The fire incident risk assessment of the MSHA incident database identified four general locations, the active face, belt areas, gob and sealed areas, and electrical installations as the most significant risk areas for fire events during 2000 to 2012. This investigation shows that the fire incidents at the "Active Face" happened more frequently during this time period relative to the remaining locations. This result is likely caused by

the concentration of personnel and potential ignition sources that are present in the active face. Because of this increased activity, the severity of fire incidents that do occur is mitigated by the amount of safety policies and technologies implemented at the active face. In contrast, the "Belt Area" had the highest average severity in comparison with the remaining locations and a moderate frequency. This higher relative severity resulted from a number of incidents in which a belt fire resulted in either significant injuries or long periods of mine inactivity. However, given the fairly simple operational nature of belt areas, the frequency of fire incidents during this time period was likely suppressed. The four locations highlighted in this study will be the focus of further studies regarding fire simulation and mitigation methodologies with a specific concentration on the "Active Face" and the "Belt Area".

3.7. Acknowledgements

This research was developed under Contract No. 200-2014-59669, awarded by the National Institute for Occupational Safety and Health (NIOSH). The findings and conclusions in this report are those of the authors and do not reflect the official policies of the Department of Health and Human Services; nor does mention of trade names, commercial practices, or organizations imply endorsement by the U.S. Government.

3.8. Bibliography

ISO/IEC Guide 51, (1999). Safety Aspects-Guidelines for their inclusion in standards, 2nd ed. ISO/IEC, Geneva.

Van Duijne, F. H., Van Aken, D., Schouten, E. G., (2008). Considerations in developing complete and quantified methods for risk assessment. Science Direct. Safety Science 46, 245–254.

McDonald, L. B., and Pomroy, W. H., (1980). A statistical analysis of coal mine fire incidents in the United States from 1950 to 1977. Minneapolis, MN: U.S. Department of the Interior, Bureau of Mines, Twin Cities Research Center, IC 8830. NTIS No. PB 81-148371.

Pomroy, W. H., Carigiet, A. M., (1995). Analysis of underground coal mine fire incidents in the United States from 1978 through 1992. Minneapolis, MN: U.S. Department of the Interior, Bureau of Mines, Twin Cities Research Center, IC9426. NTIS No. PB 95-253720.

De Rosa, M., (2004). Analyses of mobile equipment fires for all U.S. surface and underground coal and metal/nonmetal mining categories, 1990-1999. National Institute for Occupational Safety and Health, IC 9467. DHHS (NIOSH) Publication No. 2004-105.

Joy, J., Griffiths, D., (2007). National Industry Safety and Health Risk Assessment Guideline, Version No. 7, Minerals Industry Safety and Health Centre (MISHC), University of Queensland, Australia.

4. Simulation of a Methane Fire Event at a Coal Mine Working Face with Consideration of Ventilation Curtain Damage

This paper was published on 2016 Transactions of the Society for Mining, Metallurgy & Exploration, Vol. 340, pp. 120-126. https://doi.org/10.19150/trans.7336. Ali Haghighat conducted the majority of the work and wrote the paper with editorial input from coauthors: Dr. Kray Luxbacher, and Dr. Brian Lattimer. Please cite this article as: Haghighat, A., Luxbacher, K., Lattimer, B. (2016). Simulation of a methane fire event at a coal mine working face with consideration of ventilation curtain damage. 2016 Transactions of the Society for Mining, Metallurgy & Exploration, Vol. 340, pp. 120-126.

4.1. Abstract

Mine face ignition due to high levels of methane is one of the most common fire incidents in underground coal mines. In continuous miner headings, depending on the magnitude of the ignition or resulting fire, auxiliary ventilation controls may be damaged or dislodged, affecting the ventilation into the area. A computational study was conducted to investigate the effects of different levels of damage to an exhausting ventilation curtain in a continuous miner heading, and the impact on ventilation to the face. The computational fluid dynamics software Fire Dynamics Simulator (FDS) Version 6.0 was used to predict the conditions that develop due to a 200-kW fire in the face following a methane ignition with different levels of assumed ventilation curtain damage. Smoke layer depth, temperature and mass flow inby the last open crosscut were used to evaluate the impact of no damage to the curtain, partially dislodged curtain, and fully removed curtain. As more of the ventilation curtain was damaged, smoke depth and temperature outby the fire increased. With the full removal of the curtain, the smoke accumulated from the last open crosscut to the face, with the ventilation completely bypassing the continuous miner region.

4.2. Introduction

Active working faces in underground coal mines are one the most hazardous locations in terms of fire events. According to Mine Safety and Health Administration (MSHA) data analysis, the highest number of nonfatal fire incidents were reported at mining faces, intersections and crosscut areas compared with other locations from 2000 to 2012, with about 464 fire incidents reported at active working faces, most consisting of

methane ignitions (MSHA, 2016). In some cases, these ignition incidents were followed by localized fire. The ignitions themselves are high-risk incidents due to the potential to raise float dust and damage ventilation systems, particularly auxiliary systems that move air into dead end cuts, such as ventilation curtain or tubing. Further, an active fire in the face, coupled with a damaged system, creates further risk, and the atmosphere near-fire is difficult to predict. Depending on the magnitude of an ignition or fire, and the degree of damage to auxiliary ventilation controls, the atmosphere near the fire can change substantially. In this study, the state of the auxiliary ventilation was varied based on the assumption that as a face ignition increases in magnitude, auxiliary ventilation will be affected proportionally. Five computational fluid dynamics (CFD) scenarios were considered to investigate the smoke-layer depth, temperature, visibility, mass flow rate and air velocity in an entry with a continuous miner located in an active (dead-end) cut. Visibility and temperature from floor to roof were investigated, and the height of the interface between the smoke-laden layer and the cooler layer, called interface height, at various points from the face outby to the last open crosscut were determined. Fire Dynamics Simulator (FDS) Version 6.0, specialized CFD software for the simulation of fire, was used to predict the conditions that develop due to a 200-kW fire at a coal mine face following a methane ignition under varying levels of auxiliary ventilation damage. Most entry fires are reported as fuel-controlled fires as they are rarely restricted to air access (Ingason, Li and Lönnermark, 2014). Thus, the fire in these models was assumed to be a fuel-controlled fire. Mine fires are difficult to control, because there is typically only a narrow time window for personnel to approach the fire, limited qualitative information available, or communicated, about the fire, and scarce quantitative information characterizing the event. Modeling of multiple scenarios allows for assessment of the safest and most efficacious response to local fires. Such fires, in the absence of an immediate and successful response, can rapidly escalate to events that compromise the entire ventilation system and the safety of all personnel in the mine. These scenarios also have potential applications in training and educating fire brigades and mine rescue teams. This study was carried out to accomplish three main objectives. First, to assess visibility and temperature in the entry for anyone approaching the fire. Second, to develop an understanding of conditions that result from several ventilation damage scenarios, and third, to use this

knowledge to determine the smoke layer depth through interface and fresh air heights study.

4.3. Geometry, Initial and Boundary Conditions

In this study, five different scenarios based on different assumed ignition magnitudes were considered for investigation of a methane fire at the coal face. It was assumed that the ignition and fire occurred during continuous miner production, and that the miner was backed out of the face, which is common procedure. The ignition magnitudes were not quantified; rather, their effect on the auxiliary ventilation was assumed to range from minimal to completely destroyed. In every case, a methane fire was assumed to have been started by the initial ignition event. The fire was set on the floor at the center, close to the face. The airway, curtain and continuous miner were simulated according to the geometry shown in Figure 4.1: number 8 entry, with the exhausting line curtain set to the right side. The geometry and ventilation are generally based on a partner mine in the United States.

The width and height of the entries were 6 and 1.8 m (20 and 6 ft), respectively. The length of the entry that had the continuous miner in it was set at 15 m (50 ft) and the distance from the outlet to the curtain was set at 2.8 m (9 ft). The outlet corresponds to the outby end of the exhausting line curtain. The curtain was installed in the entry, 0.6 m (2 ft) to the closest rib. The length of the inlet to the main entry was 1.8 m (6 ft). The inlet corresponds to the crosscut.

This fire was assumed to have a heat release rate (HRR) of 200 kW. There is no information in the literature quantifying a heat release rate for methane ignitions at working faces in underground coal mines, due to the difficulty in measuring or estimating the fuel mass loss or gas consumption in a real scenario. In general, there is quantification of HRR for various burning items, such as upholstery, wood cribs and vehicles, which can give the reader a relative sense of HRR. Hansen and Ingason (2013) measured the peak HRR of a drilling rig and a loader fire at 29.4 MW and 15.9 MW, respectively, and the maximum HRR of a single wood crib was measured at about 180 kW (Hansen, 2015). Also, the U.S.

National Institute for Occupational Safety and Health (NIOSH) conducted different experiments for better understanding of mine fires, and used a natural gas burner with rated HRR of 44 to 114 kW (Trevits et al., 2009). Yuan and Lazzara (2004) used 230-kW, 1-MW and 3-MW diesel fuel fires in experiments to investigate the effect of ventilation and preborn time on water mist extinguishing. There are also standards for HRR in vehicle fires. The HRR for a passenger car fire is recommended to be set at about 5 to 10 MW in simulations (National Fire Protection Association, 2011). Given these values, particularly the gas burner values, 200 kW is assumed to be reasonable for a methane-fed, fuel-controlled fire.

According to MSHA mine fire accident reports from 2000 to 2012, most fires at working faces were reported as small fires. Although there is a lack of information in terms of HRR, there are some data in terms of flame height and physical size of the fire at working faces. To justify the fire parameters in this research, we refer to a mine fire incident in 2000 in which it was reported that an ignition occurred when the continuous miner operator was brushing the floor. The flame size was reported to be 0.25 m (0.8 ft) high and 1 m (3.3 ft) long by 1 m (3.3 ft) wide. In this research we simulated the same height and physical size of methane fire in the presence of curtain at the face.

The methane was ignited on a surface that was 1 m (3.3 ft) long and 1 m (3.3 ft) wide. The heat of combustion and soot yield for the methane fire were considered to be 55.5 MJ/kg and 0.1 kg/kg, respectively. All thermal and physical parameters of Pittsburgh bituminous coal, such as density, thermal conductivity and specific heat, were set according to experimental analysis (Singer and Tye, 1979). The emissivity of the coal was set at 0.96. The curtain consisted of a composite of double-layered, high-temperature ceramic fiber textile, rated at 3,000 °F (1,649 °C) with continuous use, sewn together using ceramic thread and buffered on both sides with an approved 0.9-mm (35-mil) polyethylene plastic brattice (Luzik, 1993). The high-density polyethylene was considered for the curtain properties (greater than 0.95 g/cm^3). The density, thermal conductivity and specific heat of the curtain were set at 1,300 kg/m3, 0.5 W/m-K and 1.9 kJ/kg-K, respectively. Due to the ceramic fiber textile and polyethylene outer layer of brattice, the heat of combustion for

the curtain was set at 43,600 kJ/kg (Tewarson, 1995). All of the thermal and physical properties of steel, including specific heat, thermal conductivity, emissivity and density, were used for the simulation of the continuous miner. The specific heat and conductivity of steel were varied according to different temperatures. In FDS, we assumed that reliable numerical results can be achieved when the grid size is $\leq 0.1D^*$ (McGrattan, Baum and Rehm, 1998), where D^* is representative of the characteristic length scale that corresponds to the total HRR of a fire plume (Baum and McCaffrey, 1989; Yuan et al., 2014).

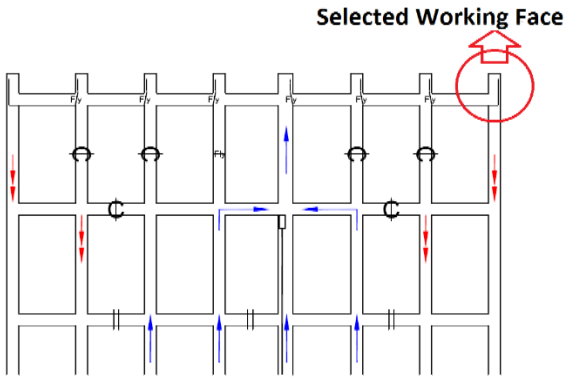

Figure 4.1. Schematic view of working faces

Therefore, a grid size of 5 cm (2 in.) was considered for the numerical analysis of the 200-kW methane fire in this study. The T squared approach was used for the growth of the methane fire at the face (Ingason, 2009). The decay time period for methane fire was not considered in the study as the focus of the research in this paper was to investigate the effect of curtain length on the height of smoke-laden layer at the fire source, as well as the amount of smoke movement upstream of the fire. The growth of the fire at the face was assumed to be medium to slow growth. Therefore, the fire growth coefficient was set at 0.00347 kW/s2 (Kim and Lilley, 2002).

The volume flow rate at the inlet was set at 6.61 m3/s (14,000 cfm) and the outlet was set to open. The working face, continuous miner, coal seams, fire source, inlet and outlet, exhausting ventilation curtain location in different scenarios, and axes are depicted in Figure 4.2. Numerous parameters were calculated, including visibility and temperature at different points in the entry. A no-slip boundary condition was considered for all walls and objects in the domain.

According to the assumed pre-ignition intensity, five different scenarios, each with increasingly damaged curtain, were considered for the investigation of different parameters at various parts of the entry. Smoke layer depth, temperatures and mass flow into the continuous miner area were used to evaluate the impact of no damage to the curtain, partially dislodged curtain, and full removal of the curtain. The model geometry is shown in Figure 4.2, and damage to the curtain can also be seen for each scenario. In scenario 1, no damage was assumed. For the partially dislodged curtain, it was assumed that the curtain was damaged—essentially removed—6 m (20 ft), 15 m (50 ft) and 21 m (69 ft) from the face for scenarios 2, 3 and 4, respectively. The whole curtain was removed from the computational domain in scenario 5 (Figure 4.2).

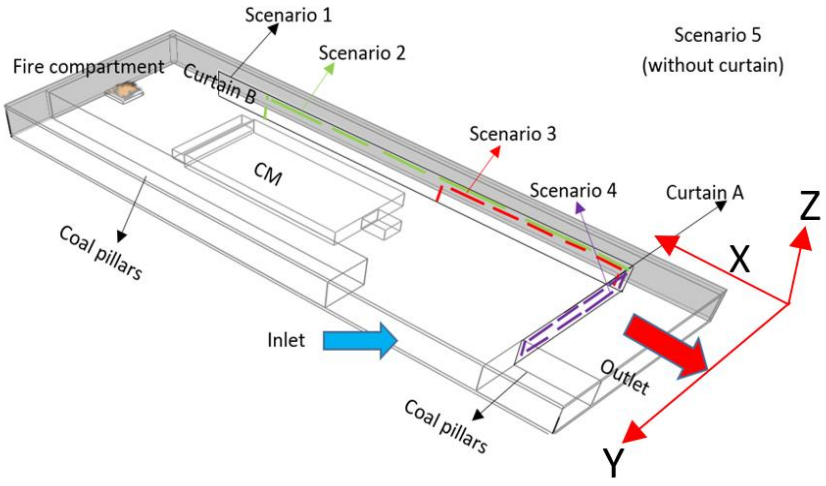

Figure 4.2. Working face and objects for all scenarios (isometric view)

4.4. Interface Height

Smoke behavior analysis is important in terms of mine rescue training and best firefighting practice. According to the mine rescue manual, personnel in the incident command post (ICP) need to quickly gain an understanding of the fire location, fire specifications, and conditions near the fire area. Smoke can limit visibility to the degree that it is difficult for personnel to even approach the fire, and, if they do approach, it may still be nearly impossible to assess the magnitude and involvement. Further, the soot and carbon monoxide (CO) expected to be present with smoke pose a considerable hazard to barefaced personnel (Enright and Ferrier, 2015). All of these parameters affect the ability

of section personnel, as well as specially trained mine rescue teams or fire brigades, to approach and assess a fire, and communicate conditions.

Interface height is one of the primary parameters used for understanding smoke layer depth. Because of the buoyancy effect, the generated hot smoke in the fire plume tends to move up to the top of the enclosure and relatively cool air remains lower. The height of the interface between the smoke-laden layer and the cooler layer is defined as the interface height (He, Fernando and Luo, 1998). Both the smoke layer depth, and the smoke progress into the entry—upstream of the continuous miner—can be studied through interface and fresh air height studies. The following study concentrates on the effect of the ventilation curtain on the interface height, which allows for the understanding of conditions for barefaced miners, mine rescue teams and fire brigade teams during a methane fire at the working face. Hence, the interface height was investigated for smoke behavior analysis in all simulations at different locations of the working face. Although smoke rollback study is important for designing the emergency plan during fire events in underground mines, this topic is beyond the scope of this research. The upwind transport of the smoke, or rollback, occurs when the air velocity is less than critical velocity or the fire's intensity has increased sufficiently. The reason lies in the buoyancy forces associated with the temperature of the smoke plume that cause it to overcome the inertial forces of the ventilation (Friel et al., 2006). The air velocity considered in this study was well above critical velocity.

The zone approach was used to calculate the interface height. In this approach the cross section is divided into a top hot layer and lower cool layer zones, as explained in detail by Brani and McCaffrey (1992) and Jones et al. (1993). It was shown in He, Fernando and Luo (1998) that using this approach reduces the complexity of computation with acceptable result accuracy compared with other approaches. In the zone approach, the interface height is calculated according to:

$$Z_{int} = \frac{T_1(I_1 I_2 - H^2)}{I_1 + I_2 {T_1}^2 - 2T_1 H} \tag{4-1}$$

where Z_{int} is the interface height in meters, T_1 is the lower layer temperature in °C, H is the ceiling height from the floor in meters, and I_1 and I_2 are in meters and calculated by:

$$I_1 = \int_0^H T(z)dz \tag{4-2}$$

$$I_2 = \int_0^H \frac{1}{T(z)}dz \tag{4-3}$$

where $T(z)$ is the continuous function defining temperature T in °C as a function of height above the floor z, where 0 and H are the floor and ceiling heights in meters, respectively (McGrattan et al., 2014). The fresh air height is therefore not the same as the interface height according to the zone approach. The height of fresh air is determined according to the average temperature and visibility, along with the height of the entry at different sections in all scenarios. Fresh air, for these purposes, is defined as air having no combustion products, a maximum temperature of 20 °C and visibility of 30 m (98 ft).

4.5. Results

In all scenarios, it was assumed that the inlet volume flow rate was 6.61 m^3/s (14,000 cfm) and the HRR of methane fire was 200 kW. The T squared approach was used for the growth of the methane fire at the face (Ingason, 2009). The fire growth coefficient, the α value, was set at 0.00347 kW/s^2. The HRR increased during the first four minutes of the event and then remained constant until the end of the simulation time (Figure 4.3). The same initial and boundary conditions were assigned to all scenarios except for the curtain length. Various parameters, including temperature, visibility, velocity, heat flux and mass flow rate were calculated at different cross sections of the entry.

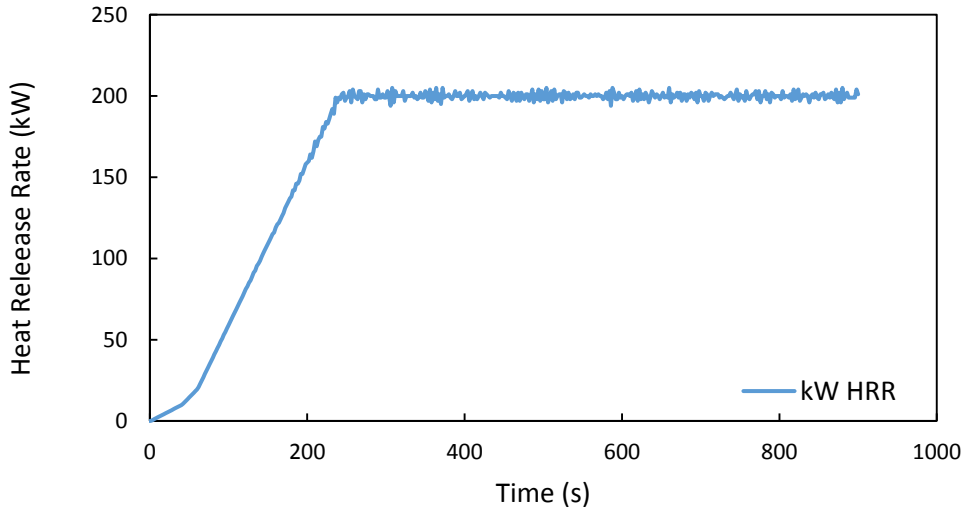

Figure 4.3. Heat release rate over simulation time

4.5.1. Temperature/Visibility for All Scenarios at Different Sections of the Entry

The temperature and visibility along the height of the entry at different locations and the mass flow rate in all five scenarios were investigated for two main reasons: (1) for use in the interface height calculation, and (2) to understand the progression of smoke into the upwind side of the fire source. This approach allows for the investigation of smoke layer depth, fresh air height and interface height in fire incidents in underground mines. This work is expected to contribute to future research that examines increased speed for such simulations and translation to the field for practical training of mine fire fighters.

The location of the slice file, average temperature and average visibility along the height of the entry from the mine floor to the roof at different heights at x = 20.8 m (68 ft), which is 2.5 m (8 ft) from the fire source center, and 900 s in scenario 1 are shown in Figures 4.4 and 4.5. Each point on the temperature and visibility line graphs represents the average temperature and visibility from the left rib to the right rib at the indicated height at 900 s. The interface height was calculated using Eqs. (1), (2) and (3) at each cross section of the entry in FDS. The height of fresh air was determined from the average temperature and visibility at different heights.

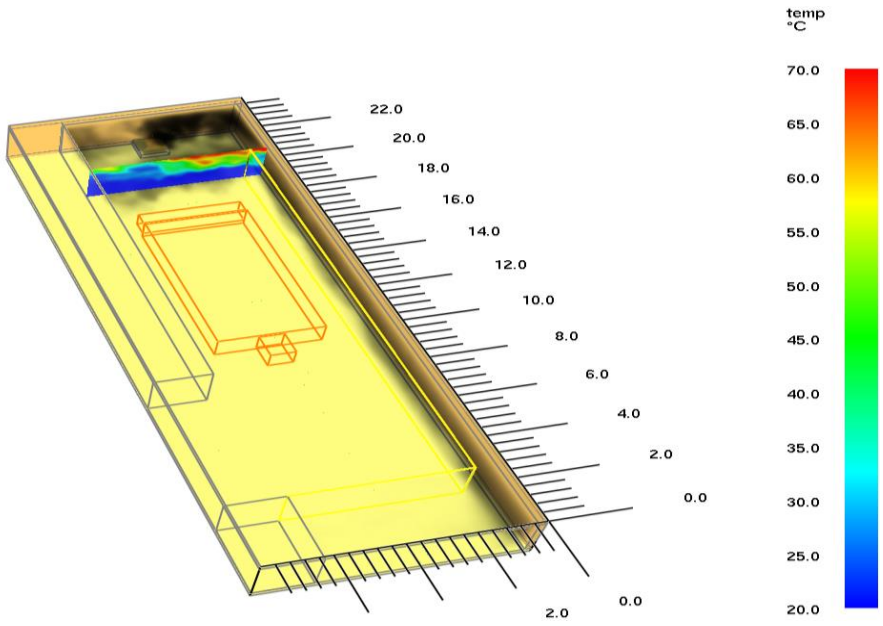

Figure 4.4. Temperature slice file at t=900 seconds and x=20.8 m, shown in isometric view

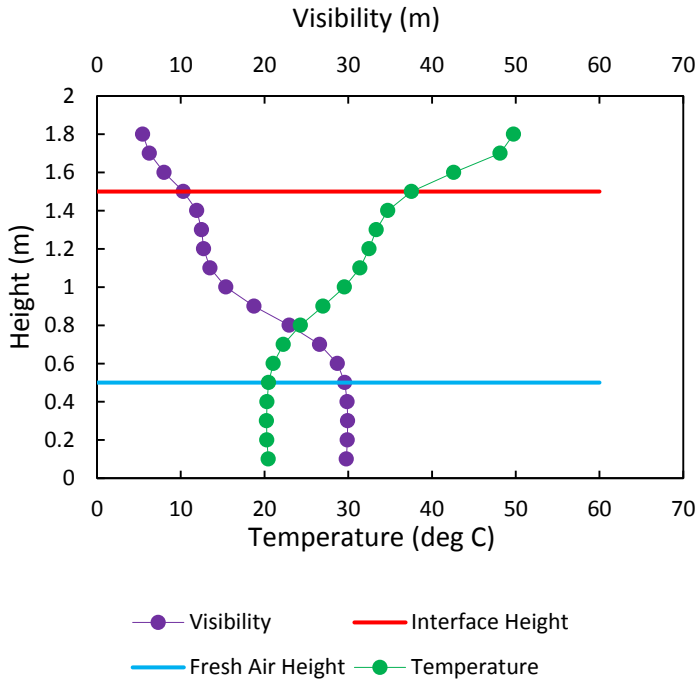

Figure 4.5. Average temperature and visibility at a cross section of the entry (normal to long axis), located at x=20.8 m, 900 s after the fire starts for scenario 1

It is evident from Figure 4.5 that the height of fresh air and interface height are about 0.5 m (1.6 ft) and 1.5 m (5 ft), respectively. The height of fresh air and interface height increased further outby the fire while the average temperature decreased considerably. The height of fresh air 4.5 m (15 ft) away from the fire source was 1.2 m (4 ft). It is noteworthy that smoke progressed into the continuous miner face by about 2.5 m (8 ft) from the mouth of the curtain, and beyond that distance the inlet was free from any smoke. The intact curtain works well in this case to control temperature and movement of smoke.

The movement of smoke outby the fire source increased in scenario 2, as shown in Figure 4.6b. According to the visibility and temperature data, the smoke reached to the floor at x = 20.8 m (68 ft), 2.5 m (8 ft) from the fire source center, while the fresh air height in scenario 1 was 0.5 m (1.6 ft). Moreover, the interface height at x = 20.8 m (68 ft) decreased to 1 m (3.3 ft). Also, the average temperature of the upper and lower layers increased dramatically. Because of shorter curtain, the smoke accumulation increased at x = 20.8 m (68 ft) in comparison with the smoke concentration at x = 20.8 m (68 ft) in scenario 1.

In scenario 2, smoke moved into the entry in the continuous miner area about 3.4 m (11 ft) outby the mouth of the curtain, as shown in Figure 4.6b. The entry was clear 9 m (30 ft) from the fire source.

Smoke behavior was similar at the continuous miner area in scenarios 3, 4 and 5. With the full removal of the curtain in the continuous miner area, the smoke accumulated through the entire depth of the continuous miner area and flowed out of the entrance to the continuous miner area, and the ventilation completely bypassed the region. After five minutes, the entire continuous miner area filled with smoke, and explosive gases such as methane can be expected to build up, though these gases have not been explicitly modeled yet and are dependent upon seam gas content, pressure and permeability, which are not considered here. In scenario 3, smoke progress against the upwind direction from the mouth of the curtain was about 5.5 m (18 ft).

The progress of smoke into the continuous miner area of the entry for all scenarios is shown in Figures 4.6a-4.6e. By briefly examining the smoke movement in all scenarios, it is evident that the smoke progress from the mouth of the curtain increased when the curtain length decreased, as expected. The smoke movement against the upwind from the mouth of the curtain in scenarios 1, 2 and 3 was 2.5 m (8 ft), 3.4 m (11 ft) and 5.5 m (18 ft), respectively. In scenarios 4 and 5, it was assumed that that the curtain was completely dislodged. The progress of smoke was tracked through monitoring of the CO concentration, soot concentration, temperature and visibility at different heights along the working face in all scenarios.

(a)

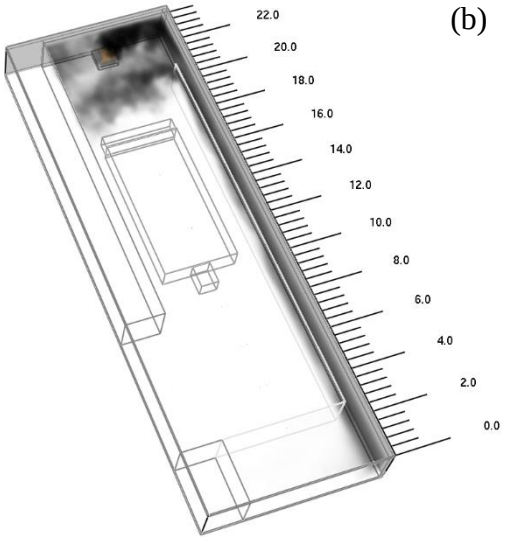

(b)

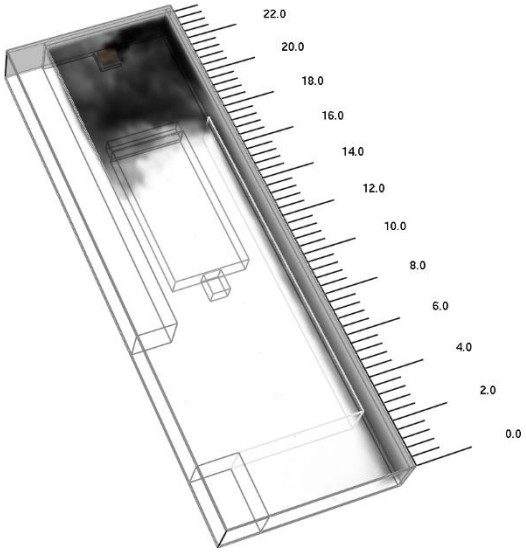

(c)

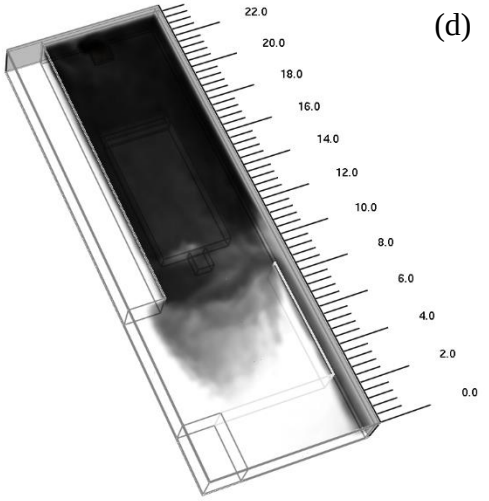

(d)

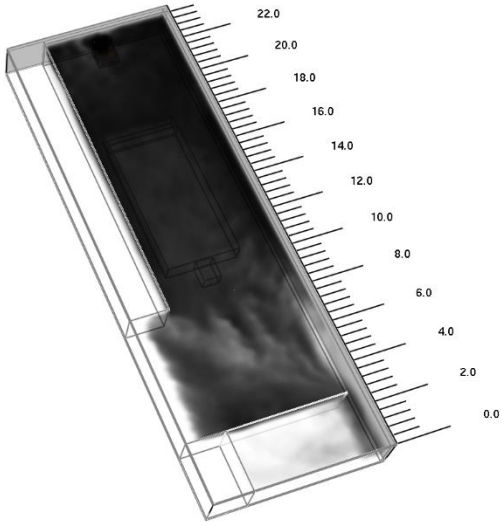

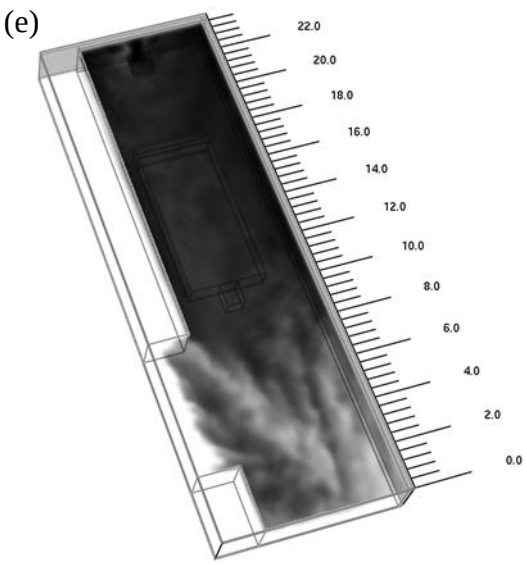

Figure 4.6. Smoke progress to the inlet in all scenarios (a) scenario 1, (b) scenario 2, (c) scenario 3, (d) scenario 4, (e) scenario 5

The average mass flow rates at the inlet and outlet were 7.88 kg/s and 7.90 kg/s. Consistent with the data displayed in Figure 4.7, it is evident that some air reaches the fire source, in spite of limited auxiliary ventilation.

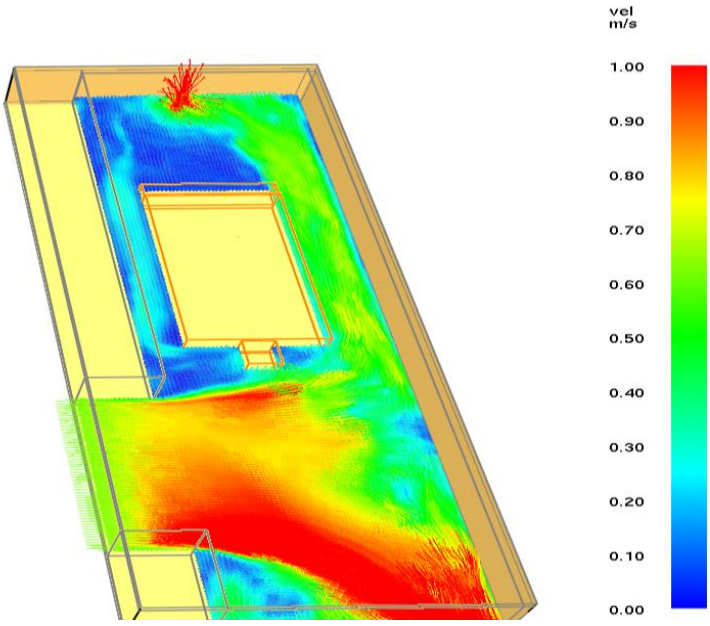

Figure 4.7. Velocity vector slice at z=0.6 m in scenario 5

The average mass flow rate of air into the continuous miner area of the entry was 0.53 kg/s at x = 8.8 m (29 ft). This study shows that 6.7 percent of the inlet mass flow of air moved to the fire source and the rest moved directly to the outlet in scenario 5, because the curtain was completely removed.

4.5.2. Interface Height and Fresh Air Height Analysis

The average interface heights along the X axis at different parts of entry for all scenarios are shown in Figure 4.8.

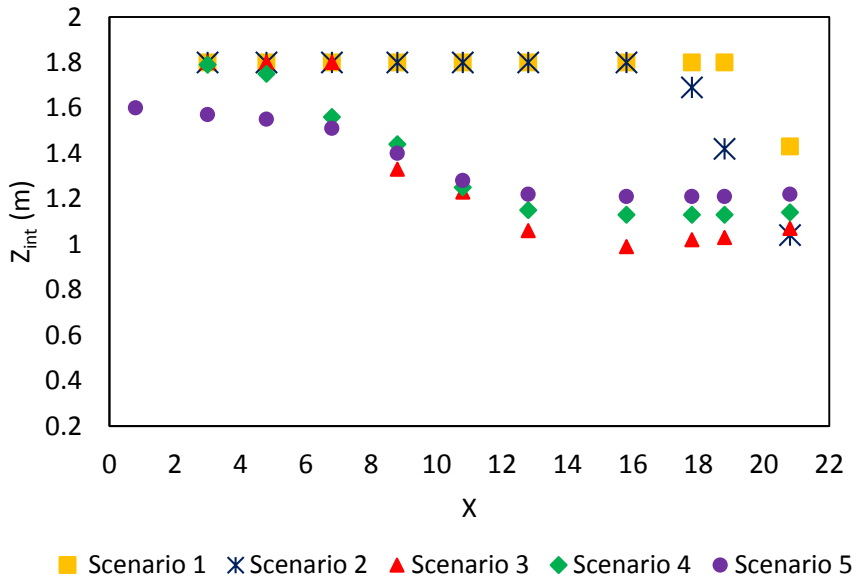

Figure 4.8. Average interface height along X axis for all scenarios

From Figure 4.8, it is evident that the interface height at x = 20.8 m (68 ft), 2.5 m (8 ft) from the fire source center, was 1.43 m (4.7 ft) in scenario 1, and the interface height decreased to 1.1 m (3.6 ft) in scenarios 2 and 3 at that section. The interface height in scenario 1 increased to 1.8 m (6 ft) at x = 18.8 m (62 ft), 4.5 m (15 ft from the fire source center, but the fresh air height at that section was 1.2 m (4 ft) (Figure 4.9).

In scenario 2, the interface height increased to 1.8 m (total entry height) at x = 15.8 m (52 ft), 7.5 m (25 ft) from the fire, while the fresh air height was 1.4 m (5 ft). In this scenario, the smoke moved outby to x = 14.4 m (47 ft), about 9 m (30 ft) from the fire

source, as shown in Figure 4.6b. It is noteworthy that the smoke progressed into the entry by about 3.4 m (11 ft) from the mouth of the ventilation curtain in scenario 2 while this length was 2.5 m (8 ft) in scenario 1.

According to the data of Figure 4.8, the interface height increased to 1.8 m (6 ft) at x = 6.8 m (22 ft) in scenario 3, while the average fresh air height was 1.2 m (4 ft) at that section. The average fresh air height reached the entry ceiling height (1.8 m or 6 ft) at x = 3 m (9.8 ft), as shown in Figure 4.9.

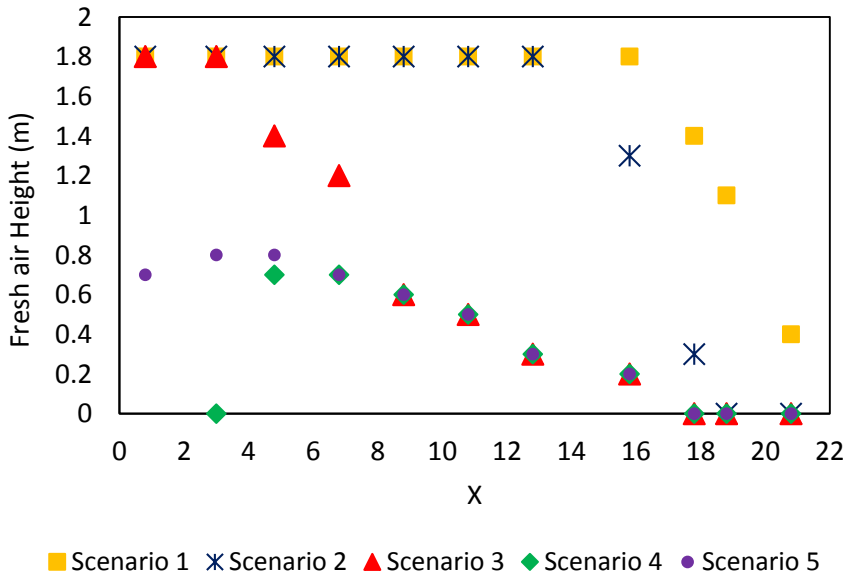

Figure 4.9. Average fresh air height along X axis for all scenarios

It is evident from Figures 4.8 and 4.9 that the average fresh air height is always less than or equal to the interface height. The average fresh air height and interface height along the X axis in scenarios 4 and 5 are shown in Figure 4.10.

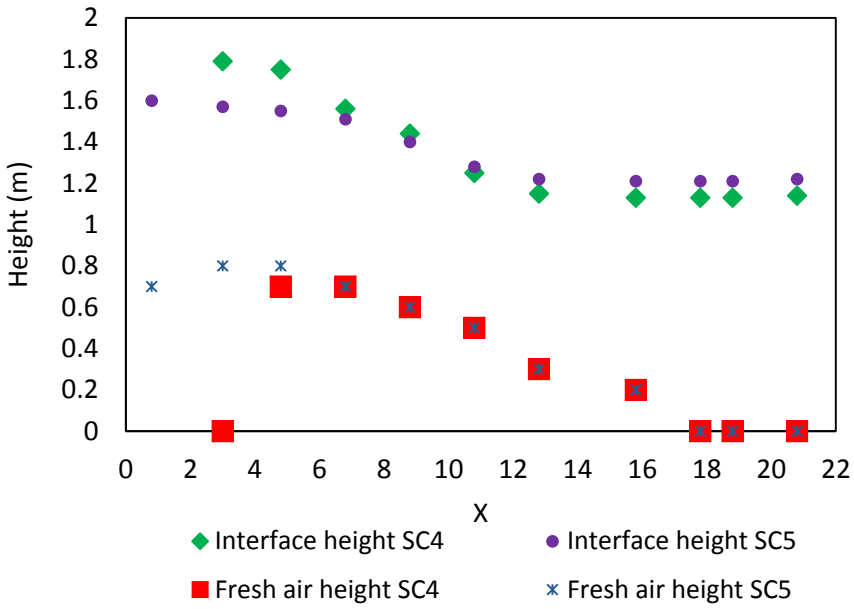

Figure 4.10. Average interface and fresh air height at different sections of the entry in scenarios 4 and 5

In scenarios 1 through 3, the fresh air height increased directly with distance from the fire source (Figure 4.9). However, in scenario 4, the fresh air height at x = 2.8 m decreased dramatically to zero. The absence of a ventilation curtain parallel to the long axis of the entry in this scenario caused smoke to accumulate just adjacent to the crosscut (Figure 4.11). The average interface height was almost the same in scenarios 4 and 5. In these two scenarios the fresh air height never intersected the interface height (Figure 4.10). In scenarios 4 and 5, the smoke progressed into the crosscut by about 1.5 m (5 ft).

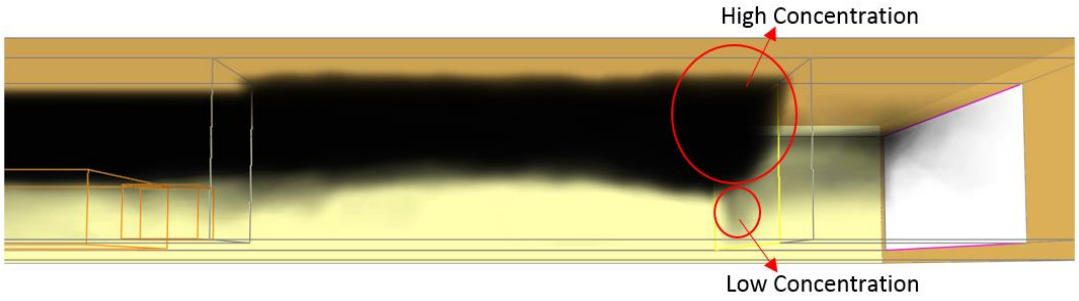

Figure 4.11. The smoke accumulation in front of curtain A. Side view, facing line curtain, the end of the continuous miner is seen to the left

This study demonstrates that curtain length plays an important role in the temperature and height of layers near a fire source and also the amount of smoke movement to the upwind side of continuous miner entry.

The smoke movement in the outby direction in the continuous miner area of entry increased as ventilation curtain damage increased. The smoke movements against the ventilation from the mouth of the curtain in scenarios 1, 2 and 3 were 2.5 m (8 ft), 3.4 m (11 ft) and 5.5 m (18 ft), respectively. In scenarios 4 and 5, it was assumed that curtain B was completely dislodged. The fresh air height and interface height increased when the distance from the fire source increased.

The height of the interface between the hot, smoke-laden upper layer and the cooler lower layer close to the fire source decreased when the curtain was dislodged partially or fully in the continuous miner area. The interface height, 4.5 m (15 ft) from the center of the fire source, moved closer to the floor by about 50 cm (1.6 ft) in scenario 2 compared with the scenario 1 interface height. With the full removal of the curtain, the smoke accumulated through the entire depth of the continuous miner area and flowed out of the entrance to the continuous miner area, and the ventilation bypassed the region.

4.6. Conclusion

The smoke propagation in an entry is dependent on different parameters, such as the location of the fire, the physical size and intensity of fire, air velocity and direction. This study examined a 200-kW fire at an active face with varying degrees of assumed damage to an exhausting ventilation curtain. In examining interface height and simulations of visibility throughout the entry, it is clear that as damage to the ventilation curtain approaches the last open crosscut it will become increasingly difficult for miners to approach the fire in order to observe conditions or fight the fire, due to limited visibility and high temperature.

These simulations are based on the geometry and ventilation of a partner mine in the United States and can be used to assess and plan for response in the event of an ignition, followed by fire on the face. The five simulations presented underscore the importance of

maintaining or immediately reestablishing face ventilation immediately after damage in order to maintain visibility and keep smoke moving to the return. The maintenance or reestablishment of ventilation allows personnel to approach the fire in order to extinguish it or observe involvement for emergency response. More broadly, these simulations can be used to train crews in firefighting approach, to assess and manage fire risk, and to develop global emergency response scenarios.

4.7. Future Work

This study examined ventilation curtain length with fixed physical fire size and HRR, two parameters which also play key roles in determining the interface height. Hence, a future study will be conducted varying HRR and physical fire size to determine the influence of these parameters on outby conditions. It is also important to characterize the concentration and temperature of smoke in upper or lower layers for tenability investigations. The following parameters can be recognized as parameters for tenability analysis: interface height, temperature, radiation, visibility, and species concentration, including carbon monoxide, carbon dioxide and oxygen.

We also acknowledge that the modeling presented here is computationally expensive in terms of time and processing capabilities. These models will serve as base models for comparison with faster modeling techniques that could be utilized in real time in an emergency scenario or, more practically, for risk assessment and emergency planning at mine operations. Fire modeling has a critical role to play in planning for emergency response, preventing such events, reacting to fires, and forensic analysis, ultimately leading to safer mines.

4.8. Acknowledgements

This research was developed under Contract No. 200-2014-59669, awarded by the National Institute for Occupational Safety and Health (NIOSH). The findings and conclusions in this report are those of the authors and do not reflect the official policies of the Department of Health and Human Services; nor does mention of trade names, commercial practices, or organizations imply endorsement by the U.S. Government.

4.9. Bibliography

Baum, H. R., and McCaffrey, B. J., 1989, "Fire induced flow field-theory and experiment," *Fire Safety Science, Proceedings of the 2nd International Symposium, Hemisphere*, New York, pp. 129-48, https://doi.org/10.3801/iafss.fss.2-129.

Brani, D. M, and Black, W. Z., 1992, "Two-zone model for a single-room fire," *Fire Safety Journal*, Vol. 19, Nos. 2-3, pp. 189-216, https://doi.org/10.1016/0379- 7112(92)90033-9.

Enright, C., and Ferrier, R. L., 2015, *Mine Rescue Manual: a Comprehensive Guide for Mine Rescue Team Members*, Society for Mining, Metallurgy & Exploration Inc., Englewood, CO, eBook, ISBN: 978-0-87335-405-9.

Friel, G.F., Yuan, L., Edwards, J.C., and Franks, R.A., 2006, "Fire-generated smoke rollback through crosscut from return to intake – experimental and CFD study," *Proceedings of the 11th U.S./North American Mine Ventilation Symposium*, University Park, PA, June 5-7, 2006, J.M. Mutmansky and R.V. Ramani, eds., Taylor & Francis Group, London, U.K., pp. 483-489, https://doi.org/10.1201/9781439833391.ch68.

Hansen, R., and Ingason, H., 2013, "Heat release rate measurements of burning mining vehicles in an underground mine," *Fire Safety Journal*, Vol. 61, pp. 12-25, https://doi.org/10.1016/j.firesaf.2013.08.009.

Hansen, R., 2015, "Analysis of methodologies for calculating the heat release rates of mining vehicle fires in underground mines," *Fire Safety Journal*, Vol. 71, pp. 194-216, https://doi.org/10.1016/j.firesaf.2014.11.008.

He, Y., Fernando, A., and Luo, M., 1998, "Determination of interface height from measured parameter profile in enclosure fire experiment," *Fire Safety Journal*, Vol. 31, pp. 19-38, https://doi.org/10.1016/s0379-7112(97)00064-7.

Ingason, H., 2009, "Design fire curves for tunnels," *Fire Safety Journal*, Vol. 44, pp. 259-265, https://doi.org/10.1016/j.firesaf.2008.06.009.

Ingason, H., Li, Y. Z., and Lönnermark. A., 2014, *Entry Fire Dynamics*, eBook, ISBN 978-1-4939-2198-0.

Jones, W. W., Peacock, R. D., Forney G. P., Reneke, P. A., and Portier, R., 1993, "CFAST-the Consolidated Model of Fire Growth and Smoke Transport," NIST Technical Note

1299, Building and Fire Research Laboratory, National Institute of Standards and Technology, Gaithersburg, MD.

Kim, H. J., and Lilley, D. G., 2002, "Heat release rates of burning items in fires," *Journal of Propulsion and Power*, Vol. 18, No. 4, pp. 866-870, https://doi.org/10.2514/6.2000-722.

Luzik, S. J., 1993, "MSHA develops new fire-resistant check curtains," Federal Register, Vol. 59, No. 96, No: 94-12054, pp.102-104, http://arlweb.msha.gov/S&HINFO/TECHRPT/MINEWSTE/FIRESCC.pdf

McGrattan, K., Baum, H., and Rehm, H., 1998, "Large eddy simulation of smoke movement," *Fire Safety Journal*, Vol. 30, pp. 161-178, https://doi.org/10.1016/s0379-7112(97)00041-6.

McGrattan, K., Hostikka, S., McDermott, R., Floyd, J., Weinschenk, C., and Overholt, K., 2014, "Fire Dynamics Simulator User's Guide," NIST Special Publication 1019, 6th Edition, Fire Research Division Engineering Laboratory, Gaithersburg, MD, SVN repository revision: 20596.

Mine Safety and Health Administration (MSHA), 2016, "MSHA Data File Downloads," U.S. Department of Health and Human Services, National Institute for Occupational Safety and Health (NIOSH), Centers for Disease Control and Prevention, http://www.cdc.gov/niosh/mining/data/default.html.

National Fire Protection Association (NFPA), 2011, "NFPA® 502, Standard for Road Tunnels, Bridges, and Other Limited Access Highways, 2011 Edition," ISBN 978-161665095-7.

Singer, J. M., and Tye, R. P., 1979, "Thermal, Mechanical, and Physical Properties of Selected Bituminous Coals and Cokes," Bureau of Mines Report of Investigations 8364, U.S. Department of the Interior, Bureau of Mines, Washington, DC.

Tewarson, A., 1995, *SFPE Handbook of Fire Protection Engineering*, 2nd Edition, P. DiNenno, C. Beyler, R. Custer and W. Walton, eds., National Fire Protection Association, Section 3, Chap. 4.

Trevits, M. A., Yuan, L., Teacoach, K., Valoski, M. P., and Urosek, J. E., 2009, "Understanding mine fire disasters by determining the characteristics of deep-seated

fires," SME Annual Conference & Expo, Feb. 22-25, 2009, Denver, CO, Society for Mining, Metallurgy & Exploration Inc., Englewood, CO, preprint 09-150, 9 pp.

Yuan, L., and Lazzara, C. P., 2004, "The effects of ventilation and preborn time on water mist extinguishing of diesel fuel pool fires," *Journal of Fire Science*. Vol 22, pp. 379-404, https://doi.org/10.1177/0734904104042438.

Yuan, L., Mainiero, R. J., Rowland, J. H., Thomas, R. A. T., and Smith, A. C. S., 2014, "Numerical and experimental study on flame spread over conveyor belts in a large-scale tunnel," *Journal of Loss Prevention in the Process Industries*, Vol. 30, July 2014, pp. 55-62, https://doi.org/10.1016/j.jlp.2014.05.001.

5. Tenability Analysis for Improvement of Firefighters' Performance in a Methane Fire Event at a Coal Mine Working Face

The following paper was submitted to Journal of Safety Research. Ali Haghighat conducted the majority of the work and wrote the paper with editorial input from coauthor: Dr. Kray Luxbacher.

5.1. Abstract

Due to the high rate of methane ignitions at active working faces in underground coal mines, this location has been the focus of many researchers, as well as safety initiatives. Multiple ignitions occur annually in US mines, and outcomes vary widely based on the magnitude of the ignition and the subsequent damage to ventilation controls or development of active fire. Depending on the magnitude of the explosion or fire, auxiliary ventilation controls, such as exhausting line curtain or tubing may be damaged or completely removed, affecting the ventilation into the area. Investigation of a typical dead end working face with exhausting ventilation was undertaken to explore firefighting conditions post ignition. Regular mining crews are trained in the fighting of mine fires, while mine rescue or fire brigade teams may also be utilized for firefighting depending upon the conditions. The research in this paper develops an approach to analyze the tenable limits in a fire event in an underground coal mine for bare-faced miners, mine rescue teams, and fire brigade teams in order to improve safety and training of personnel trained to fight fires. A detailed computational fluid dynamics (CFD) analysis was conducted to investigate temperature, visibility, radiation, and concentration of combustion products based on different damage assumptions following an ignition at the working face. The source of the combustion products analysis and the exposure effects were considered to assess the potential for harm to mine personnel, mine rescue teams, or fire brigades during a firefighting operation, taking into account their training and personal protective equipment during 5 and 15 minutes exposure. This study has shown that if the exhausting line curtain was destroyed, the situation would not be tenable for barefaced personnel. The findings were utilized to recommend the tenable limits for bare-faced miners, mine rescue team, and fire brigade teams during 15 minutes exposure to the methane fire at a coal mine

working face. The outcome of this research, applied to training, will result in the more efficient evacuation, as well as safe and effective firefighting under certain conditions.

5.2. Introduction

Tenability for fire situations has historically been considered for a number of occupied structures, to determine if conditions will allow for the escape of bare-faced occupants and if conditions are tenable for trained fire fighters to engage in firefighting or search and rescue. Tenability studies commonly consider heat effects, visibility, geometric considerations, air velocity, noise level, and toxicity during a limited time in a fire event [1-9].

Tenability has been less formally studied and defined for the case of fires in underground coal mines in the U.S. where atmospheric and regulatory considerations are substantially different than for typical surface structures. Additionally, while U.S. municipal or public emergency workers may respond to surface installations at u/g mines during an accident, they are not expected to enter a mine due to unique hazards in this environment. However, a systematic approach to tenability for personnel fighting underground coal mine fires could lead to improved safety and more efficient response. Generally, there are three groups of people that could be expected to respond to fires in underground coal mines: bare-faced mine personnel, fire brigade teams, and mine rescue teams. All underground coal miners in the US are trained in firefighting and operators are required to provide firefighting equipment including rock dust, fire hose and waterlines, and fire extinguishers, in addition to regulated automatic fire suppression systems at key locations [10]. Miners attempting to escape a mine with an active fire are encouraged to don self-contained self-rescuers (SCSRs) as soon as they suspect the atmosphere is compromised; however, most SCSRs commonly used in mines are not approved for firefighting. Therefore, for regular mine personnel, tenability for firefighting is considered for barefaced miners while tenability for escape would be considered for miners under standard escape SCSRs [11]. Fire brigade teams and mine rescue teams have similar equipment as surface fire fighters, including fire resistant clothing and rebreathers. Fire

brigade teams tend to have training that is more specialized for fire related emergencies while mine rescue teams are trained more broadly in mine emergency response.

Mine fire response varies tremendously and is complicated by the underground coal mine environment. Small fires are typically extinguished quickly by barefaced personnel. Large and involved fires would seem to call for immediate evacuation of barefaced personnel (and the donning of SCSRs); however, in the underground coal mine environment, the risk of a catastrophic methane-dust explosion during an escape is considerable, and the deployment of mine rescue teams and fire brigades can be time consuming. The decision to attempt an escape is difficult given that an explosive atmosphere could be developing and that escape routes can be several miles long. Crews must make such decisions within minutes of fire discovery. Further, while there is literature devoted to various measures that impact tenability [12], there are few examples that take a comprehensive approach to tenability. The literature that does exist is largely outside of the U.S. context and provides broad approaches without a methodology for determining tenability [13].

This work aims to investigate a scenario in which mine personnel are faced with a methane fed mine fire and a face ventilation system that is compromised to varying degrees, examining tenability for barefaced personnel and fire brigades or mine rescue team members approaching the fire. The determination of the refuge chamber location was not investigated in this study, although other researchers have considered factors such speed of travel for miners in limited visibility wearing SCSRs [14], as well as oxygen consumption under varying conditions [15] in investigating SCSR performance, optimal caching of SCSRs and where to provide refuge chambers.

Precise numerical analysis of fire scenarios can improve safety and decision making for all personnel faced with fire underground. In this study, five computational fluid dynamics (CFD) scenarios were simulated to analyze the tenability for personnel in a methane fire event in the working face of an underground coal continuous miner section. This work details preliminary investigation into the effects of different parameters such as heat and temperature, visibility, smoke layer depth, radiation and convection, and toxicity

on tenable limits were investigated thoroughly. For the purposes of this investigation, it is assumed that a face ignition has resulted in a face fire during mining production. The computational fluid dynamics software Fire Dynamics Simulator (FDS), Version 6.0 was utilized to predict the conditions that develop due to a 200 kW fire at the working face following a methane ignition with different levels of curtain damage. For a small ignition magnitude assumption, the ventilation curtain was not dislodged from its location so the curtain was 3 meters far from the face, approximately the distance prescribed by U.S. regulation (scenario 1). For increasingly powerful ignitions, it was assumed that the curtain was dislodged 6 m, 15 m, and 21 m, from the face in scenarios 2, 3, and 4 respectively. Finally, in scenario 5, the entire curtain was assumed to have been damaged. The tenability criteria were analyzed for 5 and 15 minutes exposure. The outcomes of this research were utilized to recommend the tenable limits for bare-face miners, fire brigade, and mine rescue teams in a 200 kW methane fire event at a working face. Ultimately, the developed methodology can be used for determination of tenable limits for bare-faced miners, mine rescue, and fire brigade teams under different fire events situations and conditions.

5.3. Computational Domain and Design Consideration

In this study, five different scenarios according to different assumed pre-ignition magnitudes were considered for tenability analysis in a methane fire event at a working face. This study is based on a previous study [16] with the same geometry examining smoke layer depth, fresh air height, and interface height in a fire incident under different fire scenarios. Due to the difficulty in measuring the fuel mass loss in a real case scenario, the simulated 200 kW methane fire at the working face was based on the flame height and physical size of the fire which it was reported in 2000 MSHA mine fire accident reports [17] and was explained elaborately in [16]. In this study, it was assumed that the ignited methane was on a coal surface that was 1 m long and 1 m wide. The airway and curtain were simulated according to the mine map as shown in Figure 5.1 (a), number 8 entry, with exhausting line curtain set to the right side. The width and height of the entries were 6 m and 1.8 m respectively. The length of the entry (continuous miner area) was set at 15 m. The schematic view and the dimension of the working face are shown in Figure 5.1. And

also the damage to the curtain can also be seen for each scenario in Figure 5.1 (b). Based on the standard practice in underground mines, the continuous miner (CM) was backed up to supported roof and de-energized as shown in Figure 5.1 (b).

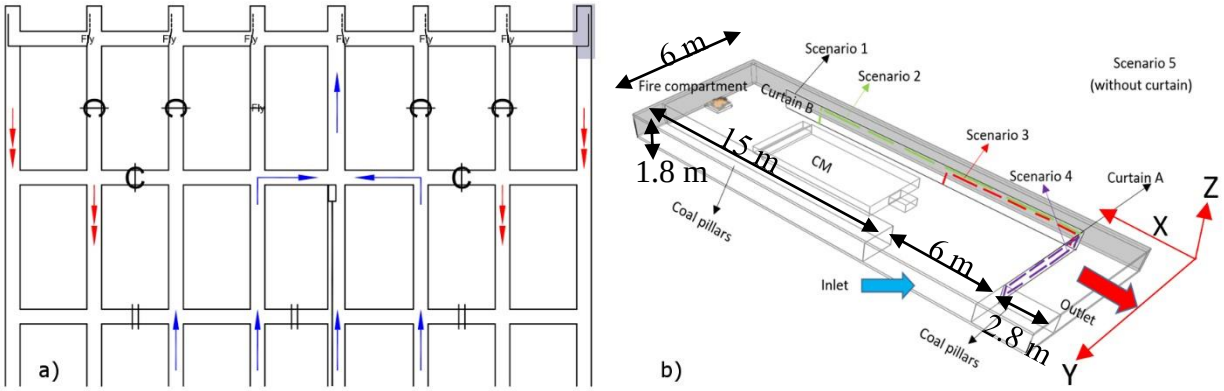

Figure 5.1. Selected working face with detailed specifications (a) schematic view of working faces with detail in shaded in the upper right, (b) The computational domain, dimensions, and the objects for all scenarios

The thickness of the coal on the wall assumed to be 0.2 m. The thermal and the physical characteristics of Pittsburgh bituminous coal [18], were considered for the characteristics of the walls in all simulations. The heat of combustion of the methane fire, and the thermal and the physical properties of the steel for the continuous miner (CM) were set according to the previous research study [16]. In some research studies, it was indicated that CO yield for methane fire can be increased by about a factor of 30 from $6xl0^{-3}$ (4-5 ppm concentration) to $1.5 \times l0^{-1}$ as the nitrogen flow is increased to the extinction limit (14.9% oxygen); therefore, 0.1 was considered as the CO yield [19-20]. The detailed characteristic of the exhausting line curtain [16, 21-22], was considered in the simulation of the scenarios 1 to 4. In scenario 5, the exhausting line curtain was removed from the computational domain.

The inlet volume flow rate was set at 6.61 m^3/s based on a partner mine volume flow rate in the United States. The T squared approach [23] with the 0.00347 kW/s^2 [24] as the fire growth coefficient was utilized for the growth of the methane fire at the face. During the first 4 minutes of the methane fire event, the HRR of the methane fire increased up to the maximum HRR (200 kW). Then, it remained constant until the end of the

simulation. The whole simulation time was set to 900 s. The no-slip boundary condition was considered for the walls and the objects in the domain. The initial and boundary conditions were the same in all scenarios except the curtain length. The grid size was set at 5 cm for the numerical analysis of the 200 kW methane fire [16] as it was recommended that the reliable numerical results in FDS can be achieved with the usage of the grid size less than equal to 0.1D* (≤ 0.1D*) [25-27]. All scenarios were simulated as shown in Figure 5.2 to demonstrate the effect of the intact and completely destroyed auxiliary ventilation system.

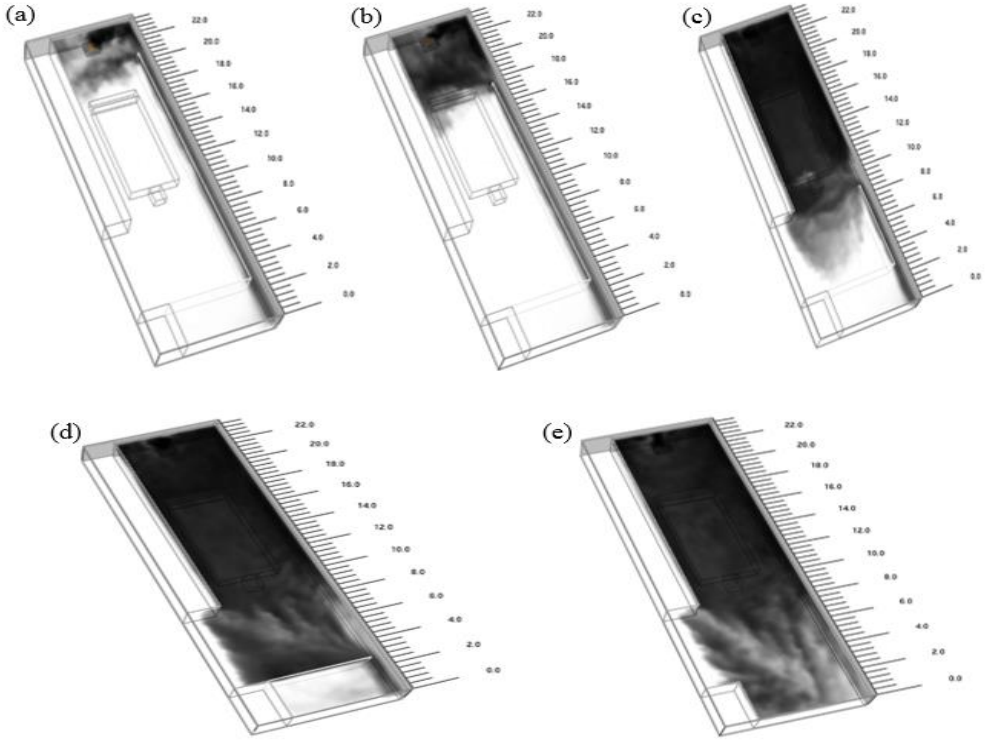

Figure 5.2. Isometric view of the smoke movement at t=900 s in all scenarios (a) scenario 1, (b) scenario 2, (c) scenario 3, (d) scenario 4, (e) scenario 5

5.4. Tenability and the U.S. Coal Mining Context

Safe escape for mining personnel is one of the most critical issues during a mine fire. It is important to note that approaching, fighting, and extinguishing a fire immediately can improve the safety since gassy coal mines can approach explosive limits, particularly when ventilation systems are negatively impacted. For both bare-faced personnel who are

well versed in firefighting techniques, and for mine rescue teams or fire brigade teams working under closed circuit oxygen, an improved understanding of tenability under various scenarios represents a significant advancement in training and potentially improved decision making during emergency response. A tenable environment is defined as an environment that supports human life for a specific period of time. The goal of tenability analysis in a fire event is to provide guidance for the safety of personnel who would consider approaching an underground fire in standard mining personal protective equipment (PPE) or more specialized firefighting PPE. Tenability criteria are often set at incapacitation for an average person. In this research study, more conservative criteria were utilized, since it was assumed that the fire fighters must travel out of the mine without assistance.

It is instructive first to describe the personnel who would be expected to fight fires as well as their standard PPE. US law requires that mine personnel are trained in firefighting, suitable firefighting materials are available, and fire and evacuation drills are regularly held [10]. Mine personnel performing their regular jobs are expected to have SCSRs, hard hats, safety glasses, boots with metatarsal protection, hearing protection, lights, and gloves; select personnel will also have a hand held gas detectors (oxygen [O_2], methane [CH_4], and carbon monoxide [CO]). Further, every mine shall have available a group of miners specifically trained in mine rescue and firefighting [10]. These teams must be able to deploy to the mine site within one hour [11] and would be likely to have self-contained breathing apparatus (SCBA) appropriate for fire, light duty fire resistant clothing and heavy duty turnout gear, as well as access to ventilation materials and firefighting materials. Their training in search and rescue and firefighting is more extensive than that of other mine personnel.

Personnel who intend to escape a mine emergency will typically don an SCSR if they suspect the mine atmosphere is compromised, and proceed to secondary or primary escapeways where they have the benefit of powered vehicles or life lines to assist in escape. Additionally, they have access to refuge chambers and SCSR caches. This work only examines (i) barefaced mine personnel approaching a newly discovered fire; and (ii) mine

rescue or fire brigade personnel under oxygen (i.e., SCBA) approaching a fire. Surface firefighting and rescue personnel (e.g., municipal or private) are usually available only for transport and treatment of victims as they are brought out of a U.S. mine, because hazards associated with fire in underground mines are particularly specialized.

In this study, five main parameters were considered to investigate tenability for barefaced miners, fire brigade, and mine rescue teams: visibility, temperature, smoke layer depth, radiation, and toxicity. These parameters have been extensively utilized for analysis of the tenable limits in the road tunnels [1]. In addition, it was assumed that the main mine ventilation system operates continuously [10]. The concentration of toxic species effects (e.g., CO, CO_2) for the fire brigade and mine rescue teams were not considered for tenability analysis since the team members carry self-contained breathing apparatus (SCBA). They are designed to provide oxygen for at least 4 hours and are appropriate for firefighting. For barefaced mine personnel, the toxicity of CO and CO_2 are considered, as well as O_2 deficiency. For both bare-faced teams and teams under oxygen, explosibility should be considered in comprehensive tenability analysis. If personnel observe or expect combustion the advance of people into an explosive atmosphere (e.g., 5-15% methane in the presence of standard oxygen) is not tenable because the risk of fatal injury is immediate and imminent. However, in this preliminary study, emissions of methane from the coal strata were not incorporated, so we did not consider explosibility.

5.4.1. Temperature and Heat Effects

Radiation from hot gases and areas and convection from hot gases are two main sources of heat exposure for mine personnel during firefighting in underground coal mines. It is noteworthy that the percentage of water vapor in the combustion products plays a key role on burning of the respiratory systems. The inhalation of the air, containing less than 10% water vapor, cannot influence on the burning of the respiratory system. Generally, the tenability limits for skin burns are lower than for burns to the respiratory tract. By inhalation of the saturated water vapor air with a temperature above 60°C (140°F), the respiratory tract thermal burns happen [1,2]. Tenability for temperature during a fire event depends on the dose of heat over a period of time. A longer exposure to a lower temperature

or heat flux is usually more tolerable than a short exposure to a high radiant heat flux or temperature [2]. In NFPA® 502, Equation (5-1) was recommended for calculation of time of exposure to a certain amount of temperature.

$$t_{exp} = (1.125 \text{ x } 10^7)\, T^{-3.4} \tag{5-1}$$

where t_{exp} is time of exposure to reach a FED of 0.3 in min; T is temperature (^oC). For the calculation of the maximum exposure time without incapacitation in equation (5-1), some crucial factors (ex: evacuees were lightly clothed, zero radiant heat flux, the constant exposure temperature, and the FED is less than or equal to 0.3 (≤ 0.3)) were considered [2].

The tenability limit for the exposure of skin to radiant heat is approximately 2.5 kW/m^2 [28]. It is likely that people can tolerate exposure at this level for 30 minutes or longer [1]. Our simulation also considers convected heat from hot gases which are the dominant source of heat transfer during a fire incident in underground coal mines. Pain and skin burns can occur at air temperatures above 120^O C [2]. The rate of heat transfer from hot air to the skin via convention depends on different parameters including the rate of ventilation, humidity, air temperature, and clothing [29-30].

5.4.2. Visibility

Smoke can limit visibility to the degree that it is difficult for personnel to approach a fire, and if they do approach, it may still be nearly impossible to assess the magnitude and involvement [16]. An atmosphere will usually reach the tenability limits for visibility well before the limits for gas concentrations, temperature, and radiation [31].

Visibility and the processes affecting it are crucial not only for the safety of self-evacuation of people in the mine, but also for fire brigade and mine rescue teams since the infrared cameras are not utilized in rescue missions in underground mines. Visibility has an immense impact on walking speed during evacuation period or fighting the fire. Jin and Yamada proposed a relationship between the visibility and walking speed [32]. Frantzich and Nilsson proposed an equation (Equation (5-2)) for calculation of walking speed.

$$u_w = -0.1423.C_s + 1.177 \quad (5\text{-}2)$$

where C_s and u_w are extinction coefficient and walking speed respectively. If visibility (V_s) is used as the independent parameter, Equation (5-3) can be utilized for calculation of walking speed [31].

$$u_w = 0.5678.V_s + 0.3033 \quad (5\text{-}3)$$

Numerous experiments have been carried out by different scientists on the determination of walking speed during fire incidents. However, based on the Swedish building code, the basic unhindered walking speed was recommended at 1.5 m/s. For children or people with disabilities, the walking speed was recommended to be set to 0.7 m/s [31].

Consistent with the data of several different experiments which were plotted in tunnel fire dynamics book in terms of walking speed as a function of visibility, it was concluded that the walking speed range was changed from 0.2 m/s to 1.5 m/s when the visibility was in the range of zero to 10 m [33-35]. Therefore, in this study, the mean velocity (0.85 m/s) was selected as the walking speed for evacuation time calculation and speed. However, it is noteworthy that the walking speed could be changed for injured evacuees, elder mine personnel, or on the other hand for mine rescue, fire brigade teams. In addition, the evacuation path, the slope of the airways, and the mine height can influence the travel speed. Hence a comprehensive experiment is needed for precise calculation of walking speed in underground mines. However, based on previous study on the travel speed of the miners in heavy smoke situation, it was evident that the average travel speed was 0.4 m/s which the average travel speed increased to 0.97 m/s in clean air situation [36].

FDS utilizes an approach to calculate visibility at an arbitrary 30 m distance based on the soot yield of combustible materials [37]. For purposes of this work tenable visibility limits were set to 10 m; however, this is one of the most subjective criteria, and depending on circumstances firefighters may proceed in more limited visibility.

5.4.3. Toxicity

In this study, the O_2 deficiency and the effects of CO and CO_2 for barefaced personnel were considered to investigate the toxicity in order to recommend the tenable limits during a methane fire event in an underground coal mine. Carbon monoxide decreases the possibilities for the blood to take up, carry and deliver oxygen to the tissues, and combines with the hemoglobin in the blood to form carboxyhemoglobin (COHb) [3]. CO produces negative health effects including neurological effects, such as cognitive impairment, dizziness, and unconsciousness [38], and can be fatal at high concentrations. The detrimental effects of different levels of COHb on human health are summarized in [39, 40].

Carbon dioxide affects the time to incapacitation in two different ways. At low concentrations, CO_2 acts as a stimulus, increasing the breathing rate, and influencing the uptake of other asphyxiant gases (e.g., CO), and, at concentrations greater than 5%, CO_2 can become an asphyxiate [31], with risk of unconsciousness within a few minutes when the concentration of CO_2 is above 7% [5]. In this study, all numerical calculation in terms of toxicity was carried out at Z= 1.5 m as the height for barefaced miners, as it expected they would make every effort to stay below the smoke layer.

5.4.4. Calculation of Exposure Levels and Tenability Criteria

When examining both heat and toxicity, the best indicator of exposure is dosage over time. Additionally, the stimulus effect of CO_2 can increase uptake of CO, so the additive and multiplicative effects of these gases should be considered. Fractional Effective Dose (FED) is an indicator of dosage and can be calculated for exposure to heat or gaseous species. Fractional Effective Dose is calculated based on a 15 minute exposure time, following the method proposed by Purser [4], and displayed in Equation (5-4):

$$FED_{tot} = (FED_{CO} + FED_{CN} + FED_{NOx} + FLD_{irr}) \times HV_{CO2} + FED_{O2} \quad (5\text{-}4)$$

For this study, only CO_2, O_2, and CO were considered. Given the relatively short simulation time, standard oxygen was maintained, so oxygen deficiency was not considered, and the equation is simplified to Equation (5-5):

$$FED_{tot} = (FED_{CO}) \times HV_{CO2} + FED_{O2} \quad (5\text{-}5)$$

In equation (5-5), FED_{CO}, HV_{CO2}, and FED_{O2} can be calculated according to Equations (5-6), (5-7), and (5-8) [4].

$$FED_{CO} = \int_0^t \frac{C_i}{(C.t)_i} dt = \int_0^t 2.764\ x\ 10^{-5}\ (C_{CO}(t))^{1.036}\ dt \quad (5\text{-}6)$$

$$HV_{CO2} = \frac{exp\ (0.1903 C_{CO2}(t) + 2.0004)}{7.1} \quad (5\text{-}7)$$

$$FED_{O2} = \int_0^t \frac{dt}{exp\ [8.13 - 0.54(20.9 - C_{O2}(t))]} \quad (5\text{-}8)$$

where t is time in minutes and C_{O2}, C_{CO2} are the O_2 and CO_2 concentration in percent. C_{CO} is the CO concentration in ppm. The HV_{CO2} is defined as the hyperventilation factor induced by carbon dioxide [4].

While it is clear that FED gives a more comprehensive measure of health effects, providing better tenability criteria, it is not practical to calculate dosage in real time for miners in active fire scenarios. Table 5.1 summarizes criteria proposed by various groups and includes Short Term Exposure Limits (STEL), based on a 15-minute dose, as well as Ceiling (C) limits which should not be exceeded. These data are used to inform the proposed tenability criteria.

Table 5.1. Criteria for exposure to various products and effects of fire

Note: STEL is Short Term Exposure Limit (15 minute dose) and C is ceiling limit.

Standard	CO (ppm)	CO2 (%)	O2 (%)	Heat	Temperature
ACGIH	25 TWA	3.0 STEL	19.5	--	--
NIOSH	200 C	3.0 STEL	19.5	--	--
OSHA	50 TWA	3.0 STEL	19.5	--	--
MSHA (coal)	400 STEL	3.0 STEL	19.5	--	--
MSHA (M/NM)	400 STEL	1.5 STEL	19.5	--	--
NFPA 502	450 STEL		19.5	2.5	60

(MSHA, 2016; NFPA, 2011; OSHA, 2016.)

5.5. Results and Discussion

5.5.1. Smoke Layer Depth, Temperature, and Visibility Results

The fire smoke level is the main factor for a safe escape. Because it can influence visibility and increase risk of incapacitation. The interface height [41, 42] and the fresh air height [16] were considered for investigation of smoke layer depth at different parts of the continuous miner area.

The mean temperature and the mean visibility, the mean interface height, and the mean fresh air height along the height of the entry at the different cross section for scenarios 1 to 5 were calculated. The mean interface height and fresh air height along the X axis at t=900 s at different parts of the entry for all scenarios are shown in Figure 5.3.

Based on the simulation results, it was evident that as ventilation curtain damage increased, the smoke movement in the outby direction in the continuous miner area of entry increased. In addition, by getting further from the fire source, the fresh air height and interface height increased. The upstream smoke movement from the mouth of the exhausting line curtain in scenarios 1, 2 and 3 were 2.5 m, 3.4 m, and 5.5 m respectively. In spite of limited auxiliary ventilation in scenarios 4 and 5, some air reaches the fire source. However, in general, the smoke accumulated through the entire depth of the continuous miner area. It is noteworthy that the thickness of the hot, smoke-laden layer close to the fire source increased when the curtain was dislodged partially or fully in the continuous miner area as shown in Figure 5.3. All in all, we refer the readers to [16] for detailed interface height and fresh air height study based on different levels of damage to an exhausting line curtain in continuous miner area. The average temperature for different layers along the height of tunnel was calculated as shown in Figure 5.4 to analyze the tenability criteria for bare faced miners, mine rescue teams, and fire brigade teams. The average temperature for two different layers at both sides of the interface height along the x axis are illustrated in Figure 5.4.

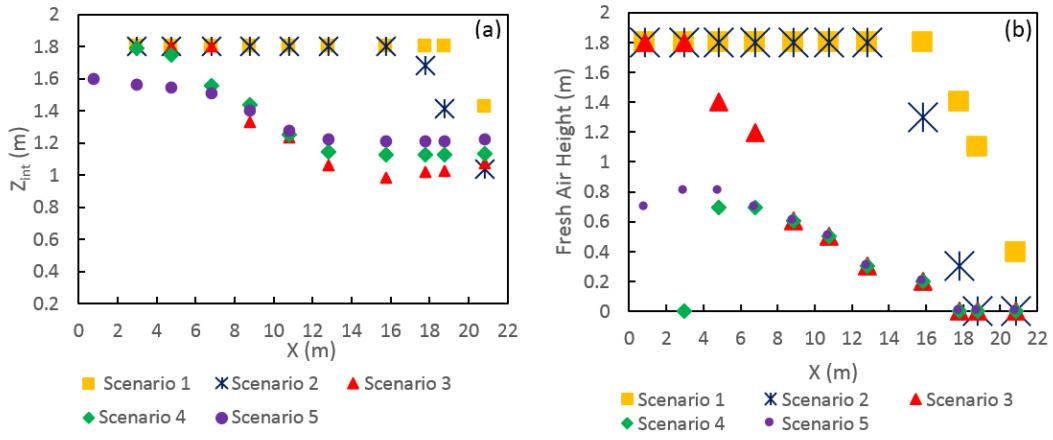

Figure 5.3. Average height of different layers along the x axis at 900 s (a) Average interface height (b) Average fresh air height

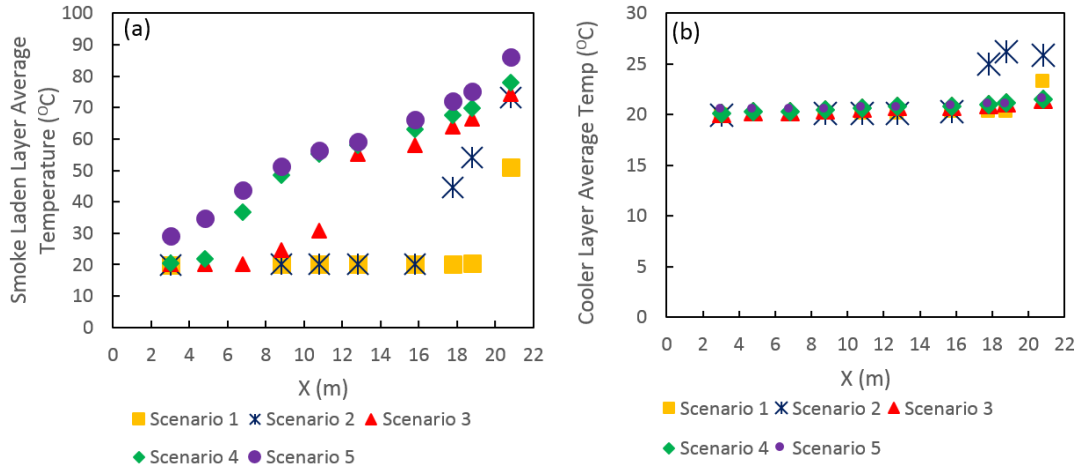

Figure 5.4. Average temperature of different layers along the x axis at 900 s (a) smoke-laden layer temperature (b) cooler layer temperature

The average cooler layer height is the average temperature of the layer from floor to the interface height (Figure 5.4 (b)), and the average temperature of the smoke-laden layer is the average temperature of the layer from interface height to the ceiling. In Figure 5.4 (a), it is evident that average temperature of the smoke-laden layer is close to that of the cooler lower layer temperature (20°C) for scenarios 1 to 4 at 4.5 m, 7.5 m, 16.5 m, and 20.3 m from the fire source. In addition, the average temperatures of the cool layer close to the fire source for scenarios 1 and 2 were only slightly higher when compared to

scenarios 3, 4, and 5. Moreover, it was evident that by getting further from the fire source the smoke-laden layer temperature decreased. According to Figure 5.4 (a), by decreasing the exhausting line curtain by about 3 m, the average temperature increased by about 23 ^{O}C at X= 20.8 m. The average temperature of the smoke-laden layer in the continuous miner area for scenarios 3, 4, and 5 were calculated almost the same as shown in Figure 5.4 (a). This study has shown that the length of the curtain played a key role in the average temperature of the smoke-laden layer close to the fire source.

For the calculation of the visibility along the height of the tunnel at different cross section, the height of 1.5 m was considered since it was assumed that the bare faced miners, mine rescue and fire brigade teams would try to stay below the smoke layer. The mean visibility at the height of 1.5 m at different cross sections of the tunnel in scenario 1 through 5 was calculated as shown in .Figure 5.5 (a). Consistent with the data of Figure 5.5 (a), it was evident that the mean visibility at different parts of the continuous miner area at z = 1.5 m was less than 10 m in scenarios 3, 4, and 5. However, the mean visibility was more than 10 m in scenarios 1 and 2, when we get further from the fire source by about 4.5 m and 7.5 m respectively. In addition, a location (4.5 m away from the fire) was considered to investigate the mean visibility along the height of the tunnel at selected cross section as shown in Figure 5.5 (b). The criterion for the selection of the location was based on the distance that both the barefaced personnel and mine rescue teams or fire brigades would approach. Each point on the visibility line graph (Figure 5.5 (b)) represents the average visibility from the left rib to the right rib at X= 18.8 m (4.5 m away from the fire source) at the indicated height at 900 s for all scenarios. According to Figure 5.5 (b), the 10 m visibility at that cross section was achieved at height of 1.8 m, 1.1 m, 1.1 m, 0.7 m, 0.9 m, and 1.1 m in scenarios 1, 2, 3, 4, ad 5 respectively. Overall, the study of the mean visibility has shown that the length of the exhausting line curtain has had an immense impact on the visibility at different cross sections. Moreover, the effect of the ventilation curtain length on the mean visibility at different height of the tunnel close to the fire source was consequential.

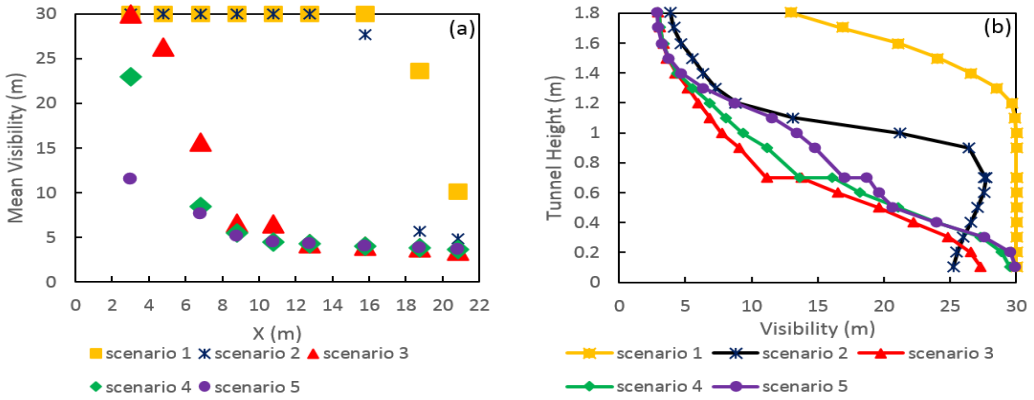

Figure 5.5. Mean visibility at 900 s (a) along the length of the tunnel at z= 1.5 m (b) along the height of the tunnel at x= 18.8

5.5.2. Toxicity Results

In this study, the concentration of CO, CO_2, and O_2 at different sections of a working face during 900 seconds of methane fire were calculated to investigate the toxicity rate at the working face of an underground coal mine. The average personnel height should be considered for investigation of toxicity at associated location. Therefore, a 1.5 m as the height for barefaced miners was selected, as it expected they would make every effort to stay below the smoke layer. The effect of the exhausting ventilation curtain length on an average mass fraction of CO and O_2 at 900 seconds at z=1.5 m are shown in Figures 5.6 (a) and (b) respectively. It is evident that the concentration of CO passed the TWA level while O_2 was maintained at more than 19.5% (TLV) at all locations. Furthermore, the exhausting ventilation curtain substantially impacted the decrease of the CO concentration around the continuous miner in scenarios 1 and 2. As can be seen in Figure 5.6 (a), the CO concentration decreased when the distance from the fire source increased. However, in scenario 4, the CO concentration increased at X=2.8 m, 20.5 m from the fire source to 147 ppm. The reason lies in the absence of a ventilation curtain parallel to the long axis of the entry in scenario 4 which it contributed to the accumulation of the smoke in just adjacent to the crosscut. Consistent with the data of CO_2 concentrations along the height of the tunnel at different cross sections, it was evident that the CO_2 concentrations in in scenarios 1 and 2 (scenarios with exhausting line curtain in continuous miner area) were less than the TWA level (0.5%) during 900 seconds while the concentration of CO_2 exceeded the

TWA level when the ventilation curtain was removed from the continuous miner area (scenarios 3, 4, and 5). The CO_2 concentration in scenarios 3, 4, and 4 were calculated by about 0.7% in continuous miner area at X=18.8 m.

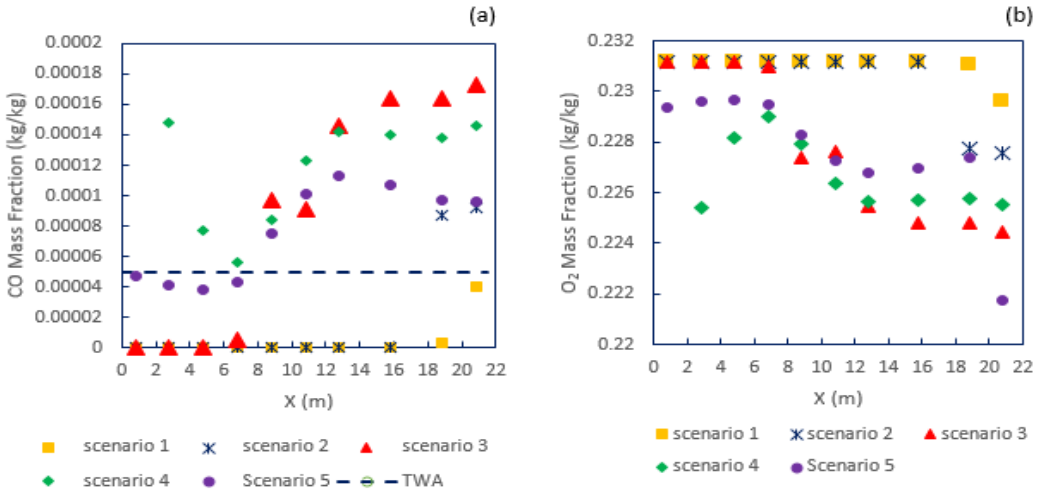

Figure 5.6. Average mass fraction, 4.5 m far away from the fire at z= 1.5 m, t =900 s (a) average CO mass fraction (b) average O_2 mass fraction

5.6. Preliminary Tenability Recommendations

Average values for toxicity, temperature, and heat were calculated during 5 different periods of time after the initiation of a methane fire at a coal mine working face in all scenarios. The least and the most damage to the curtain scenarios (scenario 1 and 5) results are shown in Table 5.2. We assume that both barefaced personnel and mine rescue teams or fire brigades would approach within 4.5 m of the fire, so this location was selected as the area for investigation of tenable limits for mine personnel, fire brigade, and mine rescue teams during firefighting. Next, 1.5 m was selected as the height for barefaced miners, as it expected they would make every effort to stay below the smoke layer. Therefore, results for the concentrations of gases, fractional incapacitating doses, temperature, and visibility are investigated at that height. The simulation results indicate that the smokeless sections for scenarios 1, and 2 are at about 6 m, and 9 m from the fire source. Moreover, the visibility is more than 10 m at those sections when there is curtain at the working face. Smoke behaved similarly at the continuous miner area in scenarios 3,

4, and 5. With the full removal of the ventilation curtain, the smoke accumulated through the entire depth of the entry and ventilation bypassed the region. After 4 minutes (when the HRR reached 200 kW), the whole CM area filled with smoke.

The proposed tenability criteria for barefaced firefighters and mine rescue or fire brigade teams, along with the data from scenarios 1 and 5, at 5 and 15 minutes are shown in Table 5.2. Tenability criteria were developed based on the various limits given in Tables 5.1 and 5.2. For barefaced miners approaching the fire the most conservative limits were utilized for several reasons. First, there is some uncertainty associated with the application of FED (equations 5-4 through 5-8) to individuals; and second, evacuation from a mine fire is complicated by long evacuation paths (on the order of miles) and the donning and changing of SCSRs. Miners experiencing CO intoxication can find their abilities to make critical decisions impaired, so a conservative ceiling value of 200 ppm for CO was utilized. There is speculation that impairment due to intoxication complicates evacuation and has contributed to fatal injuries in mine fires.

Table 5.2. Average concentration of toxic and physical hazards and fractional incapacitating dose for 15 min periods during methane fire at a coal mine working face with full curtain (scenario 1)

Time (min)	scenario 1		scenario 5		Proposed Tenability Criteria (15 min exposure)*	
	5	15	5	15	Bare-faced Mine Personnel	Mine Rescue/ Fire Brigade
CO Concentration (ppm)	0	0	**270**	**280**	200 ppm	<125000
CO_2 Concentration (%)	0.07	0.08	**0.7**	**0.7**	<0.5	--
O_2 Concentration (%)	23	23	22.1	22	>19.5	--
Fractional Effective Dose	--	0.0243	--	**1.447**	<1	--
Temperature at height 1.5 (^{O}C)	23.7	23.7	**90.5**	**95.3**	<60	<100
Visibility (m)	23.4	25.8	**1.3**	**1.3**	>10	>10
Interface Height (m)	1.8	1.8	1.18	1.12	--	--
Smoke-laden Layer Average Temp. (^{O}C)	20.2	20.5	**83**	**84**	<60	<100
Cool Layer Average Temp. (^{O}C)	20.2	20.5	21.1	21.4	<60	<100
Radiant Heat Flux (kW/m^2)	0.09	0.1	0.1	0.13	<2.5	<5.0

Note: simulation results that exceed proposed criteria for barefaced personnel are bold.

5.6.1. Tenability for Barefaced Miners

In scenario 5 incapacitation by heat was reached at 2 min 36 sec when the temperature of the smoke-laden layer exceeds 60°C (140°F). Furthermore, the time to the tenability limit of 10 m for visibility was reached by 1 min 16 sec. So, for scenario 5 it would not be tenable for barefaced mine personnel to approach and fight a 200 kW fire. Conservatively, the miners would be exposed to CO intoxication and they would certainly be exposed to unacceptable heat levels and compromised visibility. The FED is higher than 1 which also indicates untenable conditions for scenario 5. On the other hand, in scenario 1, various tenable limits, including FED, were not exceeded. Fire approach and firefighting under scenario 1, intact ventilation, is tenable for barefaced miners, at least up to 15 minutes. They also must assess the risk of explosion when deciding whether to fight a fire or evacuate, so evacuation is not without risk. In examining these scenarios for a fire of about 200 kW, it is clear that if the face ventilation has been destroyed (scenario 5) the situation is not tenable for barefaced personnel. First, they may be exposed to intoxicating levels of CO, and the subsequent disorientation could hamper later evacuation attempts. Next, the visibility is quite low, and the temperature near the fire is not tenable as it exceeds 60°C, and this personnel is not in turnout gear.

5.6.2. Tenability for Mine Rescue Teams and Fire Brigades

The previous section details tenability for barefaced miners in standard work clothes. Tenability is entirely different for mine rescue or fire brigade teams in the same situation. There is no tenability limit in terms of gas toxicity since the teams carry breathing apparatus (SCBAs). Teams must be cautious of explosive atmospheres, particularly explosive levels of CO and methane; the lower limits are 12.5% and 5%, respectively, in the presence of standard oxygen. Mine rescue teams and fire brigades do not typically carry infrared cameras but are prepared to work in lower visibility and often tether themselves together. Gas temperature and flame radiation were considered for investigation of tenable limits for rescue teams in underground mines, assuming that they are in standard fire turnout gear. Heat related tenability limits for fire fighters in turnout gear are reported as high as gas temperature $\leq$ 100°C (212°F), and radiation $\leq$ 5 kW/m^2 [43]; however, these are probably not tolerable in a full 15 minute dose.

The visibility limit of 10 m was reached at 1 min 16 sec and the visibility continued to decrease with time. Therefore, after 5 minutes, the rescue teams do not have enough visibility at a height of 1.5 m to fight the fire. Again, visibility is perhaps the most subjective tenability criteria, and near zero visibility is not uncommon during firefighting. This is a criterion that teams may consider on the ground, possibly proceeding under low visibility under certain circumstances. Visibility can be substantially improved if teams install ventilation as they approach the fire which is standard practice for teams traveling a mine during emergencies.

Ultimately, both scenarios are tenable with the exception of visibility for specially equipped mine rescue and fire brigade teams, at least up to 15 minutes. It is likely that such teams would be approaching the fire long after the 15 minute mark, and the simulation should be expanded to consider up to at least 1 hour.

5.7. Conclusion

Numerical fire simulation was utilized to investigate a specific set of scenarios in an active continuous miner face, ventilated by exhausting line curtain. Tenability criteria were researched and proposed for approaching a mine fire in an active coal mine face. This study illustrates that the status of ventilation controls has a substantial effect on tenability for personnel engaged in firefighting. This work applies to the training of mine personnel in responding to face fires: it is reasonable to miners that they can consider barefaced firefighting when ventilation controls are intact and they are actively monitoring the atmosphere, but evacuation or reventilation is necessary if ventilation controls are destroyed. This scenario is best left to mine rescue or fire brigade teams. These scenarios should be studied over a longer period of time than 15 minutes to further inform mine rescue and fire brigade approach.

Broadly, this study can inform further work in the ways miners are trained in firefighting, and be utilized to further develop tenability criteria for various personnel in underground coal mines. First, we recognize that mine personnel is extensively trained in firefighting and have access to firefighting equipment, so their preparation differs from that

of the average structure occupant on the surface. Fire simulation, in concert with reasonable tenability guidelines, can be used to train miners as to when approaching fire barefaced is appropriate and when evacuation is the best option. These simulations, applied to training will result in more efficient evacuations (e.g., the decision to leave can be made quickly and with less delay), as well as safe and effective firefighting under certain situations. Also, it is clear that while US regulation provides for firefighting training and equipment for all mine personnel, provision of basic firefighting PPE and a limited number of SCBAs could allow for immediate control of fires that could not otherwise be approached by barefaced personnel.

Finally, future work must account for explosibility by further examining combustion of methane and the effect of various strata emission levels. Additionally, tenability criteria should be further examined and formalized for various mine fire scenarios, as this approach can lead to more effective decision making for personnel faced with fire and supervisory personnel during emergencies, ultimately improving safety by mitigating fire early.

5.8. Acknowledgements

This research was developed under Contract No. 200-2014-59669, awarded by the National Institute for Occupational Safety and Health (NIOSH). The findings and conclusions in this report are those of the authors and do not reflect the official policies of the Department of Health and Human Services; nor does mention of trade names, commercial practices, or organizations imply endorsement by the U.S. Government.

5.9. Bibliography

1. National Cooperative Highway Research Program (NCHRP) Synthesis 415. (2011). Design fires in road tunnels. A synthesis of highway practice. Project 20-05, Topic 41-05. ISSN 0547-5570. ISBN 978-0-309-14330-1. Library of Congress Control No. 2010943183.
2. NFPA® 502. Standard for Road Tunnels, Bridges, and Other Limited Access Highways. 2011 Edition. ISBN: 978-161665095-7.

3. Purser, D. A., (1995). SFPE Handbook of Fire Protection Engineering, *Toxicity Assessment of Combustion Products*. National Fire Protection Association, Quincy, Massachusetts, 2nd edition.
4. Purser, D. A., (2002.) SFPE Handbook of Fire Protection Engineering, *Toxicity Assessment of Combustion Products.* National Fire Protection Association, Quincy, Massachusetts,3rd edition, 206-207.
5. Purser, D. A., (2008). Assessment of Hazards to Occupants from Smoke, Toxic Gases, and Heat. *The SFPE Handbook of Fire Protection Engineering*, 4th ed. edn. Quincy: National Fire Protection Association., 2–96 –2–193.
6. PIARC, "Fire and Smoke Control in Road Tunnels" 05.05.B, La Defense, France, 1999.
7. ASHRAE Handbook: HVAC Applications, American Society of Heating and Air-Conditioning Engineers (ASHRAE), Atlanta, Ga., 2007.
8. Assessment of the Safety of Tunnels Study, European Parliament, Science and Technology Options Assessment, IP/A/STOA/FWC/2005-28/SC22/29, IPOL/A/STOA/ 2006-26, Brussels, Belgium, May 2006.
9. Kim, H. K., Lönnermark, A., Ingason, H., (2010). Effective Firefighting Operations in Road Tunnels. SP Technical Research Institute of Sweden. SP Report. ISBN 978-91-86319-46-5. ISSN 0284-5172. Borås.
10. US Code of Federal Regulations. CFR, Title 30 (Mineral Resources) Part 75. Mandatory safety standards- underground coal mines, 2016: http://www.ecfr.gov/.
11. US Code of Federal Regulations. CFR, Title 42 (Public Health) Part 84. Approval of Respiratory Protective Devices, 2016: http://www.ecfr.gov/.
12. Perera, I. E., and Litton, C. D., (2011). A detailed study of the properties smoke particles produced from both flaming and non-flaming combustion of common mine combustibles. Fire Safety Science, volume 10, 213-226: 10.3801/IAFSS.FSS.10-213.
13. Mendham, F. Cliff, D., and Horberry, T., (2012). A quantitative approach to engineering fire life safety in modern underground coal mines, 12th Coal Operators' Conference, University of Wollongong & The Australasian Institute of Mining and Metallurgy, 326 - 334.
14. Kissell, F. N. and Litton, C. D., (1992). How smoke hinders escape from coal mine fires. Mining Engineering, volume 44 (1). http://www.osti.gov/scitech/biblio/5875791

15. Pollard, J. P., Heberger J. R., and Dempsey P. G., (2015). Development of a model to determine oxygen consumption when crawling. Transactions of the Society for Mining, Metallurgy, and Exploration, volume 338 (1): 441-447. http://www.ncbi.nlm.nih.gov/pubmed/26997858
16. Haghighat, A., Luxbacher, K., Lattimer, B., 2016. "Simulation of methane fire event at a coal mine working face with consideration of ventilation curtain damage". 2016 Transaction of the Society for Mining, Metallurgy & Exploration, Vol 340, pp. 120-126.
17. Mine Safety and Health Administration (MSHA), 2016, "MSHA Data File Downloads," U.S. Department of Health and Human Services, National Institute for Occupational Safety and Health (NIOSH), Centers for Disease Control and Prevention, http://www.cdc.gov/niosh/mining/data/default.html.
18. Singer, J. M., and Tye, R. P., 1979, "Thermal, Mechanical, and Physical Properties of Selected Bituminous Coals and Cokes," Bureau of Mines Report of Investigations 8364, U.S. Department of the Interior, Bureau of Mines, Washington, DC.
19. Mulholland, G. W., Janssens, M. L., Yusa, S., Twilley, W. and Babrauskas, V., 1991. The Effect of Oxygen Concentration on CO and Smoke Produced By Flames. *Fire Safety Science, volume 3*: 585-594. doi:10.3801/IAFSS.FSS.3-585
20. Gülder Ö. L., Intasopa, G., Joo, H. I., Mandatori, P. M., Bento, D. S., Vaillancourt, M. E., (2011). Unified behaviour of maximum soot yields of methane, ethane and propane laminar diffusion flames at high pressures. *Combustion and Flame, volume 158*: 2037–2044.
21. Luzik, S. J., 1993, "MSHA develops new fire-resistant check curtains," Federal Register, Vol. 59, No. 96, No: 94-12054, pp.102-104, http://arlweb.msha.gov/S&HINFO/TECHRPT/MINEWSTE/FIRESCC.pdf
22. Tewarson, A., 1995, SFPE Handbook of Fire Protection Engineering, 2nd Edition, P. DiNenno, C., Beyler, R., Custer and W. Walton, eds., National Fire Protection Association, Section 3, Chap. 4.
23. Ingason, H., 2009, "Design fire curves for tunnels," *Fire Safety Journal*, Vol. 44, pp. 259-265, https://doi.org/10.1016/j.firesaf.2008.06.009.

24. Kim, H. J., and Lilley, D.G., 2002, "Heat release rates of burning items in fires," Journal of Propulsion and Power, Vol. 18, No. 4, pp. 866-870, https://doi.org/10.2514/6.2000-722.
25. McGrattan, K., Baum, H., and Rehm, H., 1998, "Large eddy simulation of smoke movement," *Fire Safety Journal*, Vol. 30, pp. 161-178, https://doi.org/10.1016/s0379-7112(97)00041-6.
26. Baum, H. R., and McCaffrey, B. J., 1989, "Fire induced flow field-theory and experiment," *Fire Safety Science, Proceedings of the 2nd International Symposium, Hemisphere*, New York, pp. 129-48, https://doi.org/10.3801/iafss.fss.2-129.
27. Yuan, L., Mainiero, R. J., Rowland, J. H., Thomas, R. A. T., and Smith, A. C. S., 2014, "Numerical and experimental study on flame spread over conveyor belts in a large-scale tunnel," Journal of Loss Prevention in the Process Industries, Vol. 30, July 2014, pp. 55-62, https://doi.org/10.1016/j.jlp.2014.05.001.
28. Babrauskas, V., (1979). Technical Note 1103. National Bureau of Standards, Washington.
29. Berenson, P. J., Robertson, W. G., (1972). In Bioastronautics Data Book, Biotechnology, Virginia.
30. Simms, D. L., Hinkley, P. L., (1963). Fire Research Special Report No. 3, Her Majesty's Stationary Office, London.
31. Ingason, H., Li, Y. Z., Lönnermark, A., (2015). Tunnel Fire Dynamics. Springer New York. ISBN 978-1-4939-2199-7.
32. Jin, T., Yamada, T., (1985) Irritating Effects of Fire Smoke on Visibility. Fire Science and Technology 5 (1):79-89.
33. Jin, T., (1978). Visibility through smoke. Journal of Fire & Flamability. 9:135–157.
34. Fridolf, K., Andrée, K., Nilsson, D., Frantzich, H., (2013). The impact of smoke on walking speed. Fire and Materials.
35. Fridolf, K., (2014). Walking speed as function of extinction coefficient. Personal communication, Jan. 10.
36. Trackemas, J. D., Thimons, E. D., Bauer, E. R., Sapko, M. J., Zipf, R. K., Jr., Schall, J., Rubinstein, E., Finfinger, G. L., Patts, L. D., LaBranche, N., (2015). "Facilitating the use of built-in-place refuge alternatives in mines". U.S. Department of Health and

Human Services, Centers for Disease Control and Prevention, National Institute for Occupational Safety and Health, DHHS (NIOSH) Publication No. 2015-114, RI 9698.

37. Mulholland, G, 1995. SFPE Handbook of Fire Protection Engineering, second edition, Section 2/ Chapter 15, (eds: P DiNenno, C Beyler, R Custer and W Walton) (National Fire Protection Association).
38. Prockop, L. D., & Chichkova R. I., (2007.) Carbon monoxide intoxication: an updated review. Journal of Neurological Sciences, volume 262 (1-2): 122-130.
39. Nelson, G. L., (1998). Carbon Monoxide and Fire Toxicity: A Review and Analysis of Recent Work. Fire Technology 34 (1):39–58
40. Varon, J., Marik, P. E., Fromm, R. E., Gueler, A., (1999). Carbon Monoxide Poisoning: A Review for Clinicians. The Journal of Emergency Medicine 17 (1):87–93
41. Brani D. M, Black W. Z., (1992). "Two-zone model for a single-room fire". Fire Safety Journal, Vol. 19, Nos. 2-3, pp. 189—216.
42. Jones, W. W., Peacock, R. D., Forney G. P., Reneke, P. A., Portier, R., (1993). "CFAST- the Consolidated Model of Fire Growth and Smoke Transport". NIST Technical Note 1299, Building and Fire Research Laboratory, National Institute of Standards and Technology, Gaithersburg, MD 20899-0001, USA.
43. Ingason, H., (2005). TG2.2– Target criteria. UPTUN Report WP2– task Group 2.

6. Airflow Simulation Cost Reduction for an Underground Space Environment Based on POD

This paper was submitted to the Computers & Fluids. Ali Haghighat conducted all the CFD works and Dr. Alan Lattimer conducted all the ROM works with technical and editorial input from coauthors: Dr. Jeff Borggaard, Dr. Serkan Gugercin, Dr. Brian Lattimer, and Dr. Kray Luxbacher.

6.1. Abstract

Underground mine ventilation system design and hazard assessments require numerous simulations to support evaluating the risk and overall safety of the system. These simulations have domains that span kilometers and require higher resolution in areas with increased hazards. In this research, the use of computationally efficient reduced-order models (ROMs) was explored for the high resolution areas of a mine simulation. A ROM was produced to predict the flow field of a complex tunnel geometry (Continuous Miner (CM) working face) using proper orthogonal decomposition (POD) to reduce the simulation cost in the nonlinear model. A full order CFD model was developed using Fluent for ventilation at the continuous miner face, and a comprehensive study was conducted to assess the model accuracy and convergence. CFD model results were then used to construct a ROM using proper orthogonal decomposition (POD) with the method of snapshots, and ROM predictions were compared to the full order CFD model. A sensitivity study of the ROM with respect to various inlet velocity boundary conditions was utilized to examine the results near the known solution. The ROM was able to increase the computational efficiency by over three orders of magnitude while retaining the physics and producing results within 5% of the full order CFD model.

6.2. Introduction

Underground mine ventilation systems are critical to emergency response, particularly fire, and to the routine control of strata gas, dusts, and diesel particulate matter. Simulations are used to assist in ventilation system design as well as to predict conditions that support comprehensive assessment and management of risk, emergency response, and best design for occupational health. These analyses commonly require numerous

simulations to determine the impact of different variables on the safety level provided by the ventilation system. In the most hazardous areas where mine personnel are working, detailed simulation results are required to adequately understand the conditions during operations. As a result, there is a need in the mining community to have detailed models that are computationally efficient to support these design and hazardous risk assessments.

The focus of the research in this paper is to develop an accurate and efficient airflow model for a continuous miner (CM) face region in an underground mine. The continuous coal miner (CM) face is a hazardous operating region in the mine due to the potential for high levels of methane gas and coal dust during the mining process. Due to this gas release, frictional ignitions pose a considerable risk at the active working face in underground coal mines. The ignitions are initiated by methane conflagrations that may be gas fed or ignite the coal face. According to non-fatal fire reports of the Mine Safety and Health Administration (MSHA), active working faces are one of the most common locations where non-fatal injuries occur [1]. More accurate models of the ventilation conditions at the coal miner face are needed to improve the safety in this area during normal operation as well as during emergency events such as fires.

The ventilation systems in underground mines are commonly designed using network models such as VnetPC [2, 3], Ventsim Visual™ [4, 5], or other software specifically designed for the mining industry. These models are designed to provide a prediction of airflows over an entire mine, which may range over kilometers. To facilitate fast prediction of the overall performance of the ventilation, the physics of the airflow are simplified by treating sections of the mine where the conditions are spatially uniform as branches and nodes. Depending on the application, the network may be solved based on mass or volumetric balance. Although the simulation cost is decreased significantly using these models, detailed results are not available in areas where the geometry or flow is complex. Therefore, there is a crucial need to provide efficient ventilation models for complex underground space environments, such as the continuous coal miner (CM) working face, with high accuracy and low computational cost.

Detailed simulations of ventilation can be generated using computational fluid dynamics (CFD) to approximate solutions to the Navier-Stokes equations. These partial differential equations are well-suited to model ventilation to a high degree of accuracy [6, 7]. This technique is commonly used for assessment of ventilation in smaller sections of underground spaces [8-14]. However, this technique is costly, and even with high performance workstations, complex domains may require days to solve. As a result, this technique is not acceptable for use in ventilation design and hazard analyses where numerous simulation variations are required.

Reduced-order models (ROM) are explored in this paper as an efficient simulation method to predict the airflow conditions in the CM region. The goal is to assess the local conditions that may lead to a hazardous operating conditions with substantially reduced simulation cost. The proposed methodology can be applied to decrease the ventilation simulation cost of all underground spaces, such as transportation tunnels and underground storage facilities. As suggested in [15-20], there is an increased need to create low dimensional, high fidelity, surrogate models that capture the dynamics of the system. For a comprehensive picture of ROM methods, we recommend the overview by Antoulas [21] and [18, 22, 23], as well as the introduction to Section 6.5. ROM has been used for steady and unsteady models arising in many industrial applications [24-29], but there is scant evidence in the literature that ROM has been applied to mine ventilation systems.

In this research study, a CFD model for the CM face region was produced in ANSYS Fluent with detailed analysis performed to assess the accuracy of the predictions and ensure convergence. While there are many proposed model order reduction methods, this paper focuses on the most popular method for fluids, the proper orthogonal decomposition (POD) [30-33]. The POD-based ROMs are commonly used due to their ability to robustly handle predictions of nonlinear systems and their historical application to fluids. The basic theory of POD is discussed, including the benefits and limitations associated. Results are then presented for a POD-based ROM produced for the CM face region. The CFD model and ROM results are compared for various input ventilation velocities to evaluate the sensitivity of the ROM to changing the input conditions. Also,

the overall accuracy and increase in computational efficiency is provided for the application of ROM in this scenario.

6.3. CFD Simulation Consideration

The geometry of the CM, curtain and mine face were designed according to the JOY 14CM27 Continuous Miner dimensions, with a simplified geometry. The working face tunnel dimensions are shown in Table 6.1, and are consistent with dimensions at a partner mine. A continuous miner face is essentially a dead end tunnel that may be up to 45 m long. In this example, a curtain is constructed during active mining to exhaust air, allowing dilution of contaminants at the dead end face, and for gas and dust to be swept away from the miner. The curtain was simulated 60 cm to the nearest wall, and airflow exhausts from the face behind the curtain.

Table 6.1. CM face region domain dimensions used in the simulation

Face Dimension	Size (m)
Length	15.24
Width	5.50
Height	1.83

Since most of the airflow only moves on the top and sides of the CM under actual conditions, the detailed CM structure was considered inconsequential for this study. The detailed structure of the CM can have an immense impact on the cost of the simulation, so a simplified model was utilized. The CM geometry dimensions used in the simulation are illustrated in Figure 6.1 and Table 6.2. The thickness, length, and height of the ventilation curtain in the simulation were 0.002, 12, and 1.83 m; respectively. In the field, the curtain is constructed with wooden support so that it forms a relatively rigid wall.

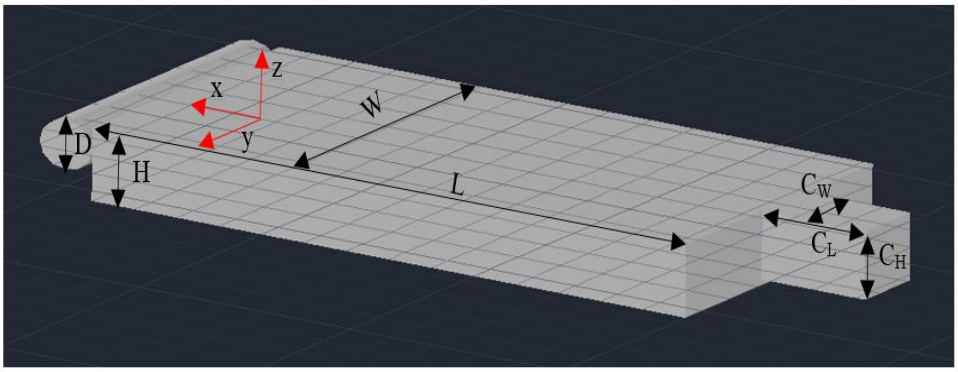

Figure 6.1. Continuous miner schematic view

Table 6.2. CM dimensions used in the simulation

CM Dimension	Size (m)
Length (L)	7
Width (W)	3.35
Height (H)	0.92
Drum Diameter (D)	0.6
Chain Conveyor Boom Length (C_L)	1.2
Chain Conveyor Boom Height (C_H)	0.6
Chain Conveyor Boom Width (C_W)	0.8

6.3.1. Governing Equations

The simulation of airflow at the CM face was studied by solving the Navier–Stokes equations using the realizable k-ϵ turbulence model within the software FLUENT. The three dimensional continuity equations and time averaged Navier-Stokes along with the boundary conditions were solved using a finite volume method.

The air was assumed to be constant temperature in this study, so the energy equation was not included in this model. Thus, equations (6-1) -- (6-4) were solved for an incompressible, isothermal flow with constant viscosity.

$$\frac{\partial u}{\partial x}+\frac{\partial v}{\partial y}+\frac{\partial w}{\partial z}=0 \tag{6-1}$$

$$\rho\frac{Du}{Dt}=-\frac{\partial p}{\partial x}+\mu\vec{\nabla}^2u \tag{6-2}$$

$$\rho\frac{Dv}{Dt}=-\frac{\partial p}{\partial y}+\mu\vec{\nabla}^2v \tag{6-3}$$

$$\rho \frac{Dw}{Dt} = -\frac{\partial p}{\partial z} + \mu \vec{\nabla}^2 w \tag{6-4}$$

Equations (6-1) -- (6-4) with four unknowns (*u, v, w, and p*) were solved for incompressible, isothermal flows with constant μ, where *u, v, w, p, and* μ represent the velocity component along the x-axis, the velocity component along the y-axis, the velocity component along the z-axis, pressure, and viscosity respectively and also **u** = (*u*, *v*, *w*).

The realizable *k-*ϵ model is beneficial when the flow has erratic behavior such as rotation, separation, or boundary layers under strong adverse pressure gradients. On the other hand, the weakness of the standard *k-*ϵ model or other traditional *k-*ϵ models lies with the modeled equation for the dissipation rate (ϵ). It should be considered that the equation for the turbulent kinetic energy (*k*) is the same as that in the standard *k-*ϵ model. As Shih [34] proposed in 1995, the realizable *k-*ϵ model differs from the standard *k-*ϵ model in two ways. First, the realizable *k-*ϵ model has a new formula for the turbulent viscosity. Second, for the transport of the mean-square vorticity fluctuation, a new proposed transport equation for the dissipation rate ϵ is derived from an exact equation.

6.3.2. Transport Equations for the Realizable *k-*ϵ Model

The modeled transport equations for k and ϵ in the realizable *k-*ϵ model are defined by

$$\frac{\partial}{\partial t}(\rho k) + \frac{\partial}{\partial x_j}(\rho k u_j) = \frac{\partial}{\partial x_j}\left[(\mu + \frac{\mu_t}{\sigma_k})\frac{\partial k}{\partial x_j}\right] + G_k + G_b - \rho\epsilon - Y_M + S_k \tag{6-5}$$

$$\frac{\partial}{\partial t}(\rho \epsilon) + \frac{\partial}{\partial x_j}(\rho \epsilon u_j) = \frac{\partial}{\partial x_j}\left[(\mu + \frac{\mu_t}{\sigma_\epsilon})\frac{\partial \epsilon}{\partial x_j}\right] + \rho C_1 S_\varepsilon - \rho C_2 \frac{\epsilon^2}{k+\sqrt{\nu\epsilon}} + C_{1\epsilon}\frac{\epsilon}{k} C_{3\epsilon} G_b + S_\epsilon \tag{6-6}$$

where

$$C_1 = \max\left[0.43, \frac{\eta}{\eta+5}\right] \tag{6-7}$$

$$\eta = S\frac{k}{\epsilon} \tag{6-8}$$

$$S = \sqrt{2S_{ij}S_{ij}} \tag{6-9}$$

$$\mu_t = \rho C_\mu \frac{k^2}{\epsilon} \tag{6-10}$$

In these equations, G_k and G_b represents the generation of turbulent kinetic energy due to the mean velocity gradients and due to buoyancy respectively. The contribution of the fluctuating dilatation in compressible turbulence to the overall dissipation rate is shown by Y_M and C_2 and $C_{1\epsilon}$ are constants. The turbulent Prandtl numbers for k and ϵ are shown by σ_k and σ_ϵ respectively. For a more complete description of all the terms and default values for the k-ϵ constant, refer to [34, 35].

6.3.3. Element Quality Assessment

Regardless of the type of discretization that is used in the model, characterization of mesh quality is essential. The accuracy and stability of the numerical computation are influenced by the quality of the mesh. Three different grid sizes, producing a range of computational cells (97,051; 595,772; and 3,680,961) were generated, and the Grid Convergence Index (GCI) was utilized to study the effect of changing the mesh size on the error. The element quality, the aspect ratio, and the skewness of the cells were investigated to understand model performance. Finally, a fourth mesh with over 18 million cells was produced for the grid independence study.

The normal curvature angle and the growth rate for generating the grid cells were set to 18^o and 1.2, respectively for all models. The minimum edge length was set to 3.2×10^{-3} m. The minimum and the maximum cell size, and the maximum face size were changed to generate different mesh sizes. A fine center span angle was considered for generating cells for all discretizations, and the transition from the minimum size to the maximum size was set to be slowly varying as shown in Table 6.3.

Table 6.3. Mesh characteristics for different cell sizes

Number of cells	Average element quality	Average aspect ratio	Average skewness	Min size (m)	Max face size (m)	Max size (m)
97,051	0.792	3.443	0.277	0.0024	0.238	0.476
595,772	0.821	2.209	0.243	0.0024	0.108	0.239
3,680,961	0.824	1.952	0.244	0.0024	0.045	0.219
18,845,331	0.833	1.866	0.231	0.00024	0.024	0.048

Using a mesh of adequate geometrical quality is an important part of controlling discretization error. The orthogonality, expansion and aspect ratio (or stretching) are defined as the effective parameters in categorizing the significant measures of mesh quality [35]. The schematic view of 97,051 tetrahedral cells is shown in Figure 6.2.

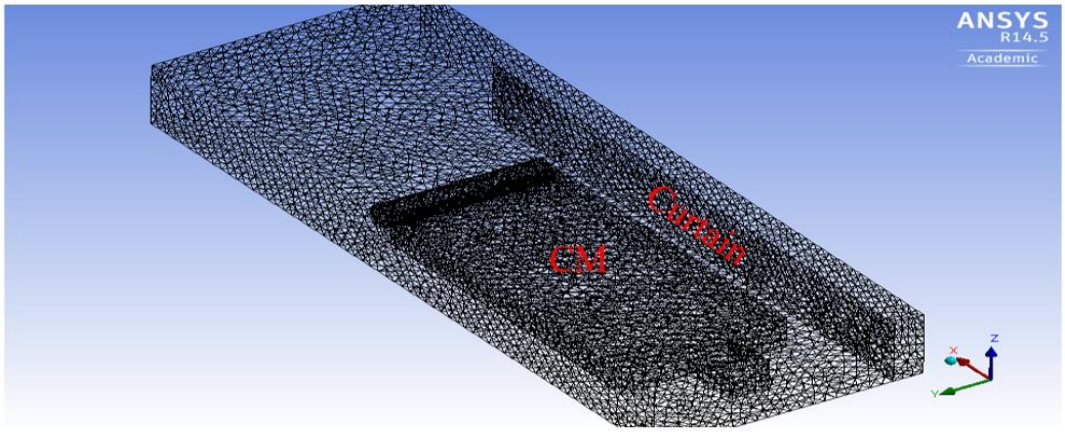

Figure 6.2. Schematic view of 97,051 elements

6.3.3.1 Aspect ratio

The accuracy and the stability of the numerical analysis are related to the quality of the mesh. The three main parameters that influence the quality of the mesh are node point distribution, smoothness, and skewness. A poor mesh quality can present conditions that are not representative of the actual physics of the system or can cause an over-diffusive solution and convergence difficulties. The quality of the mesh is referred as the orthogonal quality of a given cell, and we refer the reader to [35, 36] for details on the calculation of mesh quality. In general, the mesh quality spectrum ranges from 0 to 1, with the former

representing a degenerate mesh quality, and the latter an excellent mesh quality [35]. The other indicators of mesh quality are the aspect ratio and the skewness of the generated mesh. A study was conducted to investigate the effect of aspect ratio and skewness changes on the mesh quality of computational domain.

The aspect ratio is a measure of stretching the cell. The aspect ratio is defined as the maximum to the minimum value ratio of any of the normal distances between either the cell centroid and the face centroids or the cell centroid and nodes [35].

The minimum mesh size was held constant for generating the first three different numbers of cells while the maximum face sizes and the maximum cell sizes varied. In Table 6.3, it is evident that the average aspect ratio decreased dramatically when the number of cells increased from 97,051 to 3,680,961 cells. So, the element quality increased significantly with refinement; however, a conspicuous improvement in mesh quality was not observed when increasing to18 million cells. This study shows that increasing the number of cells did not necessarily improve the quality of simulation results thus we could infer a converged result. By increasing the number of cells, the computation time increases dramatically. The element quality distribution for all four mesh sizes is illustrated in Figure 6.3.

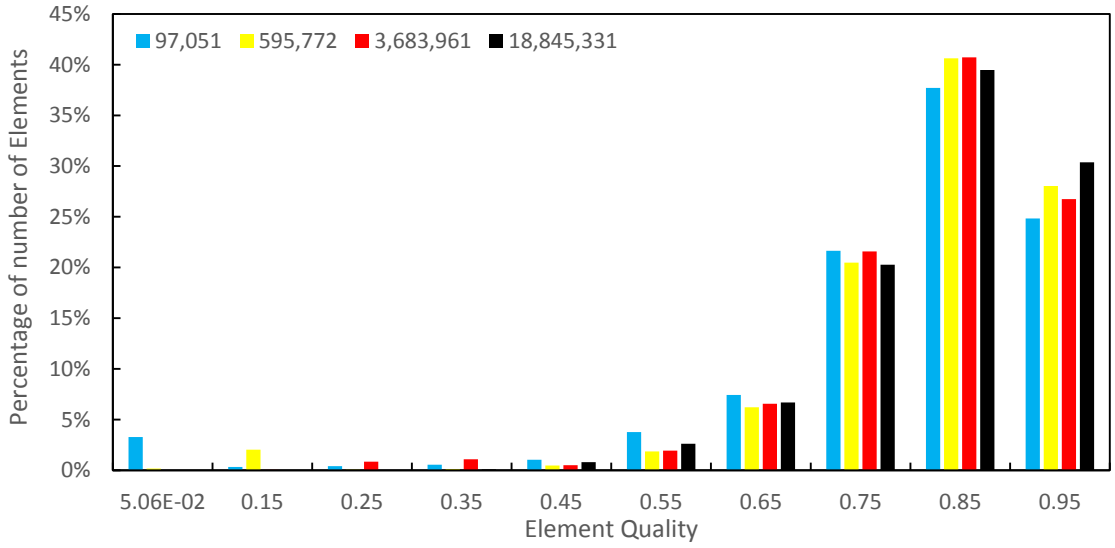

Figure 6.3. Comparison of element quality distribution for four different mesh sizes

6.3.3.2 Skewness

The skewness of a grid is an important parameter to assess the quality and suitability of the mesh. Equation (6-11) was used for determination of the grid skewness.

$$Skewness = 1 - \left(\frac{Cell\ Size}{Optimal\ Cell\ Size}\right) \tag{6-11}$$

Consistent with the data in Table 6.3, it is evident that skewness and aspect ratio together play a key role in the quality of the mesh. We conclude from our analysis of mesh quality and the corresponding convergence of the CFD simulations that we are confident in our full-order CFD model. We provide details of the full-order model below.

6.3.4. Geometry, Initial, and Boundary Conditions of Full-Order CFD Model

High-order numerical modeling was accomplished using FLUENT, the CFD module of the ANSYS Workbench 14.5 software. Field measurements were utilized to design and initialize a simulation. Double precision was considered for the calculation of the problem. The pressure-based approach was used to investigate the low-speed, incompressible airflow in the tunnel. The viscous model is set using the realizable k-ε model with standard wall functions for near wall treatment. The physical properties of the air are treated as constants with a density of 1.225 kg/m^3 and a viscosity of 1.7894e-05 kg/m-s. The transient model was considered for running all simulations.

A 0.9 m/s uniform inlet velocity boundary condition was applied. The flow rate weighting for all outflow boundaries is set to 1 (backside of the curtain). All surfaces were treated using a no-slip boundary condition. The turbulent backflow intensity was assumed to be 5%, and the turbulent viscosity ratio was set to 10. The SIMPLE algorithm was used as the solution method for the pressure-velocity coupling. Second-order upwinding was considered for spatial discretization of momentum, turbulent kinetic energy, and the turbulent dissipation rate. A second-order implicit formulation was used for the time-stepping. The convergence criterion was set to 1x10^{-5} for continuity, kinetic energy (k) and turbulent dissipation (ε) equations. Under relaxation factors for pressure, momentum and turbulent kinetic energy were set to 0.3. The models were run until the solutions converged to a steady state solution. CFD post-processor and Tecplot 360 software were utilized for

visualization and investigation of different parameters. The velocity contour plot and streamlines at 0.3 m above the floor are shown in Figure 6.4.

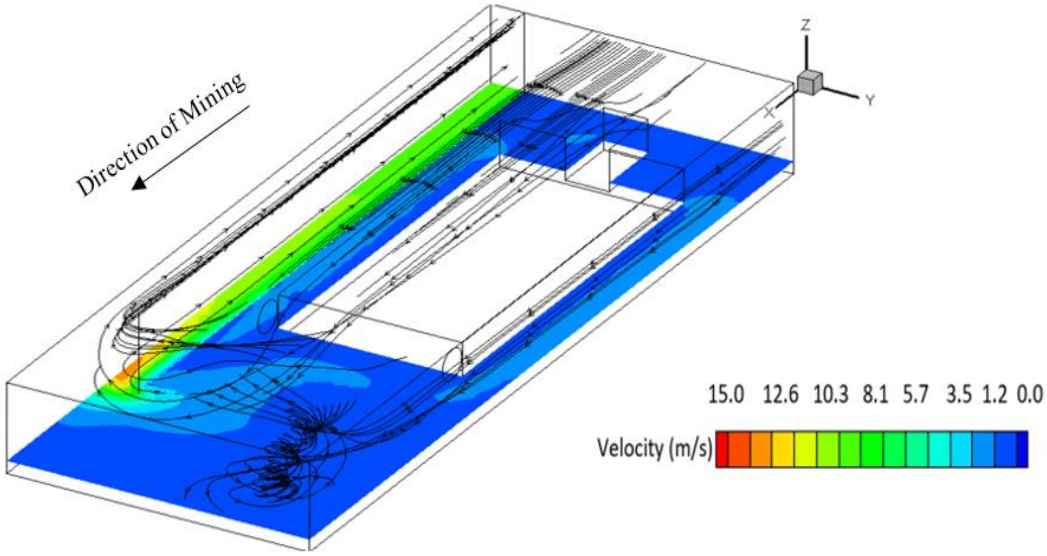

Figure 6.4. Velocity contour plot and streamlines at z=0.3 m

The magnitude of the velocity at two points and along two lines were calculated for model comparison during each simulation as shown in Figure 6.6. Point 1 was assigned at the height of 0.8 m and 0.2 m from the outlet, and Point 2 was assigned to 11 m from Point 1. Two-line monitors were assigned horizontally and vertically between Points 1 and 2 and at Point 1 respectively as shown in Figure 6.5 for sensitivity analysis of generated cell sizes.

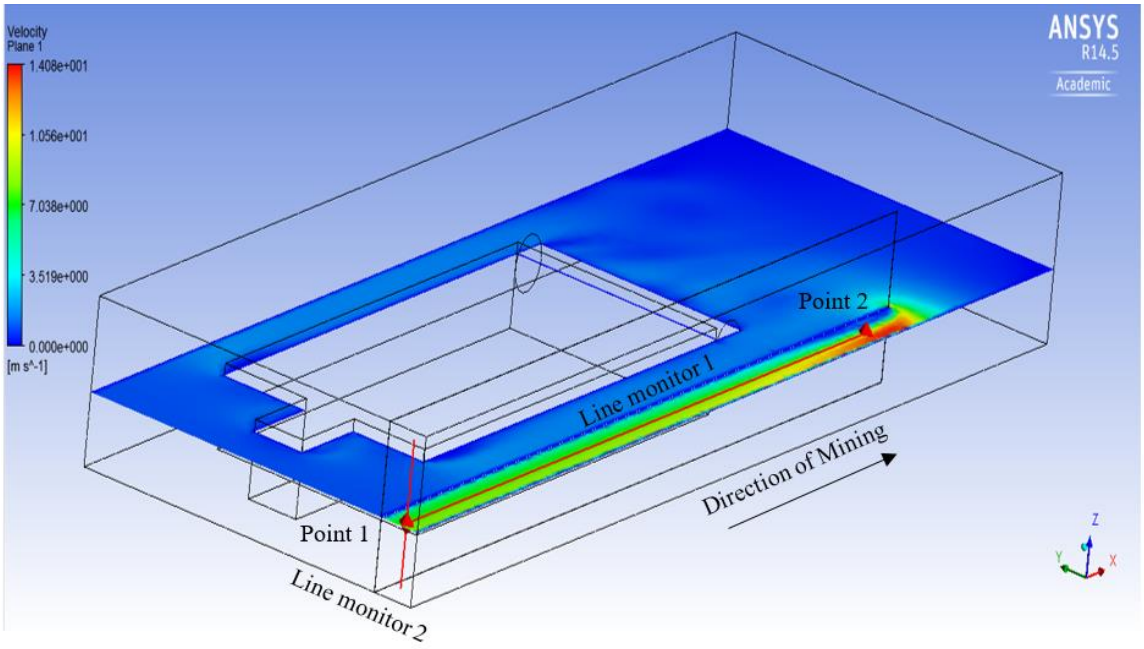

Figure 6.5. Selected points and lines for calculation of airflow velocity

6.4. Sensitivity Analysis

Air enters the face at a velocity of 0.9 m/s and exits from the back side of the curtain. Studying the streamlines on Figure 6.4, it is evident that vortices at the left side of the face were produced due to the redirection of air and turbulent behavior. Air at Point 2 has a higher velocity compared to Point 1. The study of velocity at Points 1 and 2 through time based on the first three mesh sizes (when the steady state was achieved) showed that with the coarse mesh, the velocity at Point 1 was close to the velocity at Point 2; however, when using the medium or fine mesh, the velocity from Point 1 to Point 2 changed significantly. The velocity magnitude at Points 1 and 2 according to the cell numbers at t =10 s are shown in Table 6.4. This study shows that for capturing the exact behavior of airflow at critical points with complex fluid structure such as close to the wall and at the turning points, a high resolution model is required.

Table 6.4. Velocity magnitude at points 1 and 2 according to the cell numbers at t = 10s

Cell number	Velocity at point 1 (m/s)	Velocity at point 2 (m/s)
97,051	7.4	8.3
595,772	7.5	10.4
3,680,961	7.7	11.7

The calculated velocity cross the Line monitor 1 was utilized in order to analyze the airflow behavior according to the different mesh sizes. The velocity at *t* =10 s based on coarse, medium, and fine meshes models was calculated through the Line monitor 1 and plotted in Figure 6.6.

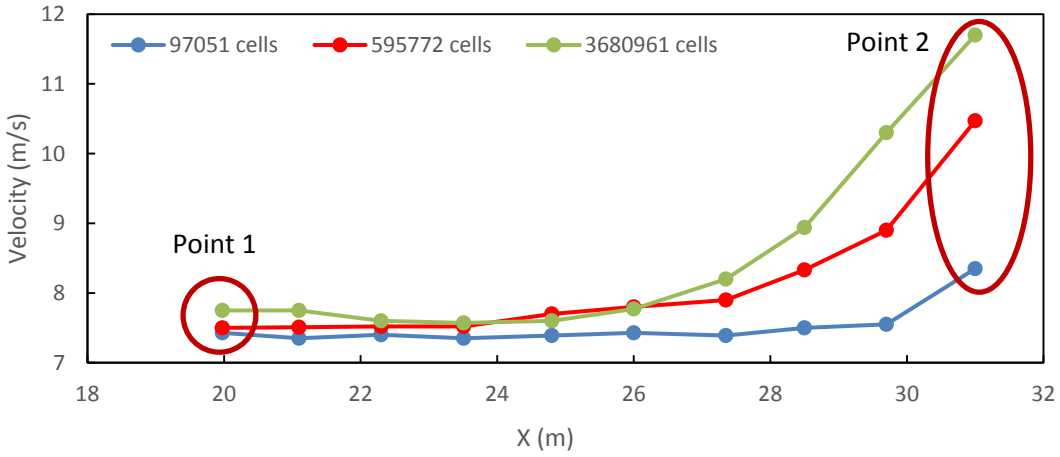

Figure 6.6. Comparison of velocity magnitude at t =10 s for three different mesh sizes across Line monitor 1

As shown in Figure 6.6, the velocity difference at Point 2 between the coarse and fine mesh is about 29% while this difference decreased noticeably to 11% between the medium and fine mesh. This study has again shown that by implementing the finer mesh, the physics of the flow structure at the specific points, can only be captured with high fidelity CFD. Therefore, a substantial difference in the results at Point 2 was observed when 3,680,961 cells were utilized compared to 97,051 cells. To investigate the effect of mesh size changes on the numerical results, the velocity across the Line 2 at t= 10 s was also calculated for our three mesh sizes. The Line 2 monitor was 10 cm from the floor and

ceiling of the outlet. The velocity magnitude according to different mesh sizes at t =10 s along the Line 2 at two different heights was calculated as shown in Table 6.5.

Table 6.5. Comparison of velocity magnitude at t =10 s for three different mesh sizes close to floor and ceiling at the outlet (start and end points of Line monitor 2)

Cell number	Velocity at z = 0.1 m	Velocity at z = 1.7 m
97,051	5.1	5.4
595,772	7.8	8.4
3,680,961	8.3	7.7

As shown in Table 6.5, using the coarse mesh, the monitored velocity at z=0.1 m (close to the floor) was 5.1 m/s while the velocity at the same location for medium and fine meshes was 7.8 and 8.3 m/s, respectively. By increasing the number of cells from 97,051 cells to 3,680,961 cells, the velocity at z = 0.1 m (close to the floor) increased while the same trend was not observed for the velocity at z= 1.7 m (close to the ceiling). Overall, this study has shown that the appropriate level of grid resolution should be determined for analysis of airflow velocity at the CM working face tunnel and either mesh convergence studies or adaptive mesh refinement strategies should be used. In this study, we analyzed the numerical error based on GCI method. Our confidence of the solution on the 3.6 M cells mesh based on simulations performed at an 18.8 M cell mesh allows us to evaluate the quality of ROMs by comparison to 3.6 M cell simulations.

6.4.1. GCI Method for Discretization Error Estimation

One of the most important issues in numerical computations is finding the appropriate level of grid resolution. This is a function of the flow conditions, type of solver, geometry, an5d other variables. One is often left to start with a grid resolution and then conduct a series of grid refinements to assess the effect of the grid resolution.

Roache [37] explained a consistent manner for calculation of a grid convergence index to estimate the discretization error based on Richardson Extrapolation (RE). This approach was used to estimate the discretization error in the CM face model. Three different mesh sizes were considered in the GCI calculation.

First of all, the representative cell, mesh or grid size *h* was calculated based on the following equation for three dimensions.

$$h = \left[\frac{1}{N}\sum_{i=1}^{n}(\Delta A_i)\right]^{1/3} \tag{6-12}$$

where ΔA_i is the area of the *ith* cell, and *N* is the total number of cells used for the computations. The average velocity at the outlet (V_{mag}) is the key variable of interest in this study. Hence, the converged solution for this quantity is needed. Then the grid refinement factor was calculated according to Equation (6-13)

$$\mathrm{r} = \frac{\mathrm{h_{coarse}}}{\mathrm{h_{fine}}} \tag{6-13}$$

It is common practice to set the grid refinement factor, $r=h_{coarse}/h_{fine}$, greater than 1.3. The grid refinement should be done systematically and the usage of geometrically similar cells is recommended.

For this study where three meshes were employed, the calculation of the apparent order *p* of the method is based on $h_1 < h_2 < h_3$ and

$$\mathrm{r_{21}} = \frac{\mathrm{h_2}}{\mathrm{h_1}} \tag{6-14a}$$

$$\mathrm{r_{32}} = \frac{\mathrm{h_3}}{\mathrm{h_2}} \tag{6-14b}$$

So the grid refinement factor for the first-second and second-third meshes, respectively, was calculated according to the Equations (6-14a) and (6-14b), where p is expressed by

$$p = \frac{1}{\ln(\mathrm{r_{21}})}\left|\ln\left|\frac{\varepsilon_{32}}{\varepsilon_{21}}\right| + q(p)\right| \tag{6-15a}$$

$$q(p) = \ln\left[\frac{\mathrm{r_{21}}^{p}-s}{\mathrm{r_{32}}^{p}-s}\right] \tag{6-15b}$$

$$s = 1.sign\left(\frac{\varepsilon_{32}}{\varepsilon_{21}}\right) \tag{6-15c}$$

where $\varepsilon_{32} = \emptyset_3 - \emptyset_2$, $\varepsilon_{21} = \emptyset_2 - \emptyset_1$, and $\emptyset_i$ corresponds to the key variable in the ith mesh. The average velocity at the outlet was selected as the key variable in this study. The

$q(p)$ is calculated zero for constant amount of r (6-15b).Therefore, in this case, (6-15b) and (6-15c) were not calculated. The extrapolated values of the interested variable can be calculated using the following equation:

$$\emptyset_{\text{ext}}{}^{21} = \frac{\text{r}_{21}{}^{p}\emptyset_1 - \emptyset_2}{\text{r}_{21}{}^{p} - 1} \tag{6-16}$$

By the usage of Eqn. (6-17), the relative error was estimated for calculation of GCI for fine mesh (Eqn. (6-19)). The extrapolated relative error was estimated according to Eqn. (6-18) To estimate the amount of error on the fine mesh.

$$e_{\text{a}}{}^{21} = \left|\frac{\emptyset_1 - \emptyset_2}{\emptyset_1}\right| \tag{6-17}$$

$$e_{\text{ext}}{}^{21} = \left|\frac{\emptyset_{\text{ext}}{}^{21} - \emptyset_1}{\emptyset_{\text{ext}}{}^{21}}\right| \tag{6-18}$$

$$\text{GCI}_{\text{fine}}{}^{21} = \frac{\text{F}_\text{s}\text{e}_{\text{a}}{}^{21}}{\text{r}_{21}{}^{p} - 1} \tag{6-19}$$

where F_s is the safety factor. A 1.25 as the safety factor for comparison among three meshes was suggested by Roache [38]. The results of all calculations for three different cells according to the four different time step are illustrated in Table 6.6. The $\text{GCI}_{\text{coarse}}{}^{32}$ was not investigated since the focus of this study was on the error quantification for the finer meshes.

Table 6.6. Discretization error for average velocity according to different time step

Characteristics	∅= Average Outlet Velocity at t=0.1 s	∅ = Average Outlet Velocity at t=0.01 s	∅ = Average Outlet Velocity at t=0.005 s	∅= Average Outlet Velocity at t=0.001 s
Fine Mesh Elements (N1)	3,680,961	3,680,961	3,680,961	3,680,961
Medium Mesh Elements (N2)	595,772	595,772	595,772	595,772
Coarse Mesh Elements (N3)	97,051	97,051	97,051	97,051
r_{21}	1.83	1.83	1.83	1.83
r_{32}	1.83	1.83	1.83	1.83
$\emptyset_1$ (m/s)	7.25956	7.25814	7.25725	7.25441
$\emptyset_2$ (m/s)	7.21694	7.21688	7.21684	7.21678
$\emptyset_3$ (m/s)	7.20725	7.23325	7.24485	7.24515
p	2.45108	1.52973	0.60649	0.46742
$\emptyset_{ext}^{21}$	7.272	7.285	7.349	7.3697
e_a^{21}	0.6%	0.6%	0.6%	0.5%
e_{ext}^{21}	0.2%	0.4%	1.2%	1.6%
GCI_{fine}^{21}	0.2%	0.5%	1.6%	2.0%

As shown in Table 6.6, it is evident that the numerical uncertainty in the fine grid GCI for average velocity at the outlet for different time steps of 0.1, 0.01, 0.005, and 0.001 seconds are calculated as 0.2 %, 0.4%, 1.2%, and 1.6% respectively. The estimated error on the fine mesh was 0.2% for average outlet velocity with the usage of 0.1 seconds as the time step and 2.0% for 0.001 seconds as the time step.

6.4.2. Grid Independent Study

The grid independent study was conducted to ensure that the solution is also independent of the grid resolution. The grid independent solution was checked by plotting a graph of the average velocity at the outlet versus the number of cells in the simulation. The average velocity at the outlet according to four different cell sizes are shown in Figure 6.7.

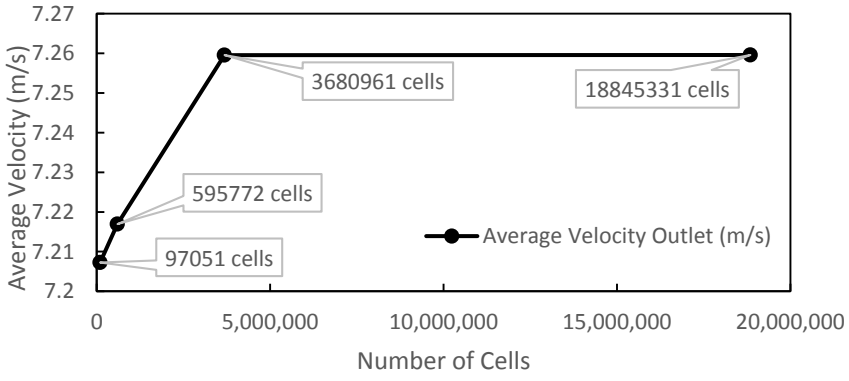

Figure 6.7. Number of cells versus average velocity at outlet according to 4 different cell sizes

As shown in Figure 6.7, the average velocity at the outlet changed from 7.21 m/s to 7.26 m/s when the number of cells was modified from approximately 100,000 cells to 3,700,000 cells while no discernable change in the average outlet velocity was observed when the grid size was changed from 3,700,000 to 18,800,000 cells. This study showed that 3 million cells represent a sufficient grid size when using 0.1 s as the time step.

The velocity contour plot at z = 1.0 m is illustrated in Figure 6.8 based on different grid sizes. According to Figure 6.8, the improvement in resolution and results precision was observed as the number of cells increased from 97,051 to 3,680,961 ((a) through (c)), with minor change between 3,680,961 to 18,845,331 cells ((c) to (d)).

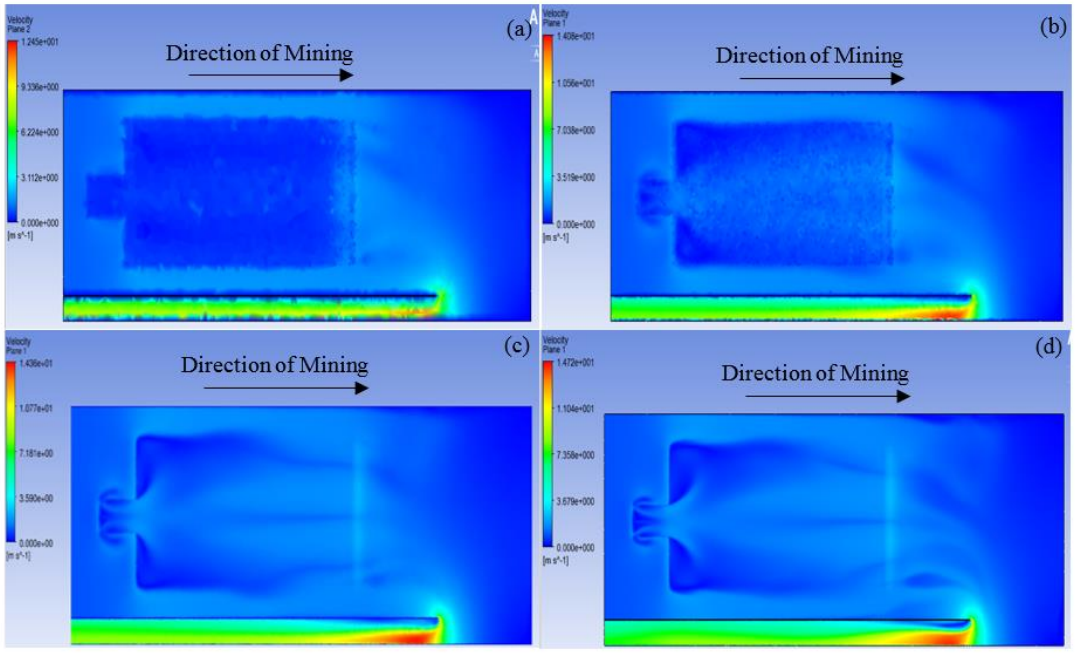

Figure 6.8. Velocity contour plot at z=1.0 m for four different grid sizes (a) 97,051 cells, (b) 595,772 cells, (c) 3,680,961 cells, (d) 18,845,331 cells

The four simulations have shown good agreement considering the extreme variation in size and the number of cells. The fine cases (c and d) show more detail than the other simulations, but even the coarse simulation has established the main features of the flow and velocity field. As seen in Table 6.6 and Figure 6.7, the 3,680,961 cell mesh is adequate for investigation of airflow behavior at the CM face region regarding accuracy and simulation cost.

6.4.3. Time Step Dependency Test

The time step dependency analysis was conducted to achieve the optimum time step for calculation of the problem with the usage of different cell sizes. Four various time steps (0.1, 0.01, 0.005, and 0.001 seconds) were selected for the three different grid sizes with the intention of investigating the average velocity at the outlet. The results for two different cell sizes are shown in Table 6.7.

Table 6.7. Average velocity for two different cell sizes according to different time steps

Time step (s)	3,680,961 cells	97,051 cells
	Velocity (m/s)	Velocity (m/s)
0.1	7.26	7.21
0.01	7.26	7.23
0.005	7.26	7.24
0.001	7.25	7.25

It is noteworthy that a change of the time step did not have a significant impact on the average velocity at the outlet for 3,680,961 cells case. However, for the coarse mesh, the average velocity changed from 7.21 m/s to 7.25 m/s when the time step decreased from 0.1 to 0.001 s. Hence, based on the simulation results from Table 6.7, a 0.1 s time step was determined to be sufficient for 3,680,961 cells case.

6.5. Reduced Order Models for CFD

Model order has an immense impact on the cost of simulation and control. Therefore, model reduction strategies can be helpful to circumvent the simulation cost problem. For systems with linear dynamics, there are numerous methodologies for effective, optimal model reduction. For example, one can apply gramian based methods such as Balanced Truncation [39, 40] or rational interpolation based methods such as the Iterative Rational Krylov Algorithm [41]. These transfer function based methods have been recently extended to systems with special nonlinearities, for example, to bilinear [42-44] and quadratic nonlinearities [45, 46]. We refer the reader to [17, 19, and 47] for recent surveys on model reduction. For general nonlinearities, the model reduction is most commonly achieved by Proper Orthogonal Decomposition (POD) [30, 48]. In POD, one first obtains a matrix of snapshots using some benchmark simulations and then obtains the model reduction basis from a truncated SVD of this snapshot matrix. Finally, one applies Galerkin projection of the governing equations onto the low-dimensional space spanned by the POD basis. The result is a small system of nonlinear ordinary differential equations (ODE) that can replace the complexity of the FLUENT simulations while retaining nearly the same accuracy as long as the physics remain close to one of the benchmark simulations.

A general algorithm as shown in Figure 6.9 was utilized for comparison of ROM to CFD to determine if ROM is a reasonable technique for the cost reduction, and can reperesent a practical range of flow physics.

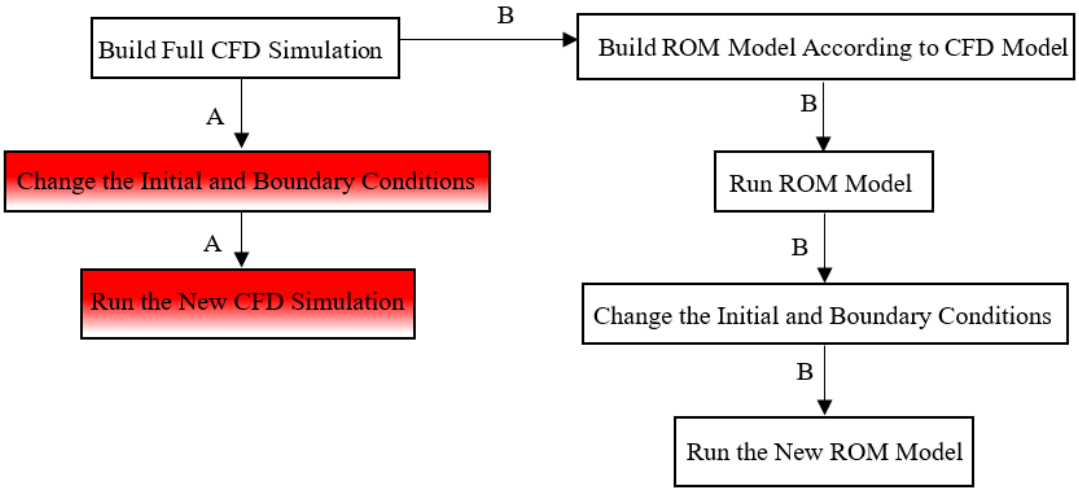

Figure 6.9. An algorithm for determining the efficacy of ROM simulation cost reduction

As can be seen in Figure 6.9, the two approaches (A and B) were determined for analysis of airflow behavior at a CM tunnel face. The common approach is building and running the CFD model (A). If the initial or boundary conditions are changed, the new changes should be applied to the CFD model, and, again, the CFD model will be run with the new input initial or boundary conditions. The other approach, which we present for mining applications, is the ROM approach (B). In this approach, the ROM model is built according to the first CFD simulation. So, the cost of this approach is just one CFD simulation. However, if the initial or boundary conditions are changed, the new changes can be input into the ROM model to simulate the results. Therefore, there is no need to build a new CFD model if the model parameters are only being perturbed by a relatively small amount. This results in substantial computational savings (e.g. the elimination of red color blocks in Figure 6.9). With the ROM approach (B), the cost of simulation is decreased by several orders of magnitude. The medium mesh (595,772 cells) of the CFD model was

utilized for building the ROM model. Running each CFD model for calculation with 595,772 cells took approximately two hours with 35 processors.

6.5.1. Basic Description of Reduced Order Modeling Using POD

POD is one of the most common techniques which is utilized for non-linear systems [49-52]. For this paper, we modeled the airflow in the mine using the Navier-Stokes equations for isothermal, incompressible flows as shown in Equation (6-20). This model is well suited for typical flow speeds and temperatures of mines.

$$\frac{\partial \mathrm{u}}{\partial t} - \mu \nabla^2 \mathrm{u} + (\mathrm{u} \cdot \nabla)\mathrm{u} + \nabla p = 0$$
$$\nabla \cdot u = 0 . \tag{6-20}$$

For any given time and n spatial nodes in the domain, we can write the velocity flow of the air, $\mathrm{u} = [u\ v\ w]^{\mathrm{T}} \in \mathrm{R}^{3n}$, as a combination of a centering vector $\bar{\mathrm{u}}(\mathrm{x})$ and an infinite set of basis vectors, $\phi_i(x)$.

$$\mathrm{u}(t, \mathrm{x}) = \bar{u}(x) + \sum_{i=1}^{\infty} \phi_i(\mathrm{x}) a(t) . \tag{6-21}$$

Then an r-dimensional approximation of the velocity, (6-22), can be created by using r basis vectors. Here we have decomposed the basis into its *u, v,* and *w* components as $\phi_i(\mathrm{x}) = [\phi_i^u(x)\ \phi_i^v(x) \phi_i^w(x)]^T$.

$$u(t, \mathrm{x}) \approx \tilde{u}(t, \mathrm{x}) = \bar{u}(x) + \sum_{i=1}^{r} \phi_i^u(x)\, a(t)$$
$$v(t, \mathrm{x}) \approx \tilde{v}(t, \mathrm{x}) = \bar{v}(x) + \sum_{j=1}^{r} \phi_j^v(x)\, a(t)$$
$$w(t, \mathrm{x}) \approx \tilde{w}(t, \mathrm{x}) = \bar{w}(x) + \sum_{k=1}^{r} \phi_k^w(x)\, a(t) \tag{6-22}$$

To find an appropriate basis for the system, we first generate $k > r$ full-order snapshot solutions, $\mathrm{S} = [\mathrm{u}_1 \mathrm{u}_2 \ldots \mathrm{u}_k]$, for the velocity field using ANSYS Fluent. We generate the POD modes by performing a singular value decomposition (SVD) of S and then select the first r singular vectors, $\Phi = [\phi_1 \ldots \phi_r]$. Using the POD modes, Φ, as the basis functions

for the approximation in (6-22), we are guaranteed the best *r* dimensional representation of the snapshot solutions in the L_2- norm. In Figure 6.10, we show an example of this approximation at the CM face. Further, if the anticipated behavior of the system is close to the snapshot solutions, we can expect to represent that behavior reasonably well with the POD basis functions given by Φ.

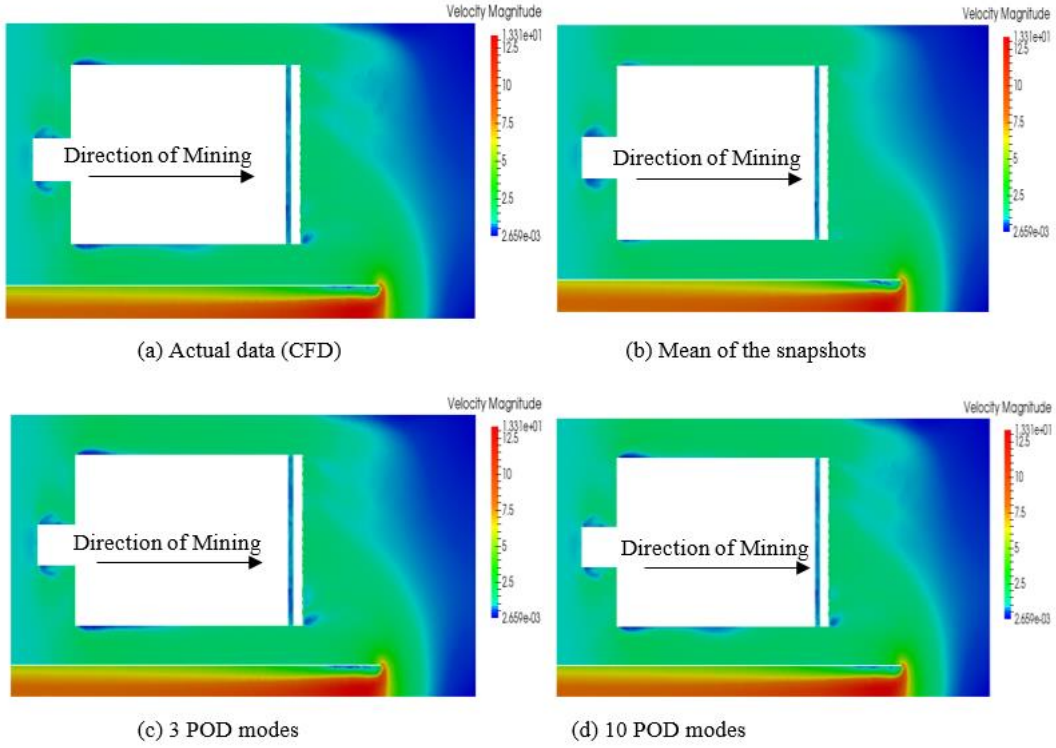

Figure 6.10. Comparison of the airflow in the full model versus the airflow at the same time step generated using various POD modes (plan view)

Using these POD modes as test functions, we substitute (6-22) into the weak formulation of equation (6-20). We define the inner product over the domain Ω by

$$(f, g) = \int_{\Omega} f(t,x)g(t,x)dV \ . \tag{6-23}$$

For example, the weak form in the *u* direction is given by

$$(u_t, \phi^u) = -\left(uu_x + vu_y + wu_z, \phi^u\right) - 2\mu\,(u_x, \phi_x^u) - \mu\left(u_y + v_x, \phi_y^u\right) - \mu(u_z + w_x, \phi_z^u) \ . \tag{6-24}$$

We can now substitute the approximation for u from (6-22) into (6-24) for each ϕ_i, i = 1,...,r and apply the linearity properties of the inner product to obtain

$$\sum_{j=1}^{p} (\phi_j^u, \phi_i^u)\dot{a}_j = -(c^u c_x^u, \phi_i^u) - \left(c^u \sum \phi_{k,x}^u a_k, \phi_i^u \right) - \left(c_x^u \sum \phi_j^u a_j, \phi_i^u \right) - \left(\sum \phi_j^u a_j \sum \phi_{k,z}^u a_k, \phi_i^u \right) - \left(c^v c_y^u, \phi_i^u \right) - \left(c^v \sum \phi_{k,y}^u a_k, \phi_i^u \right) - \left(c_y^u \sum \phi_j^v a_j, \phi_i^u \right) - \left(\sum \phi_j^v a_j \sum \phi_{k,z}^u a_k, \phi_i^u \right) - (c^w c_z^u, \phi_i^u) - \left(c^w \sum \phi_{k,z}^u a_k, \phi_i^u \right) - \left(c_z^u \sum \phi_j^w a_j, \phi_i^u \right) - \left(\sum \phi_j^w a_j \sum \phi_{k,z}^u a_k, \phi_i^u \right) - 2\mu \left(c_x^u, \phi_{i,x}^u \right) - 2\mu \sum (\phi_{k,x}^u, \phi_{i,x}^u)\, a_k - \mu \left(c_y^u, \phi_{i,y}^u \right) - \mu \sum (\phi_{k,y}^u, \phi_{i,y}^u)\, a_k - \mu \left(c_x^v, \phi_{i,y}^u \right) - \mu \sum (\phi_{k,x}^v, \phi_{i,y}^u)\, a_k - \mu \left(c_z^u, \phi_{i,z}^u \right) - \mu \sum (\phi_{k,z}^u, \phi_{i,z}^u)\, a_k - \mu \left(c_x^w, \phi_{i,z}^u \right) - \mu \sum (\phi_{k,x}^w, \phi_{i,z}^u)\, a_k. \quad (6\text{-}25)$$

Similar formulations are applied for each velocity direction. Note that $\nabla \cdot \phi = 0$, so we can ignore the incompressibility condition and the pressure. Applying this leads to an *r*-dimensional system of Ordinary Differential Equations (ODEs) that can be solved to obtain the POD basis coefficients, $a(t)$, for a given time interval $t = [0, t_f]$. Plugging these coefficients into our approximation (6-22), we can recover an approximation to the full-order model. For a complete description of the POD technique the reader is referred to [32, 33, and 48].

6.5.2. Benefits and Limitations

POD excels as a model reduction technique when used to simulate solutions around a known solution. So, if there is an existing known flow where the data is generated either experimentally or computationally via a full-order simulation, the POD can be used to approximate flows sufficiently close to the known flow [48]. While some ROM techniques are focused on the input to output mappings, POD is designed to recreate the entire state space as a linear combination of the individual POD modes. Thus, it is a good technique to use if the focus is to obtain an approximation of what the flow is doing in the entire space.

However, due to its dependence on snapshots, POD is very dependent on the quality and quantity of snapshots. First, the snapshot solutions must be representative of the types of solutions being modeled. For example, the kinematic viscosity and inlet velocity of the snapshots should be close to the values being used in the reduced order model (ROM).

Note that "close" is an application-dependent term. One of the main objectives of this paper is to evaluate the quality of POD-ROMs in the mine ventilation setting. Since POD determines the most prominent flow modes using an eigenvalue computation, the number of reliable modes is about ten percent of the total number of snapshots in most cases [53]. So, if there are one hundred snapshots, then we can expect to obtain at most ten reliable POD modes. Finally, creating the actual ROM from the POD modes can be challenging for complex fluid flows. In particular, solving the ROM quickly requires the computation of several matrices. These matrices must then be stored and then loaded when the ROM is being solved.

6.5.3. ROM Results

The POD vectors and reduced order model were created using the snapshots generated from a FLUENT simulation run with a 0.9 m/s input velocity. The simulation results were then exported into MATLAB®. We note that FLUENT solves for the velocity at the center of each volume element, but exports the data averaged to the nodes. The consequence of this is that average output velocity as calculated from exported data varies slightly from the internal FLUENT calculation. There were 100 data snapshots created from 0.1 to 10.0 seconds. Due to the accuracy of the eigenvalue solver, the reduced order model was restricted to up to ten POD modes. The total computational time required for generating these modes and the associated reduced order model was 7.55 minutes with 1 processor. Compare this to requiring over 2 hours just to compute solution snapshots. Using the initial condition from the snapshots and the reduced order model, the system was integrated forward in time from 0.1 to 10 seconds to generate an approximate solution. This computation took approximately 0.5 seconds to complete. The resulting error between the actual system (as simulated in ANSYS Fluent) and the ROM is given in Table 6.8. The error is the same order of magnitude of the error between the CFD simulations with 500 K vs. 3.6 M cells.

Table 6.8. The error between the actual and reduced order model (ten modes, r=10) velocity profiles at 10.0 seconds

$\overline{U}_{\text{in}}$	$\overline{U}\text{out}^{Act}$	$\overline{U}\text{out}^{ROM}$	$\overline{\%U}\text{out}^{Err}$	$\%U^{Err}$
0.90	7.0903	7.0912	0.0121	4.9970

Further, the average velocity at the outlet over time was investigated and it was compared it to the reduced order model. As is shown in Figure 6.11, the ROM is a good approximation of the actual system over the entire time interval.

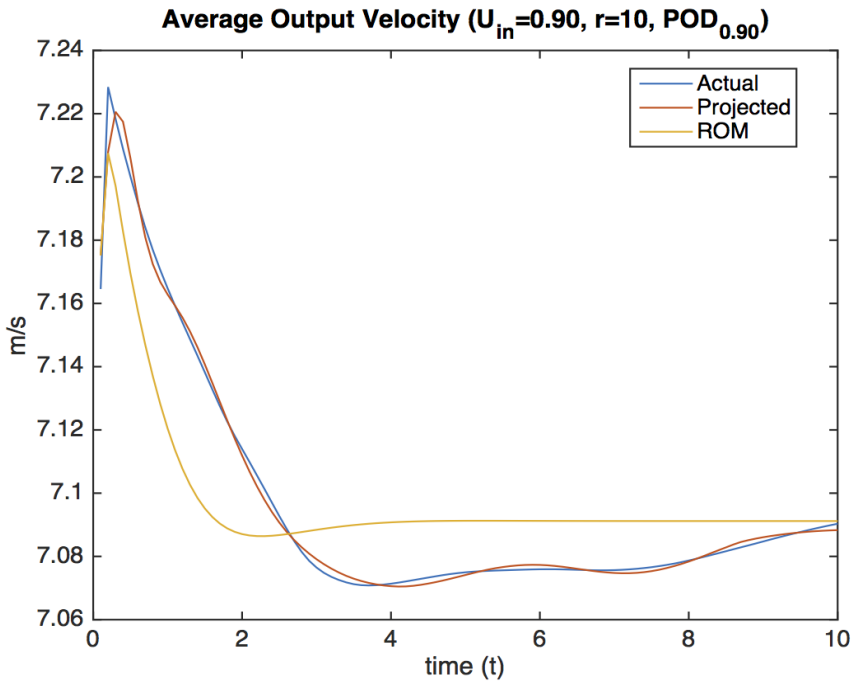

Figure 6.11. Comparison of the airflow in the full order model versus the airflow at the same time step generated using POD modes

While these results are promising, they are ultimately just an approximation to the simulation that we already had. Therefore, the total time to create this ROM was the two hours required to generate the actual data plus the seven to eight minutes necessary to generate the ROM. However, the benefit of reduced order modeling is the ability to use the ROM created for one initial condition to approximate nearby solutions without having to generate the full solution. Thus, it is ideal for generating ensembles of flow solutions. The time savings, as shown in Table 6.9, compound as each subsequent solution is generated from the original ROM.

Table 6.9. Approximate computation times in hh:mm:ss for full order versus reduced order models

$\overline{U}_{\text{in}}$ (m/s)	Full Model	ROM
0.90	2:00:00	2:08:00
0.88	2:00:00	0:00:03
0.92	2:00:00	0:00:03
Total	6:00:00	2:08:06

In examining Table 6.9 there are considerable savings in computational time when using ROM to consider various input velocity scenarios, but these savings are only useful if reasonable accuracy can be achieved. In order to test the accuracy, we generated full solutions at input velocities of 0.88 m/s and 0.92 m/s. Each of the solutions took approximately two hours to compute on a 35 processor high-performance computer. We then computed the solutions using the previously generated ROM but changed the initial conditions to the alternate input velocities. To load the ROM required about 2 seconds and creating the approximate solution took about 0.5 seconds. The error comparison in Table 6.10 shows that the approximate solutions compare favorably to the actual solutions. Further, as with the earlier simulation, we can see in Figure 6.12 that the ROM solution does a good job of approximating the average output velocity over the entire time of the simulation.

Table 6.10. The error between the actual and reduced order model velocity profiles at 10.0 seconds

$\overline{U}_{\text{in}}$	$\overline{U}\text{out}^{Act}$	$\overline{U}\text{out}^{ROM}$	$\overline{\%U}\text{out}^{Err}$	$\%U^{Err}$
0.88	6.9315	6.9328	0.0180	5.0221
0.92	7.2491	7.2494	0.0048	4.9951

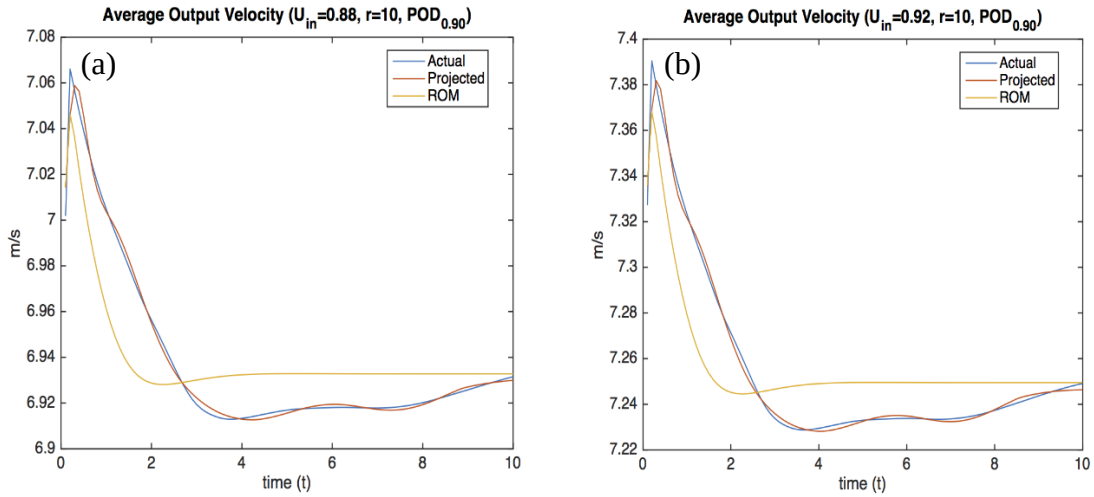

Figure 6.12. Comparison of the airflow in the full model versus the airflow at the same time step generated using various POD modes (a) $\bar{U}_{in}$ = 0.88 m/s (b) $\bar{U}_{in}$ = 0.92 m/s

6.6. Conclusion

This study provides a detailed solution of the airflow in the continuous miner face region using the CFD software as well as a computationally efficient ROM produced using results from the model results. CFD model results were produced for a range of grid sizes and time steps to evaluate convergence. The detailed sensitivity analysis was developed to investigate the simulation performance. The GCI method was applied to calculate the discretization error in the simulations. The estimated error on the fine mesh was 0.2% for average outlet velocity with the usage of 0.1 s as the time step. A change of the time step did not considerably impact the average velocity at the outlet, except for the coarsest mesh (97,000 cells). The improvement in resolution and results precision was achieved as the number of cells increased from 97,051 to 3,680,961 with inconsequential change between 3,680,961 and 18,845,331 cells. It was evident that the 3 million cell results with 0.1 s as the time step are the most efficient number of cells and the time step for investigation of airflow behavior at the CM face region regarding accuracy and simulation cost.

A ROM was developed using proper orthogonal decomposition (POD) to provide a prediction of the entire simulation region state space. POD vectors were utilized for representation of the entire state space as a linear combination of the individual POD

modes. ROM was applied to a continuous miner face with 10.1 m^2 cross section and 15.2 m in length. The ROM resulted in significant increases in computational efficiency (more than 3 orders of magnitude). ROMs were then used to predict conditions with different input conditions, resulting predictions with error of less than 5%. It is evident that ROM is an effective tool for approximating several possible solutions near a known solution, resulting in significant time savings over calculating full solutions and suitable for ensemble calculations. The inlet velocity was not varied substantially here, but we have demonstrated that ROM can be used to effectively study the effect of varying input parameters on an initial model, with relatively few computational resources. Future work will examine the sensitivity of various parameters, including velocity, to further investigate the parameter space in which ROM is reasonably accurate surrogate model.

Due to the large size of transportation tunnels, this technique is applicable for reduction of underground space environments airflow simulation cost such as simulation of the airflow in the subways, metro stations, road tunnels, train tunnels, and parking lots. This approach may also be applicable to a broad range of mining simulations, such as fire dynamics simulations in underground environments, underground mine fires or transportation tunnel fires, with lower cost compared to common CFD practice. It is noteworthy that the quality and quantity of the snapshots played a key role on the creation of the POD modes. In addition, the creation of the actual ROM from the POD modes is challenging for complex fluid flow structures such as airflow in the mine airways. Solving the ROM of more complex flows would likely involve many more basis functions and thus more cost.

6.7. Acknowledgements

This research was developed under Contract No. 200-2014-59669, awarded by the National Institute for Occupational Safety and Health (NIOSH). The findings and conclusions in this report are those of the authors and do not reflect the official policies of the Department of Health and Human Services; nor does mention of trade names, commercial practices, or organizations imply endorsement by the U.S. Government.

6.8. Bibliography

1. Haghighat, A., Luxbacher, K., Lattimer, B., Simulation of methane fire event at a coal mine working face with consideration of ventilation curtain damage. 2016 Transactions of the Society for Mining, Metallurgy & Exploration, 2016; Vol. 340, pp. 120-126.
2. McPherson, M. J., Subsurface ventilation engineering, First edition, CHAPMAN & HALL. Ventilation Network Analysis, Chapter 7, 1993.
3. Kocsis, K. C., New ventilation design criteria for underground metal mines based upon the "Life-Cycle' airflow demand schedule. Ph.D. dissertation, the faculty of graduate studies, mining engineering, The University of British Columbia, Vancouver, Canada, August 2009.
4. Widzyk-Capehart, E., Watson, B., Agnew gold mine expansion mine ventilation evaluation using Ventsim. The 7th international mine ventilation congress. 2001.
5. Brake, D. J., Fire modelling in underground mines using Ventsim Visual VentFIRE Software, Australian mine ventilation conference / Adelaide, Australia, 2013.
6. Layton, W., Introduction to the numerical analysis of incompressible viscous flows. SIAM, 2008.
7. Elman, H. C., Silvester, D. J., and Wathen, A. J., Finite elements and fast iterative solvers: with applications in incompressible fluid dynamics. Oxford University Press, 2014
8. Hargreaves, D.M., Lowndes, I. S., The computational modeling of the ventilation flows within a rapid development drivage. Tunnelling and Underground Space Technology 22, (2007) 150-160.
9. Diego, I., Torno, S., Toraño, J., Menéndez,M., Gent, M., A practical use of CFD for ventilation of underground works. Tunnelling and Underground Space Technology 26, (2011) 189-200.
10. Toraño, J., Torno, S., Menéndez,M., Gent, M., Auxiliary ventilation in mining roadways driven with roadheaders: Validated CFD modelling of dust behavior. Tunnelling and Underground Space Technology 26, (2011) 201-210.

11. Torno, S., Toraño, J., Ulecia, M., Allende, C., Conventional and numerical models of blasting gas behaviour in auxiliary ventilation of mining headings. Tunnelling and Underground Space Technology 34, (2013) 73-81.
12. Sasmito, A., P., Birgersson, E., Ly, H., C., Mujumdar, A., S., Some approaches to improve ventilation system in underground coal mines environment – A computational fluid dynamic study. Tunnelling and Underground Space Technology 34, (2013) 82-95.
13. Hurtado, J. P., Díaz, N., Acuña, E. I., Fernández, J., Shock losses characterization of ventilation circuits for block caving production levels. Tunnelling and Underground Space Technology 41, (2014) 88-94.
14. Cheng, J., Li, S., Zhang, F., Zhao, C., Yang, S., Ghosh, A., CFD modelling of ventilation optimization for improving mine safety in longwall working faces. Journal of Loss Prevention in the Process Industries 40 (2016) 285-297.
15. Antoulas, A. C., Sorensen, D. C., and Gugercin, S, A survey of model reduction methods for large-scale systems. Contemporary Mathematics, 280:193-220, 2001.
16. Chatterjee, A., An introduction to the proper orthogonal decomposition. Current Science, 78(7):808-817, 2000.
17. Baur, U., Benner, P., and Feng, L., Model order reduction for linear and nonlinear systems: A system-theoretic perspective, Arch. Comput. Methods Eng. 21 (2014), no. 4, 331–358.
18. Benner, P., Ohlberger, M., Cohen, A., and Willcox, K., Model reduction and approximation: Theory and algorithms, SIAM, 2017.
19. Benner, P., Gugercin, S., and Willcox, K., A survey of projection-based model reduction methods for parametric dynamical systems. SIAM Review 57 (2015), no. 4, 483–531.
20. Hesthaven, J. S., Rozza, G., and Stamm, B., Certified reduced basis methods for parameterized partial differential equations, Springer, 2016.
21. Antoulas, A. C., Approximation of large-scale dynamical systems, SIAM, 2005.
22. Quarteroni, A., Rozza, G., Reduced order methods for modeling and computational reduction. Modeling, Simulation & Applications, Springer, Volume 9, ISBN 978-3-319-02090-7 (eBook)

23. Noack, B. R., Morzyński, M., Tadmor, G., Reduced-Order modelling for flow control. Springer Vienna, Online ISBN: 978-3-7091-0758-4.
24. Lucia, D. J., Beran PS, Silva WA. Reduced-order modelling: new approaches for computations physics. Progress in Aerospace Sciences 2004;40:51–117.
25. Lieu, T., Farhat, C., Lesoinne, M., Reduced-order fluid/structure modeling of a complete aircraft configuration. Computer Methods in Applied Mechanics and Engineering 2006;195:5730–42.
26. Thomas, J. P., Dowell, E. H., Hall, K. C. Using automatic differentiation to create a nonlinear reduced-order-model aerodynamic solver. The American Institute of Aeronautics and Astronautics Journal 2010; 48:19–24.
27. Braconnier, T., Ferrier, M., Jouhaud, J. C., Montagnac, M., Sagaut, P. Towards an adaptive POD/SVD surrogate model for aeronautic design. Computers & Fluids 2011; 40:195–209.
28. Muld, T. W., Efraimsson, G., Henningson, D. S. Flow structures around a high-speed train extracted using proper orthogonal decomposition and dynamic mode decomposition. Computers & Fluids 2012; 57:87–97.
29. Cesur, A., Carlsson, C., Feymark, A., Fuches, L., Revstedt, J. Analysis of the wake dynamics of stiff and flexible cantilever beams using POD and DMD. Computers & Fluids 2014; 101:27–41.
30. Lumley, J. L. The Structures of Inhomogeneous Turbulent Flow. Atmospheric Turbulence and Radio Wave Propagation, pages 166–178, 1967.
31. Berkooz, G., Holmes, P., Lumley, J. L., The proper orthogonal decomposition in the analysis of turbulent flows. Annual review of fluid mechanics, 25(1):539–575, 1993.
32. Hinze, M., Volkwein. S., Proper orthogonal decomposition surrogate models for nonlinear dynamical systems: Error estimates and suboptimal control. In Dimension Reduction of Large-Scale Systems, pages 261–306. Springer, 2005.
33. Kunisch, K., Volkwein, S., Galerkin, S., proper orthogonal decomposition methods for a general equation in fluid dynamics. SIAM Journal on Numerical analysis, 40(2):492–515, 2002.

34. Shih, T. H., Liou, W. W., Shabbir, A, Yang, Z. And Zhu. J, A New Eddy-Viscosity Model for High Reynolds Number Turbulent Flows - Model Development and Validation. Computers Fluids, 24(3):227-238, 1995.
35. ANSYS, Inc., ANSYS Fluent Theory Guide Help. ANSYS Workbench 14.5, ANSYS, Inc, 2013.
36. Lo, D. S. H., Finite element mesh generation. CRC Press, Taylor & Francis Group. 2015. eBook ISBN: 978-1-4822-6687-0.
37. Roache, P.J., Verification and validation in computational science and engineering, Hermosa Publishers, 1998.
38. Roache, P.J. "Perspective: A method for uniform reporting of grid refinement studies", Journal of Fluids Engineering, Vol. 116, No. 3, pp. 405–413, 1994.
39. Moore. B., Principal component analysis in linear systems: Controllability, observability, and model reduction. IEEE Transactions on Automatic Control, 26(1):17–32, 1981.
40. Mullis, C., Roberts, R., Synthesis of minimum roundoff noise fixed point digital filters. IEEE Transactions on Circuits and Systems, 23(9):551–562, 1976
41. Gugercin, S., Antoulas, A. C., Beattie, C. A., H2 model reduction for large-scale linear dynamical systems. SIAM Journal on Matrix Analysis and Applications, 30(2):609–638, 2008.
42. Bai, Z., Skoogh, D., A projection method for model reduction of bilinear dynamical systems. Linear Algebra and its Applications, 415(2):406–425, 2006.
43. Benner, P., Breiten, T., Interpolation-based H2-model reduction of bilinear control systems. SIAM Journal on Matrix Analysis and Applications, 33(3):859–885, 2012.
44. Flagg, G. M., Gugercin, S., Multipoint Volterra series interpolation and H2 optimal model reduction of bilinear systems. SIAM Journal on Matrix and Analysis and Applications, 2015. Available as arXiv preprint arXiv:1312.2627.
45. Gu, C., QLMOR: a projection-based nonlinear model order reduction approach using quadratic-linear representation of nonlinear systems. Computer-Aided Design of Integrated Circuits and Systems, IEEE Transactions on, 30(9):1307–1320, 2011.
46. Benner, P., Breiten, T., Two-sided projection methods for nonlinear model order reduction. SIAM Journal on Scientific Computing, 37(2):B239–B260, 2015.

47. Antoulas, A. C., Beattie, C. A., Gugercin, S., Interpolatory model reduction of large-scale dynamical systems. Efficient Modeling and Control of Large-Scale Systems, pages 3–58, 2010.
48. Berkooz, G., Holmes, P., Lumley, J. L., The proper orthogonal decomposition in the analysis of turbulent flows. Annual review of fluid mechanics, 25(1):539–575, 1993.
49. Ravindran, S. S., A reduced-order approach for optimal control of fluids using proper orthogonal decomposition, International Journal for Numerical Methods in Fluids 2000; 34: 425–448.
50. Weller, J., Lombardi, E., Bergmann, M., Iollo, A., Numerical methods for low-order modeling of fluid flows based on POD, International Journal for Numerical Methods in Fluids 2010; 63: 249–268.
51. Stefanescu, R., Sandu, A., Navon, L. M., Comparison of POD reduced order strategies for the nonlinear 2D shallow water equations, International Journal for Numerical Methods in Fluids 2014; 76: 497–521.
52. Fang, F., Pain, C. C., Navon, L. M., Xiao, D., An efficient goal-based reduced order model approach for targeted adaptive observations, International Journal for Numerical Methods in Fluids 2017; 83: 263–275.
53. Golub, G. H., Van Loan, C. F., Matrix computations, volume 3. JHU Press, 2012.

7. Determination of Critical Parameters in the Analysis of Road Tunnel Fires

The following paper was submitted to International Journal of Mining Science and Technology. Ali Haghighat conducted the majority of the work and wrote the paper with editorial input from coauthor: Dr. Kray Luxbacher.

7.1. Abstract

The analysis of the fluid characteristics downstream of a fire source in transportation tunnels is one the most important factor in the emergency response, evacuation and the rescue service studies. Some crucial parameters can affect the fluid characteristics downstream of the fire. The research presented in this paper develops a statistical analysis on the computational fluid dynamics (CFD) data of the road tunnel fire simulations in order to quantify the significance of tunnel dimensions, inlet air velocity, heat release rate, and the physical fire size (fire perimeter) on the fluid characteristics downstream of the fire source. The selected characteristics of the fluid (response variables) were the average temperature, the average density, the average viscosity, and the average velocity. A two-level statistically designed program was conducted based on the eight CFD scenarios results. The prediction of the designed statistical models were assessed; then the significant parameters' effects and the parameters interactive effects on different response variables were determined individually. Next, the effect of computational domain length on the selection of the significant parameters downstream of the fire source was analyzed. In this statistical analysis, the linear models were found to provide statistically good prediction. The effect of the fire perimeter and the parameters interactive effects on the average temperature, the average density, the average velocity, and the average viscosity downstream of the fire, were found to be insignificant. By getting further from the fire source, the number of significant parameters on the response variable changes downstream of the fire decreased.

7.2. Introduction

In order to provide the fire safety plan of the occupants and the emergency response layout in the road tunnel fire situations, there is a crucial need to understand the factors that may influence the conditions of people exposed to the closed space (e.g., transportation

tunnel) fires. Due to the interaction of physical and chemical processes (turbulence, combustion, radiation, etc.) in a closed space, tunnel fires are complex phenomena [1]. As a result, fire safety in a tunnel must be carefully considered. Tunnel safety ties to the tunnel design, the tunnel management, and the emergency response. The dimensions of the tunnel (width, height, and length) which are a main parameter of the tunnel design, can play a key role in changes of the build-up heat rate and the rate of smoke stratification during the fire events. The other important parameter of the tunnel design, which affects the tunnel safety, is the ventilation system. The airflow velocity can influence the smoke propagation upstream and downstream of the fire in road tunnel fire events. The second most important element in assessing the tunnel safety, is the traffic management in transportation tunnels. A thorough understanding of the nature of the transportation vehicles (e.g., the size of the vehicles, the produced heat release rate (HRR) output from the fire during a fire event) commuting through a tunnel, can help to design safer, and more reliable emergency response layout [2].

Previous studies have shown that the smoke generation is affected by different parameters such as HRR, ventilation, the dimensions of the obstruction, etc. [3]. Babrauskas and Peacock indicated that HRR is the single most important variable in fire hazard analysis [4]. The other important parameter in terms of smoke propagation is ventilation. Since tunnel fires have limited air access points [5], the fire was assumed to be a fuel-controlled fire in this research study. Therefore, the tunnel dimension, the air velocity, the physical fire size, and the HRR are the most important parameters affecting the transportation tunnel safety.

There is an experimental study on the effect of tunnel cross section and the velocity together on gas temperatures and heat fluxes for the large HRR fire sources (HRR $\geq$ 100 MW). In that study, it was evident that maximum temperature under the ceiling was significantly dependent on the tunnel height changes, while the tunnel width changes, HRR changes, and the longitudinal velocity changes had insignificant impacts on the maximum temperature under the ceiling. In addition, it was noteworthy that by increasing the tunnel dimensions, the downstream temperature decreased. Besides, by increasing the

longitudinal velocity, the gas temperature beneath the ceiling increased [6]. Caliendo et al. conducted a study for safety evaluation of different HGV fire scenarios in the curved bi-directional road tunnels numerically. In that study the effect of the fire source position, tunnel geometry, the longitudinal velocity, and the traffic flow on different parameters such as the gas temperature, airflow velocity, visibility, toxic gas concentration, and the evacuation process were investigated; then, the worst case scenario was determined to be when the HGV was in the middle of the tunnel length [1]. And also, some studies were carried out to determine and calculate the HRR of the vehicle fires in the road tunnels experimentally and numerically in order to the design and propose reliable emergency response layout [7, 8]. Although the outcomes of the explained research studies were utilized extensively for the development of the evacuation models to analyze road tunnel safety [9-12], the interactive effect of different parameters (e.g., tunnel dimension, inlet velocity, HRR, and the fire perimeter) were not investigated. Also, the research studies on determination of the significant parameters on changes of the temperature, density, velocity, and viscosity downstream of the fire source in transportation tunnels are so limited. In addition, the effect of computational domain length on the selection of the significant parameters for changes of the fluid characteristics (e.g., average temperature, average density, average viscosity, and average velocity) downstream of the fire source was not quantified in these studies.

The focus of the research in this paper is to utilize a two-level statistical approach to investigate the effect of the tunnel dimensions, the inlet air velocity, HRR, the fire perimeter, and the parameters interactive effect on the fluid characteristics at different cross sections downstream of the fire. The eight different CFD vehicle fire scenarios for the road tunnel were simulated in Fire Dynamics Simulator (FDS), Version 6.0. The FDS core algorithm is an explicit predictor-corrector scheme, with second order accuracy in space and time with the LES turbulence model which we refer the reader to the FDS technical reference guide [13] for the detailed numerical algorithm in this software. Then, the fluid characteristics such as average temperature, average density, average velocity, and average viscosity at different tunnel cross sections were calculated. The calculated CFD results were analyzed in order to conduct a statistical analysis (a two level fractional factorial

design) for determination of the significant parameters on the mentioned fluid characteristics downstream of the fire source. The linear, quadratic and cubic statistical models were investigated and the prediction of the designed statistical models were assessed via residual analysis and the studentized residuals versus predicted values analysis. Next, the significant parameters on the fluid characteristics at a selected cross section downstream of the fire was determined based on the performed two-level fractional factorial design. Moreover, the effect of the domain length on the significant parameters determination downstream of the fire source was analyzed. The significant parameters were screened via this parametric study. The outcomes of this research can be utilized to decrease the number of simulations in future studies by determination of the significant and insignificant parameters on the change of the fluid characteristics downstream of the fire source. In addition, the findings of this study can be used to modify the tunnel design, the tunnel management (e.g., operational management, traffic management, and the engineering management), firefighting procedures, and the emergency medical assistance to have more robust emergency response layout.

7.3. Parametric Study and Design Considerations

A two-level statistically designed program was conducted to quantify the significant parameters on the responses at different cross sections, downstream of the fire. The two-level fractional factorial design has different advantages. One of the most important its advantages is that the interaction of different parameters on a specified response can be investigated. Furthermore, with the usage of factorial design, the error variance can be decreased [14]. This approach is common to be used to screen the significant parameters on various responses in different research areas [15, 16]. A two-level test program based on the fractional factorial design was performed to evaluate the effects of the heat release rate (HRR), physical fire size, tunnel cross section, and the inlet velocity on the responses such as the average temperature, the average density, the average velocity, and the average viscosity at the cross sections downstream of the fire. Therefore, four main parameters as shown in Table 7.1 were selected due to the previous research studies results. A minimum and a maximum values were selected for each parameter. In

this study, the regular van and bus sizes were used as the minimum and maximum physical fire sizes respectively in this study. Although in NFPA® 502, 2011, it is recommended that 30 MW and 10 MW be used as the peak heat release rates for the bus and the van respectively [17], for investigation of the effect of fire perimeter on different response variables, 30 MW and 10 MW were also considered for the van and the bus fire heat release rate respectively (scenarios 1, 2, 5, and 8 as shown in Table 7.3). The width, length, and the height of the van and bus used in the computational domain were 1.7 X 5.0 X 2.4 m^3 and 2.7 X 12.0 X 3.5 m^3, respectively. Two and three lane standard cross section of road tunnels [18] were considered in this study. The height of the tunnel was set to 7.7 m as the height of Gotthard tunnel in Switzerland. Although pedestrians are not permitted in road tunnels, sidewalks are required and recommended to be greater than or equal to 0.7 m [19]. Therefore, two 0.96 m sidewalks were considered in the geometry of the road tunnels. The length and the height of the whole tunnels were 960 m, and 7.7 m, respectively. The width of the tunnel for the two and three lane transportation tunnels were set to 9.6 m and 15.6 m respectively. The detailed tunnel geometry dimensions used in the simulations are shown in Figures 7.1 (a) and 7.1 (b).

Table 7.1. Two levels (a minimum and a maximum)

Parameters	Minimum	Maximum
Heat release rate (MW)	10	30
Physical fire size (m^3)	Van size (20.4)	Bus size (113.4)
Tunnel cross section (m^2)	73.7 (2 lane)	119.8 (3 lane)
Velocity (m/s)	1.5	5

All of the studies on roll back and critical velocity showed that for the 10 MW to 100 MW fires, the critical velocity varies from 2.5 m/s to 3 m/s [20-24]. It should be considered that the critical velocity can vary due to different hydraulic diameters. Therefore, a study was conducted to calculate the critical velocity for 10 MW and 30 MW vehicle fires in both two and three lane road tunnels with the following equations:

$$V_c = K_1 K_g \left[\frac{gHQ}{\rho C_p A T_f}\right]^{1/3} \quad (7\text{-}1)$$

$$T_f = \left[\frac{Q}{\rho C_p A V_c}\right] + T \tag{7-2}$$

where: V_c is critical velocity in (m/s), K_1 is Froude number factor 1, K_g is grade factor (1), g is acceleration caused by gravity (m/sec^2), H is the height of duct or tunnel at the fire site (m), Q is heat fire is adding directly to air at the fire site (kW), ρ is the average density of the approach (upstream) air (kg/m^3), C_p is specific heat of air (kJ/kgK), A is the area perpendicular to the flow (m^2), T_f is the average temperature of the fire site gases(K), and T is the temperature of the approach air in (K) [49]. The calculated hydraulic diameters for both two lane and three lane road tunnels were 8.53 m and 10.30 m, respectively. The critical velocity varied from 2.6 m/s to 3.7 m/s for 10 MW and 30 MW fires in the associated tunnels. Since the inlet velocity affects the propagation of the smoke and hot gases to the upstream and the downstream of the fire source, a velocity less than critical velocity (1.5 m/s < V_{cr}) and a velocity greater than critical velocity (5 m/s > V_{cr}) was selected for investigation of significant parameters on different responses (Ex: mean temperature, mean velocity, mean viscosity, and mean density) at different cross sections downstream of the fire.

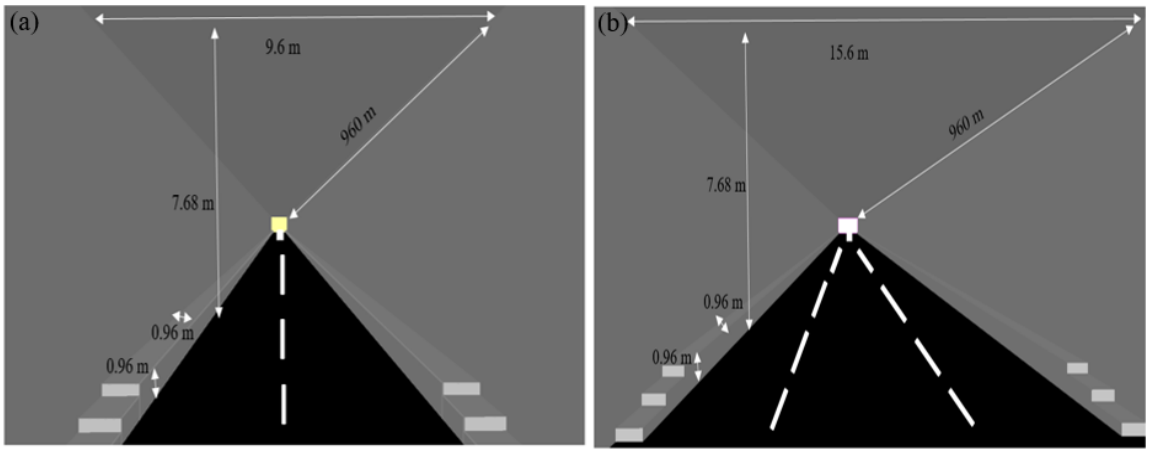

Figure 7.1. Transportation tunnel detailed dimensions (a) two lane (b) three lane

The t-squared approach was utilized for the growth of the vehicle fires [25]. Because of the simulation cost, 1 min was considered as the t_{max} in all simulations. Since the focus of this research study is to investigate the effect of some parameters on the

response variables changes during a fire event, the decay time period for vehicle fires were not considered. Flexible polyurethane foam characteristics as shown in Table 7.2 were used for vehicle fire simulation in the tunnels [26].

Table 7.2. Heat of combustion, CO, CO_2, and soot yields of vehicle fire events in simulation

Material	ΔH_T (kJ/kg)	Y_{CO2} (kg/kg)	Y_{CO} (kg/kg)	Y_{Soot} (kg/kg)
Polyurethane	25300	1.5325	0.02775	0.1875

The thermal and the physical characteristics of the concrete such as density, thermal conductivity, and specific heat [27] were considered for the characteristics of the tunnel's side walls, roof, and the sidewalks. The thermal diffusivity of concrete was set to 0.77 mm^2/s [28]. All the thermal characteristics of the concrete was based on the rock type in the concrete which was assumed to be limestone, sandstone, and chert. And also the sand and aggregate were from the same rock type at early age. The thermal and the physical characteristics of the asphalt were considered for the characteristics of the tunnel pavement. The density, thermal conductivity, and specific heat capacity of the dry asphalt with 5% air voids content were set to 2371.67 kg/m^3, 1.16 W/m°C, and 0.9637 kJ/kg°C, respectively [29]. The ambient air temperature, ambient air density, and air viscosity at ambient temperature were set at 20 ^{O}C, 1.196 kg/m^3, and 1.79e-05 kg/m/s respectively in all simulations. The no-slip boundary condition was considered for all walls, sidewalks, roof, pavement, and the objects in the domain. Fixed air flows based on two different velocities were set to the inlet of computational domain since the jet fans were assumed to be far away from the fire source. Reliable numerical results can be achieved when the grid size is $\leq 0.1D^*$ [30], where D^* is explained in detail in [31, 32]. Therefore, the rectangular cells with a grid size of 24 cm was considered for the numerical analysis based on the used heat release rates (10 MW and 30 MW) in this research study. Consequently, eight computational fluid dynamics (CFD) scenarios as shown in Table 7.3 were simulated to investigate the effect of mentioned parameters (Table 7.1) on average temperature, average density, average velocity, and viscosity at different cross sections downstream of the fire. All the vehicle fires were set at the middle of the road tunnels.

Table 7.3. CFD simulation scenarios based on different parameters

Scenarios	Parameter 1 Velocity (m/s)	Parameter 2 HRR (MW)	Parameter 3 Fire Size (m^3)	Parameter 4 Tunnel Dimension (m^2)
scenario 1	5	10	Bus (114)	2 lanes (73.7)
scenario 2	5	30	Van (20.3)	2 lanes (73.7)
scenario 3	1.5	10	Van (20.3)	2 lanes (73.7)
scenario 4	1.5	30	Bus (114)	2 lanes (73.7)
scenario 5	1.5	10	Bus (114)	3 lanes (119.8)
scenario 6	5	30	Bus (114)	3 lanes (119.8)
scenario 7	5	10	Van (20.3)	3 lanes (119.8)
scenario 8	1.5	30	Van (20.3)	3 lanes (119.8)

7.4. CFD Results and Discussion

To conduct the statistical assessment for determination of the significant parameters (e.g., HRR, physical size of the fire (fire perimeter), tunnel dimension, and airflow velocity) on the fluid characteristics downstream of the fire, there was a need to calculate the average temperature, viscosity, density, and velocity along the height of the tunnel at different cross sections in all scenarios. All parameters were calculated every 5 m upwind and downwind from the fire source and the zero line is the representative of the tunnel cross section at the center of the fire source as shown in Figure 7.2.

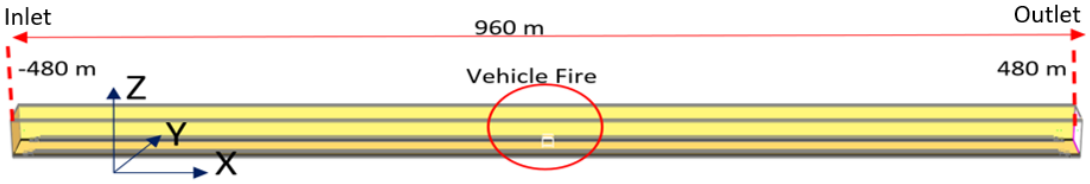

Figure 7.2. The isometric view of the computational domain

The calculated results for average temperature, average density, average viscosity, and average velocity along the height of the tunnel at different cross sections for all scenarios are shown in Figures 7.3 and 7.4. It is noteworthy that the steady-state flow condition in the tunnel was reached at t = 900 s in all scenarios. Therefore, all parameters upwind and downwind of the fire source were calculated at t= 900 s in all scenarios. Due to the considered inlet velocity less than the critical velocity in some scenarios (e.g.,

scenarios 3, 4, 5, and 8), the upwind transport of the smoke (backlayering phenomenon) was observed. The length of the backlayering (rollback) for scenarios 3, 4, 5, and 8 was calculated at 170 m, 270 m, 150 m, and 273 m respectively from the centerline of the fire source. In the rest of the scenarios (e.g., scenarios 1, 2, 6, and 7), due to the velocity greater than critical velocity, just the downwind transport of the smoke was observed.

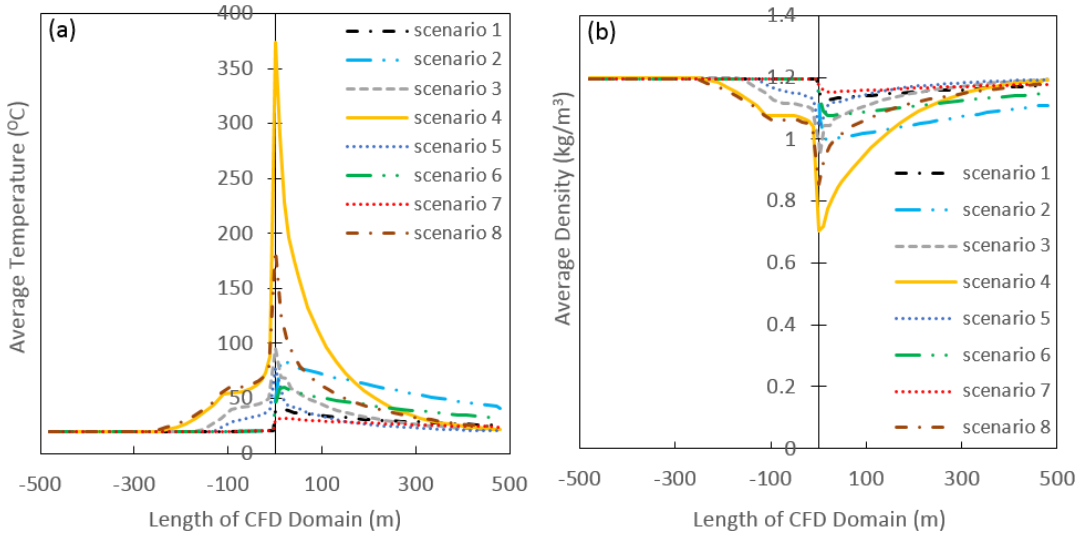

Figure 7.3. Fluid characteristics along the height of the tunnel at different cross sections of the road tunnel at t=900 s for all scenarios (0 on the x-axis represents the middle plane of fire source) (a) average temperature (b) average density

Since, just the downwind transport of the smoke was observed in scenarios with the velocity greater than critical velocity (e.g., scenario 1, 2, 6, and 7), the average temperature, average density, average viscosity, and the average velocity upstream of the fire source was calculated similar to the ambient ones as can be seen in Figures 7.3 and 7.4. According to Figure 7.3 (a), by getting further from the fire source, the average temperature along the height of the tunnel at different cross sections decreased, as expected. The decreasing temperature trend downstream of the fire continued until it eventually ends up the ambient temperature (20 ^{O}C). Consistent with the data of Figure 7.3 (a), it is evident that the average temperature was 20 ^{O}C in scenarios with the velocity greater than critical velocity (scenarios 1, 2, 6, and 7) from the inlet to 4 m from upwind of the end of the fire object, while because of the upwind transport of the smoke (rollback) in scenarios with velocity

less than critical velocity (e.g., scenarios 3, 4, 5, and 8), the average temperature at different cross sections upstream of the fire varied. The highest mean temperature at the fire source was calculated in scenario 4 (373 ^{O}C), due to the highest HRR, the lowest velocity, and the smallest tunnel cross section among all scenarios. Due to the dependency of the density to the temperature, the lowest average density at the fire source was calculated in scenario 4 as shown in Figure 7.3 (b). According to Figure 7.3 (b), it is noteworthy that no appreciable variations in average air density could be observed downstream of the fire source, when the CFD domain length is larger than 300 m. The average density upstream of the fire source was influenced by the upstream transport of smoke and hot gases (backlayering) in scenarios with velocity less than critical velocity (scenarios 3, 4, 5, and 8). However, the average density was measured as same as the inlet air density from the inlet to 4 m from upwind the end of the fire object in scenarios that the velocity was greater than the critical velocity (e.g., scenarios 1, 2, 6, and 7) as shown in Figure 7.3 (b).

The average viscosity and average velocity along the height of the tunnel at different cross sections were calculated as shown in Figures 7.4 (a) and 7.4 (b) respectively. According to Figure 7.4 (a), there were no appreciable variations observed downstream of the fire source, when the CFD domain length is larger than 100 m in all scenarios. Furthermore, the average viscosity and average velocity were measured as 1.79e-05 kg/m/s and 5 m/s, respectively, for scenarios with the velocity greater than critical velocity (scenarios 1, 2, 6, and 7) from the inlet to 4 m from upwind the end of the fire source. The rollback influenced on the average viscosity and the average velocity at different cross sections upstream of the fire source in scenarios with the velocity less than critical velocity (e.g. scenarios 3, 4, 5, and 8) as shown in Figures 7.4 (a) and 7.4 (b). Because of the highest HRR, highest velocity, and the smallest cross section in scenario 2 compared to the other scenarios, the highest viscosity was calculated at 3.5 m downstream of the fire source.

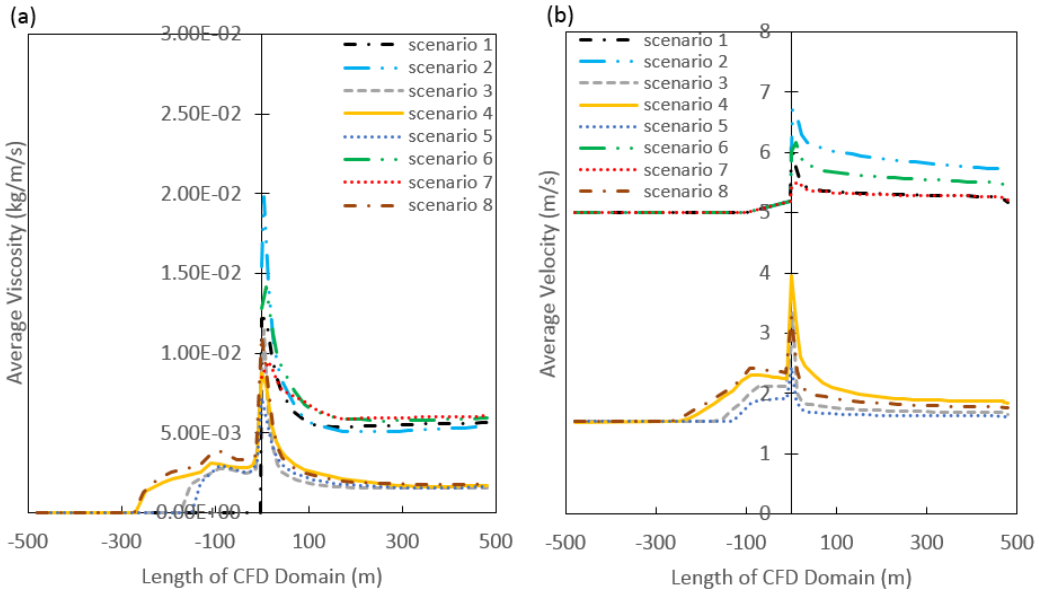

Figure 7.4. Fluid characteristics along the height of the tunnel at different cross sections of the road tunnel at t=900 s for all scenarios (0 on the x-axis represents the middle plane of fire source) (a) average viscosity (b) average velocity

7.5. Parametric Evaluation

A statistically-designed parametric study was performed to investigate the influence of independent variables (e.g., the tunnel dimension, the physical fire size, HRR, and the velocity) on the dependent responses (e.g., the mean temperature, the mean density, the mean velocity, and the mean viscosity) downstream of the fire source, statistically. Four different cross sections, shown in Table 7.4, downstream of the fire were considered to conduct the statistical analysis for determination of the significant parameters on temperature, velocity, viscosity, and density changes. Cross sections 1 to 4 were classified based on a distance from the centerline of the fire source.

Table 7.4. Selected cross sections for calculation of the average variable responses

Cross Section	Downstream Distance (m)
cross section 1	20
cross section 2	120
cross section 3	220
cross section 4	400

To evaluate the parameters and the parameters interactive effects, eight CFD simulations were developed as described in the sections 2 and 3. Next, the response variables (e.g., average temperature, average density, average velocity, and average viscosity) along the height of the tunnel at four selected cross sections (cross sections 1, 2, 3, and 4) at t= 900 s were calculated. The calculated values for the response variables 120 m downstream of the fire source (cross section 2) are provided in Table 7.5 (see Appendix A for the response variables at the cross sections 1, 3, and 4).

Table 7.5. Summary of independent parameters and measured average values for the response variable at cross section 2 (120 m downstream of the fire source) at t=900 s

Scenario no.	Response variables			
	Temperature (^{O}C)	Density (kg/m^3)	Velocity (m/s)	Viscosity (kg/m/s)
scenario 5	30.69	1.16	1.65	0.00196
scenario 8	52.77	1.09	1.88	0.00218
scenario 2	70.60	1.02	5.99	0.00551
scenario 1	33.93	1.14	5.34	0.00556
scenario 3	42.14	1.12	1.75	0.00179
scenario 4	96.59	0.97	2.05	0.00254
scenario 7	28.78	1.16	5.32	0.00623
scenario 6	48.42	1.10	5.64	0.00620

The accuracy of the prediction of the statistical model is related to the selected statistical model [33, 34]. In this statistical analysis, the linear, quadratic and cubic models were investigated. A residual analysis was conducted to make sure the statistical models are well-behaved. The normality of residuals were assessed via the normal probability plot of the studentized residuals as shown in Figures 7.5 (a) to 7.5 (d) for all models which indicates that the error terms were normally distributed when the linear model was performed.

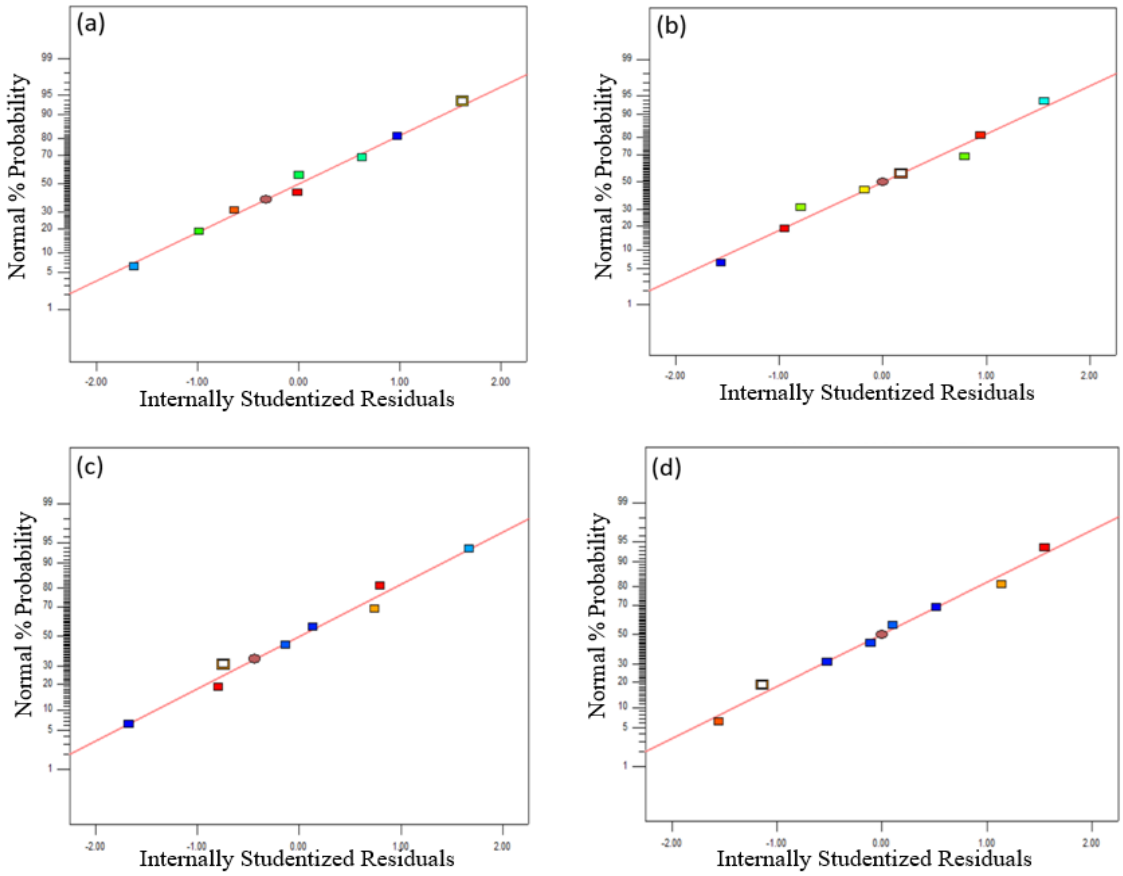

Figure 7.5. Normal plot of residuals, 120 m downstream of the fire (cross section 2) for eight scenarios at t= 900 s for different variable responses (a) average temperature (b) average density (c) average viscosity (d) average velocity

Additionally, the studentized residuals versus predicted values were investigated for three main reasons. First, they were utilized to check that the residuals bounce randomly around the 0 line which indicates that the assumption that the relationship is linear is reasonable. Second, they were used to check the residuals roughly form a horizontal band around the 0 line which indicates that the variances of the error terms are equal. Third, they were used to check that there are no outliers if no one residual stands out from the basic random pattern of residuals [35]. Consistent with the data from the studentized residuals versus predicted values plots, it was evident that there were no unusual data points in the data set. In addition, the results have shown that the variation around the estimated regression line is constant, suggesting that the assumption of equal error variances was reasonable as plotted in Figures 7.6 (a) to 7.6 (d) for average temperature, average density,

average viscosity, and average velocity at cross section 2 (120 m downstream of the fire source).

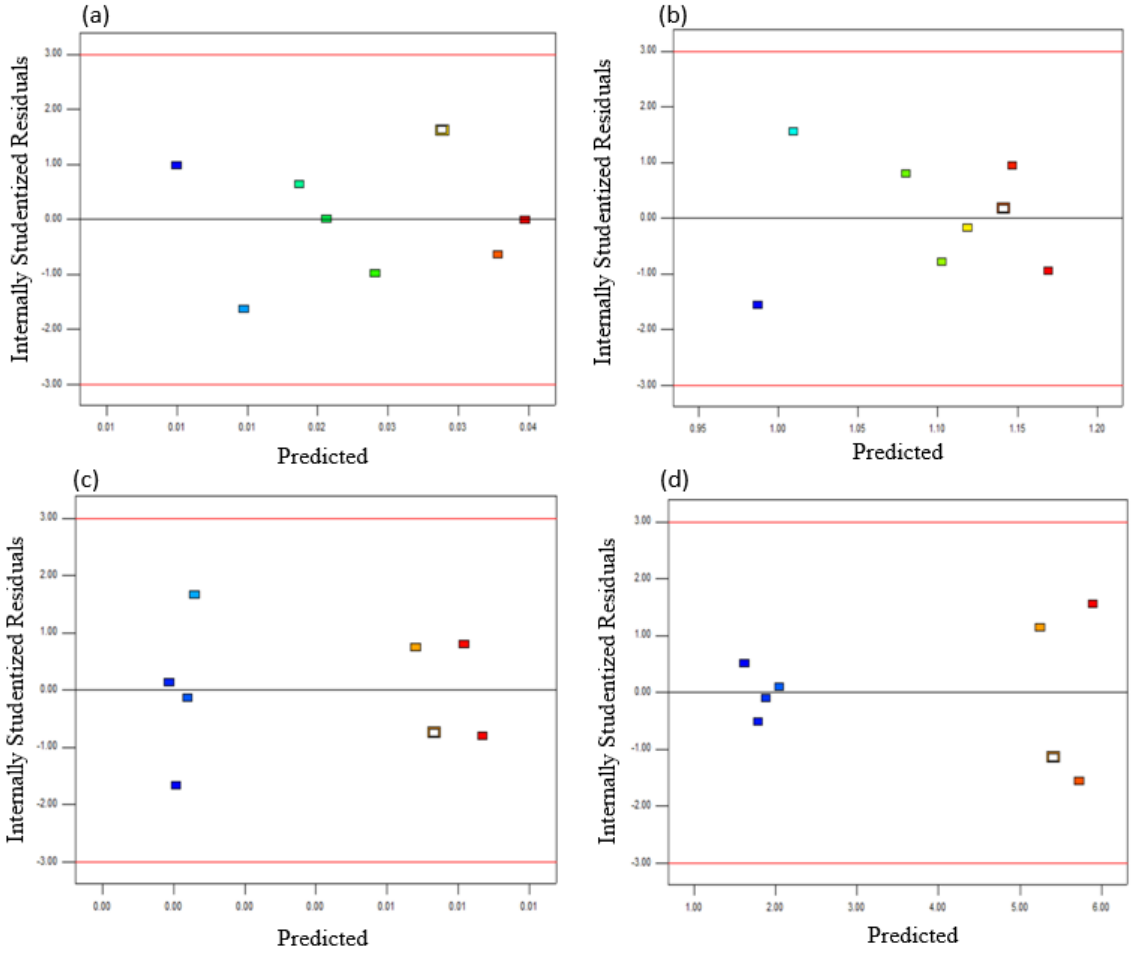

Figure 7.6. Residuals versus Predicted plots, 120 m downstream of the fire (cross section 2) for eight scenarios at t= 900 s for different variable responses (a) average temperature (b) average density (c) average viscosity (d) average velocity

The same studies were conducted at the other cross sections (cross section 1, cross section 3, and cross section 4) in order to investigate the behavior of statistical models when the cross sections were changed. The same behavior was observed when the linear model was utilized at the other cross sections. All in all, the linear models were found to provide statistically good prediction at four selected cross sections downstream of the fire source. The p-values obtained from ANOVA for linear models were calculated less than 0.05 for all models which indicates the models are significant as shown in Table 7.6 (see

Appendix B for the probability of the significant parameters or significant associated interactions on various responses at the cross sections 1, 3, and 4).

Moreover, the coefficient of determination (R^2) was utilized to show that the estimated response variables were accurate by the usage of the models. The R^2 greater than 0.9 indicated that the linear models could predict the average temperature, average viscosity, average velocity, and average density at determined interface boundary accurately. The adjusted coefficient of determination (R^2_{adj}) was quantified for each data set to show that each model was not constrained by a low degree of freedom. The difference between the coefficient of determination and the adjusted coefficient of determination was measured less than 0.0276 at cross section 2 (120 m downstream of the fire) for all of the models as shown in Table 7.6. Therefore, the required standard was met. After acceptance of the model, the parametric and parameter interaction terms were evaluated to determine the significant terms statistically. The null hypothesis for the assessment was that the corresponding coefficient value was zero. The probability of the significant parameters or significant associated interactions on various responses at cross section 2 (120 m downstream of the fire) are shown in Table 7.6 (see Appendix B for the probability of the significant parameters or significant associated interactions on various responses at the other interface boundaries). The criterion for the rejection of insignificant terms was set to a t-value greater than 0.05 confidence level. The t-values for significant parameters are shown in Table 7.6. The air velocity, HRR, the physical fire size (fire perimeter), and the tunnel dimension are characterized by A, B, C, and D respectively. Therefore, the interaction of two parameters could be distinguished via using two letters (e.g., AD is the interaction of their velocity and the tunnel dimension).

Table 7.6. Statistical significance of the parameters and their associated interactions along with fit analysis for the models at cross section 2 (120 m downstream of the fire)

Average Temperature		Average Viscosity		Average Velocity		Average Density	
Parameter	t-statistic	Parameter	t-statistic	Parameter	t-statistic	Parameter	t-statistic
Model	0.0002	Model	0.0011	Model	< 0.0001	Model	0.0073
B-HRR	<0.0001	A-Air velocity	0.0002	A-Air velocity	< 0.0001	B-HRR	0.0024
D-Tunnel dimension	0.0008	R-Squared	0.9944	B-HRR	0.0132	D-Tunnel dimension	0.0098
R-Squared	0.9904	Adj R-Squared	0.9869	R-Squared	0.9989	R-Squared	0.9794
Adj R-Squared	0.9831			Adj R-Squared	0.9975	Adj R-Squared	0.9518

The primary parameters affecting the average temperature at cross section 2 (120 m downstream of the fire) were, in order of significance, the HRR, the tunnel dimension, the air velocity, and the interaction of the air velocity and the tunnel dimension. According to the p-value results in Table 7.6, the HRR and the tunnel dimension had significant contributions on the average temperature changes compare to the other parameter effects on the average temperature (the insignificant parameters (e.g., the air velocity and the interaction of the air velocity and tunnel dimension (AD)) were excluded from the Table 7.6). The effect of the HRR and the tunnel dimension on the average temperature changes at cross section 2 (120 m downstream of the fire) are shown in Figures 7.7 and 7.8 respectively. By varying the HRR from 10 MW to 30 MW, the average temperature at cross section 2 (120 m downstream of the fire) increased conspicuously as shown in Figure 7.7. The temperature increased from 42.1 ^{O}C to 96.6 ^{O}C when the HRR changed from 10 MW to 30 MW in the two lane tunnel with a 1.5 m/s velocity.

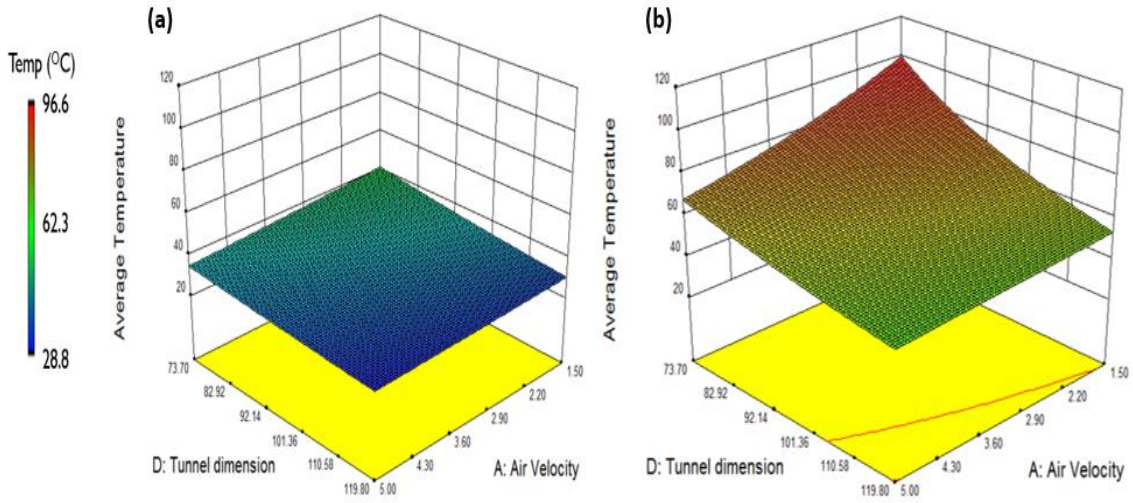

Figure 7.7. The effect of HRR, on the average temperature at cross section 2 (120 m downstream of the fire) at t=900 s (a) 10 MW fire (b) 30 MW fire

The other significant parameter on the changes of the average temperature at cross section 2 was the tunnel cross section as shown in Figure 7.8. According to Figure 7.8, by increasing the tunnel dimension from 2 lane (9.6 m width) to 3 lane (15.6 m width), the average temperature at cross section 2 (120 m downstream of the fire) significantly decreased from 100 ^{O}C to 50 ^{O}C when the HRR and the velocity were 30 MW and 1.5 m/s

respectively. In addition, it was observed that by changing the velocity from 1.5 m/s to 5 m/s, for 10 MW and 30 MW fire scenarios at cross section 2 (120 m downstream of the fire), the average temperature did not experience a drastic change except for the 30 MW fire in a two lane road tunnel as shown in Figure 7.8 (a). All in all, the average temperature in the two lane tunnel was calculated higher compared to the average temperature in the three lane road tunnel a cross section 2. It is noteworthy that changes to the physical size of the fire (fire perimeter) did not affect the average temperature at cross section 2 (120 m downstream of the fire). And also, the interactive effect of other parameters were observed insignificant on the average temperature changes, 120 m downstream of the fire source.

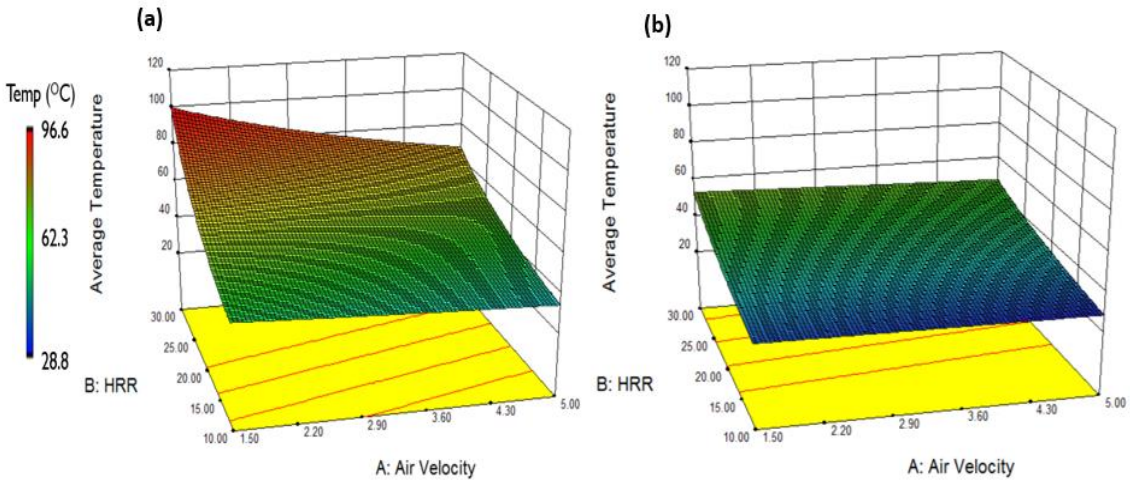

Figure 7.8. Effect of tunnel dimension, on the average temperature at cross section 2 (120 m downstream of the fire) at t=900 s (a) two lane tunnel (73.7 m^2) (b) three lane tunnel (119.8 m^2)

The air velocity was determined as the only significant parameter on the average viscosity changes at cross section 2 as shown in Table 7.6. This study indicates that the other parameter effects or parameter interactions effects on the average viscosity changes were inconsequential (e.g., the effect of HRR changes, tunnel dimension changes, the physical fire size changes), and their interaction on the average viscosity were inconsequential. According to Table 7.6, the significant parameters on the average velocity changes 120 m downstream of the fire source, in order of significance, were the inlet air velocity and the HRR. Therefore, it was observed that the mean velocity at cross section 2 (120 m downstream of the fire) was changed dramatically, by changing the inlet air velocity

and the HRR. Due to the dependency of density to the temperature, the significant parameters on average temperature and average density changes were observed the same (e.g., significant parameters were HRR and tunnel dimension) at cross section 2 (120 m downstream of the fire) as shown in Table 7.6.

7.6. Effect of Domain Length on Significant Parameters Determination

Due to complex dynamical fluid field close to the fire source, different parameters such as temperature, velocity, viscosity, and density close to the fire source could behave differently compare to the values far away from the fire source. Therefore, the significant parameters (e.g., tunnel dimension, physical fire size, HRR, and velocity) on the changes of the response variables could be different close to the fire source compare to the far away from the fire. Due to this, three different cross sections (cross section 1, cross section 3, and cross section 4) were selected to conduct a statistical analysis for determination of the significant parameters on different response variables at the selected cross sections downstream of the fire. Based on the calculated response variables at selected cross sections downstream of the fire (See Appendix A (Tables 7.7, 7.8, and 7.9)), the ANOVA test for linear models as shown in Appendix B were conducted and the significance of the models were assessed based on the p-values. The calculated p-values obtained from ANOVA for the linear models were less than 0.05 for all models which indicates that the models were significant as shown in Tables 7.10, 7.11, and 7.12. Then, the significant parameters on the selected response variables were determined at different cross sections downstream of the fire as shown in Figure 7.9.

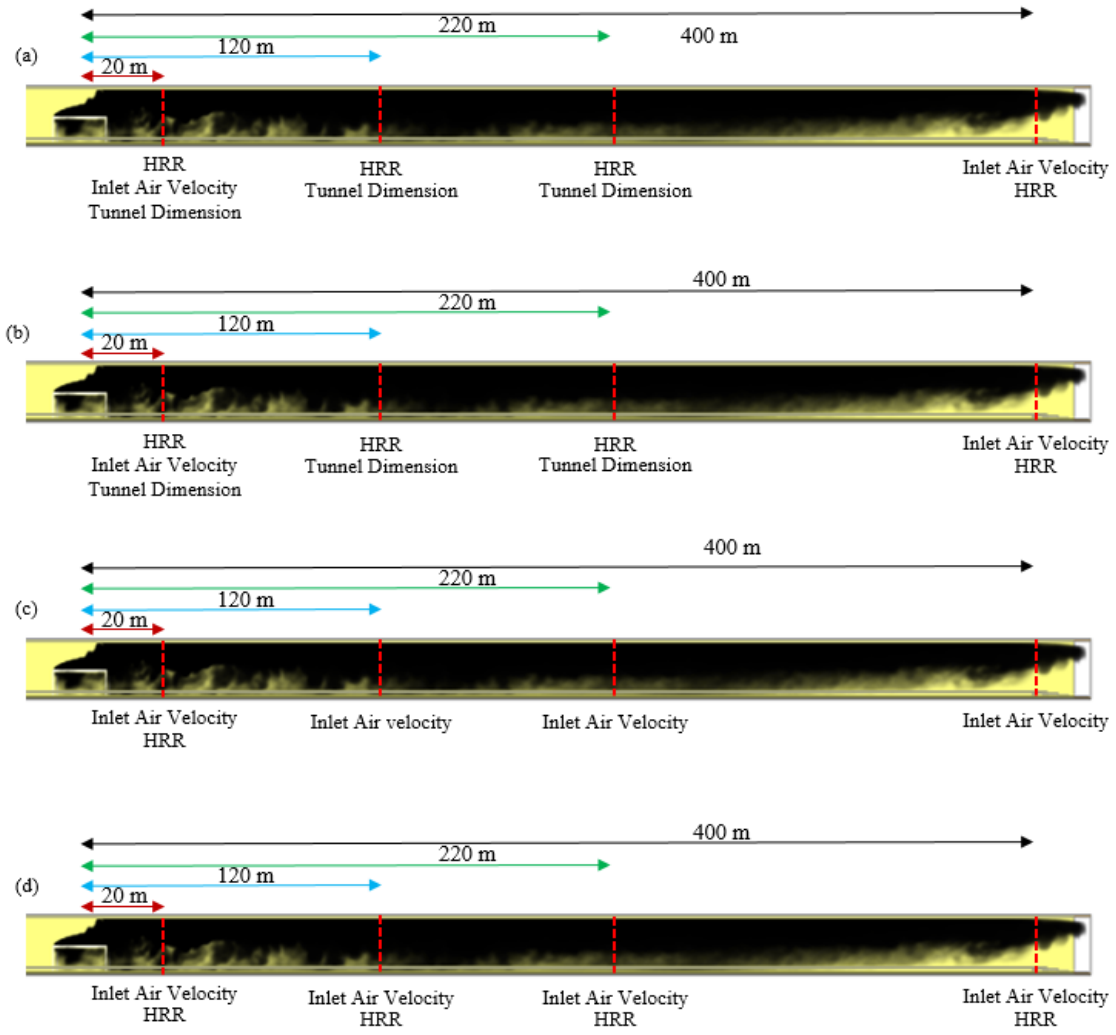

Figure 7.9. Significant parameters on different response variables at different cross sections downstream of the fire source (a) average temperature (b) average density (c) average viscosity (d) average velocity

Consistent with the data of Appendix B and Figure 7.9 (a), it was observed that by getting further from the fire source, the significance of the tunnel dimension on the average temperature at the cross sections decreased from the cross section 1 to the cross section 4. The effect of tunnel dimension on the average temperature changes was insignificant 400 m downstream of the fire source (cross section 4). It is noteworthy that the air velocity was the significant parameter on average temperature changes at cross section 1 (20 m downstream of the fire source) and the cross section 4 (400 m downstream of the fire source) as shown in Figure 7.9 (a). However, it was an insignificant parameter on average

temperature changes at the cross sections 2 and 3 (120 m and 220 m downstream of the fire source). The reason lies in the decreasing trend of the average temperature in the simulations with velocity greater than critical velocity ($V \geq V_{cr}$) compare to the results of the scenarios with velocity less than critical velocity ($V < V_{cr}$) as shown in Figure 7.10. By getting further away from the fire source, the average temperature downstream of the fire source decreased faster in the scenarios that have the velocity less than critical velocity $V<V_{cr}$ (1.5 m/s) in comparison with the scenarios that have the velocity greater than equal to the critical velocity $V \geq V_{cr}$ (5 m/s). According to Figure 7.10, the average temperature difference at the center of the fire source (X=0) was consequential for the same two scenarios with different velocities (e.g., scenarios 1 vs 3, 2 vs 4, 5 vs 7, and 6 vs 8). However, when you get further from the fire source, the average temperature difference decreased until the average temperature was equal at a given cross section as shown in Figure 7.10 (red points). The average temperature difference between two scenarios with the same HRR and tunnel dimensions, but different velocities at that point (red points), was calculated as zero. Therefore, the effect of the average velocity on the average temperature changes at that point was inconsequential. And after that, the average temperature difference again increased, so, the impact of the inlet velocity was to increase the average temperature. In addition, it was observed that the HRR was the only significant parameter on the changes of the temperature at all cross sections downstream of the fire source as shown in Figure 7.9 (a).

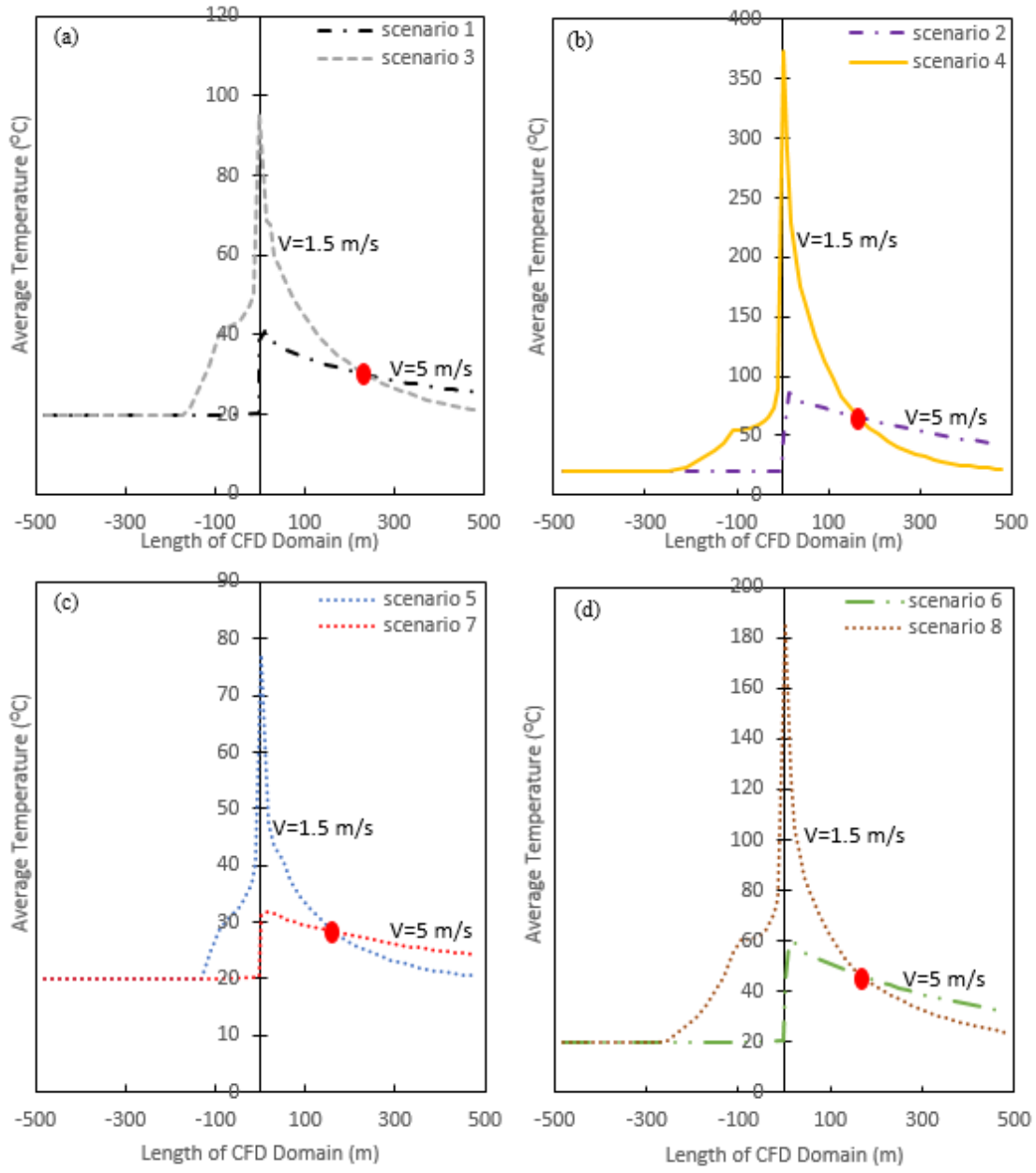

Figure 7.10. The effect of inlet velocity on the average temperature along the height of the tunnel at different cross sections in different scenarios at t= 900 s (a) scenario 1 vs scenario 3 (b) scenario 2 vs scenario 4 (c) scenario 5 vs scenario 7 (d) scenario 6 vs scenario 8

Since the density is temperature dependent, the significant parameters on the average density changes at different cross sections downstream of the fire were the same as the significant parameters on the average temperature changes, as shown in Figure 7.9 (b). Although the HRR had a significant influence on the average viscosity changes at the

cross section 1 (20 m downstream of the fire), the effect of HRR on the changes of the average viscosity at the other cross sections (cross sections 2, 3, and 4) downstream of the fire was inconsequential as shown in Figure 7.9 (c). Due to the high temperature close to the fire source in 30 MW scenarios compared to the scenarios with 10 MW fire, the HRR had a drastic impact on the average viscosity changes. At cross section 2 (120 m downstream of the fire source) and further downstream of the fire, the average viscosity was not changed significantly by changing the HRR from 10 MW to 30 MW as shown in Figure 7.9 (c). The inlet velocity was observed to be the only significant parameter effecting the average viscosity at all selected cross sections downstream of the fire. The reason lies in the upwind transport of the smoke (rollback) in the scenarios with the air velocity less than critical velocity $V < V_{cr}$ (scenarios 3, 4, 5, and 8). Therefore, the average air viscosity downstream of the fire in these scenarios is lower compare to the scenarios with the velocity greater than equal to the critical velocity $V \geq V_{cr}$ (5 m/s) (scenarios 1, 2, 6, and 7). The significant parameters on the average velocity changes at all cross sections downstream of the fire were the inlet air velocity and the HRR as shown in Figure 7.9 (d). Since the fixed flow was set at the tunnel inlet in all scenarios, the impact of tunnel cross section on the average velocity changes was insignificant. It is noteworthy that the physical size of the fire (fire perimeter) did not have the significant effect on the response variables at all cross sections downstream of the fire (from 20 m downstream of the fire to 400 m downstream of the fire).

Overall, by getting further away from the fire source, the domination of tunnel dimension on the changes of the average temperature and the average density downstream of the fire decreased. The changes of the tunnel dimension did not influence the average velocity and the average viscosity downstream of the fire (If the fixed flow were set at the inlet of the computational domain). The only two significant parameters on the changes of the average temperature, average density, and the average velocity 400 m downstream of the fire source, were HRR and the inlet velocity; and also the only significant parameter on the changes of the average viscosity, 400 m downstream of the fire was the inlet velocity. The fire perimeter was an insignificant parameter on the changes of the response variables at all cross sections downstream of the fire. It is noteworthy that the parameters interactive

effects on the response variables (e.g., average temperature, the average density, the average velocity, and the average viscosity) at all cross sections downstream of the fire were also insignificant.

7.7. Conclusion

The significance of tunnel dimensions, inlet air velocity, heat release rate, and the physical fire size (fire perimeter) on the fluid characteristics downstream of the fire source were quantified using CFD simulations data from a test program that was conducted based on a statistical two-level design known as the fractional factorial design. Based on the prediction of the designed statistical models, the linear models were found to provide statistically good prediction. The effect of computational domain length on the selection of the significant parameters downstream of the fire source was analyzed. Based on the parametric evaluation, the key parameters effects and the parameters interactive effects on different response variables (e.g., average temperature, average density, average viscosity, and average velocity) at different cross section downstream of the fire were determined individually.

It is noteworthy that by getting further from the fire source, the number of significant parameters on the response variable changes downstream of the fire decreased. This study has shown that the changes of the physical size of the fire did not influence the average temperature, average velocity, average density, and average viscosity downstream of the fire source. In addition, it was observed that the interactive effect of the parameters was inconsequential on the changes of the average temperature, average density, average velocity, and the average viscosity downstream of the fire source. Therefore, these parameters don't have to be investigated in detail in any numerical analysis study on the aforementioned response variables for 10 MW to 30 MW fires in future tunnel fire studies. It is noteworthy that the HRR changes could change the average viscosity close to the fire source (20 m downstream of the fire). However, the effect of HRR on the average viscosity was inconsequential at 120 m downstream of the fire source and further. Due to effect of the velocity on the upstream transport of the smoke (e.g., scenarios with velocity less than critical velocity ($V<V_{cr}$)), the only key parameter on the average viscosity changes at all

cross sections of the tunnel downstream of the fire was the inlet velocity. Since the density is temperature dependent, the significant parameters on the average temperature and significant parameters on the average density were the same at all cross sections downstream of the fire. The tunnel dimension was one of the key parameters on the changes of the average temperature and the average density through 20 m to 220 m downstream of the fire source; the tunnel dimension effect on the average temperature and the average density was insignificant 400 m downstream of the fire. In addition, the HRR was the only parameter which had significant impact on the average temperature and the average density at all cross sections downstream of the fire. Although the inlet velocity influenced the average temperature and the average density drastically at 20 m and 400 m downstream of the fire source (e.g., cross sections 1 and 4), an insignificant impact of the inlet velocity on the average temperature and the average density at 120 m and 220 m downstream of the fire (e.g., cross sections 2 and 3) was observed. In addition, it was evident that the average velocity at all cross sections downstream of the fire was affected significantly by the changes of the inlet velocity and the HRR. Therefore, the significant parameters on the average velocity changes at all cross sections downstream of the fire were selected as the inlet air velocity and the HRR.

The proposed statistical analysis was demonstrated to be a useful technique for screening the significant parameters on the fluid characteristics downstream of the fire source. Robust emergency response layout design and fire safety plan require numerous simulations to support evaluating the safety of the underground environment. Understanding and screening the key parameters on the fluid characteristics downstream of the fire is required for decreasing the number of fire simulations for future studies and for improving the tunnel fire safety plan of the occupants.

7.8. Acknowledgements

This research was developed under Contract No. 200-2014-59669, awarded by the National Institute for Occupational Safety and Health (NIOSH). The findings and conclusions in this report are those of the authors and do not reflect the official policies of

the Department of Health and Human Services; nor does mention of trade names, commercial practices, or organizations imply endorsement by the U.S. Government.

7.9. Bibliography

1. Caliendo, C., Ciambelli, P., De Guglielmo, M. L., Meo, M. G., Russo, P., "Numerical simulation of different HGV fire scenarios in curved bi-directional road tunnels and safety evaluation", Tunnelling and Underground Space Technology 31 (2012) 33–50.
2. Beard, A., Carvel, R., (2005). The Handbook of Tunnel Fire Safety, Part V, emergency procedures. Thomas Telford Ltd., London, (536pp., ISBN: 0727731688)
3. National Cooperative Highway Research Program (NCHRP) Synthesis 415. (2011). Design fires in road tunnels. A synthesis of highway practice. Project 20-05, Topic 41-05. ISSN 0547-5570. ISBN 978-0-309-14330-1. Library of Congress Control No. 2010943183.
4. Babrauskas, V., and Peacock, R. D., Heat release rate: the single most important variable in fire hazard. Fire Safety Journal, 1992, 18, 255-272.
5. Ingason, H., Li, Y. Z., Lönnermark, A., Tunnel fire dynamics. Springer Science+Business Media New York 2015
6. Fan, C. G., Li, Y. Z., Ingason, H., Lonnermark, A. "Effect of tunnel cross section on gas temperatures and heat fluxes in case of large heat release rate". Applied Thermal Engineering. 93. 2016 pp. 405-415.
7. Ingason, H., Lönnermark, A., "Heat release rates from heavy goods vehicle trailer fires in tunnels" Fire Safety Journal, 40 (2005) 646-668.
8. Migoya, E., García, J., Crespo, A., Gago, C., Rubio, A., "Determination of the heat release rate inside operational road tunnels by comparison with CFD calculations". Tunnelling and Underground Space Technology 26 (2011) 211–222.
9. Alonso, V., Abreu, O., Cuesta, A., Alvear, D., "An Evacuation model for risk analysis in Spanish Road Tunnels". Procedia - Social and Behavioral Sciences 162 (2014) 208 – 217.
10. Capote, J. A., Alvear, D., Abreu, O., Cuesta, A., Alonso, V., "A real-time stochastic evacuation model for road tunnels". Safety Science 52 (2013) 73–80

11. Ronchi, E., Colonna, P., Capote, J., Alvear, D., Berloco, N., Cuesta, A., "The evaluation of different evacuation models for assessing road tunnel safety analysis" Tunnelling and Underground Space Technology 30 (2012) 74–84
12. Seike, M., Kawabata, N., Hasegawa, M., "Quantitative assessment method for road tunnel fire safety: Development of an evacuation simulation method using CFD-derived smoke behavior". Safety Science 94 (2017) 116–127.
13. McGrattan, K., Hostikka, S., McDermott, R., Floyd, J., Weinschenk, C., Overholt, K., (2014). "Fire Dynamics Simulator Technical Reference Guide Volume1: Mathematical Model", NIST special publication 1018, sixth edition. FDS Version 6.1.2. Fire Research Division Engineering Laboratory Gaithersburg, Maryland, USA. SVN repository revision: 20596.
14. Montgomery, D. C., (2012). Design and analysis of experiments. John willy & sons, Inc. Eighth edition. ISBN; 978-1-118-14692-7. Canada.
15. Mukerjee, R., Wu, C. F. J., A modern theory of factorial designs. Springer 2006. ISBN: 978-0-387-31991-9.
16. Anderson, M. J., Whitcomb, P. J., DOE simplified: practical tools for effective experimentation. CRC Press, Taylor & Francis Group. Third edition 2015. ISBN: 978-1-4822-1894-7.
17. National Fire Protection Association (NFPA), "NFPA® 502, Standard for Road Tunnels, Bridges, and Other Limited Access Highways, 2011 Edition," ISBN 978-161665095-7.
18. Maidl, B., Thewes, M., Maidl, U., (2014). Handbook of tunnel engineering II, Basics and additional services for design and construction. Published 2014 by Ernst & Sohn GmbH & Co. KG. ISBN: 978-3-433-03049-3.
19. Hung, C. J., Monsees, J., Munfah, N., Wisniewski, J.,. "Technical Manual for Design and Construction of Road Tunnels — Civil Elements". AASHTO publication. U.S. department of transportation federal highway administration. Publication No. FHWA-NHI-10-034. (2009). http://www.fhwa.dot.gov/bridge/tunnel/pubs/nhi09010/tunnel_manual.pdf
20. Oka Y, Atkinson GT (1995) Control of smoke flow in tunnel fires. Fire Safety Journal. 25(4):305–32.

21. Wu, Y., Bakar, M. Z. A., (2000). Control of smoke flow in tunnel fires using longitudinal ventilation systems—a study of the critical velocity. Fire Safety Journal, 35:363–390 13.
22. Vauquelin, O., Wu, Y., (2006). Influence of tunnel width on longitudinal smoke control. Fire Safety Journal. 41:420–426.
23. Kunsch, J. P., (2002). Simple model for control of fire gases in a ventilated tunnel. Fire Safety Journal, 37(1):67–81.
24. Hwang, C. C., Edwards, J. C., (2005). The critical ventilation velocity in tunnel fires – a computer simulation. Fire Safety Journal, 40:213–244.
25. Ingason, H., (2009). Design fire curves for tunnels. Fire Safety Journal 44, 259-265.
26. Tewarson, A., (1995). SFPE Handbook of Fire Protection Engineering, second edition, Section 3, Chapter 4, eds: P DiNenno, C Beyler, R Custer and W Walton, National Fire Protection Association.
27. Bamforth, B., Chisholm, D., Gibbs, J., Harrison, T., (2008). Properties of Concrete for use in Eurocode 2: How to optimise the engineering properties of concrete in design to Eurocode 2. A cement and concrete industry publication. ISBN 1904482392, 9781904482390.
28. Laage,L. W., Greuer, R. E., Pomroy, W. H., (1995). "MFIRE users' manual". Version 2.20.
29. Hassn, A., Chiarelli, A., Dawson, A., Garcia, A., (2016). Thermal properties of asphalt pavements under dry and wet conditions. Materials and Design 91, 432-439.
30. McGrattan, K., Baum, H., and Rehm, H., (1998). Large eddy simulation of smoke movement. Fire Safety Journal, 30, 161-178.
31. Baum, H. R. & McCaffrey, B. J., Fire induced flow field-theory and experiment. In Fire Safety Science, Proc. 2nd Int. Symp. Hemisphere, New York, 1989, pp. 129—48.
32. Yuan, L., Mainiero, R. J., Rowland, J. H., Thomas, R. A. T., Smith, A. C. S., (2014). Numerical and experimental study on flame spread over conveyor belts in a large-scale tunnel. Journal of Loss Prevention in the Process Industries, Volume 30, July 2014, Pages 55–62.
33. Freedman, D., "Statistical models: theory and practice". Cambridge University Press, 2005.

34. Freedman, D., Pisani, R.., Purves, R., “Statistics”. W.W. Norton, 1998.
35. Lyman, O., Longnecker, M., An introduction to statistical methods and data analysis. 5th ed. Duxbury/Thomson Learning. 2001, ISBN: 9780534251222.

Appendix A: Chapter 7 Supplemental Data

The calculated values for the response variables at 20 m, 220 m, and 400 m downstream of the fire source (e.g., cross sections 1, 3, and 4) are provided in Tables 7.7, 7.8, and 7.9 respectively.

Table 7.7. Summary of independent parameters and measured values for the response variable at cross section 1 (20 m downstream of the fire source) at t=900 s

Scenario no.	Response variables			
	Temperature (^{O}C)	Density (kg/m^{3})	Velocity (m/s)	Viscosity (kg/m/s)
scenario 5	47.22	1.11	1.74	0.00434
scenario 8	104.07	0.98	2.11	0.00539
scenario 2	83.70	1.00	6.29	0.01107
scenario 1	39.96	1.13	5.51	0.00981
scenario 3	67.80	1.04	1.87	0.00409
scenario 4	228.90	0.77	2.61	0.00548
scenario 7	31.65	1.15	5.46	0.00891
scenario 6	60.02	1.08	5.94	0.01167

Table 7.8. Summary of independent parameters and measured values for the response variable at cross section 3 (220 m downstream of the fire source) at t=900 s

Scenario no.	Response variables			
	Temperature (^{O}C)	Density (kg/m^{3})	Velocity (m/s)	Viscosity (kg/m/s)
scenario 5	25.16	1.17	1.63	0.00167
scenario 8	38.42	1.13	1.82	0.00188
scenario 2	61.16	1.05	5.89	0.00509
scenario 1	30.75	1.15	5.31	0.00544
scenario 3	31.66	1.15	1.71	0.00156
scenario 4	50.70	1.09	1.93	0.00198
scenario 7	27.09	1.17	5.30	0.00593
scenario 6	42.38	1.11	5.59	0.00584

Table 7.9. Summary of independent parameters and measured values for the response variable at cross section 4 (400 m downstream of the fire source) at t=900 s

Scenario no.	Response variables			
	Temperature (^{O}C)	Density (kg/m^{3})	Velocity (m/s)	Viscosity (kg/m/s)
scenario 5	21.30	1.19	1.62	0.00158
scenario 8	26.63	1.17	1.78	0.00180
scenario 2	46.71	1.10	5.75	0.00529
scenario 1	26.72	1.17	5.28	0.00559
scenario 3	22.89	1.19	1.69	0.00155
scenario 4	24.76	1.18	1.88	0.00166
scenario 7	24.91	1.18	5.28	0.00603
scenario 6	34.82	1.14	5.51	0.00586

Appendix B: Chapter 7 Supplemental Data

The probability of the significant parameters or significant associated interactions on various responses 20 m, 220 m, and 400 m downstream of the fire source (e.g., cross sections 1, 3, and 4) are shown in Tables 7.10, 7.11, and 7.12 respectively.

Table 7.10. Statistical significance of the parameters and their associated interactions along with fit analysis for the models at cross section 1 (20 m downstream of the fire source)

Temperature		Viscosity		Velocity		Density	
Parameter	t-statistic	Parameter	t-statistic	Parameter	t-statistic	Parameter	t-statistic
Model	0.0003	Model	< 0.0001	Model	< 0.0001	Model	0.0077
B-HRR	< 0.0001	A-Air velocity	< 0.0001	A-Air velocity	< 0.0001	B-HRR	0.0050
A-Air velocity	0.0003	B-HRR	0.0032	B-HRR	0.0088	A-Air velocity	0.0161
D-Tunnel dimension	0.0009	R-Squared	0.9863	R-Squared	0.9929	D-Tunnel dimension	0.0321
R-Squared	0.9978	Adj R-Squared	0.9808	Adj R-Squared	0.9901	R-Squared	0.9351
Adj R-Squared	0.9950					Adj R-Squared	0.8864

Table 7.11. Statistical significance of the parameters and their associated interactions along with fit analysis for the models at cross section 3 (220 m downstream of the fire source)

Temperature		Viscosity		Velocity		Density	
Parameter	t-statistic	Parameter	t-statistic	Parameter	t-statistic	Parameter	t-statistic
Model	0.0003	Model	< 0.0001	Model	< 0.0001	Model	0.0156
B-HRR	< 0.0001	A-Air velocity	< 0.0001	A-Air velocity	< 0.0001	B-HRR	0.0044
D-Tunnel dimension	0.0016	R-Squared	0.9810	B-HRR	0.0147	D-Tunnel dimension	0.0272
R-Squared	0.9879	Adj R-Squared	0.9778	R-Squared	0.9992	R-Squared	0.9656
Adj R-Squared	0.9788			Adj R-Squared	0.9981	Adj R-Squared	0.9197

Table 7.12. Statistical significance of the parameters and their associated interactions along with fit analysis for the models at variable at cross section 4 (400 m downstream of the fire source)

Temperature		Viscosity		Velocity		Density	
Parameter	t-statistic	Parameter	t-statistic	Parameter	t-statistic	Parameter	t-statistic
Model	0.0019	Model	< 0.0001	Model	< 0.0001	Model	0.0355
A-Air velocity	0.0031	A-Air velocity	< 0.0001	A-Air velocity	< 0.0001	A-Air velocity	0.0299
B-HRR	0.0034	R-Squared	0.9894	B-HRR	0.0135	B-HRR	0.0337
R-Squared	0.9181	Adj R-Squared	0.9876	R-Squared	0.9994	R-Squared	0.9190
Adj R-Squared	0.8853			Adj R-Squared	0.9987	Adj R-Squared	0.8432

8. Development of a Methodology for Interface Boundary Selection in the Multiscale Road Tunnel Fire Simulations

This paper was submitted to the Fire Technology. Ali Haghighat conducted all of the work and wrote the paper with editorial input from coauthors: Dr. Kray Luxbacher and Dr. Brian Lattimer.

8.1. Abstract

The simulation of large complex dynamical systems such as a fire in road tunnels is costly. Therefore, there is a crucial need to design efficient models. Coupling of Computational Fluid Dynamics (CFD) models and 1D network modeling simulations of a fire event, a multiscale method, can be a useful tool to increase the computational efficiency while the accuracy of simulations is maintained. The boundary between a CFD model (near field) and a 1D model (far field) plays a key role in the accuracy of simulations of large systems. The research presented in this paper develops a novel methodology to select the interface boundary between the 3D CFD model and a 1D model in the multiscale simulation of vehicle fire events in a tunnel. A detailed fluid dynamics analysis was utilized to determine the interface boundary between CFD and 1D models during vehicle fire events in a road tunnel. The effect of changes in heat release rate (HRR) and air velocity on the selection of an interface boundary was investigated. An indirect coupling strategy was utilized to couple CFD models to 1D models at the selected interface boundary; then, the coupled models results were compared to the full CFD model results. The calculated error between CFD and coupled models for mean temperature and velocity at different cross sections is less than 5%. The findings were used to recommend a modification to the selection of interface boundary in multiscale fire simulations in the road tunnels and more complex geometries such as mines.

8.2. Introduction

The simulation cost of a complex dynamical system is an important consideration in engineering design and analysis, especially in fire protection engineering. One of the most common numerical approaches is computational fluid dynamics (CFD). The CFD

numerical analysis is often utilized for precise studies of fluid behavior in underground space environments (Ballesteros-Tajadura et al., 2006; Diego et al., 2011; Stefopoulos et al., 2007; Yuan et al., 2007). This kind of numerical analysis is common to be utilized near fire field. For large domains such as road tunnel environments, network modeling software, one-dimensional (1D) simulations, can be a useful tool for fire analysis at the far field, because of low computational requirements. However, the 1D modeling approach cannot analyze the characteristics of complex flow regions encountered close to the fire source. Therefore, the multiscale methodology is a useful approach to couple a CFD solver with a 1D model to maintain the accuracy and increase the computational efficiency. This approach has been used extensively in different fields. This technique was applied successfully in environmental engineering, mechanical engineering, and bio engineering (Choi et al., 2012; Kuprat et al., 2013; Nobile, 2009; Wang and Chen, 2008). The advantage of proposed method is the reduction in the overall computation time.

Coupling methods have been used in the simulation of airflow and fire in the transportation tunnels. Colella et al. coupled CFD and 1D models of a tunnel ventilation system to decrease the ventilation simulation cost in transportation tunnels. This approach allows for the complexity of full CFD models of flow in tunnels and the inaccuracies of simplified 1D models can be avoided (Colella et al., 2009). Colella et al. also worked on simulation of tunnel ventilation flows during fires. In that study, a simple 1D network approach was utilized to simulate tunnel regions where the flow structure is 1D (far field), and for flow conditions require three-dimensional (3D) resolution (near field), CFD was utilized. Different fire sizes ranging from 10 MW to 100 MW were investigated with a variable number of velocities. Both direct and indirect coupling strategies in steady state condition were utilized and compared. Several multiscale simulations were run to identify the interface boundary limit which is referred to as the interface boundary independence study. In this study, the CFD domain was gradually increased while the 1D domain was gradually decreased. Then the associated average error was calculated with the following norm:

$$\varepsilon_{\varphi} = \frac{\sum_{j=1}^{N} |\vartheta_{j,CFD} - \vartheta_{j,ms}|}{N\overline{\vartheta_{CFD}}} \tag{8-1}$$

where $\vartheta_{j,CFD}$ and $\vartheta_{j,ms}$ are the values calculated in each grid point j belonging to the reference section of interest and $\overline{\vartheta_{CFD}}$ is the averaged predicted by the full CFD simulation. The subscripts *CFD* and *ms* refer to the full CFD and multiscale simulation results. The summation over j is extended to all the N grid points belonging to the specific section of the domain under study. The average of parameters, such as average temperature and average longitudinal velocity, were used for calculation of errors. It was recommended that the location of downstream interface boundary should be at a distance from the fire larger than 13 times the hydraulic diameter (D_h) when the velocity is close to the critical velocity (Colella et al., 2011a). The recommended ratio between hydraulic diameter and the distance from the fire to the downstream interface boundary provided good agreement with the same ratio which was recommended by Van Maele for different fire scenarios in a small scale tunnel (Van Maele and Merci, 2008). In addition, the multiscale approach was utilized to study the transient flow interaction between a growing fire and a ramping-up ventilation scenario. The time required to reach critical velocity conditions to remove rollback was investigated in that study. The results from multiscale approach showed that the required computing time decreased by 40 times without any loss of accuracy compared to the full CFD model (Colella et al., 2011b). In previous research studies, several multiscale simulations were simulated in order to determine the interface boundaries (Colella et al., 2011a). The lowest average error between CFD and coupled models at different cross sections was the criterion for selection of the interface boundary. Therefore, an iterative method was utilized to reduce the boundary, and to compare the coupled model with the full-order CFD model across the entire domain. However, in this study, a novel methodology was developed based on the fundamental physics of fluid, including the physics of the fluid structure, turbulent kinetic energy (TKE), and the vortex dynamics to determine the interface boundaries. Since this methodology considers the physical mechanism driving flow it can easily be applied to different underground spaces with more complex geometry.

In addition, in previous research studies, the Reynolds-Averaged Navier-Stokes (RANS) equations were used for simulation of the turbulent fluctuations of CFD results. This approach, which has been largely used to simulate fire and smoke propagation (Breuer et al., 1996; Colella et al., 2011a, 2011b; Galdo Vega et al., 2008; Van Maele and Merci, 2008; Wang and Chen, 2008; Wu and Baker, 2000), can provide results for mean quantities with acceptable accuracy at moderate cost. However, this approach has its own limitations. Van Maele and Merci applied and compared both RANS and Large Eddy Simulation (LES) approaches for well-ventilated horizontal tunnel fires. The measured critical velocity in the experiment was compared to LES and RANS simulations, and the temperature contours of the LES simulations for 30 kW fire showed better agreement with the experimental results than the RANS simulations results. Moreover, the turbulent thermal diffusion in the LES simulation showed better agreement than in the RANS simulations due to the large-scale unsteadiness in the LES (Van Maele and Merci, 2008). LES bears less modeling uncertainties such as wakes of bluff bodies' structure in comparison with RANS, because the flow behavior is dominated by large-scale anisotropic vortical structures (Frohlich and Von Terzi, 2008). Although RANS simulations have lower computation cost, by a factor of 10 to 100 (Breuer et al., 1996), LES was preferred for this study for the reasons just described.

This research focuses on the development of a methodology to determine the interface boundary region upstream and downstream of a fire source in the transportation tunnels to decompose the domain into 3D and 1D domains via detailed fluid dynamics analysis. Consistent with the data from previous research studies, the interface boundary should be located in the regions where the flow structure is 1D (Colella et al., 2009, 2010, 2011a; Van Maele and Merci, 2008). In order to determine the interface boundary, it is necessary to find the region where the flow-field is quasi-1D, meaning that the streamwise component of the fluid dominates the flow-field (Colella et al., 2011b). On the other hand, the continuity of the following quantities at the interface boundaries (i and j, as shown in Figure 8.1) should also be met (Formaggia et al., 2001).

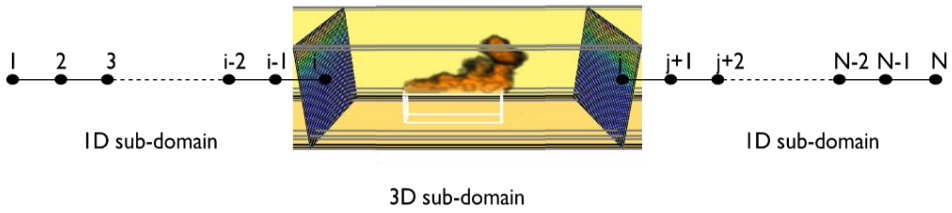

Figure 8.1. Decomposition of the global domain into 1D and 3D sub-domains (after (Colella et al., 2011a))

$$Area\ A(a^-) = A(a^+) \tag{8-2}$$

$$Mean\ pressure\ p(a^-) = p(a^+) \tag{8-3}$$

$$Mean\ velocity\ \bar{v}(a^-) = \bar{v}(a^+) \tag{8-4}$$

$$Mean\ Temperature\ \bar{T}(a^-) = \bar{T}(a^+) \tag{8-5}$$

Therefore, since the mean information of fluid (mean velocity, mean temperature, mean pressure) are transferred at the 1D-3D interface in both directions, all the node values of the 3D model at the interface should be almost uniform and close to the mean values. Under these circumstances, the single value (mean value) of the 3D model at the interface boundary can be the precise representation of all the nodes in that cross section of a dynamic system. Therefore, a detailed fluid dynamics study was conducted to investigate the distribution and behavior of the longitudinal velocity component (u-velocity) and transversal velocity components (v- and w-velocities) of all nodes at different cross sections. In order to determine the quasi-1D flow structure region, there is a need to investigate the tendency of fluid particles to rotate in the system, the physics of the vortex dynamics, and also the intensity of turbulence of the system. Due to this, the mean vorticity along the X, Y, and Z axes and the mean turbulent kinetic energy at different cross sections of the tunnel were analyzed.

The computational fluid dynamics software Fire Dynamics Simulator (FDS), Version 6.0 was used to determine the regions where the flow structure is 3D versus quasi-1D. The FDS core algorithm is an explicit predictor-corrector scheme, with second order accuracy in space and time. Turbulence in this software is modeled via (LES) (McGrattan

et al., 2014). LES has been used extensively for the simulation of the fire in different research areas such as fire plume studies, flame height studies, plume temperature, mine fires, and etc. (Frohlich and Von Terzi, 2008; Gutiérrez-Montes et al., 2009; Haghighat et al., 2016; Heskestad, 2008; Hurley and Munguia, 2009; Liang et al., 2003; Ma and Quintiere, 2003; McGrattan et al., 1998; Yuan et al., 2014). The formulation of the equations and the numerical algorithm are described elaborately in the FDS technical reference guide to which we refer the reader (McGrattan et al., 2014). For the road tunnel fire scenarios two different velocities and two different heat release rates (HRR) were utilized to investigate the effect of HRR and velocity changes on the selection of 1D-3D interface boundary. The interface boundary regions were determined according to study results. Then, the 1D models were simulated via VentFIRE™ in order to couple to the full CFD simulations. VentFIRE™ is a module of Ventsim Visual program which the transport of the smoke and heat are simulated via a discrete sub-cell transport and node mixing method (Ventsim Visual™, 2016). The indirect coupling strategy was utilized for coupling of CFD models to 1D models; the coupled results were compared to the full CFD and 1D models. Ultimately, a methodology was developed and recommended for selection of the interface boundary for multiscale simulation of fire in road tunnels.

8.3. Simulation Consideration

Three computational fluid dynamics (CFD) scenarios were considered to investigate the significant parameters for the selection of interface boundaries for the development of a multiscale methodology applied to road tunnel fire simulations. FDS was utilized to predict the conditions that develop due to the 10 MW and 30 MW vehicle fires in a 2 lane road tunnel. A two lane standard cross section of a road tunnel (Maidl et al., 2014), as considered in this study. The height of tunnel was set to 7.7 m. Although pedestrians are not permitted in road tunnels, the sidewalks are required and recommended to be greater than or equal to 0.7 m (Hung et al., 2009). Therefore, two 0.96 m sidewalks were considered in the geometry of the road tunnels. The thickness of the walls were set to 0.24 m. The length, the width, and the height of the whole tunnel was 960 m, 9.6 m, and

7.7 m, respectively. The detailed tunnel geometry dimensions used in the simulations are shown in Figure 8.2.

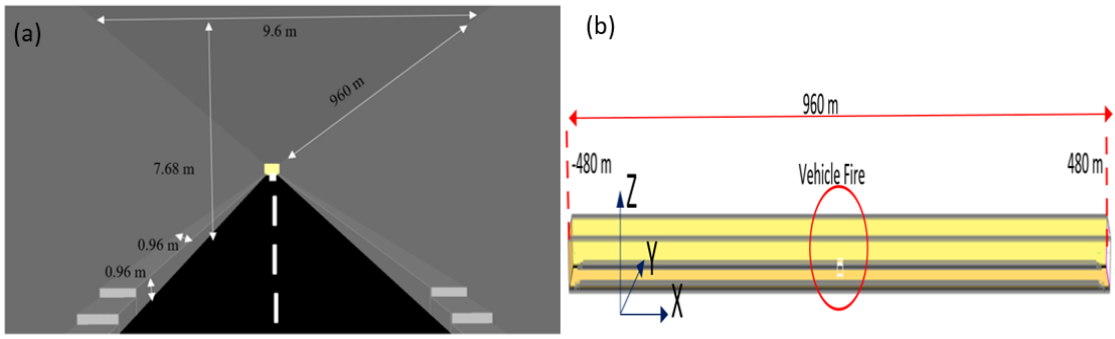

Figure 8.2. Two lane transportation tunnel dimensions and layout (a) tunnel dimension (b) isometric view of the computational domain

Previous studies have shown that smoke generation is affected by different parameters, including HRR, ventilation, and the dimension of the obstruction (National Cooperative Highway Research Program (NCHRP) Synthesis 415, 2011). Babrauskas and Peacock discussed the HRR as the single most important variable in fire hazard (Babrauskas and Peacock, 1992), while the other important parameter in terms of smoke propagation is ventilation (Beard and Carvel, 2005).

Studies examining roll back and critical velocity show that the critical velocity varies from 2.5 m/s to 3 m/s for the 10 MW to 100 MW fires (Hwang and Edwards, 2005; Kunsch, 2002; Oka and Atkinson, 2006; Vauquelin and Wu, 2006; Yuan et al., 2014). Critical velocity varies based on the hydraulic diameter of a tunnel. Thus, the critical velocity was calculated for 10 MW and 30 MW vehicle fires in the simulated road tunnel in this study with the following equations:

$$V_c = K_1 K_g \left[\frac{gHQ}{\rho C_p A T_f}\right]^{1/3} \tag{8-6}$$

$$T_f = \left[\frac{Q}{\rho C_p A V_c}\right] + T \tag{8-7}$$

where: V_c is critical velocity in (m/s), K_1 is Froude number factor 1, K_g is grade factor (1), g is acceleration caused by gravity (m/sec^2), H is the height of duct or tunnel at the fire site (m), Q is heat fire is adding directly to air at the fire site (kW), ρ is the average density of the approach (upstream) air (kg/m^3), C_p is specific heat of air (kJ/kgK), A is the area perpendicular to the flow (m^2), T_f is the average temperature of the fire site gases (K), and T is the temperature of the approach air in (K) (National Fire Protection Association (NFPA), "NFPA® 502, 2011). The calculated hydraulic diameter for the two lane road tunnel was 8.53 m. The critical velocity varied from 2.6 m/s to 3.7 m/s for 10 MW and 30 MW fires in the associated tunnel. The effect of various air velocities on back layering phenomenon in the simulated road tunnels is shown in Figure 8.3.

Figure 8.3. The effect of different velocities on smoke propagation of 10 MW and 30 MW vehicle fires in the road tunnel at t=100 s (a) 10 MW, 1.5 m/s (b) 10 MW, 2.8 m/s (c) 10 MW, 5 m/s (d) 30 MW, 1.5 m/s (e) 30 MW, 3.7 m/s (f) 30 MW, 5 m/s

According to NFPA® 502, the maximum tolerable air velocity under emergency conditions for motorists is 11 m/s. Also, the minimum air velocity should be enough to prevent the smoke rollback (National Fire Protection Association (NFPA), "NFPA® 502, 2011). In this study, a velocity less than critical velocity (1.5 m/s < V_{cr}) was selected for investigation of interface boundary region where the smoke and hot gases propagates to the upstream and the downstream of the fire. Moreover, a velocity greater than critical velocity (5 m/s ≥ V_{cr}) was selected for investigation of interface boundaries when the smoke propagates just downstream of the fire. The main purpose of selected velocities was, to investigate the effect of air velocity changes on the interface boundaries determination. Two different HRR (10 MW, 30 MW) were considered as the peak heat release rates for the van and the bus fires respectively (National Fire Protection Association (NFPA), "NFPA® 502, 2011). The t-squared approach was used for the growth of the vehicle fires. The time to reach maximum HRR (t_{max}) for van fire and bus fire were recommended to be

5 min and 10 min, respectively (Ingason, 2009). However, because of the simulation cost, the t_{max} was set to 1 min. Since the focus of the research in this paper is to develop a methodology for selection of interface boundaries for fire simulations in a road tunnel, the decay time period for vehicle fires were not considered in the study. Flexible polyurethane foams were utilized for vehicle fire simulation in the tunnels. The heat of combustion and the yield of fire products were set as shown in Table 8.1 (Tewarson, 1995).

Table 8.1. Heat of combustion, CO, CO_2, and soot yields of vehicle fire events used in simulation

Material	ΔH_T (kJ/kg)	Y_{CO2} (kg/kg)	Y_{CO} (kg/kg)	Y_{Soot} (kg/kg)
Polyurethane	25300	1.5325	0.02775	0.1875

Three different scenarios, as shown in Table 8.2, were simulated for investigation of different parameters in order to determine the interface boundaries. All the vehicle fires were set in the middle of the road tunnels. A bus with dimensions of 12 X 2.6 X 3.6 m^3 as the length, width, and height, respectively, was considered as the fire object for simulations.

Table 8.2. CFD simulations according to different factors

Scenarios	Velocity (m/s)	HRR (MW)	Tunnel Dimension (m^2)
scenario 1	5	10	2 lanes (73.7)
scenario 2	5	30	2 lanes (73.7)
scenario 3	1.5	10	2 lanes (73.7)

8.4. Geometry, Initial and Boundary Conditions

The thermal and the physical parameters of the tunnel wall concrete, including, density, thermal conductivity, and specific heat were set to 2400 kg/m^3, 1 W/m°C, and 0.96 kJ/kg°C, respectively (Bamforth et al., 2008). The rock types in the concrete were assumed to be limestone, sandstone, and chert, and it was assumed that the sand and aggregate were from the same rock type at an early age. The thermal diffusivity of concrete was set to 0.77 mm^2/s (Laage et al., 1995).

The physical and the thermal characteristics of asphalt depend on the air voids in the dry or wet asphalts. A 5% air voids content was assumed for consideration of different parameters. The physical and the thermal parameters of the dry pavement asphalt, including density, thermal conductivity, and specific heat capacity were set to 2372 kg/m^3, 1.16 W/m°C, and 0.9637 kJ/kg°C, respectively (Hassn et al., 2016). The no-slip boundary condition was considered for all walls and the objects in the domain. In this study, the jet fans used for tunnel ventilation were assumed to be far away from the fire source. Therefore, a fixed air flow was set at the inlet of the computational domains. The cell size near the fire source plays a key role in the accuracy and stability of the numerical computation. Reliable numerical results can be achieved when the grid size is ≤0.1D* (McGrattan et al., 1998), where D* is representative of the characteristic length scale which corresponds to the total heat release rate of a fire plume (Baum and McCaffrey, 1989; Yuan et al., 2014). The heat release rates in this study were 10 MW and 30 MW. Therefore, a grid size of 24 cm was considered for the numerical analysis. In all simulations, the ambient air temperature, ambient air density, and air viscosity at ambient temperature were set at 20 ^{O}C, 1.196 kg/m^3, and 1.79e-05 kg/m/s respectively. The simulation of vehicle fires of all scenarios at t=900 s is shown in Figure 8.4.

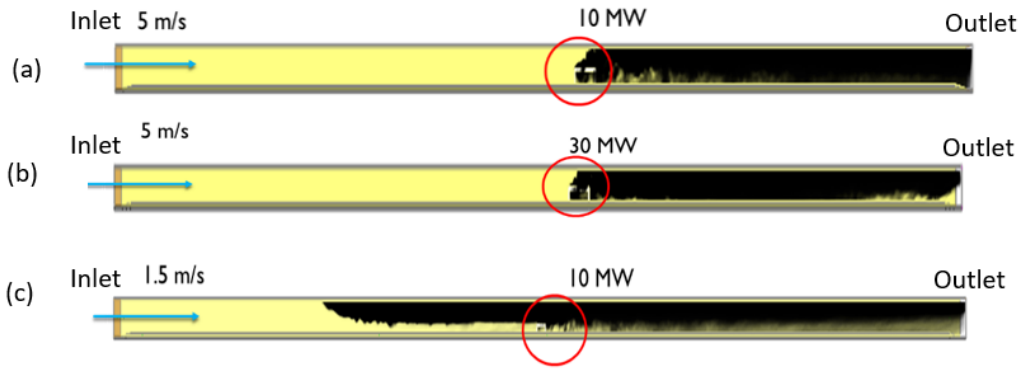

Figure 8.4. Vehicle fire and the smoke transport in the road tunnel at t=900s for all scenarios: (a) scenario 1, (b) scenario 2 (c) scenario 3

8.5. Results and Discussion

In order to determine the region where the flow structure behaves in a quasi-1D fashion, there is a need to investigate the longitudinal (u-velocity) and the transversal

velocity components (v- and w-velocities), vorticities along different axes (X, Y, and Z), and the turbulent kinetic energy at each node in 3D CFD models. All parameters were calculated every 5 m upwind and downwind from the fire source. The zero line represents the cross section of the tunnel at the center of the fire source. According to Figure 8.4 (c), the upwind transport of the smoke (rollback) occurred in scenario 3 because the air velocity in this model, was less than the critical velocity. However, just the downwind transport of smoke was observed in scenarios 1 and 2, as shown in Figure 8.4 (a) and Figure 8.4 (b). It was observed that the rollback did not advance significantly along the longitudinal axis after 900 s in scenario 3 and after that, the steady-state flow condition in the tunnel was reached. Therefore, t=900 s was selected to investigate all parameters upwind and downwind of the fire source in scenarios 1, 2, and 3.

8.5.1. Longitudinal and Transversal Velocity Components Analysis

The region where the flow structure is quasi-1D is the region where the domain can be split into distinct 3D and 1D sub-domains. In that region, the streamwise component of the velocity dominates the fluid structure. Therefore, detailed longitudinal and transversal velocity components analysis were conducted in order to determine the region where the influence of transversal velocity components on the fluid structure was inconsequential. The normality and distribution of the longitudinal velocity (u) and the transversal velocities (lateral (v-velocity) and vertical (w-velocity)) of all nodes at different cross sections of the tunnel upstream and downstream of the fire source at t=900 s for model 1 were calculated as shown in Figures 8.5, 8.6, and 8.7, respectively. All distances are from the center line of the fire.

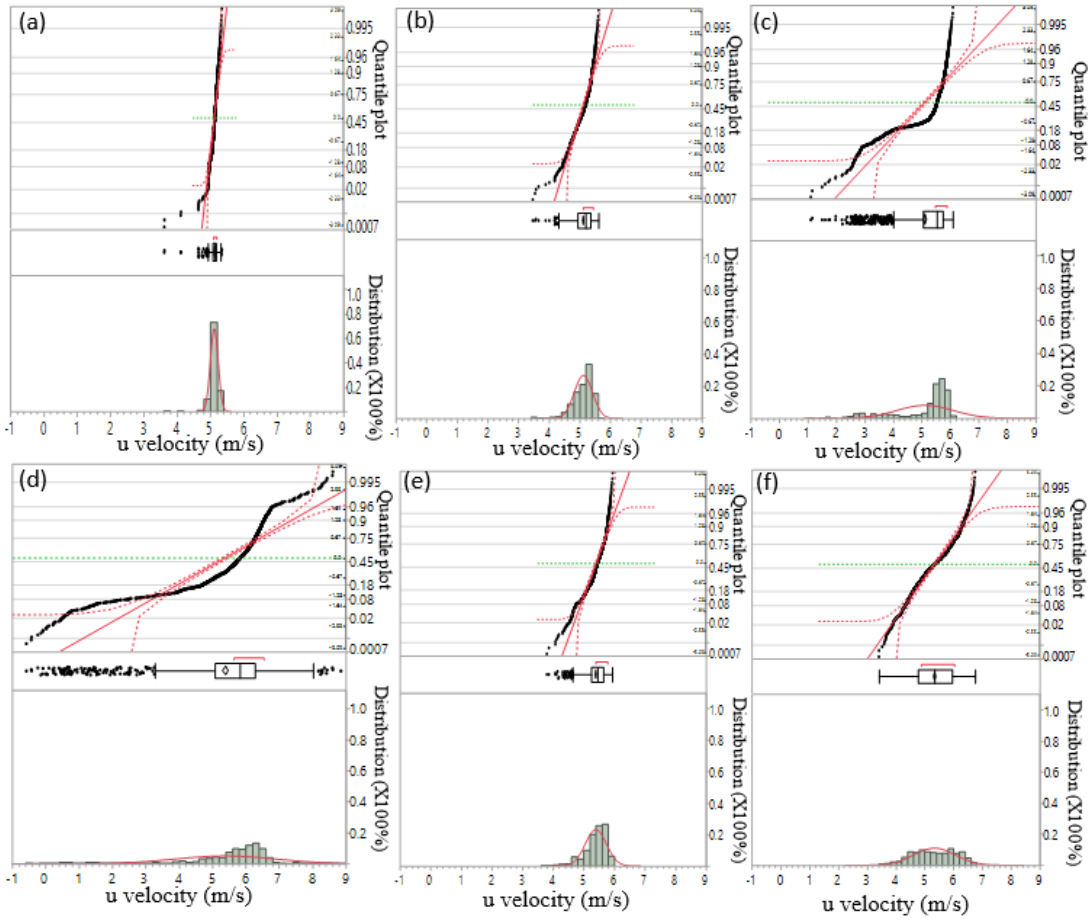

Figure 8.5. Normal quantile plots, box-and-whisker plots, and distributions of u velocity at different cross sections of the tunnel at t=900 s in scenario 1 at: (a) 430 m upstream, (b) 10 m upstream, (c) 7 m upstream, (d) 10 m downstream, (e) 100 m downstream, (f) 430 downstream

In Figure 8.5 it is evident that the longitudinal velocity (u-velocity) of all nodes along the height of the tunnel at each cross section was more normally distributed at a greater distance from the fire source (Figure 8.5a, f, e), and up to 10 m upstream of the fire (Figure 8.5b). The longitudinal velocity of all nodes at each cross section was not distributed normally up to 100 m downstream of the fire (Figure 8.5e). According to the box-and whisker plots in Figure 8.5, it is noteworthy that the dispersion of the longitudinal velocity values at cross sections increased close to the fire source as shown in Figures 8.5(c) and 8.5(d). Due to the presence of the burning object (vehicle fire) at the middle of the tunnel and the upwind transport of smoke downstream of the fire, the dynamic flow

field near the fire (from 10 m upstream of the fire source to 100 m downstream of the fire source) was not quasi-1D. This indicates that this region requires 3D simulation.

The distribution of transversal velocity components (v- and w-velocities) were similar to the distribution of longitudinal velocity components, as shown in Figures 8.6 and 8.7. The transversal velocities were not distributed normally near fire field (10 m upstream of the fire to 100 m downstream) while the normal distribution was observed at the far field regions (from the inlet to 10 m upstream and from 100 m downstream to the outlet). In addition, the variation and dispersion of transversal velocities of all nodes along the height of the tunnel at different cross sections increased by getting close to the fire source. Therefore, it was evident that the domination of transversal velocity components (v- and w-velocities) on the fluid field decreased by getting further away from the near fire region.

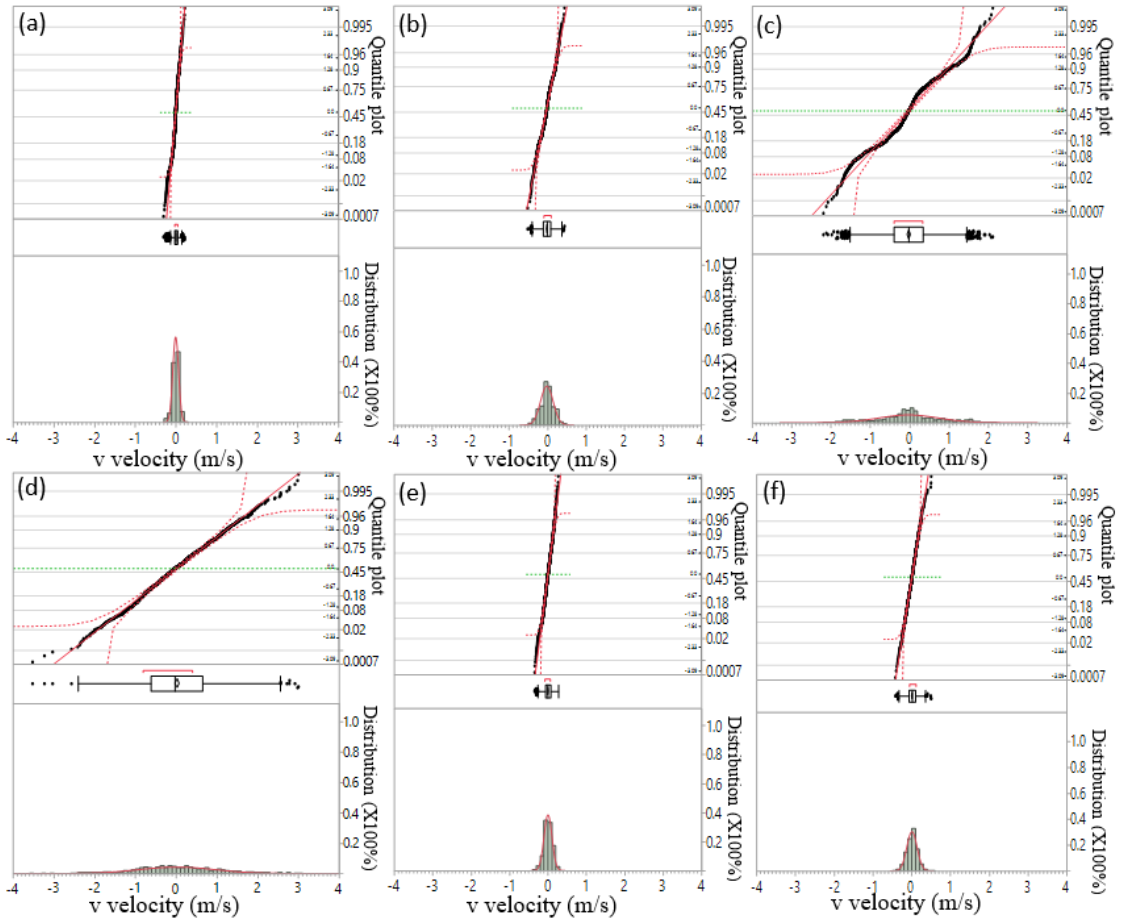

Figure 8.6. Normal quantile plot, box-and-whisker plots, and distributions of v velocity at different cross sections of the tunnel at t=900 s in scenario 1 at: (a) 430 m upstream, (b) 10 m upstream, (c) 7 m upstream, (d) 10 m downstream, (e) 100 m downstream, (f) 430 downstream

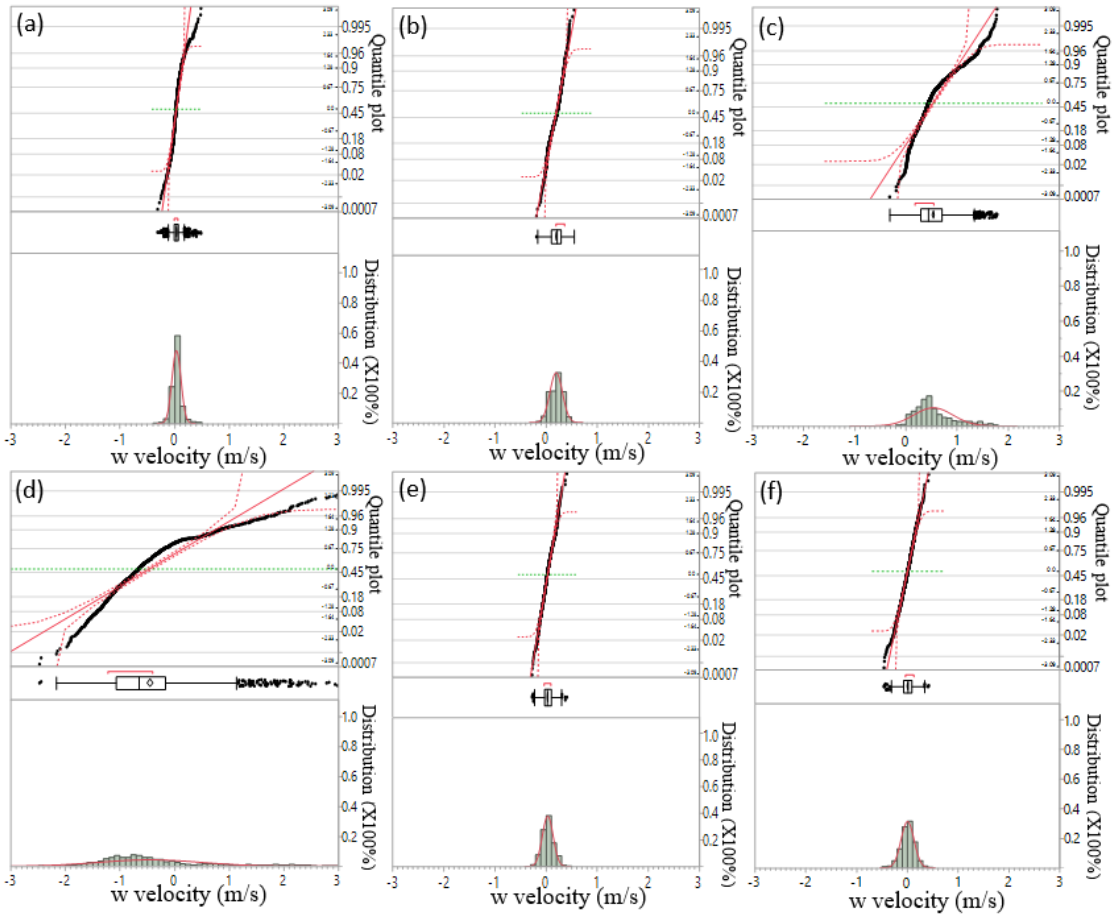

Figure 8.7. Normal quantile plot, box-and-whisker plots, and distributions of w velocity at different cross sections of the tunnel at t=900 s in scenario 1 at: (a) 430 m upstream, (b) 10 m upstream, (c) 7 m upstream, (d) 10 m downstream, (e) 100 m downstream, (f) 430 downstream

In our indirect coupling strategy, the characteristic point of 3D fire field (near fire field) (ex: mass flow rate across the boundaries, the total pressure drop across the boundaries, and the mean temperature at the boundaries) are used as the boundary condition for the 1D model (Colella et al., 2011a). The transfer of mean values of velocity, pressure, and temperature are required for the adoption of indirect coupling strategies. Therefore, a cross section at which all node values of the 3D model are nearly uniform and close to the mean values can be selected as the suitable boundary for decomposing the global domain into 3D and 1D sub-domains.

Hence, the standard deviations of velocity components (longitudinal and transversal velocity components) were calculated along the height of the tunnel at different cross sections in steady state condition in order to analyze the dispersion of the velocity components at different cross sections of the tunnel. The standard deviation of the longitudinal and transversal velocities of all nodes at t=900 along the height of the tunnel at different cross sections of the tunnel in scenario 1 are shown in Figure 8.8.

The standard deviation of the longitudinal and the transversal velocities was calculated less than 0.2 from the inlet to 10 m upstream of the fire source. After that point, it increased dramatically up to 1.6 at the centerline of the fire source. The highest dispersion of the longitudinal velocity of all nodes was calculated at the centerline of the vehicle fire. The reason lies in the sudden contraction of the cross section and the burning source which created a chaotic fluid structure in the middle of the computational domain. The sudden contraction of the cross section, due to the presence of the vehicle, and the burning source, resulted in the creation of the vorticities in the region near the fire field. The dispersion of the longitudinal and transversal velocities of all nodes decreased from the centerline of the object up to 100 downstream of the fire and it remained almost constant up to the outlet. The dispersion of the longitudinal velocity (u) of all nodes at different cross sections downstream of the fire was higher compared to the dispersion of the transversal velocities. This study has shown that the transversal velocities (v- and w- velocities) were temperature dependent just near the fire field while the temperature did not affect the dispersion of the transversal velocities of all nodes along the height of the tunnel far from the fire. On the contrary, the longitudinal velocity (u-velocity) was temperature dependent at both near and far fire fields. In other words, the streamwise component of the velocity (u-velocity) is more temperature dependent than the transversal velocity components (v- and w-velocities).

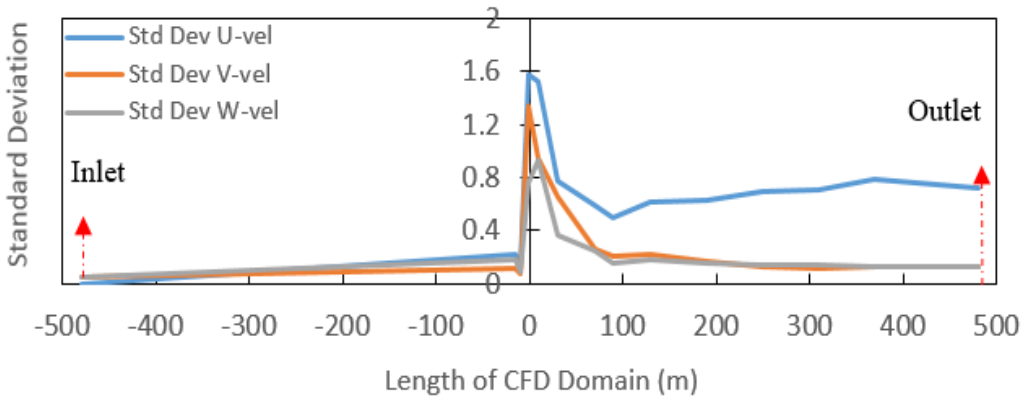

Figure 8.8. Standard deviation of u-, v-, and w-velocities at different cross sections of the tunnel in scenario 1

The contour plots of the longitudinal velocity (u velocity) and the transversal velocities (v-velocity and w-velocity) at different cross sections downstream of the fire in scenario 1 at t=900 s are shown in Figures 8.9, 8.10, and 8.11. Figures 8.9, 8.10, and 8.11 highlight the findings above and give a visual representation of the velocity fields.

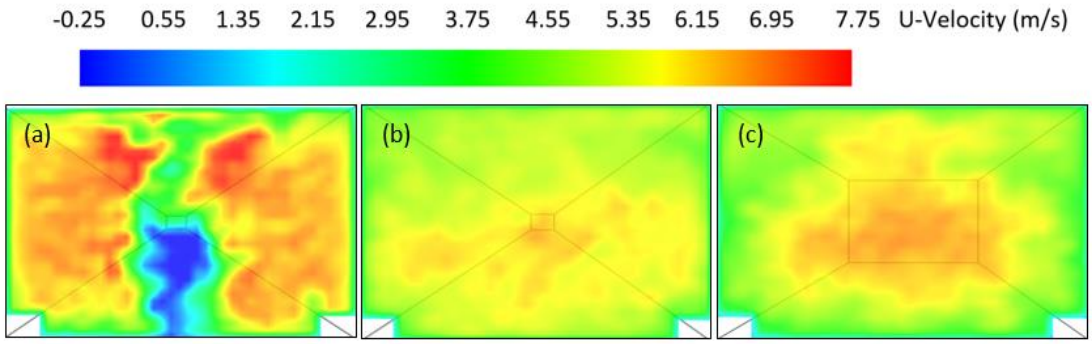

Figure 8.9. U-velocity contour plot at different cross sections of the tunnel at t=900 s: (a) 10 m downstream, (b) 100 m downstream, (c) 430 downstream

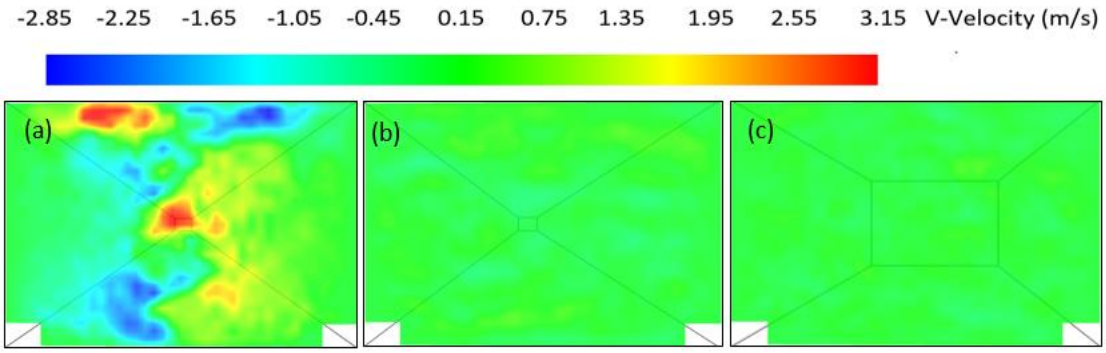

Figure 8.10. V-velocity contour plot at different cross sections of the tunnel at t=900 s: (a) 10 m downstream, (b) 100 m downstream, (c) 430 downstream

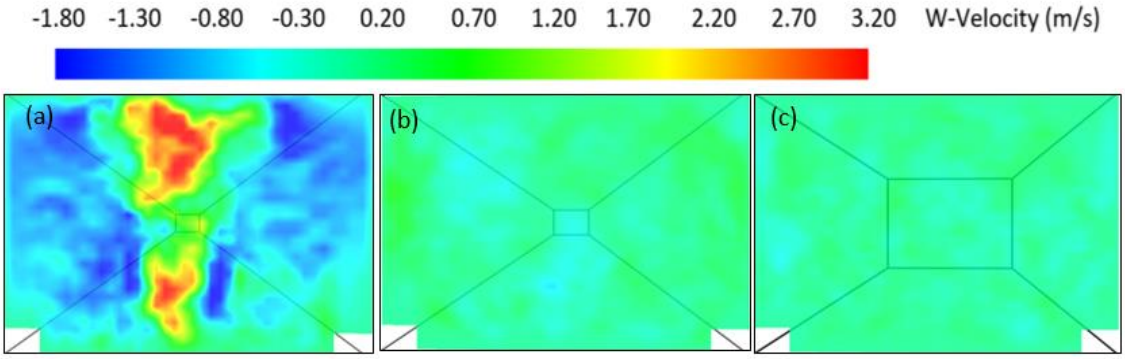

Figure 8.11. W-Velocity contour plot at different cross sections of the tunnel at t=900 s: (a) 10 m downstream, (b) 100 m downstream, (c) 430 downstream

Overall, because of the complex dynamical fluid field close to the fire (10 m upstream of the fire to 100 m downstream), the wide dispersion of the values (e.g., velocity components) was observed, dispersion decreases in the far field.

The same study was conducted for scenarios 2 and 3 in order to investigate the behavior of the longitudinal and the transversal velocity components of all nodes along the height of tunnel at different cross sections when the velocity and HRR were changed (see Appendix C for normal quantile plot, box-and-whisker plots, distributions of u-, v-, and w-velocities of all nodes, and standard deviations at different cross sections of the tunnel at t=900 s for scenarios 2 and 3). Similar dispersion characteristics near and far field of the fire were observed for scenario 2, which increased the HRR to 30 MW. Because of downwind transport of smoke and hot gases in scenario 2, the dispersion of the longitudinal and transversal velocities at different cross sections upstream of the fire did not change by

changing HRR. Therefore, the only region which the standard deviation of the transversal velocity components was affected by changing the HRR, was distinguished as a 10 m upstream of the fire to 100 m downstream as shown in Figure 8.28 (a) (See Appendix C).

It is noteworthy that by changing the HRR the dispersion of the transversal velocities (v- and w-velocities) at the near fire field were changed while the dispersion of the transversal velocities of all nodes along the height of the tunnel far from the fire was not affected. On the contrary, the longitudinal velocity (u-velocity) was temperature dependent at both near and far fire fields.

A velocity less that the critical velocity (V_{cr}) was considered in scenario 3. Therefore, because of the backlayering phenomenon, the distribution and the dispersion of longitudinal velocity of all nodes along the height of the tunnel at a different cross section upstream of the tunnel were different in comparison with the longitudinal velocity values of all nodes at upstream in scenarios 1 and 2 (Figure 8.28 (b)). Consistent with the data of Figure 8.25 (See Appendix C), it is evident that the longitudinal velocity of all nodes at different cross sections from the inlet to 170 m upstream of the fire was positive and had a normal distribution. From 170 upstream of the fire to the centerline, the negative longitudinal velocity at some nodes of different cross sections was calculated. The reason lies in the buoyancy forces associated with the temperature of the smoke plume, which causes it to overcome the inertial forces of the ventilation air (Friel et al., 2006). The smoke propagated in opposite direction of the stream as shown in Figure 8.12. Therefore, this region was not considered as the upstream interface boundary since the quasi-1D flow-field criterion was not met. In addition, according to Figure 8.28 (b) (see Appendix C), the dispersion of longitudinal velocity of all nodes at different cross sections from the inlet to 180 m upstream of the fire source remained constant and after that, it increased dramatically. This study has shown that not only the whole backlayering region but also 10 m before that region should not be considered as the upstream interface boundary region. The longitudinal and the transversal velocity components downstream of the fire were distributed normally from 100 m downstream of the fire up to the outlet. According to Figure 8.28 (b) (see Appendix C), the standard deviation of the longitudinal and the

transversal velocities along the height of the tunnel at different cross sections from the inlet to the outlet remained constant except for the region 180 m upstream of the fire to 100 m downstream of the fire.

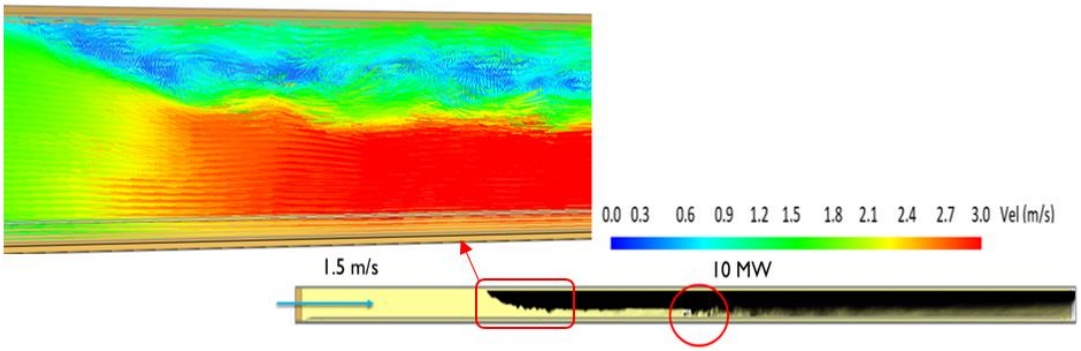

Figure 8.12. Created vortices at the tip of the rollback and the airflow velocity streamlines on the middle plane at t=900 s

8.5.1.1 Mean velocity and mean velocity components

The mean velocity and its components along the height of the tunnel at different cross sections in scenario 1 were investigated in order to distinguish the near and far fields via determination of the significance of the mean components of the velocity on the fluid structure at different cross sections of the tunnel. In addition, due to the continuity of the average velocity at the 3D-1D interface boundaries, the mean velocity (8.13 (a)) and its components (8.13 (b), 8.13 (c), and 8.13 (d)) along the height of the tunnel at different cross sections were investigated as shown in Figure 8.13.

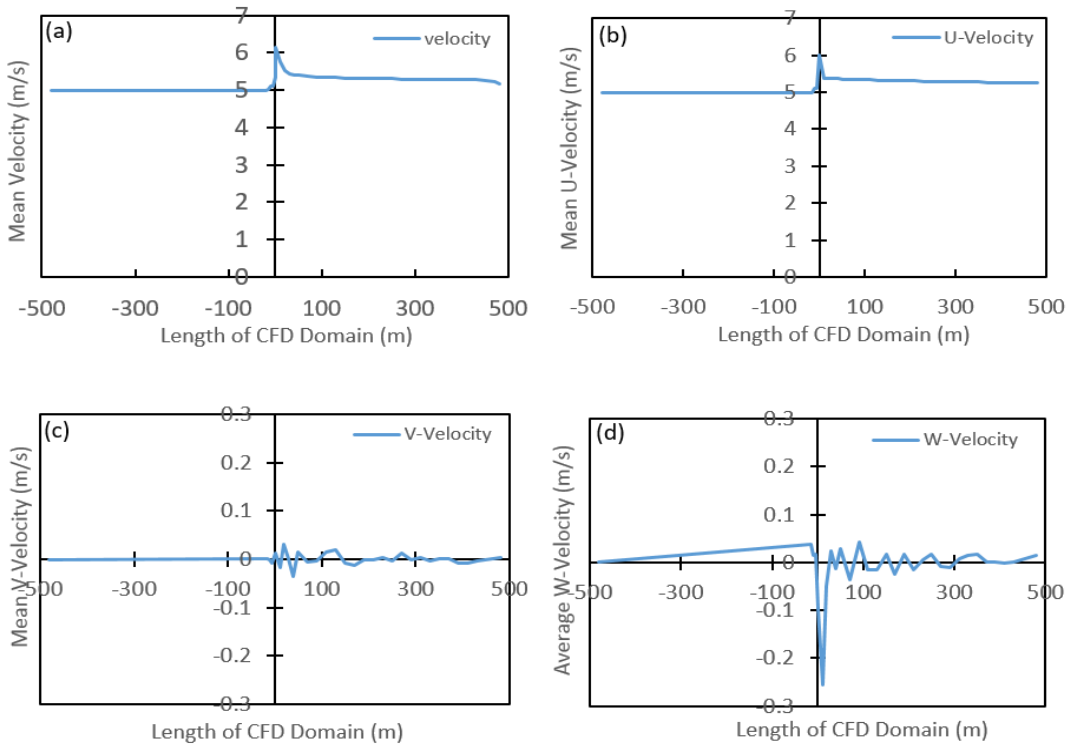

Figure 8.13. The mean velocity and its components along the height of the tunnel at different cross sections at t=900 s in scenario 1 (a) velocity (b) u-velocity (c) v-velocity (d) w-velocity

It is noteworthy that the mean velocity and the mean longitudinal velocity (u-velocity) at a different cross section of the tunnel behaved the same except the near fire field. The reason lies in the erratic behavior of the mean transversal velocities (v-velocity and w-velocity) near the fire source as shown in Figure 8.13 (c) and Figure 8.13 (d). Consistent with the data of Figure 8.13 (b) it was evident that the mean longitudinal velocity (u-velocity) remained constant from the inlet to 10 m upstream of the fire and after that, it experienced large fluctuations to 20 m downstream of the fire. Then, it leveled off up to the outlet. The mean longitudinal velocity upstream and downstream of the fire were calculated at 5 m/s, and 5.3 m/s, respectively. The magnitude of the mean longitudinal velocity compared to the mean transversal velocities is significantly higher at different cross sections of the tunnels as shown in Figures 8.13 (b), 8.13 (c), and 8.13 (d). According to Figures 8.13 (c) and 8.13 (d), the mean transversal velocities are sporadic from 10 m upstream to 100 m downstream of the fire and after that, they display only marginal

fluctuations. The mean transversal velocities (v- and w-velocities) at upstream of the fire remained constant from the inlet to 10 m upstream of the vehicle fire. According to Figure 8.13 (c), the mean v-velocity fluctuated from -0.05 m/s to 0.05 m/s in that region while the mean w-velocity (Figure 8.13 (d)) fluctuated from -0.25 m/s to 0.04 m/s in the same region. The effect of the mean transversal velocities on mean velocity was observed to be consequential at near fire field, 10 m upstream to 100 m downstream of the fire. Consequently, this study has shown that the longitudinal velocity (u-velocity) dominated the fluid field far from the fire source. Hence, the fluid field in that region was quasi-1D.

The mean velocity and the mean longitudinal and transversal velocities in scenario 2 behaved similarly to scenario 1 (see Appendix D for mean velocity, mean longitudinal velocity (u-velocity), and mean transversal velocities (v-velocity and w-velocity) along the height of the tunnel at different cross sections at t=900 s for scenarios 2 and 3). According to Figure 8.29 (see appendix D), the effect of the mean transversal velocities (v- and w-velocities) on the mean velocity in scenario 2 was consequential in the near fire field (10 m upstream to 100 m downstream of the fire source). However, in other cross sections of the tunnel, the mean longitudinal velocity (u-velocity) dominated the flow field in scenario 2. Due to the higher HRR (30 MW) in scenario 2, the mean velocity values were higher downstream of the fire in comparison with the same values in scenario 1. Due to the rollback phenomenon in scenario 3, the flow did not behave as a 1D fluid in the region from 170 upstream of the fire to the centerline as shown in Figure 8.30 (See Appendix D). The mean velocity and the mean velocity components at different cross sections downstream of the fire in scenario 3 behave similarly to the same region in scenarios 1 and 2. Therefore, the flow field was dominated by the longitudinal velocity (u-velocity) at different cross sections downstream of the fire except for the region from the centerline of the fire to 100 m downstream. Moreover, the velocity of airflow remained constant from the inlet to 180 m upstream of the fire and then it increased up to 90 m upstream of the fire as shown in Figure 8.30 (a) (see Appendix D). From 90 m upstream of the fire to 2 m upstream of the fire source, the airflow velocity changes were inconsequential. The velocity increased dramatically from 2 m upstream of the fire to 3 m downstream and then it decreased drastically up to 50 m downstream of the fire and it leveled off up to the outlet.

This study has shown that from 170 m upstream of the fire to 100 m downstream of the fire, the transversal velocity component effects were consequential. In this region, the longitudinal velocity is not the dominant component of the fluid field. Therefore, the interface boundaries should be located beyond this region.

This study has shown that the effect of the temperature on the mean transversal velocities along the height of the tunnel at different cross sections close to fire is more consequential compared to the region far from the fire. Due to this, the mean transversal velocities played a key role on the changes of the mean velocity in the near fire field. However, the effect of the mean transversal velocities on the changes of the mean velocity at the far fields was not significant. Therefore, the mean longitudinal velocity was the dominant component of the airflow velocity on the fluid structure.

8.5.1.2 Ratio between maximum longitudinal and maximum transversal velocities

For adoption of the multiscale methodology, the CFD (3D) and 1D models should be applied to the near field and far field, respectively. Hence, there is a need to determine the quasi-1D region in the computational domain. According to the previous studies, it was evident that the flow structure was quasi-1D when the maximum longitudinal velocity ratio was almost twice the maximum transversal velocities (Van Maele and Merci, 2008). Therefore, a study was conducted to investigate the maximum longitudinal velocity ratio to the maximum transversal velocities along the height of the tunnel at different cross sections in the steady state condition as shown in Figure 8.14.

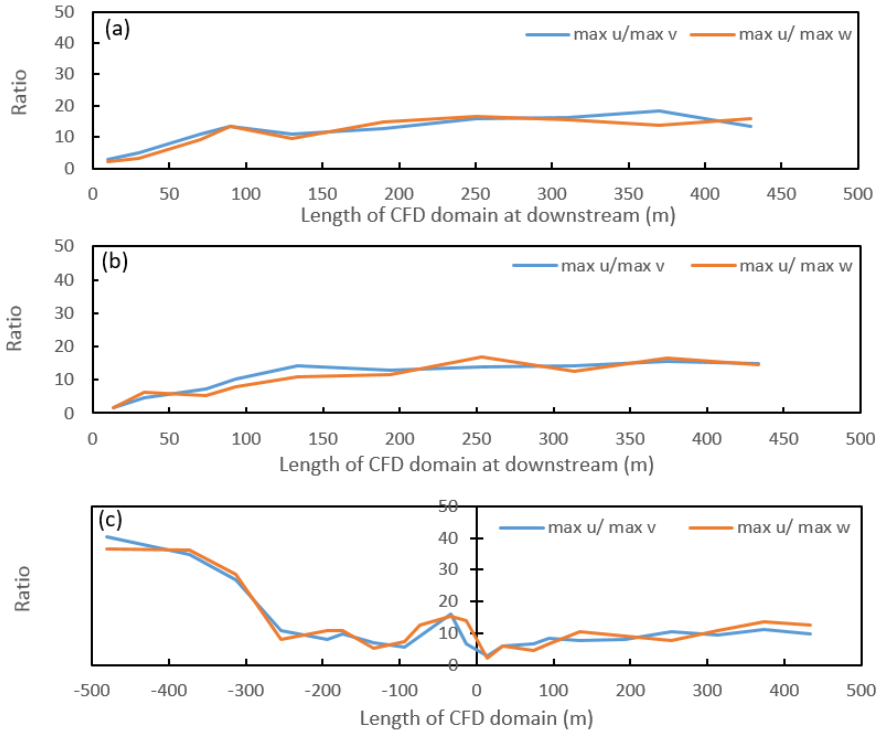

Figure 8.14. The maximum longitudinal velocity ratio to the maximum transversal velocities along the height of the tunnel at different cross sections at t=900 s: (a) scenario 1, (b) scenario 2, (c) scenario 3

Due to the transport of smoke and hot gases downstream of the fire source in the scenarios 1 and 2, the ratio of maximum longitudinal velocity to maximum transversal velocities different cross sections just downstream of the fire was investigated. However, because of the back layering phenomenon in the scenario 3, the investigation of maximum longitudinal velocity ratio to the maximum transversal velocities was carried out on the whole domain. Figure 8.14 shows that the ratio increased dramatically within the first 100 m downstream of the fire in all scenarios and after that, the values remained within the range of 10 to 20. Consistent with the data of the maximum longitudinal velocity ratio to the maximum transversal velocities downstream of the fire, it was evident that beyond 100 m downstream of the fire the flow is almost one-dimensional because of the domination the longitudinal velocity in the fluid field. In addition, this study has shown that by the change in HRR, the domination of longitudinal velocity on the fluid flow did not change significantly.

The maximum longitudinal velocity ratio to the maximum transversal velocity was calculated within the range of 28 to 40 from the inlet to 300 m upstream of the fire in scenario 3. Then the ratio decreased noticeably to 8, at 250 m upstream of the fire. The ratio experienced marginal fluctuation from 250 m to 90 m upstream of the fire. The maximum longitudinal velocity ratio to the maximum transversal velocities experienced sporadic behavior from 90 m upstream of the fire to the centerline. The reason lies in that the smoke layer depth, and the temperature close to the fire source. This study has highlights the previous findings that close to fire source the domination of the transversal velocities on the fluid structure increased. Moreover, the ratio was within a range of 10 to 20 in the quasi-1D region downstream of the fire source. Therefore, a ratio of at least 10 was recommended to indicate that longitudinal velocity component is dominant.

8.5.2. Turbulent Kinetic Energy and Vorticity Analysis

The energy content of eddies in turbulent flows is characterized by Turbulent Kinetic Energy (TKE); larger TKE values indicate higher energy content of eddies. The existence of eddies indicates the rotation of the fluid particles or vorticity. Therefore, diffusion will be intensified with the existence of eddies. Since the turbulent flows are dissipative, the kinetic energy of larger eddies will be transferred to the smaller ones, and finally, the kinetic energy of the smallest eddies will be converted into heat due to the viscous shear stresses. In some cases, backscatter phenomenon can occur which it means that because of the interaction of the smaller eddies with each other, the kinetic energy will be transferred to the larger eddies (Black, 1966; Hinze, 1975; Townsend, 1956). In order to determine the region where the transversal velocity components have an inconsequential effect on the fluid field, the tendency of fluid particles to rotate (vorticity) along the different axes (X, Y, and Z), was investigated. In addition, for characterizing the intensity of turbulence of a system, the Turbulent Kinetic Energy (TKE) analysis along the height of the tunnel at different cross sections was conducted. Then the one-dimensional flow pattern region was determined by the usage of mean TKE and mean vorticity analysis. The mean TKE of the cross sections and the mean vorticity along X, Y, and Z axis at different cross sections along the height of the tunnel at t=900 for all scenarios were calculated as shown in Figure 8.15.

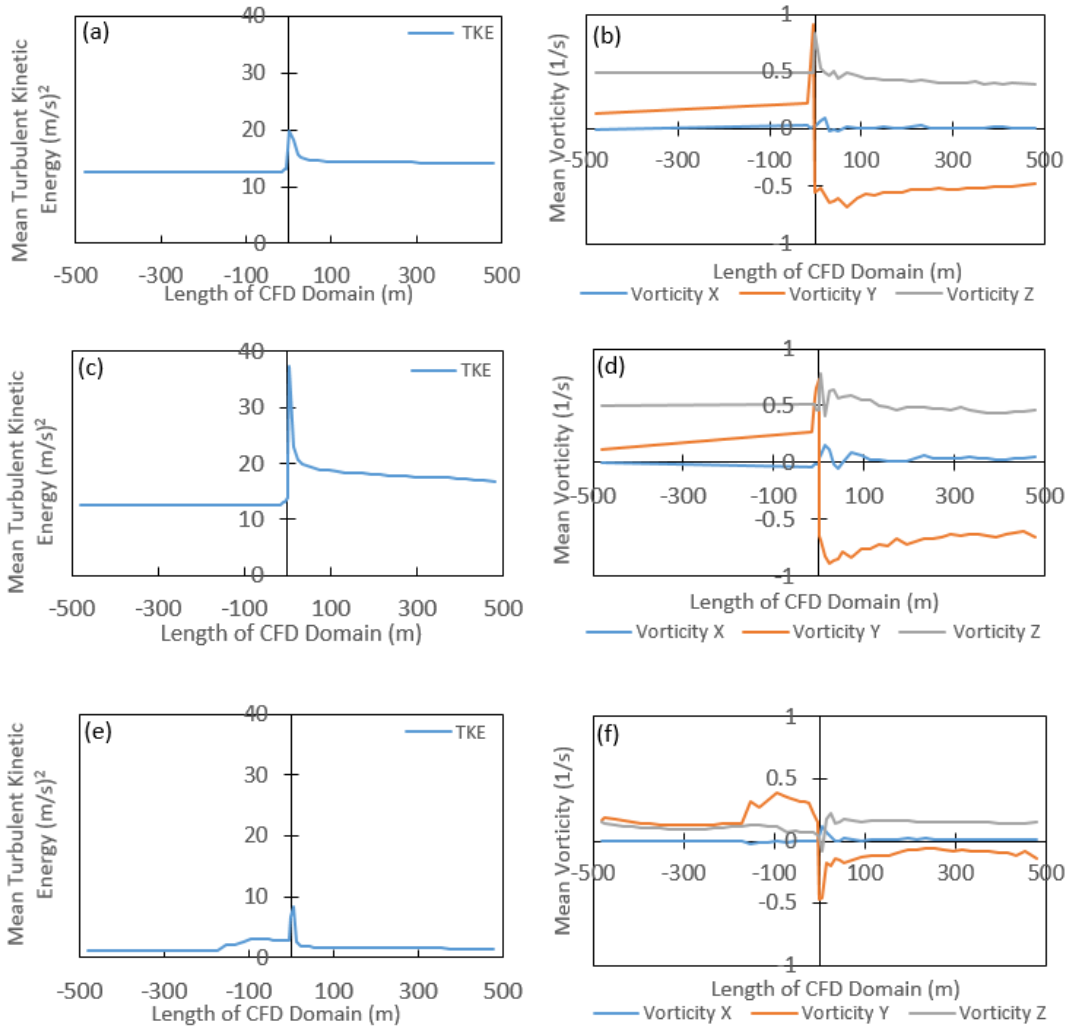

Figure 8.15. The mean TKE and the mean vorticity along the height of the tunnel at different cross sections at t=900 in all scenarios: (a) mean TKE scenario 1, (b) mean vorticity scenario 1, (c) mean TKE scenario 2, (d) mean vorticity scenario 2, (e) mean TKE scenario 3, (f) mean vorticity scenario 3

According to Figure 8.15 (a), the mean TKE at different cross sections in scenario 1 remained constant from the inlet to 10 m upstream of the fire. After that point it TKE fluctuated substantially to 50 m downstream; then, it leveled off up to the outlet. Consistent with the data of the vorticity along X, Y, and Z axis in scenario 1 (Figure 8.15(b)), it was evident that the mean vorticity along X, Y, and Z axes experienced high fluctuations in a region 10 m upstream of the fire to 100 m downstream. The changes of the mean vorticity along X, Y, and Z axes at different cross sections of the tunnel in scenario 1 were

inconsequential as plotted in 8.Figure 15 (b). When HRR was altered, the trend of the mean TKE and the mean vorticity along X, Y, and Z axis at different cross sections did not change; however, the values changed as shown in Figures 8.15(c) and 8.15(d). Therefore, the mean TKE and the mean vorticity along a different axis in scenario 2 experienced erratic behavior from 10 m upstream of the fire to 100 m downstream. This study has shown that the fluid particles had the highest tendency to rotate along X, Y, and Z axis at the near fire field.

The behavior of the mean TKE and the mean vorticity along X, Y, and Z axis downstream of the fire in scenario 3 was observed to have the same as the behavior of associated values in scenarios 1 and 2 as shown in Figures 8.15(e) and 8.15(f). Due to lower velocity in scenario 3 compare to scenario 1 and 2, the mean TKE and the mean vorticity downstream of the fire were calculated lower than the values in scenario 1 and 2. The values remained constant from the inlet to 170 m upstream of the fire. Because of the backlayering phenomenon in scenario 3, the mean TKE and the mean vorticity along the Y and Z axes experienced substantial fluctuations from 170 m upstream of the fire to the centerline. The vorticity along the X axis was almost zero at all cross sections except the regions close to the fire source. Consequently, it was evident that the intensity of turbulent kinetic energy and the rotation tendency of fluid particles remained constant in the regions where the flow field is quasi-1D.

According to the longitudinal and the transversal velocity components analysis and the TKE and the vorticity analysis, the quasi-1D regions were determined in order to couple 3D to 1D models. The upstream and downstream interface boundaries were determined for all scenarios as shown in Figure 8.16.

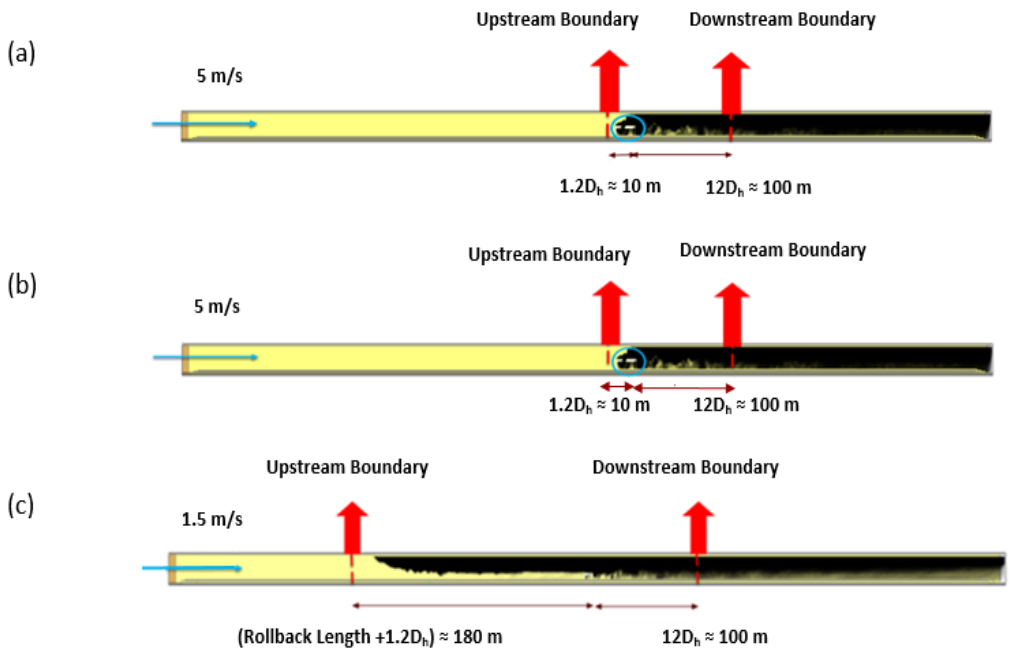

Figure 8.16. Selected interface boundaries at upstream and downstream of the fire source (a) scenario 1 (b) scenario 2 (c) scenario 3 (Not to scale)

Based on the physics of the fluid structure, TKE, and the vortex dynamics, interface boundaries were placed 10 m upstream of the fire source and 100 m downstream for scenarios 1 and 2. Because of the consequential effect of the transversal velocity components (v and w velocities) on the flow field characteristic near the fire field at upstream, the upstream interface boundary could not be moved closer than 10 m to the fire object (the calculated distance was from the centerline). The distance from upstream interface boundary to the tip of the object was 0.5 D_h (4 m). The downstream boundary was calculated to be at least 12 times the hydraulic diameter (D_h) which indicated agreement with previous work (Colella et al., 2011a; Van Maele and Merci, 2008). The same downstream interface boundary was selected for scenario 3 as scenarios 1 and 2. Due to significant effect of the transversal velocities (v- and velocities) on the fluid flow field close to the tip of the backlayering, the upstream interface boundary was selected 10 m further from the tip of the backlayering at 180 m upstream of the fire in scenario 3 as shown in Figure 8.16(c). It was observed that the fluid flow field at that section was quasi-1D. Therefore, the near fire field (the region between upstream and downstream interface boundary) was determined as shown in Figure 8.16 for all scenarios.

8.6. Coupled Simulation Results

The 1D models were simulated using VentFIRE in order to couple to the full CFD simulations. The multiscale calculations were conducted using indirect coupling strategy with the near fire field characteristic curves implemented in the 1D models. The characteristic curves of near fire field (CFD region) are required in the indirect coupling of 3D models to 1D models (Colella et al., 2010, 2011a). Therefore, the near fire field characteristic points for all scenarios were plotted in terms of mass flow rate versus total pressure drop across the domain boundaries as shown in Figure 8.17.

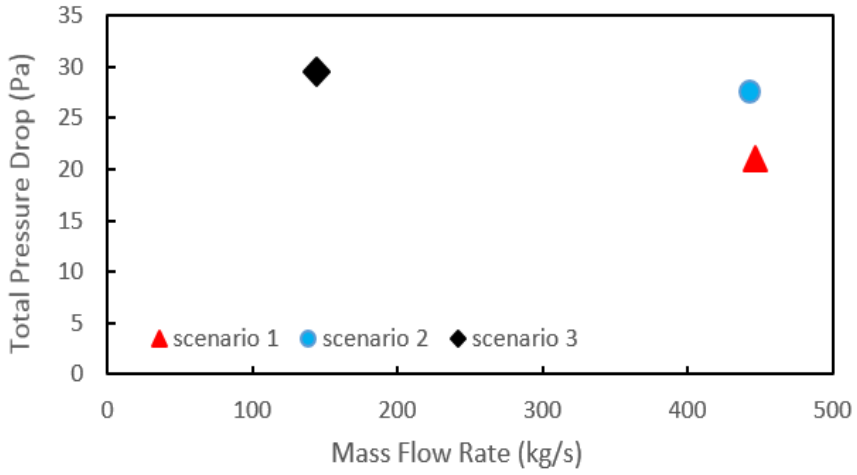

Figure 8.17. Characteristic points of the near fire filed region for all scenarios

Since the continuity of the mean temperature should be met at the interface boundary, the mean temperature along the height of the tunnel at different cross sections of CFD model was calculated as shown in Figure 8.18.

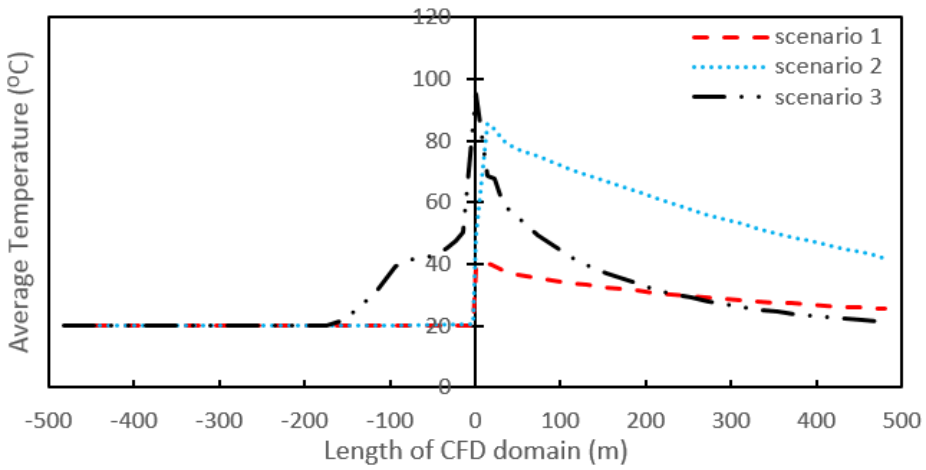

Figure 8.18. Mean temperature along the height of the tunnel at different cross sections at t=900 s in all scenarios

Figure 8.18 shows that the mean temperature upstream of the fire in scenarios 1 and 2 is the same. However, the mean temperature in scenario 3 within the first 170 m upstream of the fire source was higher due to backlayering. The highest mean temperature downstream of the fire along the height of the tunnel at different cross sections was calculated in scenario 2, due to the higher HRR. The mean temperature at the interface boundaries for different scenarios was calculated in order to couple to 1D models as shown in Table 8.3.

Table 8.3. The mean temperature at the interface boundaries for different scenarios

Scenarios	Upstream Interface Temperature (^{O}C)	Downstream Interface Temperature (^{O}C)
Scenario 1	20	34.3
Scenario 2	20	71.7
Scenario 3	20	43.8

The coupled model was simulated and the associated average temperature and velocity errors in the coupled scenarios compare to the full domain CFD simulations were calculated as shown in Figure 8.19 (see Figure 8.20 for comparison of coupled model results to 1D models' results for scenarios 1, 2, and 3). According to Figure 8.19, the mean temperature and the mean velocity errors at different cross sections after downstream

interface boundary were calculated at less than 5%. The error before upstream interface boundary was calculated as a 0%.

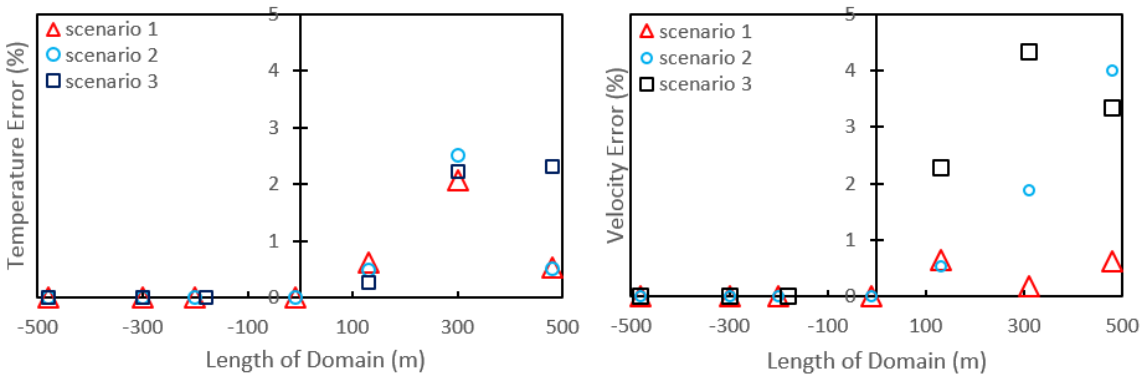

Figure 8.19. The calculated error between CFD and coupled models for mean temperature and velocity at different cross sections before and after determined interface boundaries for all scenarios: (a) temperature error, and (b) velocity error

Figure 8.20, shows that the mean temperature errors between 1D and the coupled model at the outlet were 49.2%, 66.5%, and 86% in scenarios 1, 2, and 3, respectively. Due to the inability of VentFIRE to precisely simulate rollback phenomenon, a higher percentage of error of the mean temperature scenario 3 was observed. If we assume that the 3D simulation over the whole domain is most representative of reality, then the coupling approach results in a drastic improvement in agreement for the mean temperature results at the far fire field when compared with a 1D simulation over the whole domain. In addition, the mean velocity along the height of the tunnel at the inlet and outlet was improved.

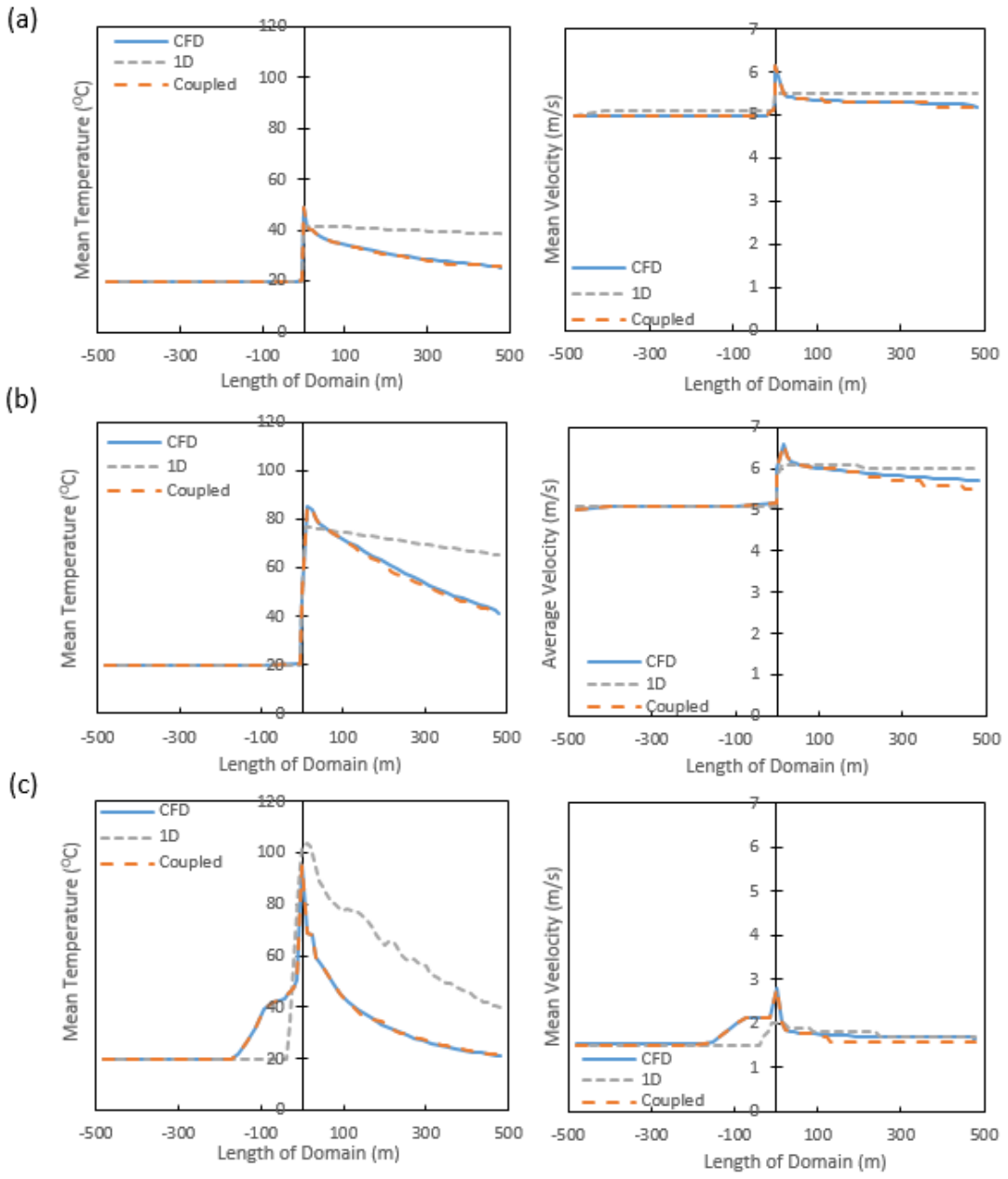

Figure 8.20. Mean temperature and mean velocity comparison between CFD, 1D, and the coupled models at different cross sections of the tunnel for all scenarios (a) scenario 1 (b) scenario 2 (c) scenario 3

8.7. Modified Procedure for Selection of Interface Boundary in Multiscale Methodology

Based on the velocity components analysis and the TKE and the vorticity analysis, it is recommended the interface boundary selection procedure for indirect coupling of 3D and 1D models. First, the CFD model is simulated and the inlet velocity of the domain is determined. If the determined inlet velocity is greater than or equal to V_{cr}, the upstream interface boundary is selected at least $0.5D_h$ from upwind the end of the fire object. If the selected inlet velocity is less than V_{cr}, the roll back length should be calculated and ($1.2\ D_h$ m + rollback length) should be selected as the upstream interface boundary. For the determination of the downstream interface boundary in both $V \geq V_{cr}$ and $V < V_{cr}$ scenarios, the longitudinal and the transversal velocities analysis and the mean TKE and mean vorticity analysis for the outlet cross section should be conducted. Next, the $12D_h$ cross section from the centerline of the object is selected as the downstream interface boundary which number 12 is the coupling variable (C_V). If the longitudinal velocity of all nodes is streamwise, and the distribution of the longitudinal and transversal velocities are almost similar to the outlet values, and the standard deviation of the longitudinal and transversal velocities of the determined section are less than 0.3 compared to the outlet values, that cross section can be accepted as the downstream interface boundary. If one of the explained requirements was not met, then $(Cv +1)*D_h$ is selected as the downstream interface boundary to repeat the longitudinal and the transversal velocities analysis and the mean TKE and mean vorticity analysis for that selected downstream interface boundary. The method will be iterated till all requirements are met. Ultimately, that cross section is accepted as the downstream interface boundary.

It is crucial to consider that the tunnel used in this study was a straight tunnel with just a burning object in the computational domain. If other objects or fire sources (e.g., vehicles) were considered in the simulation domain, the same study should be conducted for determination of the interface boundaries before and after the extra objects are included in the tunnel, because of the effect of the temperature and the presence of the objects on the fluid structure in the computational domain. By utilizing this approach, the interface

boundaries can be easily selected and adequately applied to couple 3D and 1D simulations as shown in Figure 8.21. In Figure 8.21, IB_{Up}, IB_{Down}, and C_v are upstream interface boundary, downstream interface boundary, and coupling variable respectively.

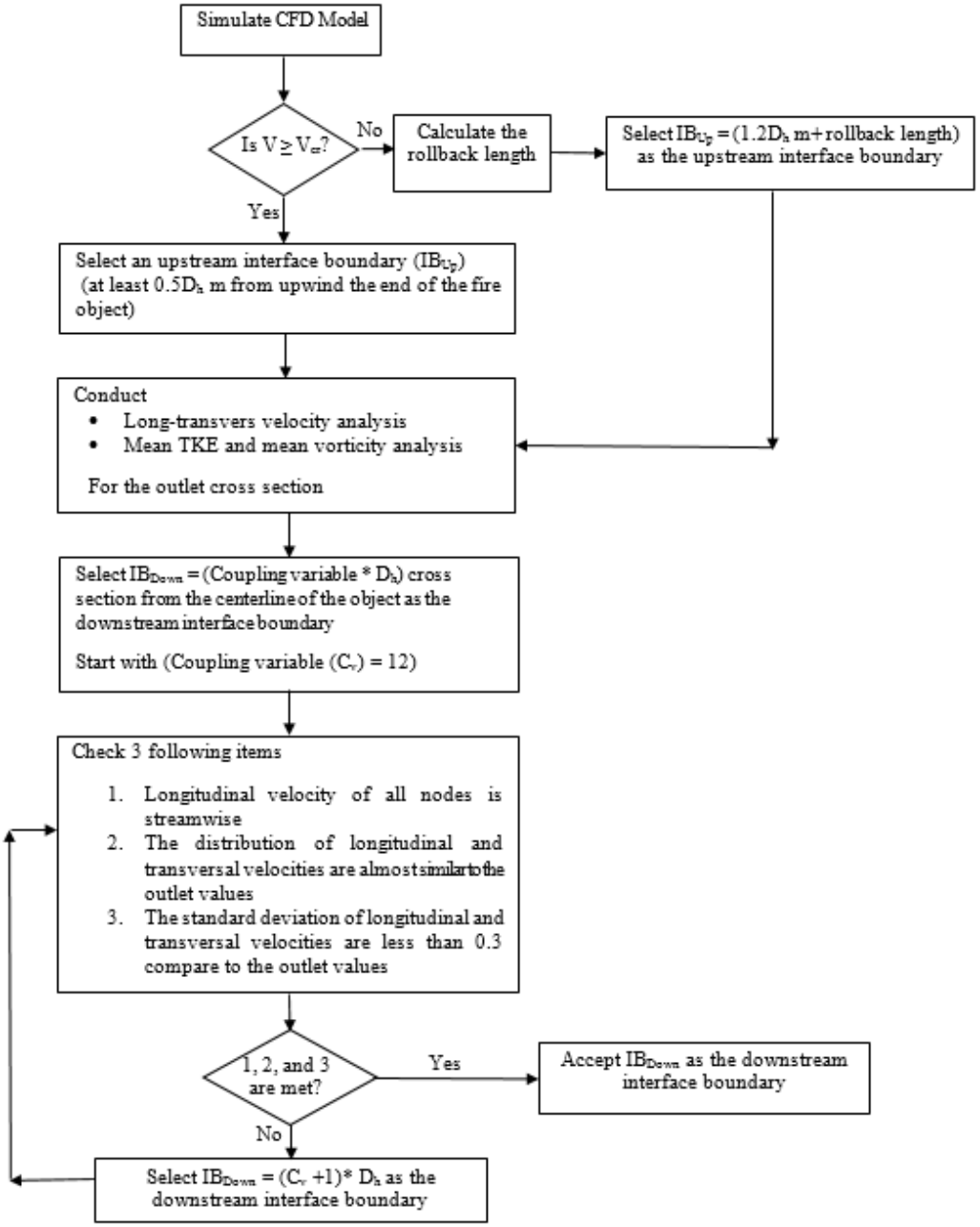

Figure 8.21. Decision making algorithm for determination of interface boundary to couple 3D and 1D fire simulations in tunnels

8.8. Conclusion

The fundamental longitudinal and the transversal velocities analysis and the TKE and the vorticity analysis for the steady state condition of the full CFD models were utilized to determine interface boundaries for coupling of 1D and 3D simulations. The selected downstream interface boundary was $12D_h$ m downstream of the fire for the simulations. The upstream interface boundary selection depends on the utilized velocity in the model. The upstream interface boundary was selected at ($0.5\ D_h$) 4 m upstream the tip of the object when the velocity was greater than equal to the V_{cr}. In the simulations with backlayering ($V < V_{cr}$), the interface boundary was selected 10 m further from the tip of the rollback ($1.2\ D_h$). The novel methodology was applied to a tunnel with 73.73 m^2 cross section and 960 m in length. The indirect coupling strategy was utilized to couple 3D sub-domain to 1D sub-domains. The calculated temperature and velocity errors between multiscale models and the full CFD models were less than 5%. It was evident that the longitudinal velocity component was affected by the temperature more than the transversal velocity components in the whole computational domain. In other words, the longitudinal velocity (u-velocity) was temperature dependent in the whole computational domain while the transversal velocity components (v and w velocities) were temperature dependent just at the near field. It was observed that the temperature did not impact the transversal velocities at the far field. Due to this, the fluid field was observed the quai-1D fluid which the longitudinal velocity dominated the fluid structure.

Consequently, a novel iterative methodology was developed according to the physics of the fluid structure, TKE, and the vortex dynamics for selection of interface boundary to couple 3D and 1D models for all kinds of fire in the road tunnel or more complex underground space environments. Additionally, the work agrees well with previous work that uses a more exhaustive systematic method (gradually increasing the CFD domain and decreasing the 1D domain until a predetermined error level is encountered.) The proposed methodology was demonstrated to be a useful technique for the determination of near and far fire fields, and could be applied across a broad range of flow simulations.

8.9. Acknowledgements

This research was developed under Contract No. 200-2014-59669, awarded by the National Institute for Occupational Safety and Health (NIOSH). The findings and conclusions in this report are those of the authors and do not reflect the official policies of the Department of Health and Human Services; nor does mention of trade names, commercial practices, or organizations imply endorsement by the U.S. Government.

8.10. Bibliography

Babrauskas, V., and Peacock, R. D., Heat release rate: the single most important variable in fire hazard. *Fire Safety Journal*, 1992, 18, 255-272.

Ballesteros-Tajadura, R., Santolaria-Morros, C., Blanco-Marigorta, E., Influence of the slope in the ventilation semi-transversal system of an urban tunnel. Tunnelling and Underground Space Technology 21 (2006) 21–28.

Bamforth, B., Chisholm, D., Gibbs, J., Harrison, T., Properties of Concrete for use in Eurocode 2: How to optimise the engineering properties of concrete in design to Eurocode 2. A cement and concrete industry publication. ISBN 1904482392, 9781904482390. (2008).

Baum, H. R., McCaffrey, B. J., Fire induced flow field-theory and experiment. In Fire Safety Science, Proc. 2nd Int. Symp. Hemisphere, New York, 1989, pp. 129—48.

Beard, A., Carvel, R., The Handbook of Tunnel Fire Safety, Thomas Telford Ltd., London, (536pp., Hardbound, ISBN: 0727731688) (2005).

Black, T. J., Proc. Heat transfer and fluid mech. Ins., 1966.

Breuer, M., Lakehal, D., Rodi, W., Flow around a surface mounted cubical obstacle: Comparison of LES and RANS–results. In M. Deville, S. Gavrilakis, and I.L. Ryming, editors, Computation of 3D Complex flows, volume 53 of Notes on Numerical Fluid Mechanics, pages 22–30. Vieweg Verlag, 1996. https://link.springer.com/chapter/10.1007%2F978-3-322-89838-8_4.

Choi, J.; Lin, C. L., Multiscale numerical analysis of airflow in CT-based subject specific breathing human lungs http://ir.uiowa.edu/etd/2685 (accessed Nov 21, 2012).

Colella, F., Rein, G., Borchiellini, R., Carvel, R., Torero, J. L., Verda, V., "Calculation and design of tunnel ventilation systems using a two scale modelling approach". Building and Environment Journal. 2009; 44. 2357-2367.

Colella, F., Rein, G., Reszka, P., Carvel, R., Torero, J. L., "Analysis of the ventilation system in the dartford tunnels using a multiscale modelling approach". TUST 2010; 25: 423-32

Colella, F., Rein, G., Borchiellini, R., Torero, J. L., "A Novel Multiscale Methodology for Simulating Tunnel Ventilation Flows During Fires". Fire Technology. ISSN:0015-2684. 2011a; pp. 221 - 253.

Colella, F., Rein, G., Verda, V., Borchiellini, R., "Multiscale modeling of transient flows from fire and ventilation in long tunnels". Computer & Fluids. 51. 2011b; pp. 16–29

Diego, I., Torno, S., Toraño, J., Menéndez,M., Gent, M., A practical use of CFD for ventilation of underground works. Tunnelling and Underground Space Technology 26, (2011) 189-200.

Formaggia, L., Gerbeau, J.F., Nobile, F., Quarteroni. A., "On the coupling of 3D and 1D Navier-Stokes equations for flow problems in compliant vessels". Comput. Methods Appl. Mech.Engrg. 191 (2001) 561-582.

Friel, G. F., Yuan, L., Edwards, J. C., and Franks, R. A., "Fire-generated smoke rollback through crosscut from return to intake – experimental and CFD study", Proceedings of the 11th U.S./North American Mine Ventilation Symposium, University Park, Pennsylvania, June 5-7. Mutmansky JM, Ramani RV. eds., London, U.K.: Taylor & Francis Group, pp. 483-489.\ (2006).

Frohlich, J., Von Terzi, D., "Hybrid LES/RANS Methods for the Simulation of Turbulent Flows". Progress in Aerospace Sciences. 2008; Volume 44. Pp. 349 – 377.

Galdo Vega, M., Arguelles Diaz, K.M., Fernandez Oro, J.M., Ballesteros Tajadura. R., Santolaria Morros, C. Numerical 3D simulation of a longitudinal ventilation system: memorial tunnel case. Tunn Undergr Space Technol, 2008; 23(5):539–551

Gutiérrez-Montes, G,. Sanmiguel-Rojas, E., Viedma, A., Rein, G., Experimental data and numerical modelling of 1.3 and 2.3 MW fires in a 20 m cubic atrium. Building and Environment, 2009; 44:1827–1839, 2.

Haghighat, A., Luxbacher, K., Lattimer, B., "Simulation of methane fire event at a coal mine working face with consideration of ventilation curtain damage". 2016 Transactions of the Society for Mining, Metallurgy & Exploration, 2016; Vol. 340, pp. 120-126.

Hassn, A., Chiarelli, A., Dawson, A., Garcia, A., Thermal properties of asphalt pavements under dry and wet conditions. 2016; Materials and Design 91, 432-439.

Heskestad, G., SFPE Handbook of Fire Protection Engineering, chapter Fire Plumes, Flame Height and Air Entrainment. National Fire Protection Association, Quincy, Massachusetts, 4th edition, 2008. 7, 25, 144, 146

Hinze, J. O., "Turbulence", McGraw-Hill series in mechanical engineering, 2nd Edition, 1975

Hung, C. J., Monsees, J., Munfah, N., Wisniewski, J., "Technical Manual for Design and Construction of Road Tunnels — Civil Elements". AASHTO publication. U.S. department of transportation federal highway administration. Publication No. FHWA-NHI-10-034. (2009). http://www.fhwa.dot.gov/bridge/tunnel/pubs/nhi09010/tunnel_manual.pdf

Hurley, M., Munguia. A., Analysis of FDS Thermal Detector Response Prediction Capability. J. Fire Protection Engineering, 20, 2009. 7

Hwang, C. C., Edwards, J. C., The critical ventilation velocity in tunnel fires – a computer simulation. Fire Safety Journal, 2005; 40:213–244.

Ingason, H., Design fire curves for tunnels. Fire Safety Journal, 2009; 44, 259-265.

Kunsch, J. P., Simple model for control of fire gases in a ventilated tunnel. Fire Safety Journal, 2002; 37(1):67–81.

Kuprat, A. P.; Kabilan, S.; Carson, J. P.; Corley, R. A.; Einstein, D. R. A Bidirectional Coupling Procedure Applied to Multiscale Respiratory Modeling. Journal of Computational Physics. 244 (2013) 148–167.

Laage, L. W., Greuer, R. E., Pomroy, W. H., "MFIRE users' manual". Version 2.20. (1995).

Liang, K. M., Ma, T., Quintiere, J. G., Rouson, D., Application of CFD Modeling to Room Fire Growth on Walls. NIST GCR 03-849, National Institute of Standards and Technology, Gaithersburg, Maryland, April 2003. 7, 10

Ma, T. G., Quintiere, J. G., Numerical simulation of axi-symmetric fire plumes: accuracy and limitations. Fire Safety Journal, 38:467–492, 2003. 7, 10

Maidl, B., Thewes, M., Maidl, U., Handbook of tunnel engineering II, Basics and additional services for design and construction. © 2014 Ernst & Sohn GmbH & Co. KG. Published 2014 by Ernst & Sohn GmbH & Co. KG.ISBN: 978-3-433-03049-3. (2014).

McGrattan, K., Baum, H., and Rehm, H., Large eddy simulation of smoke movement. *Fire Safety Journal*, 1998; 30, 161-178.

McGrattan, K., Hostikka, S., McDermott, R., Floyd, J., Weinschenk, C., Overholt, K., "Fire Dynamics Simulator Technical Reference Guide Volume1: Mathematical Model*", NIST special publication 1018, sixth edition*. FDS Version 6.1.2. Fire Research Division Engineering Laboratory Gaithersburg, Maryland, USA. SVN repository revision: 20596. (2014).

National Cooperative Highway Research Program (NCHRP) Synthesis 415. Design fires in road tunnels. A synthesis of highway practice. Project 20-05, Topic 41-05. ISSN 0547-5570. ISBN 978-0-309-14330-1. Library of Congress Control No. 2010943183. (2011).

National Fire Protection Association (NFPA), "NFPA® 502, Standard for Road Tunnels, Bridges, and Other Limited Access Highways, 2011 Edition," ISBN 978-161665095-7.

Nobile, F. "Coupling strategies for the numerical simulation of blood flow in deformable arteries by 3D and 1D models". Mathematical and Computer Modelling 49. 2009; 2152-2160.

Oka, Y., Atkinson, G.T. Control of smoke flow in tunnel fires. Fire Safety Journal. 1995; 25(4):305–32.

Stefopoulos, E. K., Damigos, D. G., Design of emergency ventilation system for an underground storage facility. Tunnelling and Underground Space Technology y 22 (2007) 293–302.

Tewarson, A., SFPE Handbook of Fire Protection Engineering, second edition, Section 3, Chapter 4, eds: DiNenno, P., Beyler, C., Custer, R., Walton, W., National Fire Protection Association. (1995).

Townsend, A. A. "The structure of turbulent shear flow" Cambridge University Press, New York, 1956.

Van Maele, K., Merci, B., Application of RANS and LES field simulations to predict the critical ventilation velocity in longitudinally ventilated horizontal tunnels. Fire Saf J. 2008; 43:598–609

Vauquelin, O., Wu, Y., Influence of tunnel width on longitudinal smoke control. Fire Safety Journal. 2006; 41:420–426.

Ventsim Visual™, Ventsim Visual™ User Guide, Chasm Consulting, Volume 1, Version 4. . 2016

Wang, L., Chen, Q., "Applications of a Coupled Multizone-CFD Model to Calculate Airflow and Contaminant Dispersion in Built Environments for Emergency Management". HVAC&R Research. 2008; Vol 14. Number 6. pp. 925-939.

Wu, Y., Bakar, M.Z.A. Control of smoke flow in tunnel fires using longitudinal ventilation systems—a study of the critical velocity. Fire Saf J. 2000; 35:363–390.

Yuan, F. D., You, S. J., CFD simulation and optimization of the ventilation for subway side-platform. Tunnelling and Underground Space Technology 22 (2007) 474–482

Yuan, L., Mainiero, R. J., Rowland, J. H., Thomas, R. A., Smith, A. C., "Numerical and experimental study on flame spread over conveyor belts in a large-scale tunnel". *Journal of Loss Prevention in the Process Industries*, 2014; *30*, 55–62.

Appendix C: Chapter 8 Supplemental Data

Longitudinal and Transversal Velocity Components Analysis for Scenarios 2 and 3

The results of the longitudinal and the transversal velocity components analysis for scenarios 2 and 3 at different cross sections at t=900 s are presented in Figures 8.22 to 8.27.the normal quantile plot, box-and-whisker plots, distributions of u, v, and w velocities of all nodes, and standard deviations at different cross sections of the tunnel were plotted during the steady state condition. In addition, the dispersion of the longitudinal and transversal velocities in scenarios 2 and 3 are demonstrated in Figure 8.28. This study has shown that the longitudinal and transversal velocities distribution in scenario 2 behaved as same as the behavior of the values in scenario 1. The scenario 3 was considered for investigation of velocity components behavior upstream and downstream of the fire during the upstream transport of smoke scenarios.

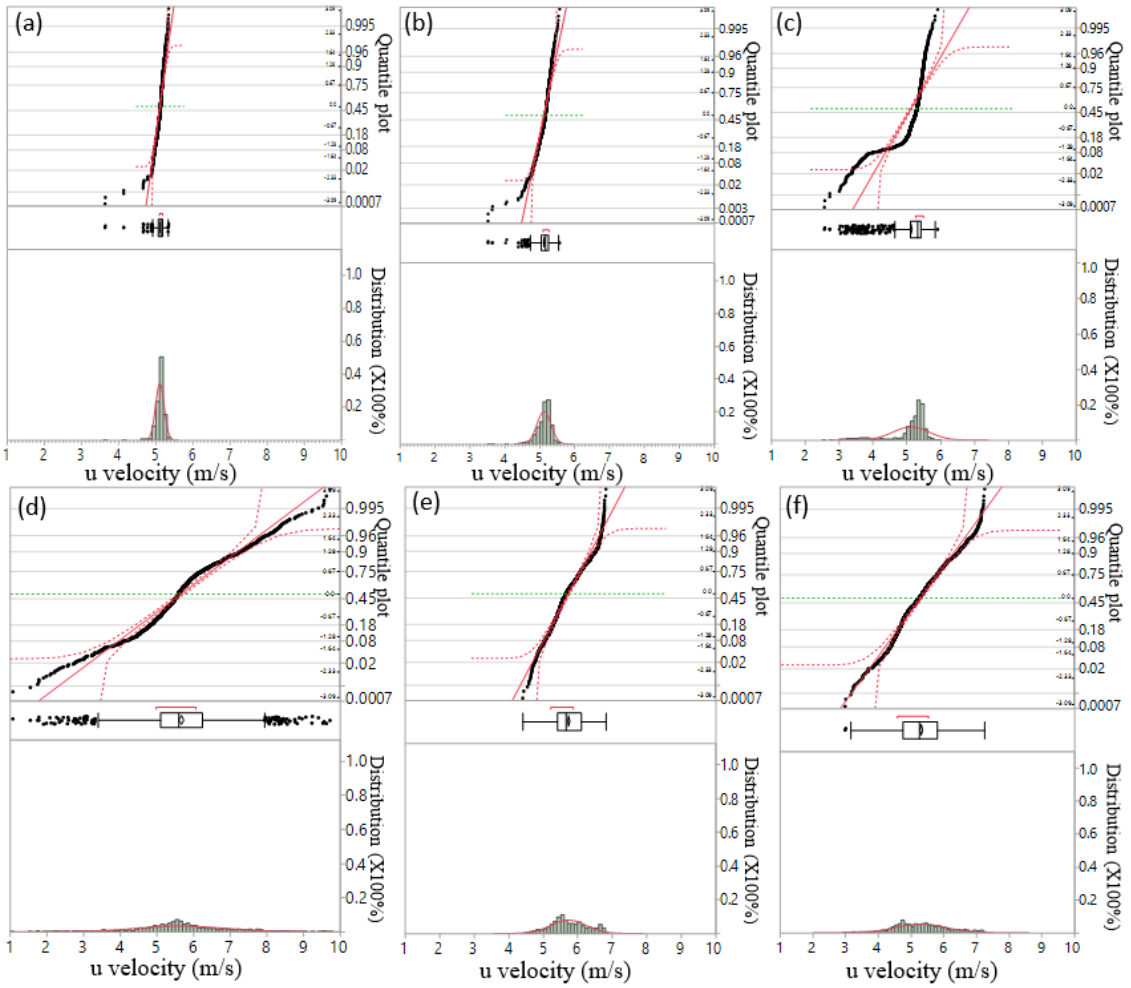

Figure 8.22. Normal quantile plot, box-and-whisker plots, and distributions of u velocity at different cross sections of the tunnel at t=900 s in scenario 2 at: (a) 430 m upstream, (b) 10 m upstream, (c) 7 m upstream, (d) 10 m downstream, (e) 100 m downstream, (f) 430 downstream

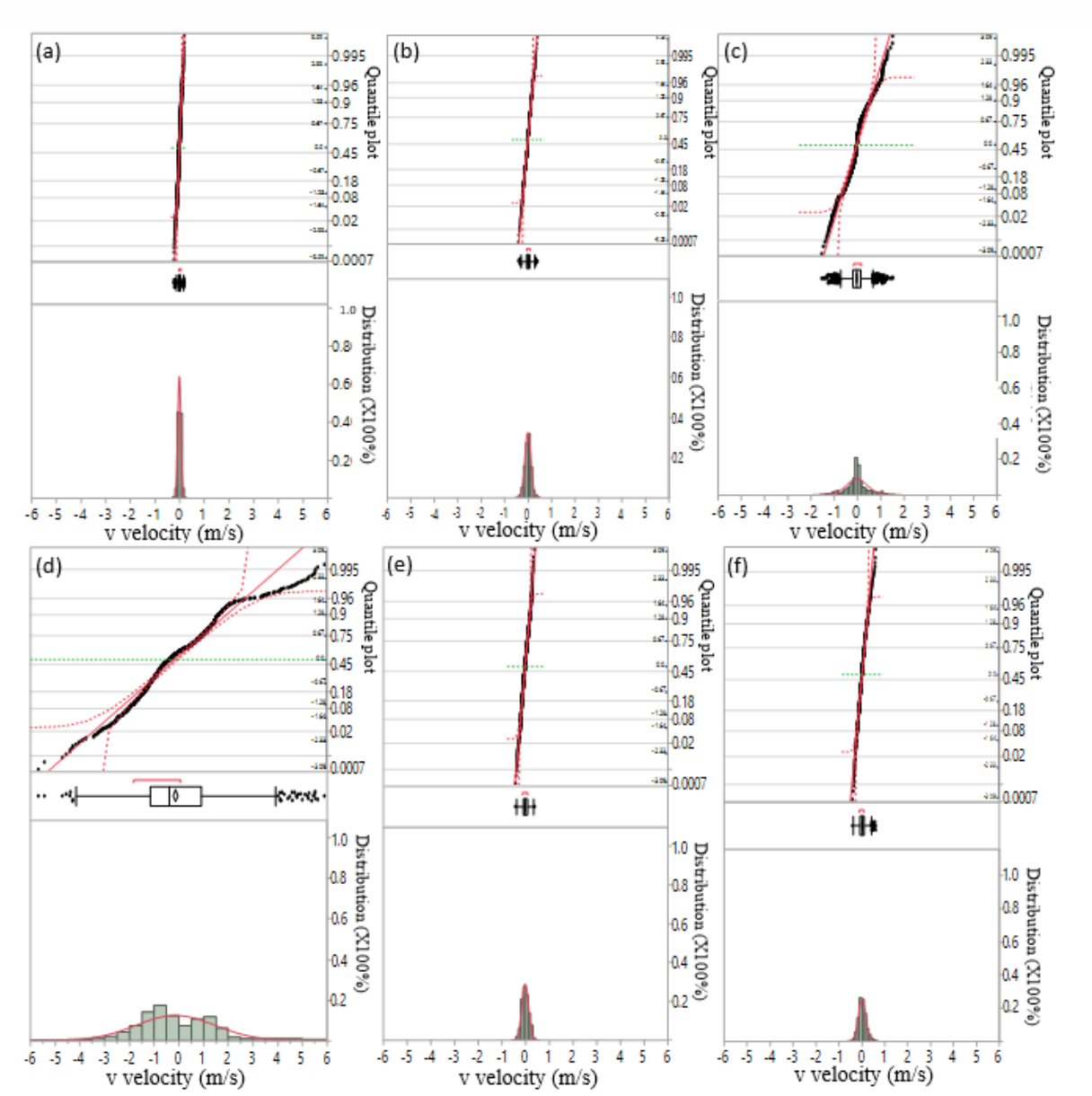

Figure 8.23. Normal quantile plot, box-and-whisker plots, and distributions of v velocity at different cross sections of the tunnel at t=900 s in scenario 2 at: (a) 430 m upstream, (b) 10 m upstream, (c) 7 m upstream, (d) 10 m downstream, (e) 100 m downstream, (f) 430 downstream

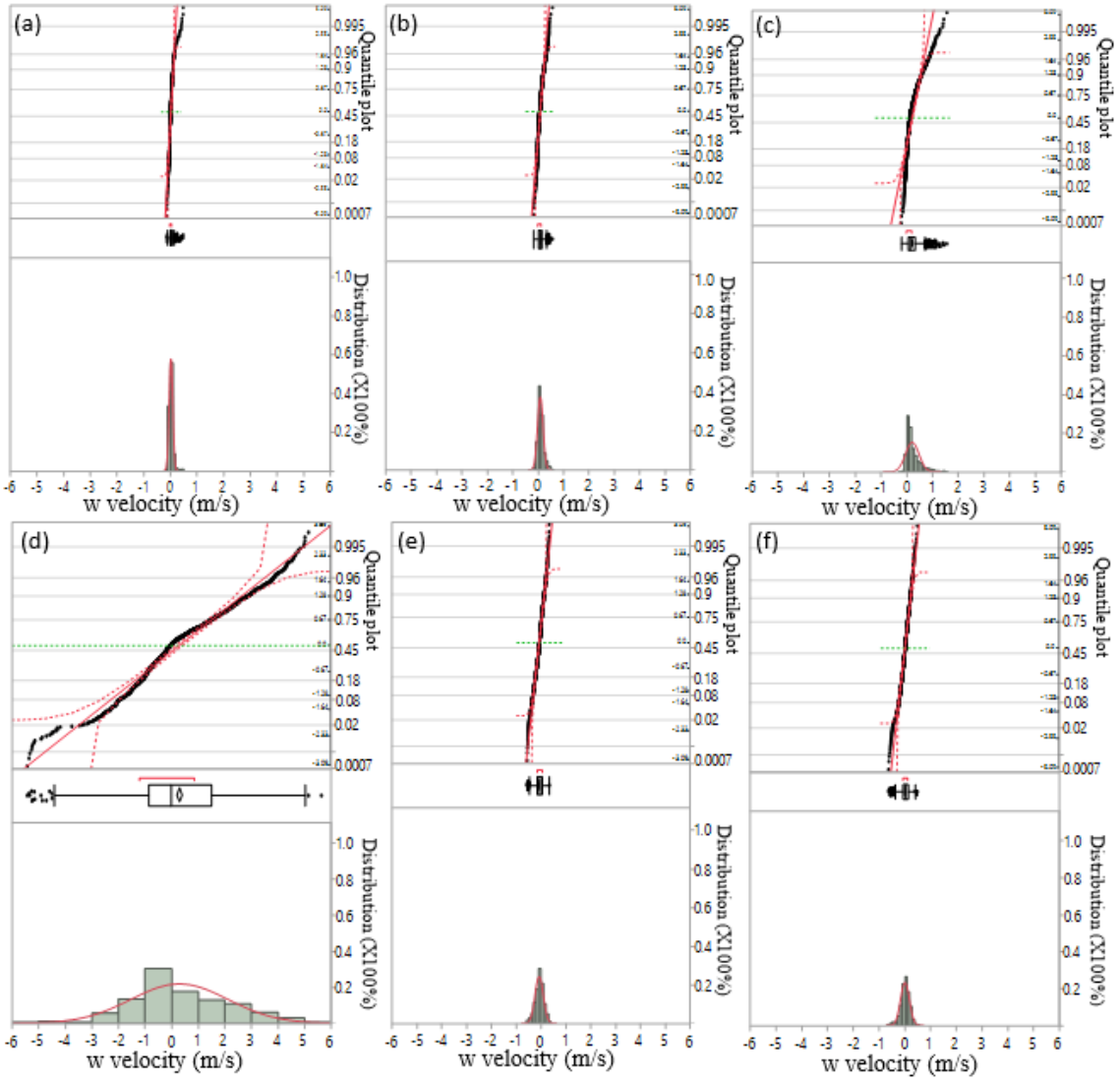

Figure 8.24. Normal quantile plot, box-and-whisker plots, and distributions of w velocity at different cross sections of the tunnel at t=900 s in scenario 2 at: (a) 430 m upstream, (b) 10 m upstream, (c) 7 m upstream, (d) 10 m downstream, (e) 100 m downstream, (f) 430 downstream

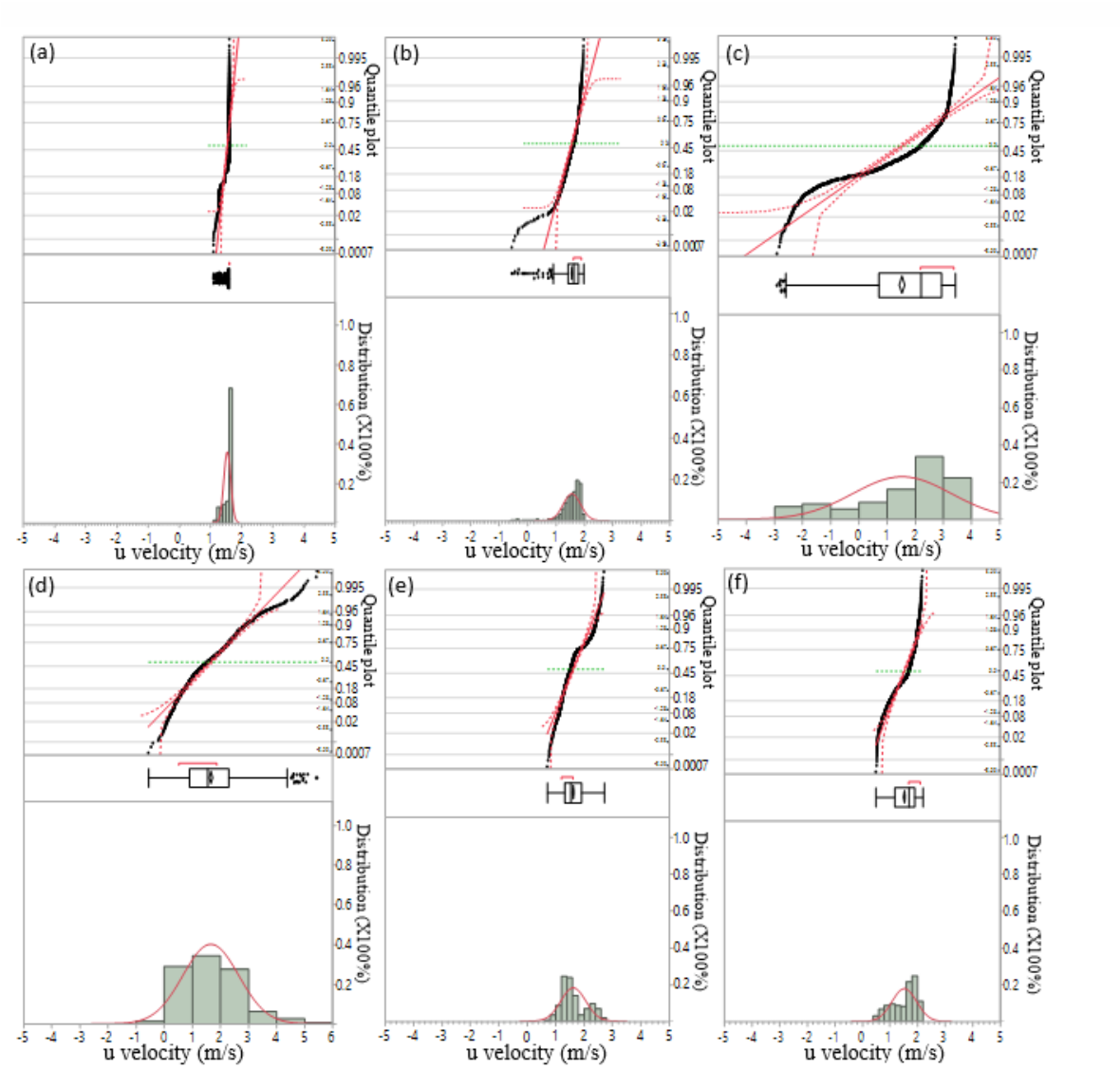

Figure 8.25. Normal quantile plot, box-and-whisker plots, and distributions of u velocity at different cross sections of the tunnel at t=900 s in scenario 3 at: (a) 430 m upstream, (b) 170 m upstream, (c) 10 m upstream, (d) 10 m downstream, (e) 100 m downstream, (f) 430 downstream

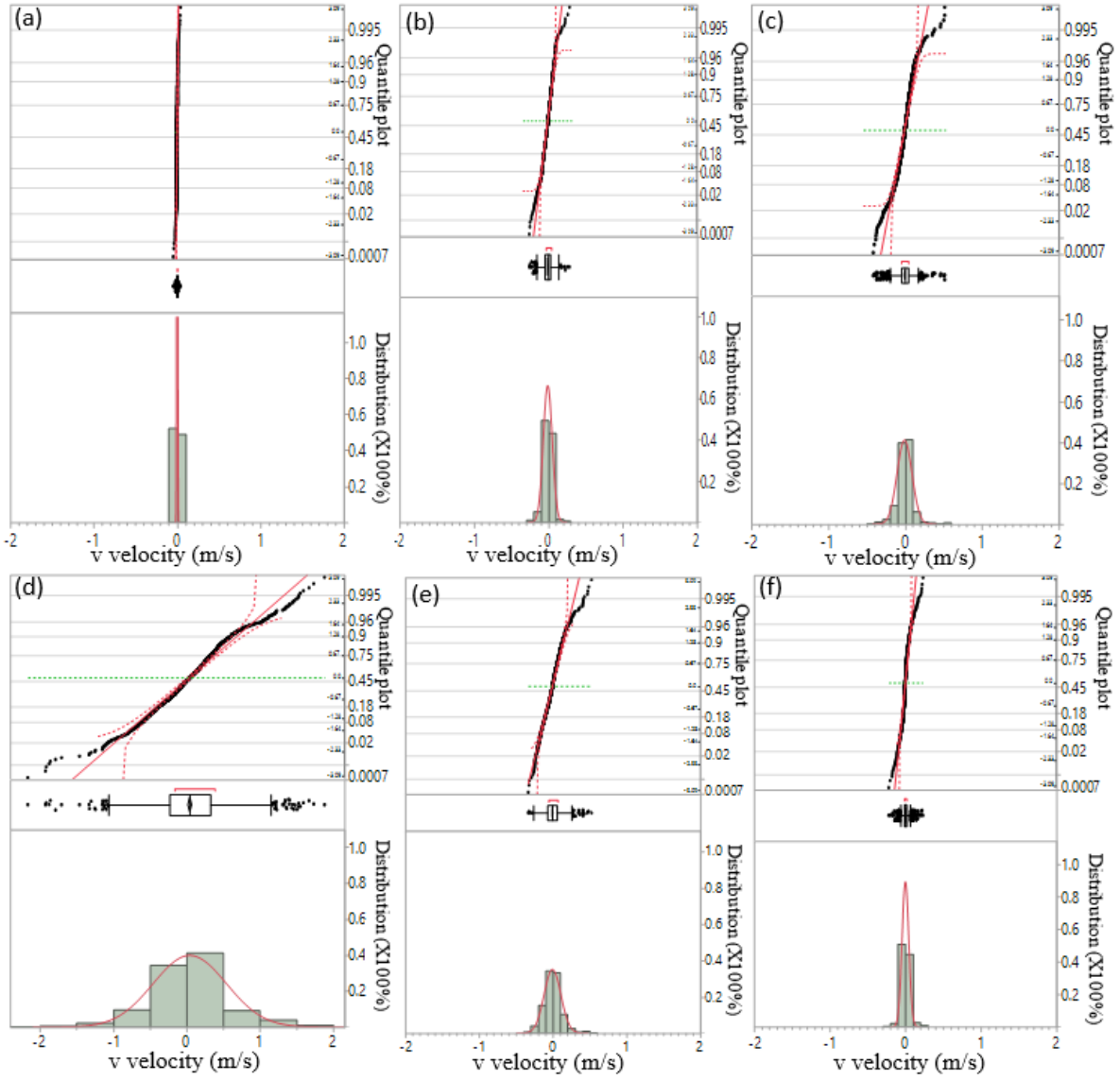

Figure 8.26. Normal quantile plot, box-and-whisker plots, and distributions of v velocity at different cross sections of the tunnel at t=900 s in scenario 3 at: (a) 430 m upstream, (b) 170 m upstream, (c) 10 m upstream, (d) 10 m downstream, (e) 100 m downstream, (f) 430 downstream

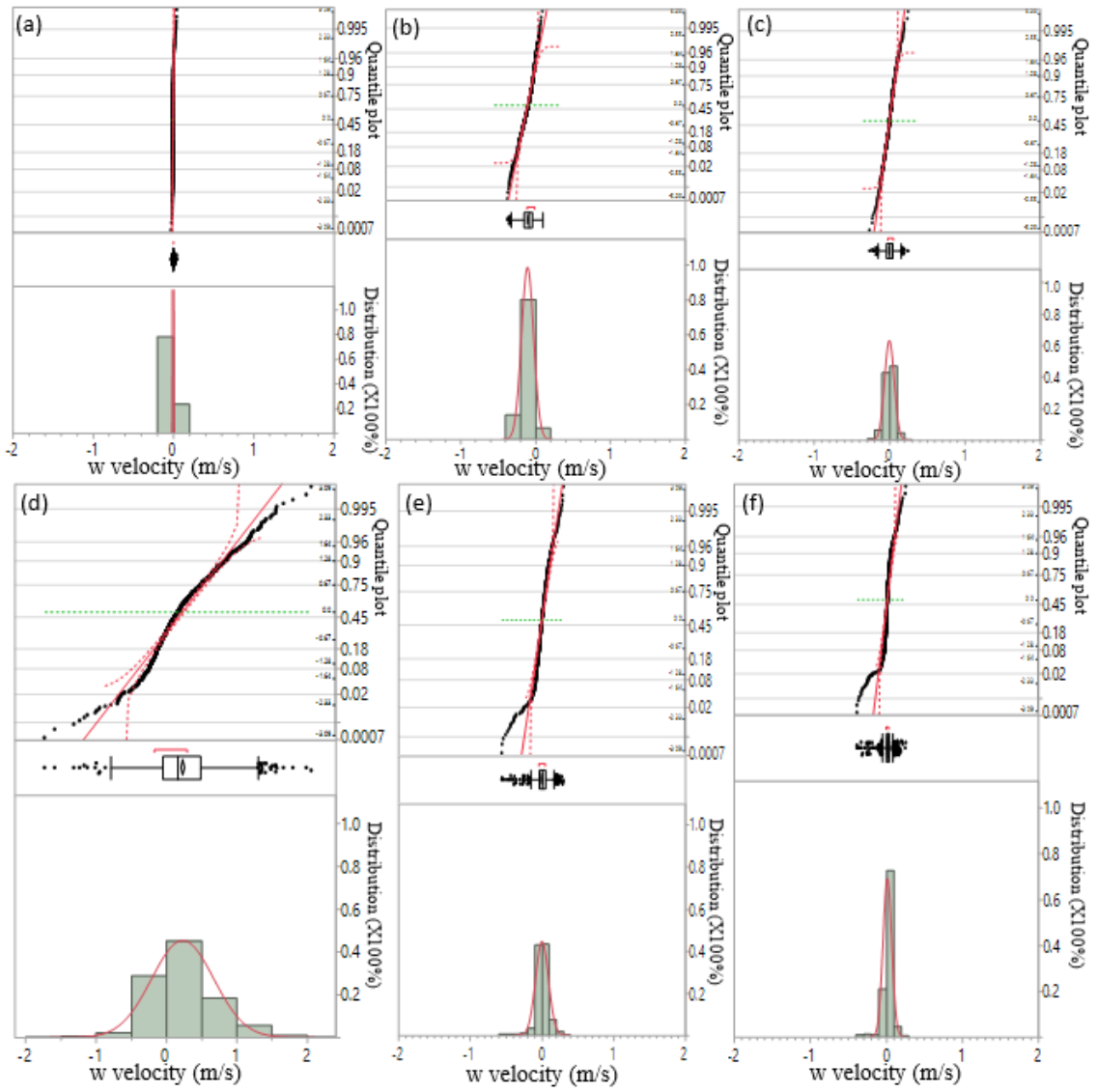

Figure 8.27. Normal quantile plot, box-and-whisker plots, and distributions of w velocity at different cross sections of the tunnel at t=900 s in scenario 3 at: (a) 430 m upstream, (b) 170 m upstream, (c) 10 m upstream, (d) 10 m downstream, (e) 100 m downstream, (f) 430 downstream

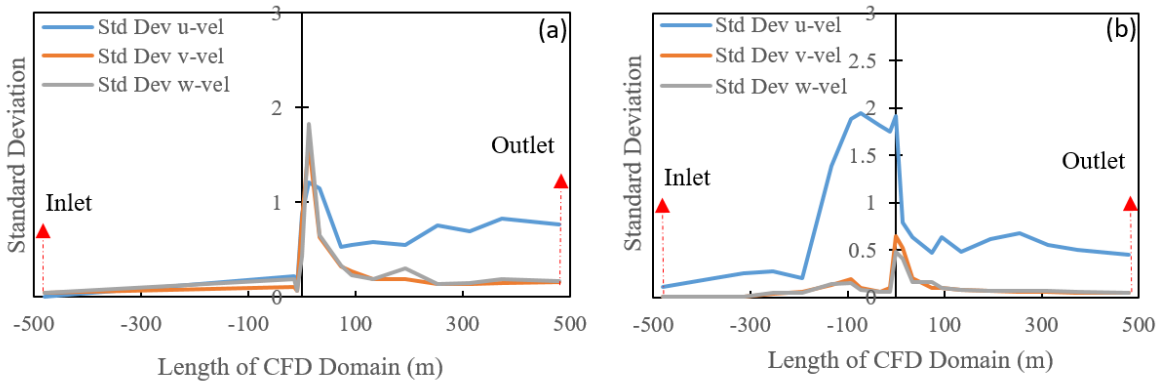

Figure 8.28. Standard deviation of u-, v-, and w velocities at different cross sections of the tunnel for (a) scenario 2 (b) scenario 3

Appendix D: Chapter 8 Supplemental Data

The Mean Velocity and Mean Velocity Components in Scenario 2 and 3

The mean velocity and mean velocity components in scenario 2 and 3 are shown in Figures 8.29 and 8.30 respectively.

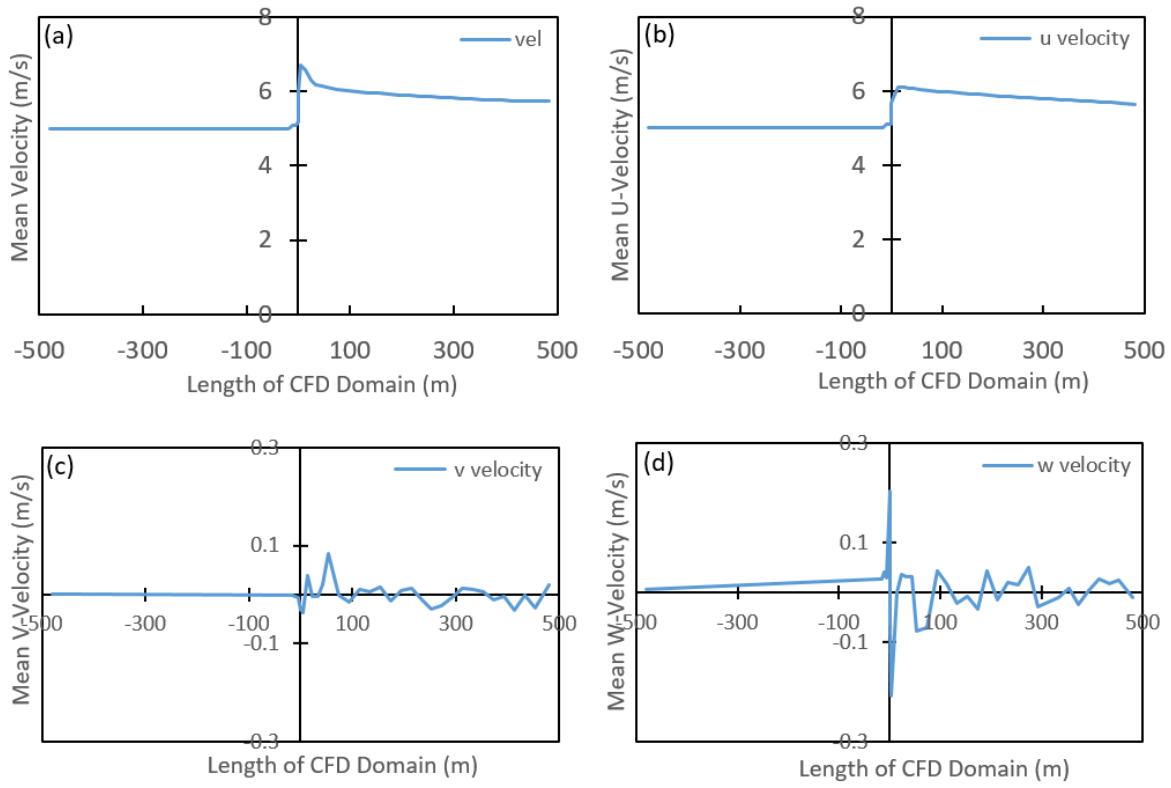

Figure 8.29. The mean velocity and its components along the height of the tunnel at different cross sections at t=900 s in scenario 2 (a) velocity (b) u velocity (c) v velocity (d) w velocity

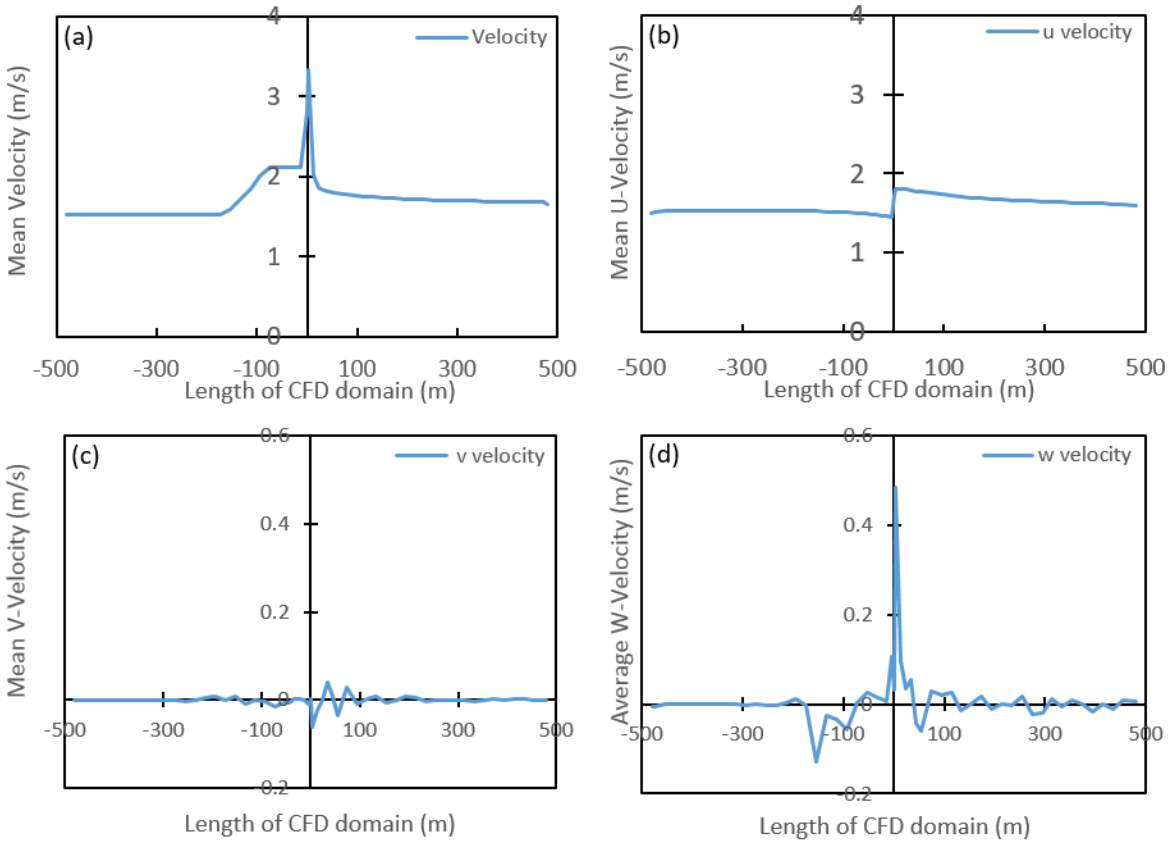

Figure 8.30. The mean velocity and its components along the height of the tunnel at different cross sections at t=900 s in scenario 3 (a) velocity (b) u velocity (c) v velocity (d) w velocity

9. Novel Methodology for Determination of Interface Boundary in the Multiscale Mine Fire Simulations

The following paper was submitted to Journal of Fire Science. Ali Haghighat conducted the majority of the work and wrote the paper with editorial input from coauthor: Dr. Kray Luxbacher.

9.1. Abstract

The numerical modelling cost of large complex dynamical systems, such as fire in underground spaces or mine tunnels is one of the most important challenges in underground research. A successful multiscale methodology can be a useful technique to decrease the simulation cost while the accuracy of results are maintained. Although, the multiscale approach can increase the simulation efficiency, the precision of the results is highly dependent on the interface boundary location. The location of the interface boundary can determine the decomposition location of 3D and 1D subdomains. The research in this paper develops a novel methodology to determine the interface boundary between CFD model (near fire field) and 1D model (far field) of fire simulations at a coal mine working face under steady state conditions. The development of the methodology is based on the physics of the fluid structure, turbulent kinetic energy (TKE) of the dynamical system, and the vortex dynamics. Different working face methane fire scenarios ranging from 200 kW to 1000 kW were investigated with various inlet velocities. The impact of velocity changes, HRR changes, and the ventilation curtain position on the selection of interface boundary were also investigated. An indirect coupling strategy was utilized to couple CFD models to the 1D models at the selected interface boundary and the coupled models results were compared to the full CFD models results. The calculated error between CFD and coupled models for the mean temperature and the mean velocity at different cross sections were calculated less than 6%. An algorithm based on the results was developed for the selection of 3D-1D interface boundary for the underground mine fire simulations. The developed approach can be utilized to determine the interface boundary of multiscale simulation of different types of fire (e.g., longwall fires, electrical installation, gob fires, belt fires, etc.) in underground mines or more complex computational domains.

9.2. Introduction

Over the past century, great strides have been made in the advancement of mine fire knowledge. However, fire hazards remain a critical hazard in underground coal mines in the U.S. and around the world. Fires in underground coal mines have contributed to catastrophic events, and the possibility for the safe escape of miners and also the design of emergency plans in firefighting missions for fire brigade teams or mine rescue teams are the main concerns during a fire event in a mine. A precise fire numerical analysis before any fire events can give a detailed view of the emergency situation, and lead to better response and improved safety. However, the high computational cost of such simulations has limited their application. When they are applied, computational fluid dynamics (CFD) numerical analysis is utilized for precise studies near the fire field [1-3]. While network modeling, one-dimensional (1D) simulation, is often used for fire analysis of large computational domains such as underground mine tunnel environments. The 1D simulations technique is commonly used due to the much lower computational cost, but the physics of the complex regions encountered close to the fire source are not captured precisely. The coupling of CFD fire simulations to the 1D fire simulations (multiscale fire simulation, 3D-1D) is a useful technique to reduce the computational time without significant loss of accuracy. This technique is extensively applied in different engineering fields, such as mechanical engineering, environmental engineering, and bio engineering [4-11]. Coupling methods have also been used in the simulation of airflow and fire in the transportation tunnels [8-11].

According to previous research studies [e.g., 10], the significant parameter for accuracy of large system multiscale simulation is the location of the interface boundary between 3D and 1D simulations. Therefore, for determination of the interface boundary, there is a need to simulate several multiscale simulations. Based on the calculated lowest average error between CFD and coupled models at different cross sections, an interface boundary can be determined [e.g., 10]. Several studies have described an exhaustive systematic method for determination of 3D-1D interface boundaries [8-11]. However, in this study, a state-of-the-art methodology was developed to determine the interface

boundaries based on the fundamental physics of the fluid, including the physics of the fluid structure, turbulent kinetic energy (TKE), and the vortex dynamics. In addition, a large eddy simulation (LES) mathematical model was considered for turbulence simulation in this research study.

LES has been used extensively for the fire numerical analysis study in different research areas such as fire plume studies, flame height studies, plume temperature, mine fires, and etc. [12-19]. This approach has some advantages compared to the Reynolds-averaged Navier-Stokes (RANS) equations which were utilized in previous research studies. Based on the results of the comparison of the RANS and LES approaches for well-ventilated horizontal tunnel fires, it was evident that the temperature contours of the LES simulations for 30 kW fire show better agreement with the experimental results than the RANS simulations results. Furthermore, the turbulent thermal diffusion in the LES simulation showed better agreement than in the RANS simulations due to the large-scale unsteadiness in the LES [20]. Although RANS can provide results for mean quantities with acceptable accuracy at moderate cost for simulation of fire and smoke propagation [10, 11, 20-23], LES was selected for simulation of the turbulent fluctuations.

Previous research studies results have shown that the interface boundary should be located in the regions where the flow structure is quasi-1D which means that the streamwise component of the fluid is the dominant component on the flow-field [8-10, 20]. Moreover, in order to decompose the whole domain into 3D and 1D sub-domains as shown in Figure 9.1, the continuity of the following quantities at the interface boundaries should be met [24].

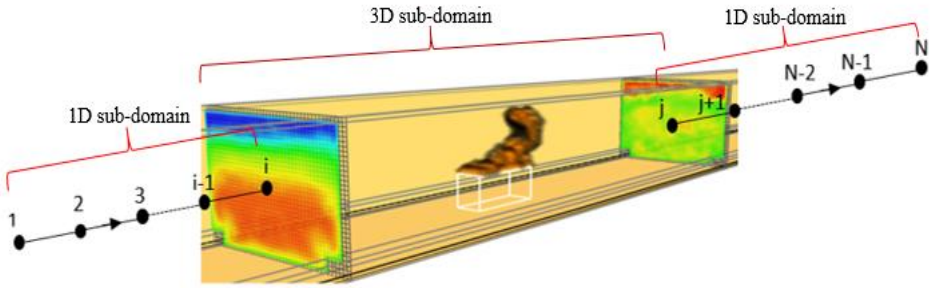

Figure 9.1. Decomposition of the global domain into 1D and 3D sub-domains (after [10])

$$Area\ A(a^-) = A(a^+) \tag{9-1}$$

$$Mean\ pressure\ p(a^-) = p(a^+) \tag{9-2}$$

$$Mean\ velocity\ \bar{v}(a^-) = \bar{v}(a^+) \tag{9-3}$$

$$Mean\ Temperature\ \bar{T}(a^-) = \bar{T}(a^+) \tag{9-4}$$

Therefore, since the mean properties of fluid (mean velocity, mean temperature, mean pressure) are transferred at the 1D-3D interface in both directions, all node values of the 3D model at the interface should be almost uniform and close to the mean values. Under these circumstances, the single value (mean value) of the 3D model at the interface boundary can be the precise representative of all the nodes in that cross section for a dynamic system.

This research study focuses on the development of a state-of-the-art methodology to determine the interface boundary in multiscale simulations of the active face fires in underground coal mines. The development of the methodology is based on the fundamental physics of the fluid structure, Turbulent Kinetic Energy (TKE) of the dynamical system, and the vortex dynamics. Detailed longitudinal and transversal velocities analyses were conducted to distinguish the region where the streamwise component of the fluid dominated the flow-field. Moreover, for determination of the quasi-1D region, there was a need to investigate the tendency of fluid particles to rotate and also the intensity of turbulence of the system. Therefore, the mean vorticity along X, Y, and Z axes and the mean turbulent kinetic energy at different cross sections of the mine tunnels were analyzed.

The computational fluid dynamics software, Fire Dynamics Simulator (FDS), Version 6.0 was utilized to determine the region where the airflow behaves as the quasi-1D fluid. The formulation of the equations and the numerical algorithm are described in detail in the FDS technical reference guide [25].

Due to the potential for high levels of methane gas and coal dust during the production at the continuous miner working face, this operating region is considered one of the most significant risk areas for fire events. Therefore, a methane fire event at a continuous miner heading as shown in Figure 9.2, number 8 entry, with the exhausting line curtain set to the right side, was considered as the computational domain. In continuous miner headings, due to different magnitudes of the ignition or resulting fire, auxiliary ventilation controls may be dislodged, affecting the ventilation into the area. Therefore, the effect of ventilation curtain removal on the selection of interface boundary, for coupling of the 3D simulations to the 1D simulations was investigated. According to the various velocities and HRR, thirteen fire scenarios were utilized to investigate the impact of velocity and HRR changes on the selection of 3D-1D interface boundary.

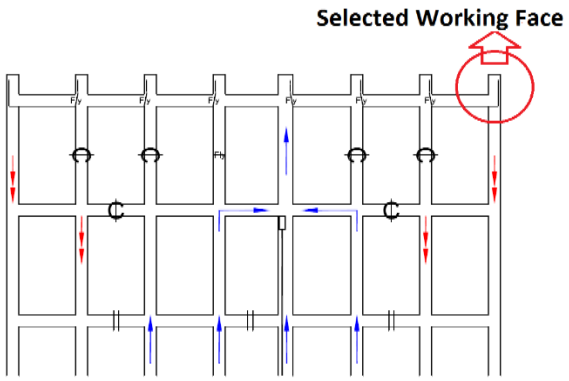

Figure 9.2. Schematic view of the selected working face (after [19])

The interface boundary regions were determined for all scenarios according to the conducted studies results. Then, the 1D models were simulated using VentFIRE^{TM} in order to couple to the full CFD simulations. An indirect coupling strategy was utilized for coupling of CFD models to 1D models; the coupled results were compared to the full CFD and 1D models. Based on the results, the interface boundary for multiscale simulation of

fire at coal mine working faces was recommended. Then, a general algorithm was developed based on the physics of the fluid structure for multiscale (3D-1D) simulation of all kinds of fire (e.g., longwall fire, gob fire, vehicle fire, electrical installation fire, and belt fire) for underground mines.

9.3. Computational Domain and Design Consideration

According to U.S. regulations, in exhausting face ventilation systems in all underground coal mines, the mean entry air velocity reaching each working face where coal is being cut should be at least 0.3 m/s [26]. In addition, the maximum air velocity at the working faces was recommended to be 4 m/s, because higher velocities can result in personnel discomfort and increased dust entrainment in the area [27]. Therefore, three different velocities as the minimum (0.3 m/s), the velocity based on a partner mine in the United States (0.6 m/s), and the maximum velocity (4.0 m/s) were considered to investigate the effect of velocity changes on the determination of 3D-1D interface boundary of the working face fire simulations.

There is no information in the literature quantifying a heat release rate for methane ignitions at the working faces in underground coal mines, due to the difficulty in measuring or estimating the fuel mass loss or gas consumption in a real scenario. Some research studies were conducted to measure the peak HRR of a drilling rig and a loader fire which they were as 29.4 MW and 15.9 MW, respectively [28]. In addition, the maximum HRR of a single wood crib was measured at about 180 kW [29].

Moreover, different experiments were conducted by the U.S. National Institute for Occupational Safety and Health (NIOSH) for better understanding of mine fires, using a natural gas burner with a rated HRR of 44 to 114 kW [30]. Additionally, an experiment was conducted on 230-kW, 1-MW and 3-MW diesel fuel fires to investigate the effect of ventilation and preborn time on water mist extinguishing [31]. Although there is a lack of information in terms of HRR, there are some data in terms of flame height and physical size of the fire at working faces. According to MSHA mine fire accident reports from 2000 to 2012, most fires at working faces were reported as small fires, such as a floor methane

fire in 2000 which the flame size was reported to be 0.25 m high and 1 m long by 1 m wide in the presence of curtain. Consistent with the data of previous research, the simulated 200 kW methane fire at a working face agreed well with the reported flame size [19]. Although none of the reported flame heights at the working faces reached to the ceiling, the maximum HRR was selected at 1000 kW, which would correspond to a flame height of about 2.7 m. Therefore, different fire scenarios ranging from 200 kW to 1000 kW were simulated in order to investigate the effect of HRR changes on the selection of a multiscale interface boundary for underground mines working face fire simulations. In this study, it was assumed that the methane was ignited on a surface that was 1 m long and 1 m wide. The thickness of the coal under the fire source was 0.2 m. The minimum, medium, and maximum values for velocity and HRR as shown in Table 9.1 were considered to investigate the effect of HRR and velocity changes on the selection of interface boundary.

Table 9.1. Selected values for design of simulations

Parameter	Minimum	Medium	Maximum
Velocity (m/s)	0.3	0.6	4.0
HRR (kW)	200	600	1000

The simulated fire in this research study was a fuel-controlled fire since the most entry fires were reported as the fuel-controlled fires [32]. It was assumed that the ignition and fire occurred during continuous miner production. In this study, the ignition magnitudes were not quantified. It is common for an ignition to damage or destroy auxiliary ventilation controls in a dead end mining face, so effects of ventilation curtain removal on the selection of 3D-1D interface boundary was investigated. The simulated scenario conditions are shown in Tables 9.2 and 9.3.

Table 9.2. Different scenarios based on the curtain position, fire size (HRR), and inlet velocity

Curtain position	Scenario	HRR (kW)	Velocity (m/s)	Curtain position	Scenarios	HRR (kW)	Velocity (m/s)
With Curtain	Scenario 1	200	0.3	Without Curtain	Scenario 4	200	0.3
	Scenario 2	200	0.6		Scenario 5	200	0.6
	Scenario 3	200	4		Scenario 6	200	4.0

Table 9.3. Different scenarios based on the curtain position, fire size (HRR), and inlet velocity

Curtain position	Scenario	HRR (kW)	Velocity (m/s)	Curtain position	Scenarios	HRR (kW)	Velocity (m/s)
With Curtain	Scenario 7	200	0.6	Without Curtain	Scenario 10	200	0.6
	Scenario 8	600	0.6		Scenario 11	600	0.6
	Scenario 9	1000	0.6		Scenario 12	1000	0.6
					Scenario 13	1000	0.3

In all scenarios, it was assumed that a methane fed fire was started by an initial ignition event. The fire was set on the floor at the center, close to the face. The geometry and ventilation are generally based on a partner mine in the United States. The width and height of the entries were 6 m and 1.8 m, respectively. The length of the entry that had the continuous miner in it was set at 15 m and the distance from the outlet to the end of the curtain was 49 m. The curtain was installed in the entry, 0.9 m from the closest rib. The length of the inlet to the main entry was 73 m. The thickness of the coal on the wall assumed to be 0.1 m for consideration of thermal conduction through the wall. The detailed tunnels geometry dimensions, continuous miner, fire source, airflow direction, and exhausting curtain utilized in all simulations are shown in Figure 9.3. The hydraulic diameter (D_h) of the tunnels was calculated at 2.769 m. The exhausting ventilation curtain was removed from the computational domain for scenarios without exhausting line curtain (scenarios 4 through 6 and also scenarios 10 through 13).

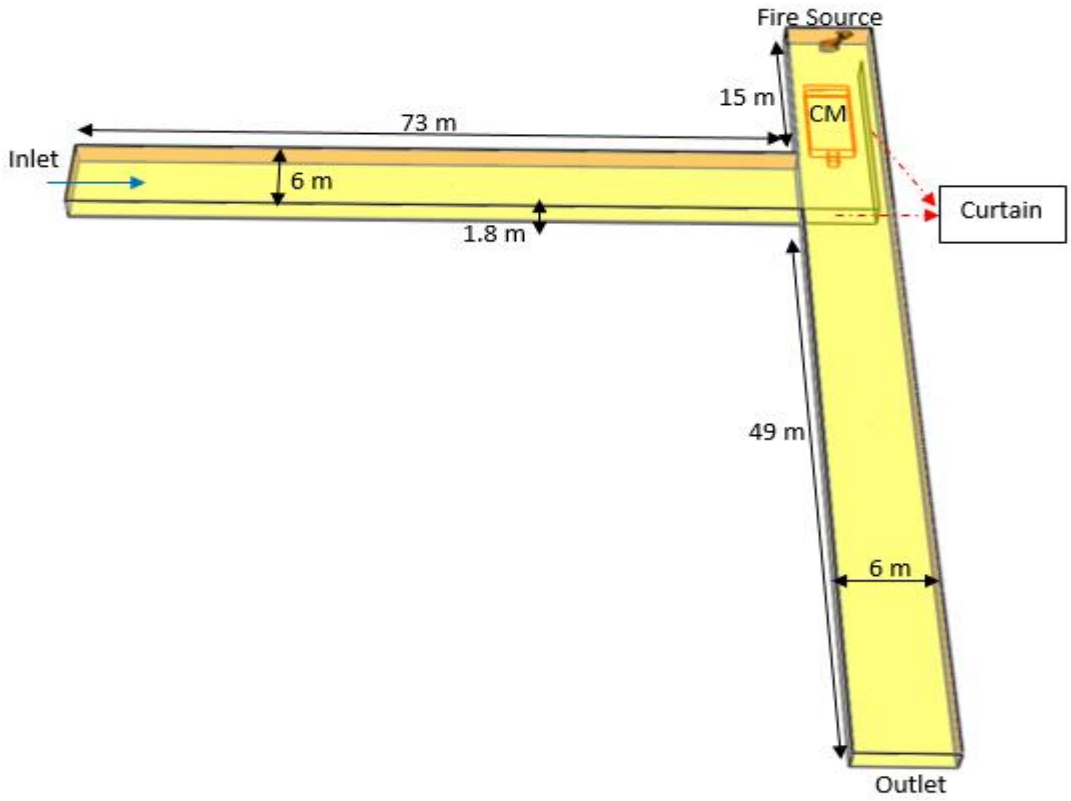

Figure 9.3. Geometry dimension and objects in the computational domain (isometric view)

Methane fire characteristics such as heat of combustion and soot yield were set to 55.5 MJ/kg and 0.1 kg/kg, respectively. The thermal and the physical characteristics of Pittsburgh bituminous coal [33], were considered for the characteristics of the walls in all simulations. The detailed characteristics of the exhausting line curtain explained in the previous research [19, 34, 35], was utilized in the simulations. For the simulation of the continuous miner body in the computational domain, the thermal and mechanical properties of steel were considered. Since the specific heat and the conductivity of the steel are temperature dependent, the referenced parameters were varied based on different temperatures. In FDS, we assumed that reliable numerical results can be achieved when the grid size is $\leq 0.1D^*$ [12], where D^* is explained in detail in [36, 37]. Therefore, grid sizes of 5 cm, 8 cm, and 10 cm were considered for the numerical analysis of the 200 kW, 600 kW, and 1000 kW methane fires respectively in this study. The t-squared approach was utilized for the growth of the methane fire at the face [38]. The decay time period for

methane fire was ignored in the study as the focus of the research in this paper was the development of a methodology for determination of 3D-1D interface boundary of the working face fire simulations. The growth of the fire at the face was assumed to be fast to ultra-fast growth, with a fire growth coefficient set at 0.16 kW/s^2 [39]. The volume flow rate at the inlet varied in the range of 3.24 m^3/s to 43.2 m^3/s and the outlet was set to open. A no-slip boundary condition was considered for all walls and objects in the computational domain.

9.4. Methodology Development for Interface Boundary Determination

The region where the flow structure is quasi-1D is the region where the longitudinal velocity is the dominant component of velocity on the fluid structure in that region [8-10, 20]. Therefore, 1D simulation can be performed on that region since the transversal velocity components do not affect the fluid structure and the results. Due to this, a detailed longitudinal and transversal velocity components analysis was conducted in order to determine the region where the longitudinal velocity dominates the fluid field. In the other words, the region where the influence of transversal velocity components on the fluid structure were inconsequential, was determined. Further, the intensity of the turbulence of the system was investigated with turbulent kinetic energy (TKE) analysis. Furthermore, in order to determine the region where the transversal velocity components have inconsequential effect on the fluid field, the tendency of fluid particles to rotate (vorticity) along different axes (X, Y, and Z), was investigated. In the worst case scenario (scenario 13 with no line curtain, and relatively high HRR and low velocity), it was observed that the rollback did not advance along the longitudinal axis after 1300 s and after that the steady-state flow condition in the tunnel was reached. Therefore, all parameters upstream and downstream of the fire source in all scenarios were investigated at t=1300 s. All parameters were calculated at all nodes along the height of the tunnel at different cross sections of the mine. All calculations are at a distance from the flow path as shown in Figures 9.4 (a) and 9.4 (b) for both curtain and curtain less scenarios respectively. The development of the methodology for selection of the interface boundary to couple 3D and 1D simulations in scenario 1 was explained in sections 9.4.1 and 9.4.2 in detail. The

methodology for the rest of the scenarios, and, also, the effect of changes in velocity, HRR, and the ventilation curtain position were investigated in section 9.5.

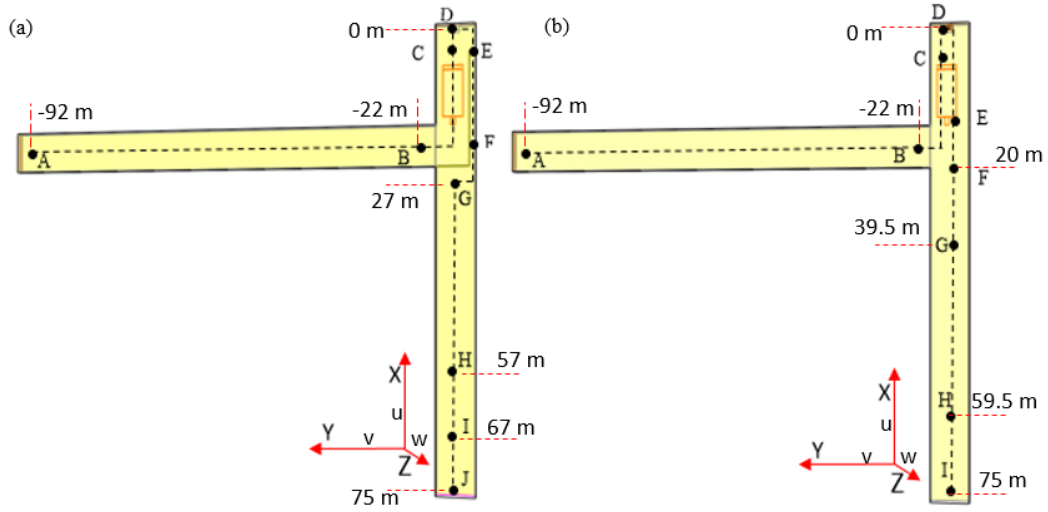

Figure 9.4. Distance from flow path and the selected cross sections for all scenarios a) scenarios with curtain (scenarios 1, 2, 3, 7, 8, and 9) b) without exhausting line curtain scenarios (scenarios 4, 5, 6, 10, 11, 12, and 13) (top View). Continuous miner is shown in orange

In all scenarios, the velocity component parallel to the airflow direction represents the longitudinal velocity component and the velocity components in the horizontal (lateral) and the vertical directions perpendicular to the airflow represents the transversal velocity components. Therefore, the velocity along the X-axis in the inlet tunnel represents the transversal velocity component in the horizontal direction while the velocity along X-axis in the outlet tunnel is the longitudinal velocity component.

9.4.1. Longitudinal and Transversal Velocity Components Analysis

The longitudinal and transversal velocity components of all nodes along the height of the tunnel at different cross sections in scenario 1 were calculated. The results were used to analyze the distribution and normality of the longitudinal velocity and the transversal velocities (lateral and vertical) of all nodes at different cross sections of the tunnel upstream and downstream of the fire source at t=1300 s. The zero line represents the cross section of the tunnel at the center of the fire source. In scenario 1, because the velocity is less than

critical velocity, the smoke progressed into the continuous miner face about 11 m outby the mouth of the curtain, as shown in Figure 9.5. However, because of the presence of exhausting line curtain, the smoke did not progress into the inlet airway. Previous research [19] has shown that the smoke progress from the mouth of the curtain depended on the curtain length. Therefore, the use of ventilation curtain can influence the transport of smoke and fluid structure upwind; consequently, the selection of interface boundary would be affected by the position of the ventilation curtain.

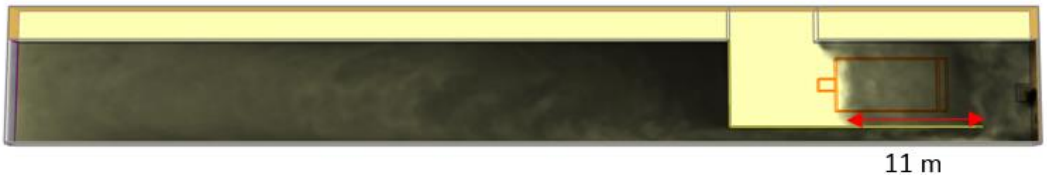

Figure 9.5. Smoke progress to the continuous miner area in scenario 1 at t=1300 s (top view)

Due to the presence of the objects (continuous miner and ventilation curtain) in the continuous miner face and the upwind transport of smoke in the continuous miner region, the dynamic flow field in the continuous miner face was not quasi-1D. Therefore, the continuous miner face is clearly not an ideal place to couple 3D and 1D simulations. On the other hand, some 1D simulation software such as MFIRE are not able to analyze the fluid structure in the narrow channels or airways (such as the airway at the backside of the curtain) [40]. Therefore, the region to decompose the domain into the 3D and 1D sub-domains should be located away from the continuous miner face region at upstream and downstream regions. In addition, because of the sudden expansion at the outlet of the exhausting line curtain, a large eddy zone at the outlet of the curtain is created. Therefore, the flow pattern is not quasi-1D at that zone. Hence, the interface boundary should be located far away from the outlet. The flow pattern based on time at the outlet of the exhausting line curtain is plotted as shown in Figure 9.6.

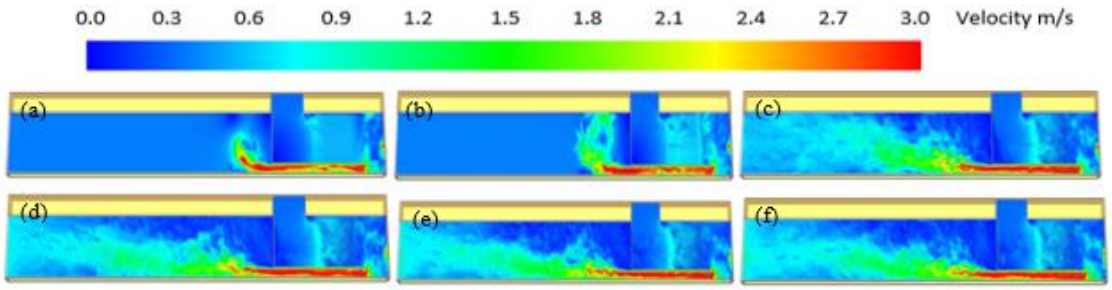

Figure 9.6. the flow pattern at the outlet of the exhausting line curtain according to different time at z = 1.3 m (a) 10 s (b) 16 s (c) 100 s (d) 200 s (e) 500 s (f) 1300 s (top view)

The normal quantile plot, box-and-whisker plots, and the distributions of the longitudinal and transversal velocities of all nodes at different cross sections of the tunnel in scenario 1 are shown in Figures 9.7, 9.8, and 9.9. All distances are from the center line of the fire source at the working face as shown in Figure 9.4 (a).

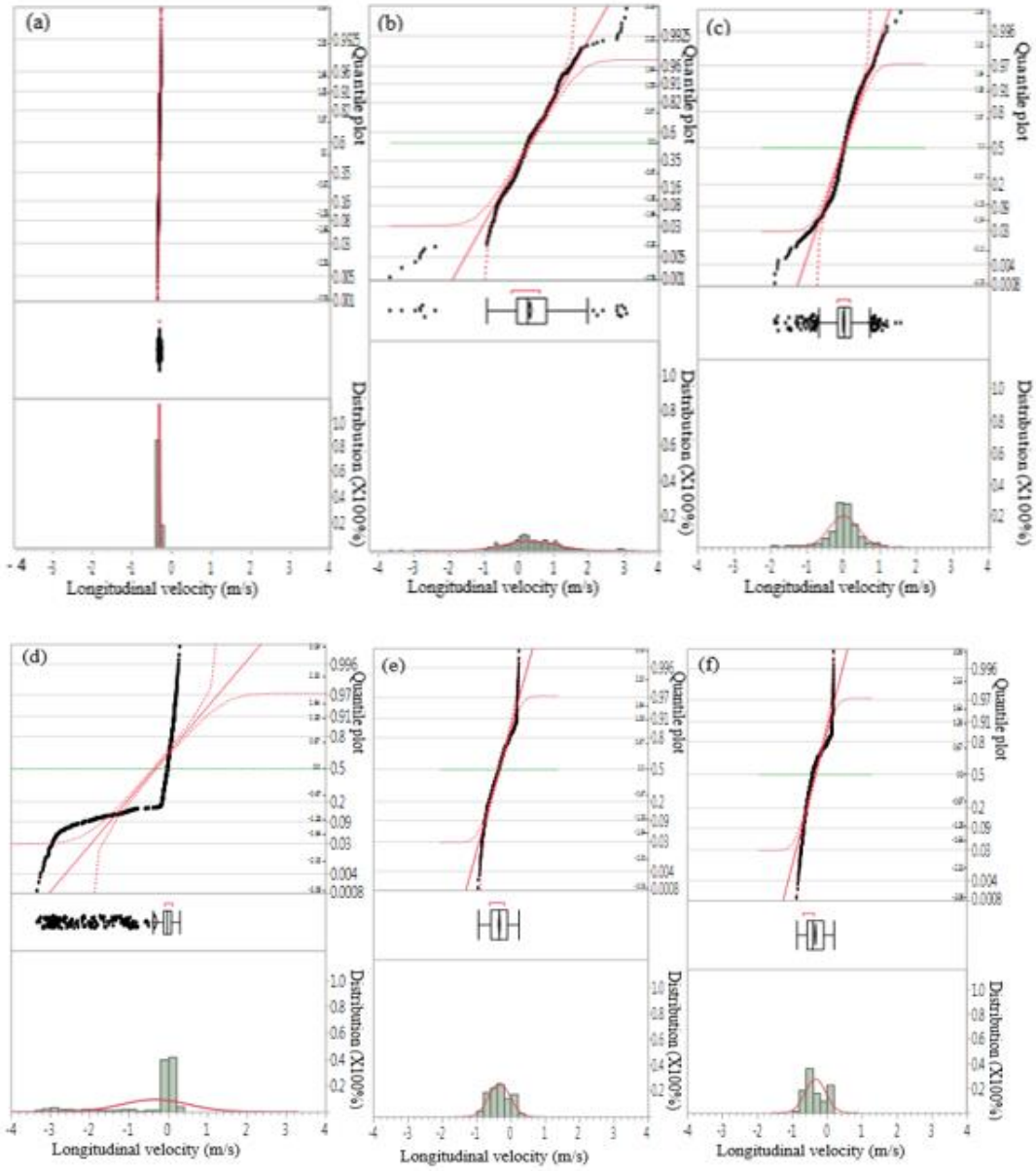

Figure 9.7. Normal quantile plot, box-and-whisker plots, and distributions of longitudinal velocity at different cross sections of the tunnels at t=1300 s in scenario 1 (a) cross section B (b) cross section C (c) cross section D (d) cross section G (e) cross section H (f) cross section I (the cross sections are based on Figure 9.4 (a))

According to the data of Figure 9.7, by getting closer to the mouth of the curtain and the fire source (Figures 9.7 (b) and 9.7 (c)), the distribution of the longitudinal velocity of all nodes along the height of the tunnel at those cross sections is not normally distributed. However, the longitudinal velocity of all nodes along the height of the tunnel at different cross sections from the inlet (cross section A) to 23 m upstream of the fire source (Figure

9.7 (a)) were distributed normally. Also, the longitudinal velocity of all nodes at each cross section was not distributed normally up to 57 m downstream of the fire (cross section H). Again, the normal distribution was observed from that cross section to the outlet (Figures 9.7 (e) and 9.7 (f)). The box-and-whisker plots in Figure 9.7 show that the dispersion of the longitudinal velocity values at cross sections increased as one moves closer to the end of the curtain at the return or the fire source as shown in Figures 9.7 (b) and 9.7 (c). Due to the sudden expansion at the outlet of the curtain, the longitudinal velocity has the highest dispersion, as shown in Figure 9.7 (d). At that section (cross section G) about 45% of the longitudinal values were in opposite direction of the air flow. However, by getting further from the cross section G, the percentage of the longitudinal velocity in opposite direction of the stream decreased. At the cross section H (30 m away from the cross section G), just 19% of the longitudinal velocity values were calculated in opposite direction of the airflow. Due to the produced eddies and the turbulent flow field in the underground mine tunnels downstream of the fire source, the percentage of the longitudinal velocity in opposite direction from that cross section up to the outlet remained constant.

The distribution of transversal velocity components in horizontal (lateral) and vertical directions, shown in Figures 9.8 and 9.9, are similar to the distribution of longitudinal velocity component. A normal distribution of the transversal velocities in horizontal and vertical directions were not observed in the continuous miner face (close to the fire source) while a normal distribution was observed far away from the fire source (e.g., from the inlet to the cross section B upstream and from the cross section H downstream to the outlet). Moreover, the spread of transversal velocity components (in horizontal and vertical directions) of all nodes along the height of the tunnel at different cross sections decreased by getting away from the continuous miner region. In the other words, the domination of transversal velocity components (in horizontal and vertical directions) on the fluid field decreased when moving away the fire source.

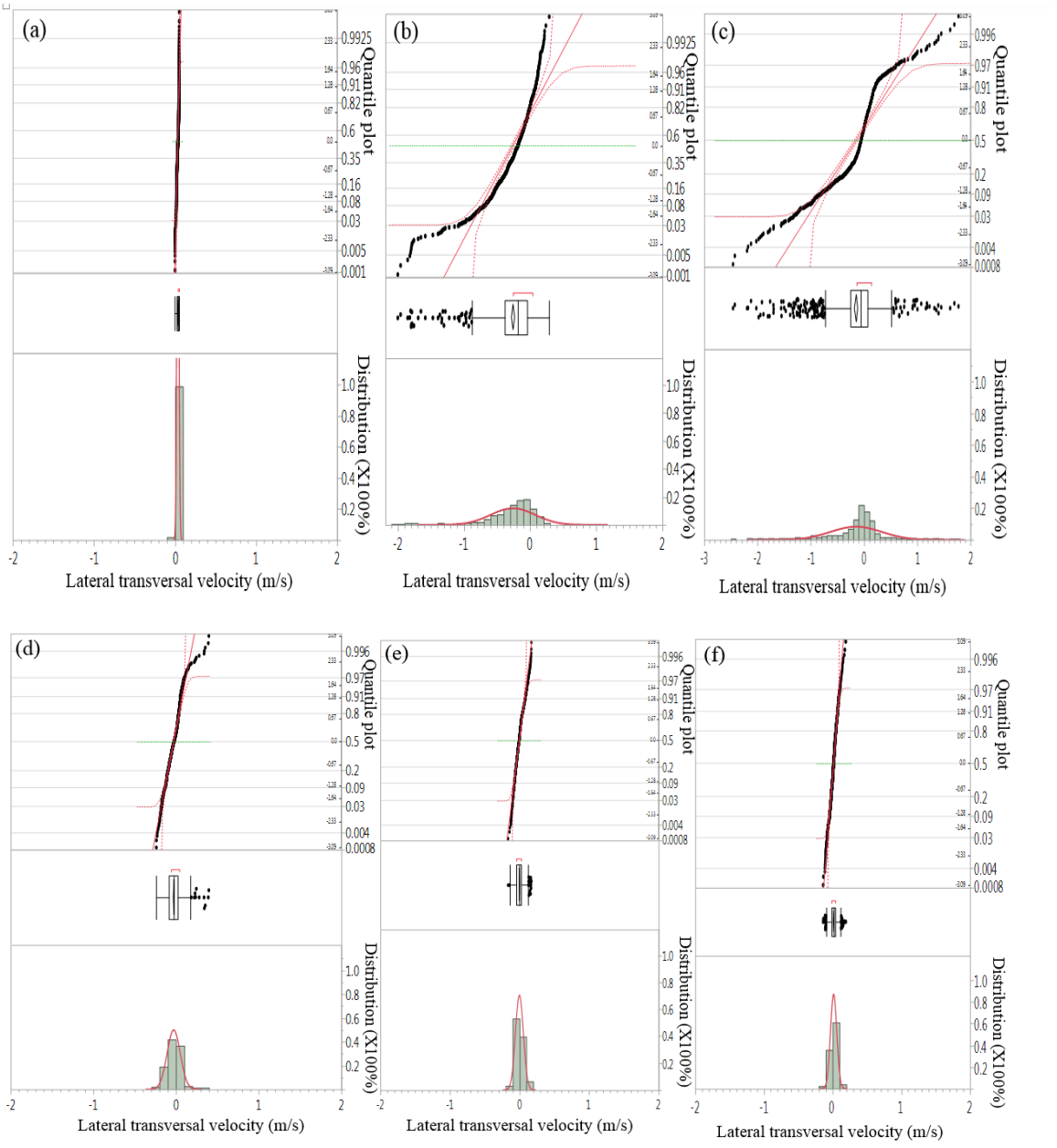

Figure 9.8. Normal quantile plot, box-and-whisker plots, and distributions of transversal velocity in horizontal direction at different cross sections of the tunnels at t=1300 s in scenario 1 (a) cross section B (b) cross section C (c) cross section D (d) cross section G (e) cross section H (f) cross section I (the cross sections are based on Figure 9.4 (a))

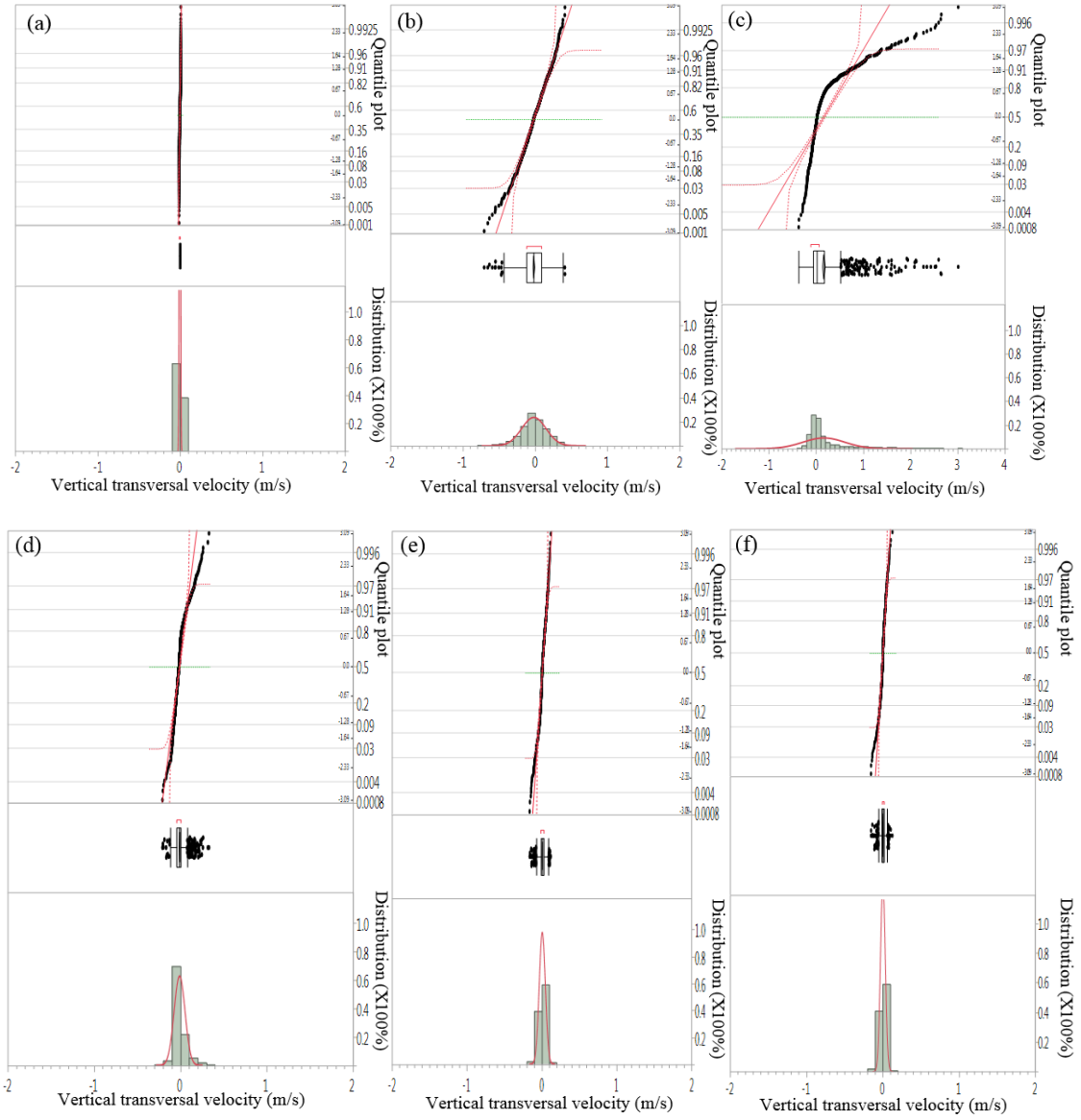

Figure 9.9. Normal quantile plot, box-and-whisker plots, and distributions of transversal velocity in vertical direction at different cross sections of the tunnels at t=1300 s in scenario 1 (a) cross section B (b) cross section C (c) cross section D (d) cross section G (e) cross section H (f) cross section I (the cross sections are based on Figure 9.4 (a))

The transfer of mean values (velocity, pressure, temperature) is required for the adoption of direct and indirect (3D-1D) coupling strategies [8-11]. For this reason, a cross section which all the nodes values of 3D model at that cross section are nearly uniform and close to the mean values can be selected as the most suitable boundary for decomposing the global domain into 3D and 1D sub-domains. In the other words, the spread of values of all nodes along the height of the tunnel at different cross section plays a key role for

determination of interface boundary and it should be investigated. Hence, a study was conducted to calculate the standard deviation of the longitudinal and the transversal velocities of all nodes along the height of the tunnel at different cross sections in steady state condition as shown in Figure 9.10.

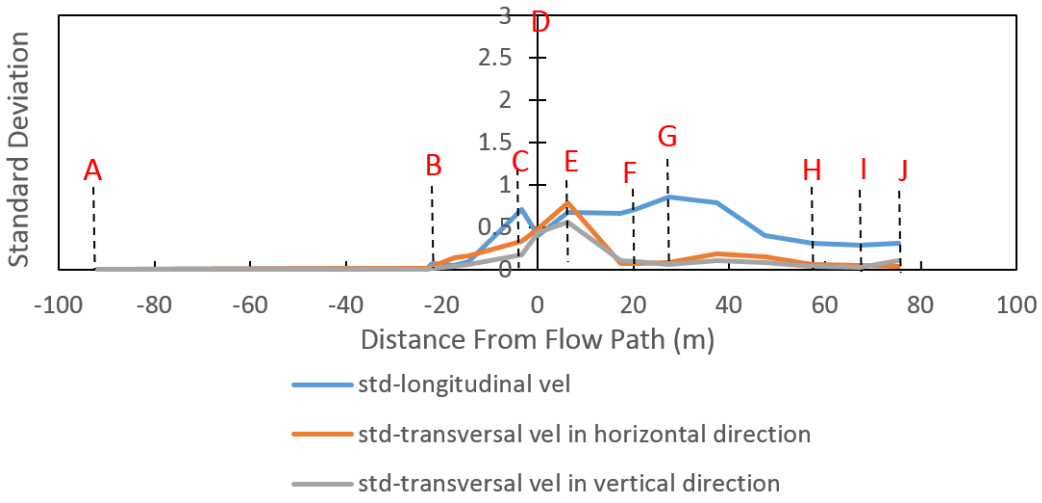

Figure 9.10. The dispersion of the longitudinal and the transversal velocities at different cross sections of the tunnels in scenario 1 at t=1300 s (the cross sections are based on Figure 9.4 (a))

Consistent with the data of Figure 9.10, the standard deviation of the longitudinal and the transversal velocities of all nodes along the height of the tunnel at different cross sections were calculated to be less than 0.02 from the inlet to 1 m to the cross cut (e.g., from cross section A to cross section B). The dispersion of the values started increasing because of three main reasons; the turning points at the cross cut, the roll back of the smoke at the continuous miner area, and the continuous miner object at the working face (e.g., cross section B to cross section C). At the center line of the fire source (cross section D), the spread of the longitudinal velocities of all nodes decreased while the spread of the transversal velocities increased (zero line represents the cross section D). The spread of the values of the nodes along the height of the tunnel increased at the mouth of the curtain (cross section E). The dispersion of the longitudinal velocity of all nodes along the height of the tunnel at different cross sections at the back side of the curtain remained constant (cross section E to cross section F), while the spread of the lateral and vertical transversal

velocities of all nodes decreased in the same region. The highest dispersion of the longitudinal velocity of all nodes was calculated at cross section G as 0.9. The reason lies in a sudden expansion of the cross section. The sudden expansion of the cross section and the ventilation curtain position contributes to the creation of vorticities in the region after the curtain (from cross section G to cross section H). From cross section G to the outlet (cross section J), the dispersion of the transversal velocities of all nodes remained relatively constant. However, the dispersion of the longitudinal velocity of all nodes decreased from the cross section G to the cross section H and then plateaued to the outlet.

Due to the complex dynamical fluid field close to the fire source, a wide dispersion of the longitudinal and transversal velocity components was calculated. However, the spread of the values decreased at the far field, after one advances beyond the auxiliary ventilation controls (i.e., line curtain). In addition, this study has shown that the streamwise component of the velocity (longitudinal velocity) was affected by the temperature in all computational domain while the transversal velocity components were influenced by the temperature just close to the fire source. In the other words, the transversal velocity components were temperature dependent close to the fire source, while the effect of the temperature on the transversal velocities was inconsequential far away from the fire source.

9.4.1.1 Longitudinal velocity ratio to transversal velocities

The ratio between longitudinal and transversal velocities can give a broad view about the fluid field structure and consequently the near and the far fire fields can be distinguished. Then, for adoption of multiscale methodology, the CFD (3D) and 1D models can be applied to the near field and far field respectively. According to the previous studies, it was evident that the flow structure was quasi-1D when the maximum longitudinal velocity ratio was almost 2 times of the maximum transversal velocities [20]. In addition, in some research studies [10, 11], the far field was named for the region where the longitudinal velocity are up to two orders of magnitude larger than the transversal velocity components. Hence, a study was conducted to calculate the maximum longitudinal velocity component ratio to the maximum transversal velocity components along the height of the tunnels at different cross sections from the inlet to the outlet in the steady state condition

as shown in Figure 9.11. Also, for investigating the ratio between the mean longitudinal and the mean transversal velocity components, there was a need to calculate the mean velocity components along the height of the tunnels at different cross sections which it is explained elaborately in section 9.4.1.2.

According to Figure 9.11, the longitudinal velocity component dominated the fluid field from the inlet to the cross section B which it is 1 m before the cross cut. After the cross section B, the air tends to turn to the continuous miner area. Therefore, the effect of transversal velocity components on the fluid structure at the cross section increased dramatically which it resulted the ratio in decreasing conspicuously. The lowest ratio was calculated at the center of the fire source indicating that this flow field was not quasi-1D. At the mouth of the curtain (cross section E), because of the turning point of the air and the complex fluid structure, the effect of the transversal velocity components is consequential. At the back side of the curtain (from the cross section E to the cross section F) the ratio increased dramatically; so, the fluid field was quasi-1D. Because of the sudden expansion of the cross section from the cross section F to the cross section G, the ratio decreased. Due to the effect of the created vorticities between cross section G to the cross section H, the impact of the longitudinal velocity component on the fluid field decreased. The maximum longitudinal velocity to the maximum transversal velocity ratios varied widely from the cross section B to the cross section H as shown in Figure 9.11. The maximum longitudinal velocity component ratio to the maximum transversal velocity components remained constant at about 6 from cross section H to the cross section J (outlet).

Overall, the complex dynamical 3D fluid field was observed from the cross section B to the cross section H. Therefore, this region was distinguished as the near fire field and the 3D CFD simulation should be applied to this region. In addition, the region between the inlet and the cross section B upstream and between the cross section H and the cross section J downstream were distinguished as the far fields (where the interface boundary could be located). Due to the transport of smoke and hot gases to the outlet, the maximum longitudinal velocity ratio to the maximum transversal velocities at the outlet was lower

than the inlet. Moreover, upstream of the fire (from the inlet to 1 m to the crosscut (0.5 D_h to the crosscut)) the dominant component of the velocity was the longitudinal velocity.

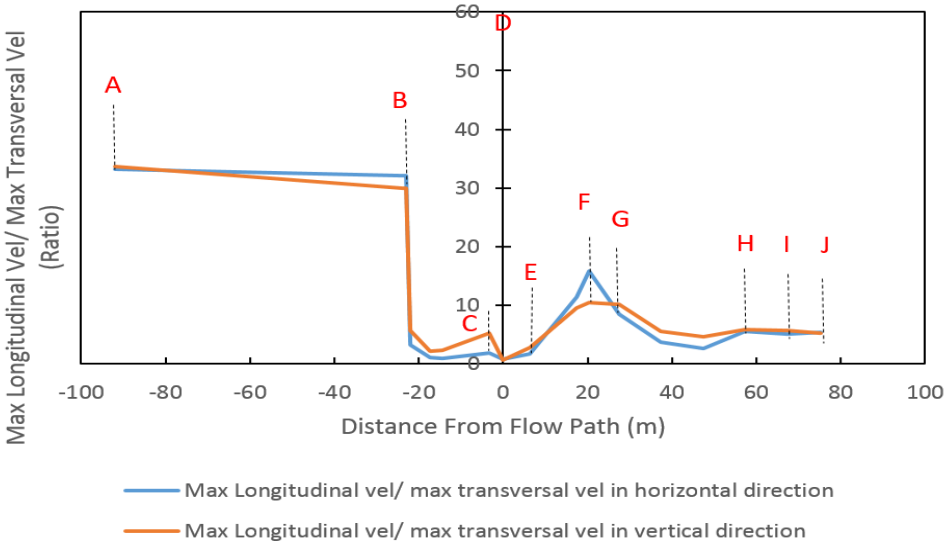

Figure 9.11. The maximum longitudinal velocity ratio to the maximum transversal velocities along the height of the tunnel at different cross sections at t=1300 s for scenario 1 (the cross sections are based on Figure 9.4 (a))

9.4.1.2 Mean velocity and mean velocity components

The mean longitudinal and the mean transversal velocity components along the height of the tunnel at different cross sections were investigated for two reasons. On one hand, the near and the far fields can be distinguished via determination of the significant component/components of the velocity on the fluid structure at different cross sections of the tunnel. On the other hand, due to the continuity of the average velocity at the 3D-1D interface boundaries, the mean velocity and its components along the height of the tunnel at different cross sections were analyzed. As shown in Figure 9.12, it is evident that the mean transversal velocity in horizontal and vertical directions in the near field (e.g., cross section B to the cross section H) experienced considerable fluctuations. In that region, the mean transversal velocities were calculated within a range of - 0.8 m/s to + 0.2 m/s, as shown in Figure 9.12 (positive and negative values correspond to the direction). From the inlet to the cross section B and from the cross section H to the outlet, the mean transversal

velocities were small. Therefore, this study has shown that the effect of the mean transversal velocities on the fluid field at those regions were inconsequential.

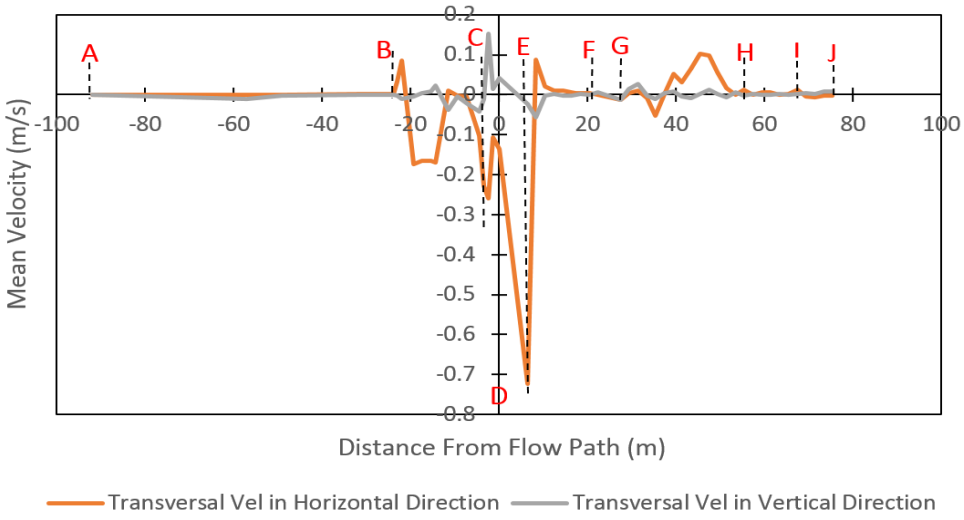

Figure 9.12. The mean transversal velocity components along the height of the tunnel at different cross sections at t=1300 s in scenario 1 (the cross sections are based on Figure 9.4 (a))

It is noteworthy that the magnitude of the mean longitudinal velocity compared to the mean transversal velocities is significantly higher at different cross sections of the tunnels as can be seen in Figure 9.13. From the inlet to the cross section B and from the cross section H to the outlet, the mean velocity remained constant and it was calculated as same as the mean longitudinal velocity. The mean velocity was higher than the mean longitudinal velocity in the near field (e.g., cross section B to the cross section H). The reason lies in the high impact of the transversal velocity components on the average velocity. Hence, the fluid field in that region was not quasi-1D.

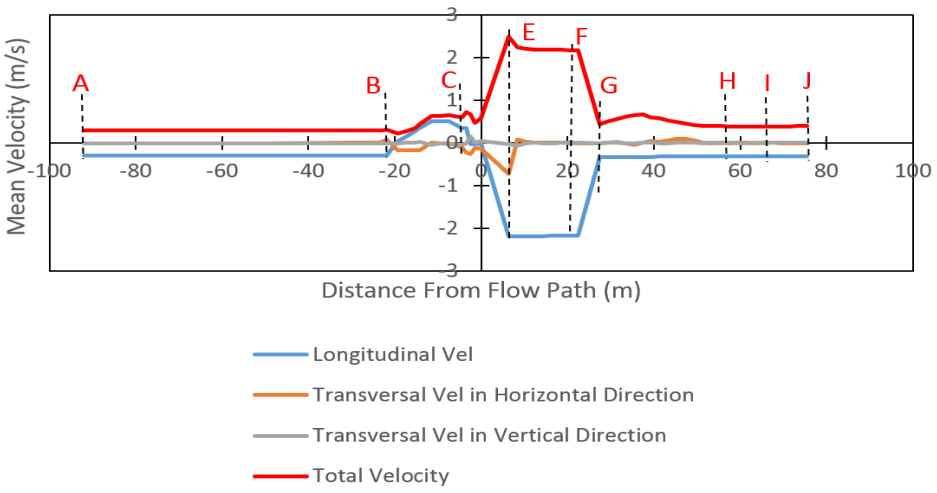

Figure 9.13. The mean velocity and its components along the height of the tunnel at different cross sections at t=1300 s in scenario 1 (the cross sections are based on Figure 9.4 (a))

9.4.2. Turbulent Kinetic Energy (TKE) and Vorticity Analysis

The TKE of a dynamical system represents the energy content of eddies in turbulent flows of that system. Although the turbulent flows are dissipative (the kinetic energy of larger eddies will be transferred to the smaller ones, and finally the kinetic energy of the smallest eddies will be converted into the heat), sometimes backscatter phenomenon (the kinetic energy will be transferred to the larger eddies via the interaction of the smaller eddies with each other,) can occur [41-43]. Due to this, a study was conducted to investigate the strength of the turbulence of the system and the tendency of fluid particles to rotate via calculation of the mean TKE and the mean vorticity along X-, Y-, and Z-axes along the height of the tunnel at different cross sections as shown in Figure 9.14. The fluid particles tend to rotate less in the quasi-1D flow regions. Therefore, the TKE of the quasi-1D fluid field (far field) should be lower than the TKE of 3D field (near field).

According to Figure 9.14 (a), the mean TKE at the near field (cross section B to cross section H) is experiencing the sporadic behavior because of the velocity fluctuations in scenario 1. However, the mean TKE at the far fields (from the inlet to the cross section B upstream and from the cross section H to the outlet) remained constant and less than 0.15 $(m/s)^2$. The highest mean kinetic energy of the turbulent flow was calculated at the mouth of the curtain in the near fire field (cross section E) by about 3.5 $(m/s)^2$. Consistent with

the data of Figure 9.14 (a), by comparison with the inlet turbulent kinetic energy, it was evident that the effect of eddies on the energy of the system from the cross section H to the outlet was inconsequential. This study has shown that the created energy content of eddies in the near fire field was dissipated at the cross section H downstream of the fire and then TKE remained constant up to the outlet.

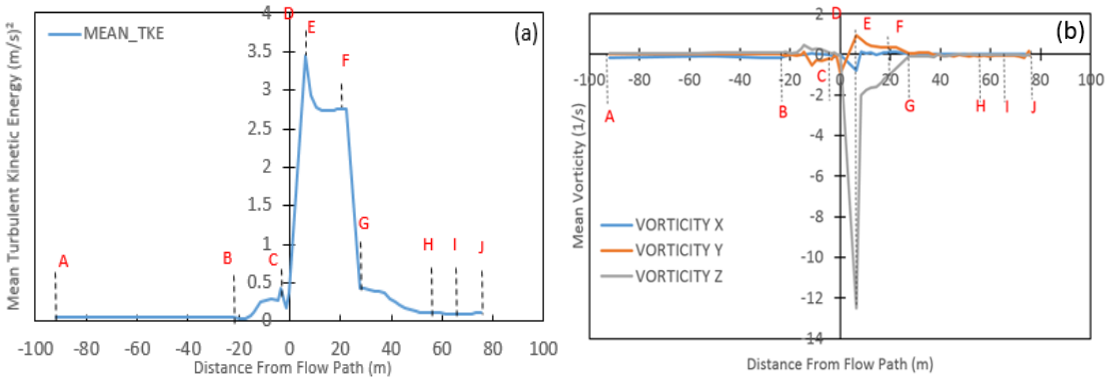

Figure 9.14. The mean TKE and the mean vorticity along the height of the tunnel at different cross sections at t=1300 in scenario 1 (a) mean TKE (b) mean vorticity (the cross sections are based on Figure 9.4 (a))

It is noteworthy that the mean vorticity along X, Y, and Z-axis (Figure 9.14 (b)) was calculated within a range of -13 (1/s) to 2 (1/s) in the near fire field (which it was started after cross section B to the cross section H) while the mean vorticity along different axis at the far fields (from the inlet to the cross section B upstream and from the cross section H to the outlet) were calculated close to zero but it was not exact zero because of the turbulence structure of the airflow in the airways. The highest mean vorticity along X, Y, and Z-axis was calculated at the mouth of the curtain in the continuous miner area (cross section E).

Overall, the higher energy content of eddies and the higher rotational structure of the fluid were calculated from the cross section B to the cross section H (near field). Because of the complex fluid structure in this region, the 3D CFD simulation has to be applied. In addition, because of the low energy content of eddies and low tendency of flow particle to rotate in the region between the inlet and the cross section B upstream and between the cross section H and the cross section J downstream (far fields), the fluid

structure could be count as the quasi-1D fluid. Therefore, the interface boundary can be located at that region for coupling of 3D models to the 1D models in multiscale underground mine fire simulations.

9.5. Effect of Velocity, HRR, and the Curtain Position Changes on Interface Boundary Selection

Different working face methane fire scenarios ranging 200 kW to 1000 kW were investigated with various inlet velocities (0.3 m/s, 0.6 m/s, and 4 m/s) in order to analyze the influence of the velocity and HRR changes on the selection of 3D-1D interface boundary in multiscale underground working face fire simulations. According to the minimum, the medium, and the maximum values for velocity and HRR as shown in Table 9.1, thirteen different scenarios shown in Table 9.2 were simulated. Previous research [19] has shown that different levels of damage to an exhausting ventilation curtain in a continuous miner heading influenced the transport of the smoke into the entry. The worst case scenario was determined as the scenario without an exhausting ventilation curtain, and the effect of the position of the ventilation curtain on the selection of 3D-1D interface boundary was investigated. In addition, the worst case scenario with the longest rollback length (scenario 13) was considered for the investigation of 3D-1D interface boundary position in multiscale underground working face fire simulations.

The same longitudinal and transversal velocity components analysis and the same TKE and the vorticity analysis (as described in sections 9.4.1 and 9.4.2 for scenario 1) were conducted to determine the near and far fields for multiscale working face fire simulations in scenarios 2 to 13. All calculations are at a distance from flow path as previously shown in Figures 9.4 (a) and 9.4 (b) for both curtain and curtain less scenarios respectively.

As shown in Appendix E, increasing the inlet velocity from 0.3 m/s to 0.6 m/s and 4.0 m/s, increased the component velocities. The mean transversal velocity in horizontal and vertical directions impacted the fluid structure drastically close to the fire source, while away from the fire, just the longitudinal velocity component dominated the fluid field. Moreover, by increasing the inlet velocity, the energy content of eddies and the rotational

structure of the fluid close to the fire source (near field) increased. However, at a certain distance away from the fire source, the created energy content of eddies was dissipated and remained constant up to the outlet. Therefore, at a certain distance away from the fire source, the tendency of the fluid particles to rotate decreased. In scenarios 2 and 3, the near field was distinguished from cross section B to the cross section H as shown in Appendix E. It is noteworthy that in the scenarios without curtain (see Appendix F), the near field domain decreased by increasing the velocity from 0.3 m/s to 4.0 m/s due to the effect of rollback on the fluid structure upstream of the fire. By increasing the inlet velocity from 0.3 m/s to 0.6 m/s and 4.0 m/s, the length of the rollback at the inlet tunnel decreased from 36 m to 8 m and 2 m, respectively, as shown in Figure 9.15. Consequently, because of the roll back length changes, the region where the fluid field is quasi-1D (far field) upstream of the fire was changed while the quasi-1D region downstream of the fire was not changed by varying the velocity. The interface boundary downstream of the fire in scenarios without curtain (See Appendix F), was calculated at 37.5 m distance from the flow path (cross section G). The quasi-1D region upstream of the fire in scenarios without curtain were calculated 3.3 m further away from the tip of the roll back. Hence, in all scenarios without curtain (scenario 4, 5, and 6), the near field was distinguished from a cross section which it is 3.3 m further away from the tip of the roll back to the cross section G (the cross sections are based on Figure 9.4(b)) as shown in Appendix F.

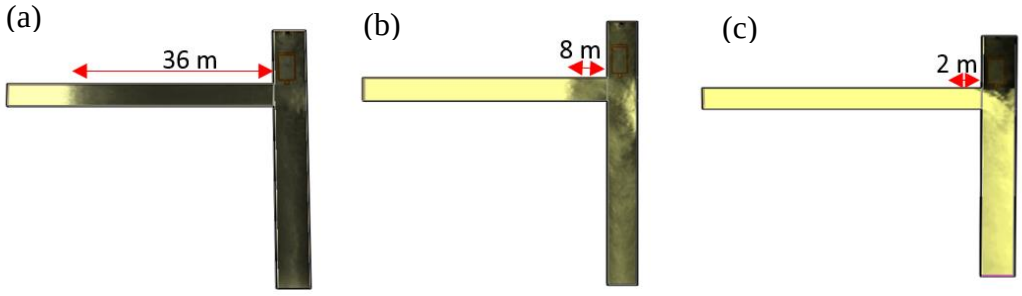

Figure 9.15. The Effect of velocity changes on the rollback length (a) scenario 4 (b) scenario 5 (c) scenario 6

By increasing the velocity from 0.3 m/s to 0.6 m/s and 4 m/s in scenarios with curtain (scenarios 1, 2, and 3), the region where the fluid structure was quasi-1D was not changed. This study has shown that the upstream and downstream interface boundaries in

scenarios with curtain were not changed by varying the inlet velocity. So, the interface boundaries were velocity independent in scenarios with exhausting line curtain. However, the upstream interface boundary in scenarios without exhausting line curtain in the computational domain is velocity dependent. The downstream interface boundary in scenarios without exhausting line curtain were not changed by varying the velocity.

In addition, a study was conducted to investigate the effect of HRR changes on the quasi-1D domain size. Therefore, two different sets of scenarios (see Appendix G and Appendix H) based on the presence of the exhausting line curtain in the computational domain were simulated as explained in Table 9.3. According to Appendix G, it was evident that by increasing HRR from 200 kW to 600 kW and 1000 kW, the near fire field (after cross section B to the cross section H) was not changed in scenarios with exhausting line curtain (scenarios 7, 8, and 9); only minor changes were observed on the magnitude of the mean velocity components, the mean TKE, and the mean vorticity at different cross sections of the mine tunnel as shown in Appendix G. According to Appendix H, the region where the fluid structure is quasi-1D, was changed in scenarios without exhausting line curtain (scenario 10, 11, and 12) by varying the HRR from 200 kW to 600 kW and 1000 kW. Because of HRR changes, the transport of smoke upstream of the fire (roll back) was changed as shown in scenarios 10, 11, and 12. By increasing the HRR from 200 kW to 600 kW and 1000 kW, the length of the rollback at the inlet tunnel increased from 8 m to 28 m and 32 m, respectively. Therefore, the upstream interface boundary was affected by the changes of HRR in scenarios without exhausting line curtain (scenario 10, 11, and 12). The quasi-1D region upstream of the fire in scenarios without curtain was calculated 3.3 m further away from the tip of the roll back up to the inlet and the downstream interface boundary (See Appendix H), was calculated at 37.5 m distance from the flow path (cross section G).

The highest HRR (1000 kW) and the lowest inlet velocity (0.3 m/s) in the computational domain without exhausting line curtain were considered as the worst case scenario (scenario 13) to investigate the effect of HRR and velocity changes at the same time on the quasi-1D region size. According to Appendix H (Figure 9.32), it was evident

that the downstream interface boundary was independent of HRR and velocity changes at the same time. The downstream interface boundary in scenario 13 (Figure 9.32) was calculated at 37.5 m distance from the flow path (cross section G) as same as the calculated downstream interface boundary in scenarios 10, 11, and 12. However, by having the highest HRR (1000 kW) and the lowest velocity (0.3 m/s), the length of the rollback at the inlet tunnel increased to 70 m. Therefore, The quasi-1D region upstream of the fire in scenario 13 was calculated 3.3 m further away from the tip of the roll back up to the inlet.

By comparison of scenarios with exhausting line curtain to the scenarios without curtain (e.g., scenario 1 to 4, scenario 2 to 5, scenario 3 to 6, scenario 7 to 10, scenario 8 to 11, scenario 9 to 12), it was evident that the presence of the exhausting line curtain influenced the domain of the quasi-1D region. Because, not only the presence of the curtain affected the transport of the smoke upstream of the fire, but also the fluid structure downstream of the fire (on account of sudden expansion) was affected by the presence of the curtain. The quasi-1D region upstream of the fire decreased while the quasi-1D downstream of the fire increased when the exhausting line curtain was removed from the computational domain (scenarios without curtain). The downstream interface boundary was 20 m closer to the fire source when the exhausting line curtain was removed from the computational domain in all scenarios. The upstream interface boundaries were rollback length dependent. Overall, the interface boundaries were affected by the presence of an object (e.g., exhausting line curtain) in the computational domain.

It was evident that the interface boundaries did not depend on the fire size (HRR) and the velocity in all scenarios with the exhausting line curtain in the computational domain. In scenarios without exhausting ventilation curtain in the computational domain, the downstream interface boundary was independent of the fire size (HRR) and the velocity while the upstream interface boundary was the fire size (HRR) dependent and the velocity dependent.

According to the longitudinal and the transversal velocity components analysis and the TKE and the vorticity analysis, the quasi-1D regions for all scenarios were determined in order to couple 3D models to 1D models. The upstream (IB_{Up}) and downstream (IB_{Down})

interface boundaries were determined for all scenarios as shown in Figure 9.16. Because of different roll back length in scenarios without curtain as shown in Table 9.4, the upstream interface boundary varied in associated scenarios. In Figure 9.16, IB_{Up}, IB_{Down}, and D_h are upstream interface boundary, downstream interface boundary, and hydraulic diameter respectively.

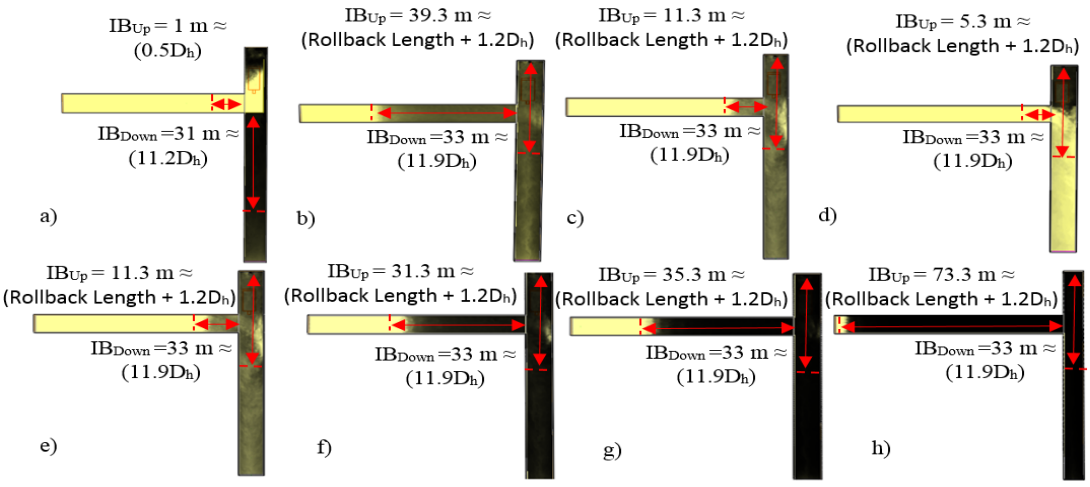

Figure 9.16. Selected interface boundaries at upstream and downstream of the fire source (a) scenarios with curtain (b) scenario 4 (c) scenario 5 (d) scenario 6 (e) scenario 10 (f) scenario 11 (g) scenario 12 (h) scenario 13 (Not to scale). Smoke is shown in black and gray

Table 9.4. Roll back length in the entry from the cross cut

Scenarios	Roll back Length (m)
Scenario 4	36
Scenario 5	8
Scenario 6	2
Scenario 10	8
Scenario 11	28
Scenario 12	32
Scenario 13	70

The upstream and downstream interface boundaries for scenarios with curtain in the computational domain (scenarios 1 to 3, 7 to 9) was calculated at least 0.5 D_h from upwind the end of the cross cut and at least 11.2D_h from downwind the end of the curtain respectively as shown in Figure 9.16(a). The upstream and downstream interface

boundaries for scenarios without curtain in the computational domain (scenarios 4 to 6, 10 to 13) was calculated at least 1.2D_h m far from the tip of the rollback and at least 11.9D_h from the fire source respectively as shown in Figures 9.16(b) to 9.16(h). The study on downstream interface boundary has indicated the excellent agreement with the previous research studies [10, 20]. Therefore, the near fire field (region between upstream and downstream interface boundaries) was determined as shown in Figure 9.16 for all scenarios.

9.6. Multiscale Simulation' Results and Design Consideration

VentFIRE^{TM} was utilized to simulate 1D models. For implementation of the multiscale methodology, the 1D simulations were coupled to the full CFD simulations. The multiscale calculations were conducted using indirect coupling strategy with the near fire field characteristic curves implemented in the 1D models. The indirect coupling strategy allows the users to get the simulation results faster compared to the direct coupling strategy. The characteristic curves of near fire field (3D CFD region) are required in indirect coupling of 3D models to 1D models [9, 10]. Therefore, the near fire field characteristic points for all scenarios were calculated in terms of mass flow rate versus total pressure drop across the domain boundaries, and these points are shown in Figure 9.17 for each scenario.

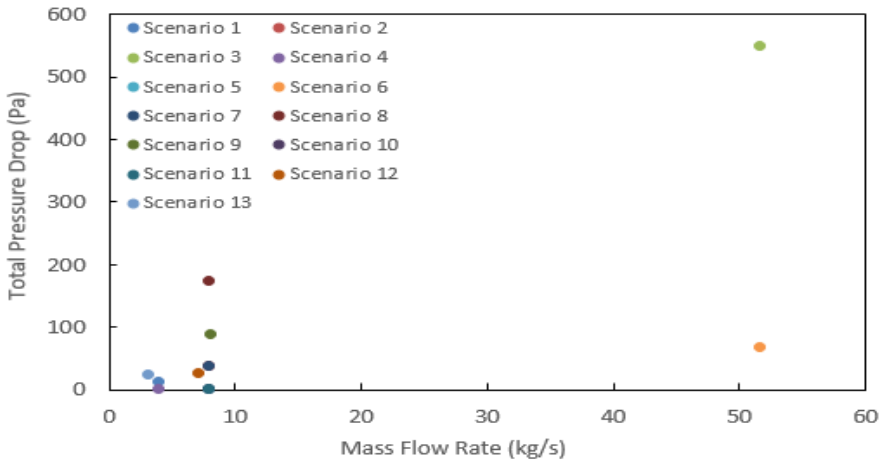

Figure 9.17. Characteristic points of the near fire filed region for all scenarios

Due to the continuity of the temperature at the interface boundaries in multiscale simulations, the mean temperature along the height of the tunnel at the selected boundaries in all CFD models were calculated as shown in Table 9.5.

Table 9.5. The mean temperature at the interface boundaries for different scenarios

Scenarios	Upstream Interface Temperature (^{O}C)	Downstream Interface Temperature (^{O}C)
Scenario 1	20	31.189
Scenario 2	20	31.339
Scenario 3	20	22.428
Scenario 4	20	28.337
Scenario 5	20	26.492
Scenario 6	20	21.139
Scenario 7	20	31.339
Scenario 8	20	52.372
Scenario 9	20	67.549
Scenario 10	20	26.492
Scenario 11	20	38.470
Scenario 12	20	46.045
Scenario 13	20	45.686

After coupling the 3D (CFD) models to the 1D models, the mean temperature and the mean velocity results along the height of the tunnels at different cross sections were selected for comparison of CFD simulations, 1D simulations, and the multiscale simulations in all scenarios as shown in Figure 9.18 and Appendix I. According to Figures 9.18, 9.33, 9.34, and 9.35, it is evident that the mean temperature and the mean velocity results were improved drastically when the multiscale methodology was used compare to the 1D model results. The highest mean temperature difference and the mean velocity difference between CFD results and 1D results were observed in the near field. Because, the 1D modeling software (such as VentFIRE^{TM}) is designed to provide a prediction of heat and fire products transfer over the huge computational domains such as entire mine, which extends kilometers in size. Therefore, for application of this type of prediction, the physics of the airflow and heat transfer are simplified by treating sections of the tunnel as nodes where the conditions are spatially uniform. Besides, some phenomenon (such as rollback) in 1D simulations are overlooked. Due to this, the physics of the fluid characteristics cannot be captured precisely as can be seen in Figure 9.18 and Appendix I. Therefore, a higher

percentage of error of the mean temperature and mean velocity between 1D and the coupled model could be observed in scenarios with the roll back.

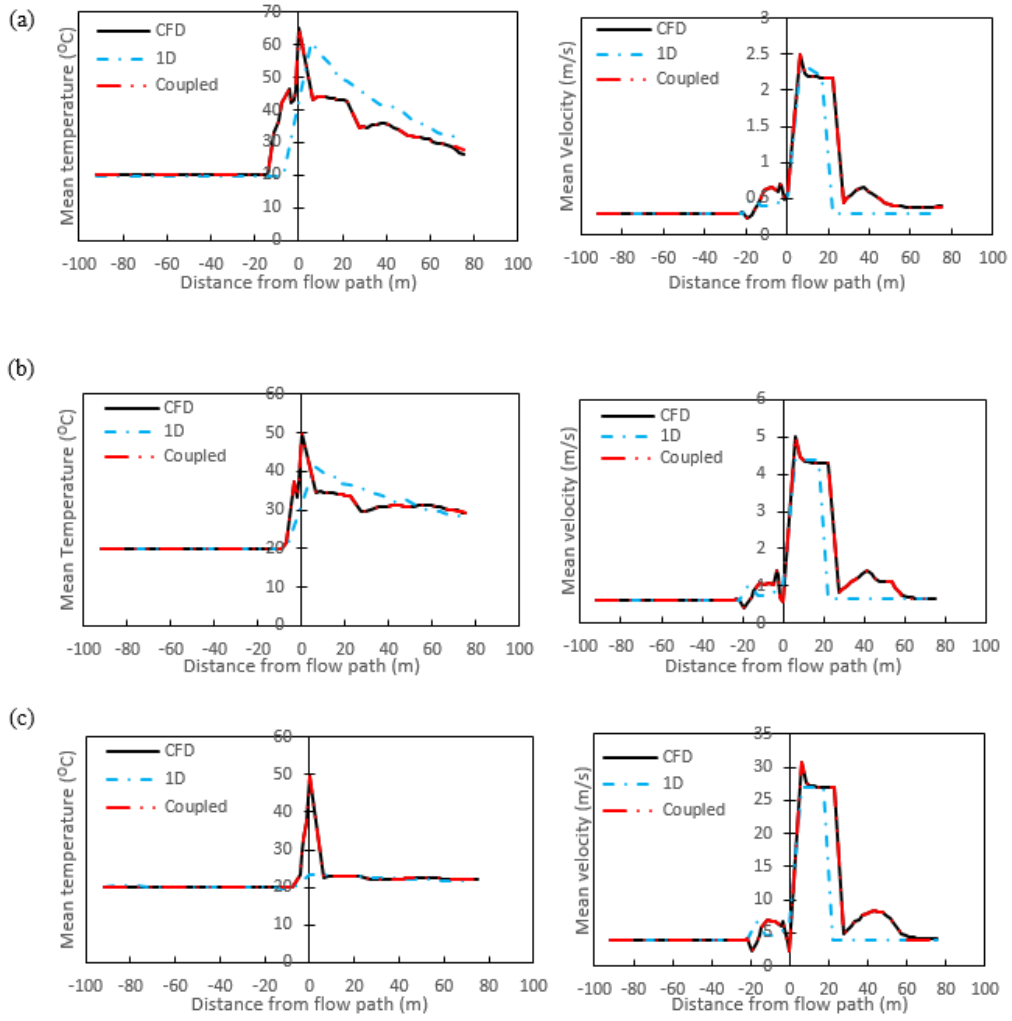

Figure 9.18. Mean temperature and mean velocity comparison between CFD, 1D, and the coupled models at different cross sections of the tunnel for all scenarios (a) scenario 1 (b) scenario 2 (c) scenario 3

The associated average temperature and the average velocity errors in the coupled scenarios compare to the full CFD scenarios at the outlet in all scenarios were calculated as shown in Figure 9.19.

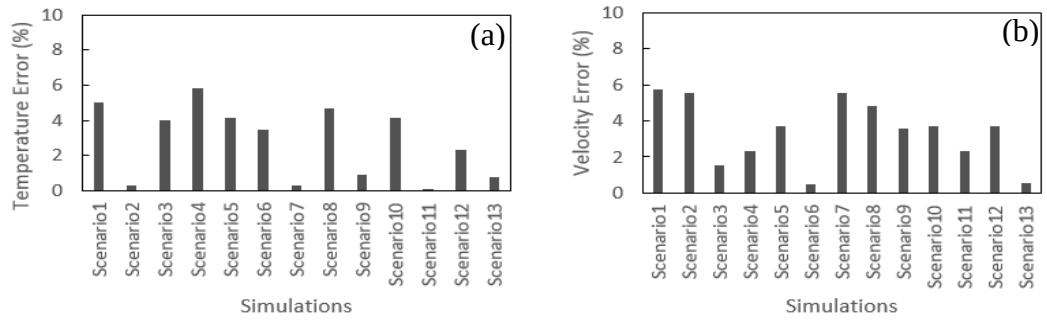

Figure 9.19. The calculated error between CFD and coupled models for the mean temperature and the mean velocity at the outlet for all scenarios (a) Temperature error (b) velocity error

According to Figure 9.19, the mean temperature error and the mean velocity errors at the outlet in all scenarios were calculated less than 6%. The error before upstream interface boundary was calculated as a 0%.

It is so crucial to consider that some natural phenomenon can be overlooked in multiscale fire simulations because of 1D sub-domains. To clarify this issue it can be referred to the "throttled" phenomenon [44] which it is assumed by The VentFIRE^{TM} when the fire source is located at a dead end tunnel (ex: coal mine working face). Due to the assumed insufficient oxygen at a dead end tunnel, the software assumes a fire with zero net airflow while in reality a bidirectional flow pattern may be established. The hot, smoke-laden upper layer travels in one direction away from the fire near the roof, while the cooler lower layer of fresh air travels to the fire source near the floor in the other direction. Therefore, the domain of the bidirectional flow pattern (Ex: dead end tunnel) should be distinguished and transferred between the inlet and the outlet airways for multiscale fire simulations since the continuity of the velocity, pressure, and temperature at the interface boundaries should be kept. In addition, this study has shown that the objects (Ex: continuous miner) in the domain, influenced the fluid structure; consequently affects the interface boundaries. Therefore, if the other objects or fire sources were considered in the simulation domain, the same study should be conducted for determination of the interface boundaries before and after the extra objects in the tunnel. Moreover, the number of nodes

used in the 1D sub-domain, can influence the multiscale simulation results. The results error decreased by increasing the used number of nodes in the 1D sub-domains.

9.7. Interface Boundary Selection Algorithm in Multiscale Mine Fire Simulations

Based on the physics of the fluid structure, TKE, and the vortex dynamics, a novel algorithm was developed for the selection of the interface boundaries as shown in Figure 9.20. First CFD model is the reference model and the most expensive part of the process. Based on the results, we recommend a computational domain of $5D_h$ upstream and $20D_h$ downstream of the fire source as the reference CFD model if the inlet velocity was greater than equal to critical velocity $V \geq V_{cr}$ (e.g., there is no rollback). However, if the inlet velocity was less than critical velocity $V < V_c$, the rollback length should be calculated and be added to the upstream computational domain. Next, the CFD model is simulated and the inlet velocity of the domain is determined. If the determined inlet velocity is greater than or equal to V_{cr}, the upstream interface boundary is selected at least $0.5D_h$ from the tip of fire source, or the cross cut, or the used upstream object. If the selected inlet velocity is less than V_{cr}, the roll back length should be calculated and ($1.2\ D_h$ m + rollback length) should be selected as the upstream interface boundary. The longitudinal and the transversal velocities analysis and the mean TKE and the mean vorticity analysis for the outlet cross section should be conducted to determine the downstream interface boundary in both $V \geq V_{cr}$ and $V < V_{cr}$ scenarios. The $12D_h$ downstream cross section from the centerline of the object is selected as the downstream interface boundary which number 12 is the coupling variable (C_V). If the distribution of the longitudinal and transversal velocities at the $12D_h$ downstream cross section are almost similar to the outlet values, and the standard deviation of the longitudinal and transversal velocities of the determined section are less than 0.3 compared to the outlet values, that cross section can be accepted as the downstream interface boundary. If one of the explained requirements was not met, then $(C_V + 1)*D_h$ is selected as the downstream interface boundary to repeat the longitudinal and the transversal velocities analysis and the mean TKE and mean vorticity analysis for that selected downstream interface boundary. The method will be iterated till all requirements are met. Ultimately, that cross section is accepted as the downstream interface boundary.

Although the recommended modified procedure for interface boundaries selection was based on the methane fire at a coal mine working face, this approach can be applied for interface boundary determination in different engineering fields. It is so noteworthy that the presence of the objects in the computational domain have an immense impact on the fluid structure and the interface boundaries. Hence, for the extra objects in the computational domain, the same study before and after the extra objects should be conducted for determination of the interface boundaries.

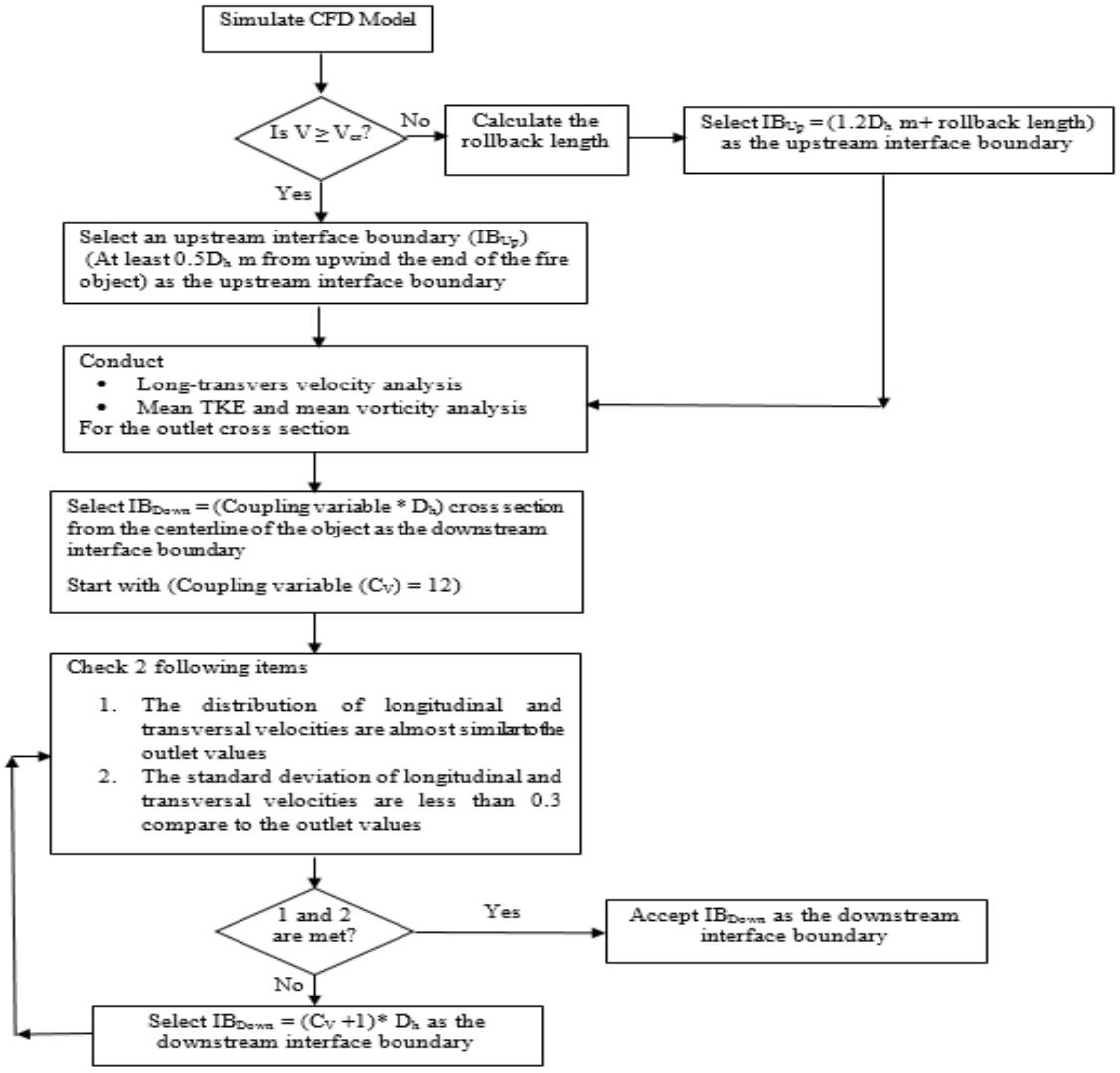

Figure 9.20. Decision making algorithm for determination of interface boundary to couple 3D and 1D fire simulations in underground mines

Therefore, with the usage of this methodology, the boundaries for decomposition of the huge complex numerical domain into the 1D and 3D sub-domains can be determined. Overall, a drastic time saving can be achieved with the usage of the proposed methodology for determination of the interface boundaries in multiscale simulations.

9.8. Conclusion

The interface boundaries were determined based on the fundamental longitudinal and transversal velocities analysis and the TKE and the vorticity analysis for steady state conditions of the methane fire in an underground mine tunnel. The novel methodology was applied to the tunnels with 10.8 m^2 cross section and 160 m in length in total. This study has shown that the longitudinal velocity component was affected by the temperature in the whole computational domain while the transversal velocity components were temperature depended just close to the fire. It was noteworthy that the temperature impact on the transversal velocities was inconsequential away from the fire source. Moreover, it was evident that the downstream interface boundaries did not depend on the fire size (HRR) and the velocity in all scenarios. However, the upstream interface boundary depends on different parameters such as the size of the fire (HRR), velocity, and the used objects in the computational domain. By comparison of scenarios with exhausting line curtain to the scenarios without curtain, it was evident that the presence of an object (the exhausting line curtain) influenced the domain of the quasi-1D region. The selected downstream interface boundary was at least $12D_h$ away from the fire source or the used object (ex: exhausting line curtain) in the numerical domain for all simulations. Due to the effects of the size of the fire (HRR), velocity, and the objects on the rollback (backlayering) phenomenon, the upstream interface boundary varied. In the simulations with backlayering ($V < V_{cr}$), the upstream interface boundary was selected at least $1.2D_h$ further from the tip of the rollback. The upstream interface boundary for scenarios without backlayering ($V \geq V_{cr}$) was calculated at least $0.5D_h$ from the upwind the end of the cross cut or the used object at the upstream of the fire source in the computational domain. The indirect coupling strategy was utilized to couple 3D sub-domain to 1D sub-domains. The calculated mean temperature and the mean velocity errors between multiscale models and the full CFD

models were less than 6%. The proposed methodology was demonstrated to be a useful technique for the determination of near and far fire fields.

Due to the large size of underground mines, the developed novel algorithm can be applied for selection of interface boundary for multiscale simulations of all kinds of fire at different regions such as longwall, gob areas, or belt areas (neutral airways). Additionally, the work agrees well with previous work that uses a more exhaustive systematic method (gradually increasing the CFD domain and decreasing the 1D domain until a predetermined error level is encountered.). This innovative methodology has broader impact which it can be applied for interface boundary determination in different engineering fields. With the usage of the proposed methodology, the precise 3D numerical analysis domain and the simplified 1D numerical analysis domains can be distinguished.

9.9. Acknowledgements

This research was developed under Contract No. 200-2014-59669, awarded by the National Institute for Occupational Safety and Health (NIOSH). The findings and conclusions in this report are those of the authors and do not reflect the official policies of the Department of Health and Human Services; nor does mention of trade names, commercial practices, or organizations imply endorsement by the U.S. Government.

9.10. Bibliography

1. Sun, X. Q., Hu, L. H., Li, Y. Z., Huo, R., Chow, W. K., Fong, N. K., Lui, G. C. H., Li, K. Y., “Studies on smoke movement in stairwell induced by an adjacent compartment fire”. Applied Thermal Engineering 29 (2009) 2757–2765.
2. Lin, C. H., Ferng, Y. M., Hsu, W. S., “Investigating the effect of computational grid sizes on the predicted characteristics of thermal radiation for a fire”. Applied Thermal Engineering 29 (2009) 2243–2250.
3. Noah L. Ryder, N. L., Sutula, J. A., Schemel, C. F., Hamer, A. J., Van Brunt. V., “Consequence modeling using the fire dynamics simulator”. Journal of Hazardous Materials 115 (2004) 149–154.

4. Wang, L., Chen, Q., (2008). "Applications of a Coupled Multizone-CFD Model to Calculate Airflow and Contaminant Dispersion in Built Environments for Emergency Management". HVAC&R Research. Vol 14. Number 6. pp. 925-939.
5. Nobile, F. “Coupling strategies for the numerical simulation of blood flow in deformable arteries by 3D and 1D models”. Mathematical and Computer Modelling 49 (2009) 2152-2160.
6. Choi, J., Lin, C.-L. Multiscale numerical analysis of airflow in CT-based subject specific breathing human lungs http://ir.uiowa.edu/etd/2685 (accessed Nov 21, 2012).
7. Kuprat, A. P., Kabilan, S., Carson, J. P., Corley, R. A., Einstein, D. R. A., Bidirectional Coupling Procedure Applied to Multiscale Respiratory Modeling. Journal of Computational Physics.
8. Colella, F., Rein, G., Borchiellini, R., Carvel, R., Torero, J. L., Verda, V., (2009). "Calculation and design of tunnel ventilation systems using a two scale modelling approach". Building and Environment Journal. 44. 2357-2367.
9. Colella, F., Rein, G., Reszka, P., Carvel, R., Torero, J. L., (2010). "Analysis of the ventilation system in the dartford tunnels using a multiscale modelling approach". TUST 2010; 25: 423-32.
10. Colella, F., Rein, G., Borchiellini, R., Torero, J. L., (2011). "A Novel Multiscale Methodology for Simulating Tunnel Ventilation Flows During Fires". Fire Technology. ISSN: 0015-2684. pp. 221 - 253.
11. Colella, F., Rein, G., Verda, V., Borchiellini, R., (2011). "Multiscale modeling of transient flows from fire and ventilation in long tunnels". Computer & Fluids. 51. pp. 16–29
12. McGrattan, K., Baum, H., and Rehm, H., Large eddy simulation of smoke movement. *Fire Safety Journal*, 1998; 30, 161-178.
13. Liang, K. M., Ma, T., Quintiere, J. G., Rouson, D., Application of CFD Modeling to Room Fire Growth on Walls. NIST GCR 03-849, National Institute of Standards and Technology, Gaithersburg, Maryland, April 2003. 7, 10
14. Ma, T. G., Quintiere, J. G., Numerical simulation of axi-symmetric fire plumes: accuracy and limitations. Fire Safety Journal, 38:467–492, 2003. 7, 10

15. Heskestad, G., SFPE Handbook of Fire Protection Engineering, chapter Fire Plumes, Flame Height and Air Entrainment. National Fire Protection Association, Quincy, Massachusetts, 4th edition, 2008. 7, 25, 144, 146
16. Gutiérrez-Montes, G,. Sanmiguel-Rojas, E., Viedma, A., Rein, G., Experimental data and numerical modelling of 1.3 and 2.3 MW fires in a 20 m cubic atrium. Building and Environment, 2009; 44:1827–1839, 2.
17. Hurley, M., Munguia. A., Analysis of FDS Thermal Detector Response Prediction Capability. J. Fire Protection Engineering, 20, 2009. 7
18. Yuan, L., Mainiero, R. J., Rowland, J. H., Thomas, R. A., Smith, A. C., "Numerical and experimental study on flame spread over conveyor belts in a large-scale tunnel". *Journal of Loss Prevention in the Process Industries*, 2014; *30*, 55–62.
19. Haghighat, A., Luxbacher, K., Lattimer, B., "Simulation of methane fire event at a coal mine working face with consideration of ventilation curtain damage". *2016 Transactions of the Society for Mining, Metallurgy & Exploration, 2016; Vol. 340, pp. 120-126.*
20. Van Maele, K., Merci, B., (2008). Application of RANS and LES field simulations to predict the critical ventilation velocity in longitudinally ventilated horizontal tunnels. Fire Saf J 43:598–609
21. Wu, Y., Bakar, M. Z. A., Control of smoke flow in tunnel fires using longitudinal ventilation systems—a study of the critical velocity. Fire Saf J. 2000; 35:363–390.
22. Galdo Vega, M., Arguelles Diaz, K. M., Fernandez Oro, J. M., Ballesteros Tajadura. R., Santolaria Morros, C., Numerical 3D simulation of a longitudinal ventilation system: memorial tunnel case. Tunn Undergr Space Technol, 2008; 23(5):539–551
23. Breuer, M., Lakehal, D., Rodi, W., Flow around a surface mounted cubical obstacle: Comparison of LES and RANS–results. In M. Deville, S. Gavrilakis, and I.L. Ryming, editors, Computation of 3D Complex flows, volume 53 of Notes on Numerical Fluid Mechanics, pages 22–30. Vieweg Verlag, 1996. https://link.springer.com/chapter/10.1007%2F978-3-322-89838-8_4.
24. Formaggia, L., Gerbeau, J. F., Nobile, F., Quarteroni. A., "On the coupling of 3D and 1D Navier-Stokes equations for flow problems in compliant vessels". Comput. Methods Appl. Mech.Engrg. 191 (2001) 561-582.

25. McGrattan, K., Hostikka, S., McDermott, R., Floyd, J., Weinschenk, C., Overholt, K., "Fire Dynamics Simulator Technical Reference Guide Volume1: Mathematical Model*", NIST special publication 1018, sixth edition*. FDS Version 6.1.2. Fire Research Division Engineering Laboratory Gaithersburg, Maryland, USA. SVN repository revision: 20596. (2014).
26. US Code of Federal Regulations. CFR, Title 30 (Ventilation) Part 75. Sec 75.326 Mean entry air velocity, Feb. 2017: https://arlweb.msha.gov/REGS/FEDREG/FINAL/1996FINL/5453(4).htm
27. McPherson, M. J. "Subsurface ventilation and environmental engineering" 1993, online edition.
28. Hansen, R., Ingason, H., (2013). "Heat release rate measurements of burning mining vehicles in an underground mine". *Fire Safety Journal*. Vol. 61, pp. 12-25.
29. Hansen, R., (2015). "Analysis of methodologies for calculating the heat release rates of mining vehicle fires in underground mines". *Fire Safety Journal*. Vol. 71, pp. 194-216.
30. Trevits, M. A., Yuan, L., Teacoach, K., Valoski, M. P., Urosek, J. E., (2009). "Understanding mine fire disasters by determining the characteristics of deep-seated fires". SME Annual Meeting and Exhibit, February 22-25, Denver, Colorado, preprint 09-150. Littleton, CO: Society for Mining, Metallurgy, and Exploration, Inc., 2009; :1-9.
31. Yuan, L., and Lazzara, C. P., 2004, "The effects of ventilation and preborn time on water mist extinguishing of diesel fuel pool fires," Journal of Fire Science. Vol 22, pp. 379-404, https://doi.org/10.1177/0734904104042438.
32. Ingason, H., Li, Y. Z., and Lönnermark. A., 2014, Entry Fire Dynamics, eBook, ISBN 978-1-4939-2198-0
33. Singer, J. M., and Tye, R. P., 1979, "Thermal, Mechanical, and Physical Properties of Selected Bituminous Coals and Cokes," Bureau of Mines Report of Investigations 8364, U.S. Department of the Interior, Bureau of Mines, Washington, DC.
34. Luzik, S. J., 1993, "MSHA develops new fire-resistant check curtains," Federal Register, Vol. 59, No. 96, No: 94-12054, pp.102-104, http://arlweb.msha.gov/S&HINFO/TECHRPT/MINEWSTE/FIRESCC.pdf

35. Tewarson, A., 1995, SFPE Handbook of Fire Protection Engineering, 2nd Edition, P. DiNenno, C. Beyler, R. Custer and W. Walton, eds., National Fire Protection Association, Section 3, Chap. 4.
36. Baum, H. R., and McCaffrey, B. J., 1989, "Fire induced flow field-theory and experiment," Fire Safety Science, Proceedings of the 2nd International Symposium, Hemisphere, New York, pp. 129-48, https://doi.org/10.3801/iafss.fss.2-129.
37. Yuan, L., Mainiero, R. J., Rowland, J. H., Thomas, R. A. T., and Smith, A. C. S., 2014, "Numerical and experimental study on flame spread over conveyor belts in a large-scale tunnel," Journal of Loss Prevention in the Process Industries, Vol. 30, July 2014, pp. 55-62, https://doi.org/10.1016/j.jlp.2014.05.001.
38. Ingason, H., (2009). "Design fire curves for tunnels". Fire Safety Journal. Vol. 44, pp. 259-265.
39. Kim, H. J., Lilley, D. G., (2002). "Heat Release Rates of Burning Items in Fires". Journal of Propulsion and Power, Vol. 18, No. 4, pp. 866-870.http://dx.doi.org.ezproxy.lib.vt.edu/10.2514/2.6011.
40. Laage, L., Greuer, R., Pomroy, W., (1995). MFIRE User's Manual Version 2.20, 110 p (United States Bureau of Mines).
41. Townsend, A. A. "The structure of turbulent shear flow" Cambridge University Press, New York, 1956.
42. Black, T. J., Proc. Heat transfer and fluid mech. Ins., 1966
43. Hinze, J. O., "Turbulence", McGraw-Hill series in mechanical engineering, 2nd Edition, 1975
44. Ventsim Visual™, Ventsim Visual™ User Guide, Chasm Consulting, Volume 1, Version 4. . 2016

Appendix E: Chapter 9 Supplemental Data

The results of the mean velocity components and the mean TKE and the mean vorticity along the height of the tunnel at different cross sections at t=1300 in scenarios 2 and 3 are presented in Figures 9.21 to 9.22. This study has shown that the domain of the near field and far filed did not change by changing the velocity.

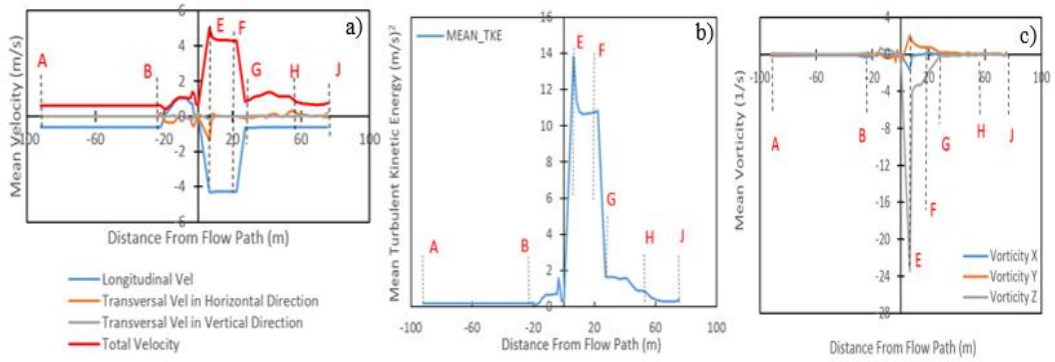

Figure 9.21. The mean velocity components, mean TKE and the mean vorticity along the height of the tunnel at different cross sections at t=1300 in scenario 2 a) velocity components b) mean TKE c) mean vorticity (the cross sections are based on Figure 9.4 (a))

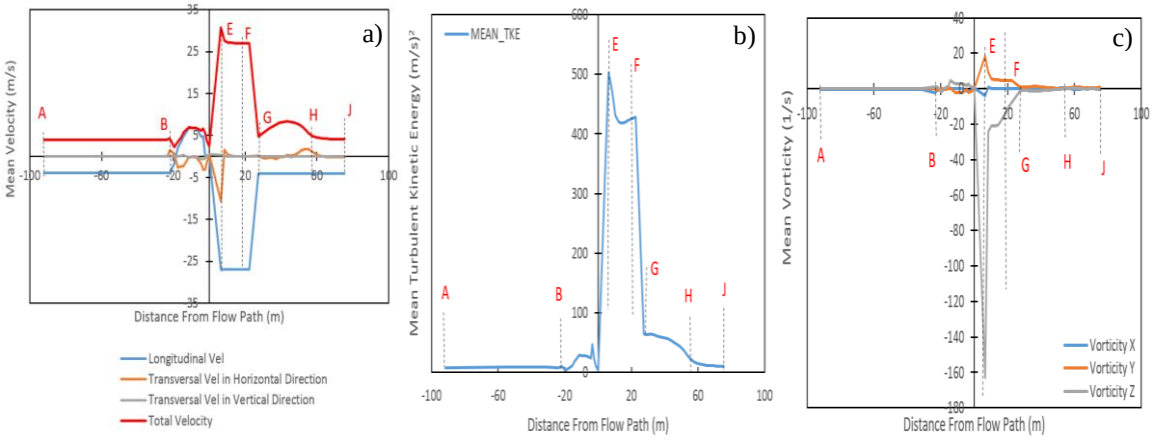

Figure 9.22. The mean velocity components, mean TKE and the mean vorticity along the height of the tunnel at different cross sections at t=1300 in scenario 3 a) velocity components b) mean TKE c) mean vorticity (the cross sections are based on Figure 9.4 (a))

Appendix F: Chapter 9 Supplemental Data

The results of the mean velocity components and the mean TKE and the mean vorticity along the height of the tunnel at different cross sections at t=1300 in scenarios 4, 5, and 6 are presented in Figures 9.23 to 9.25.

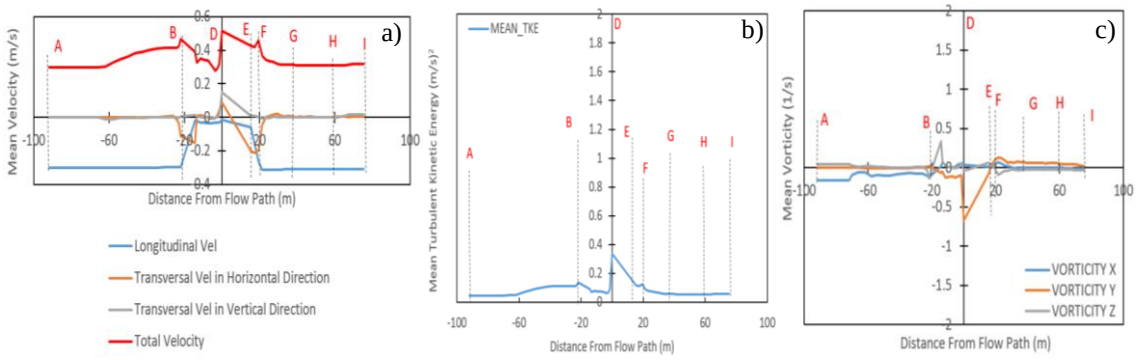

Figure 9.23. The mean velocity components, mean TKE and the mean vorticity along the height of the tunnel at different cross sections at t=1300 in scenario 4 a) velocity components b) mean TKE c) mean vorticity (the cross sections are based on Figure 9.4 (b))

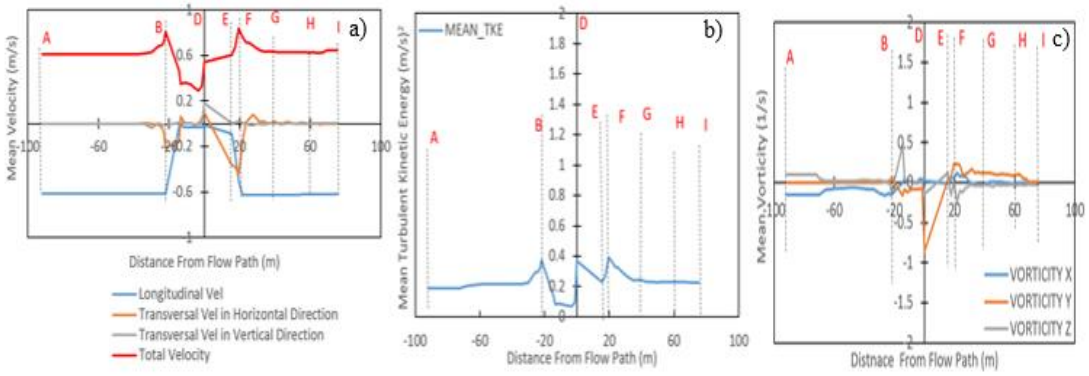

Figure 9.24. The mean velocity components, mean TKE and the mean vorticity along the height of the tunnel at different cross sections at t=1300 in scenario 5 a) velocity components b) mean TKE c) mean vorticity (the cross sections are based on Figure 9.4 (b))

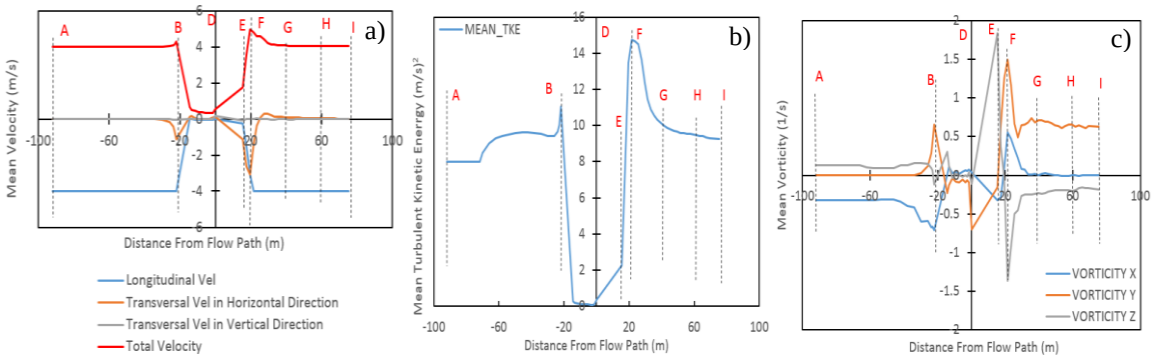

Figure 9.25. The mean velocity components, mean TKE and the mean vorticity along the height of the tunnel at different cross sections at t=1300 in scenario 6 a) velocity components b) mean TKE c) mean vorticity (the cross sections are based on Figure 9.4 (b))

Appendix G: Chapter 9 Supplemental Data

The results of the mean velocity components and the mean TKE and the mean vorticity along the height of the tunnel at different cross sections at t=1300 in scenarios 7, 8, and 9 are presented in Figures 9.26 to 9.28.

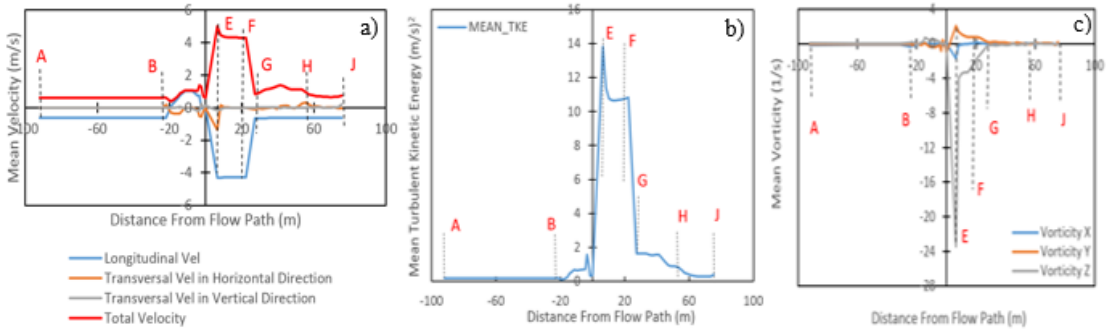

Figure 9.26. The mean velocity components, mean TKE and the mean vorticity along the height of the tunnel at different cross sections at t=1300 in scenario 7 a) velocity components b) mean TKE c) mean vorticity (the cross sections are based on Figure 9.4 (a))

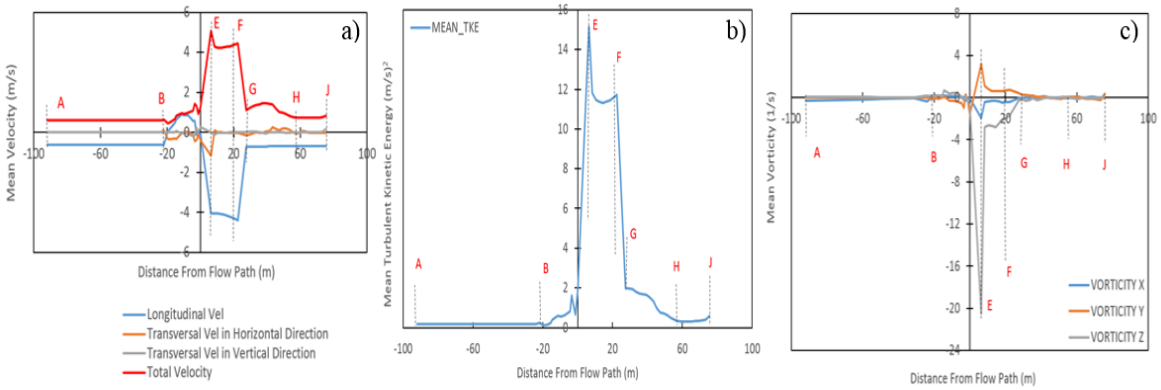

Figure 9.27. The mean velocity components, mean TKE and the mean vorticity along the height of the tunnel at different cross sections at t=1300 in scenario 8 a) velocity components b) mean TKE c) mean vorticity (the cross sections are based on Figure 9.4 (a))

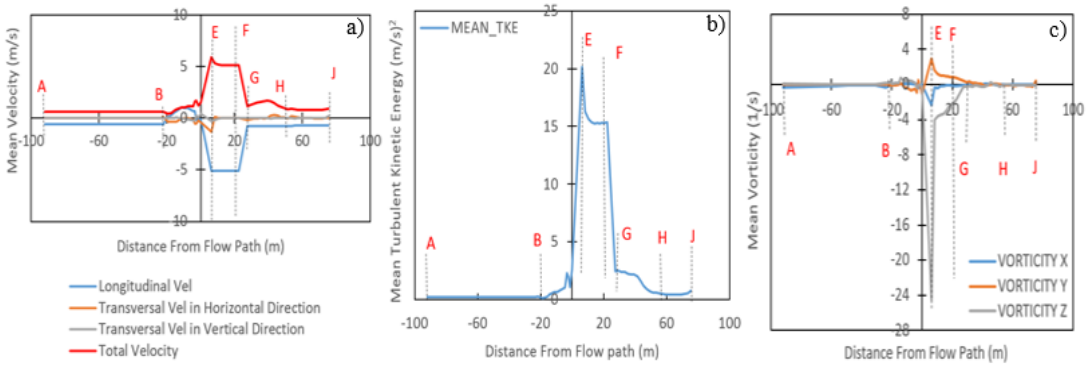

Figure 9.28. The mean velocity components, mean TKE and the mean vorticity along the height of the tunnel at different cross sections at t=1300 in scenario 9 a) velocity components b) mean TKE c) mean vorticity (the cross sections are based on Figure 9.4 (a))

Appendix H: Chapter 9 Supplemental Data

The results of the mean velocity components and the mean TKE and the mean vorticity along the height of the tunnel at different cross sections at t=1300 in scenarios 10, 11, 12, and 13 are presented in Figures 9.29 to 9.32.

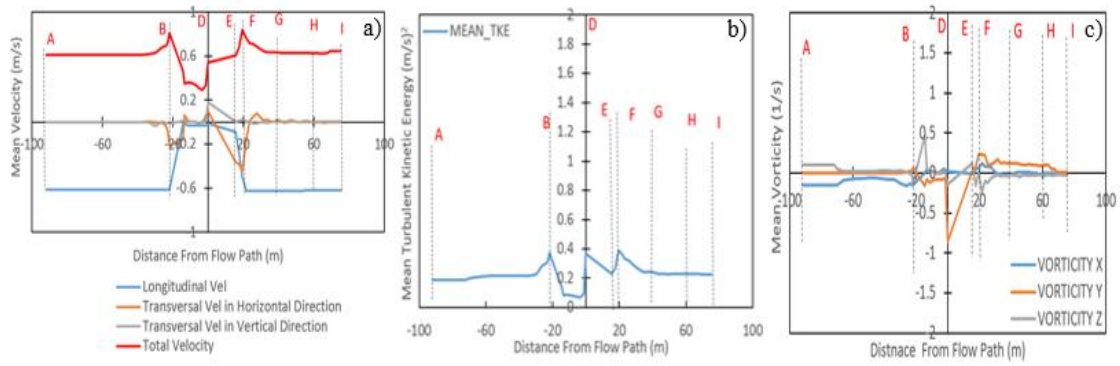

Figure 9.29. The mean velocity components, mean TKE and the mean vorticity along the height of the tunnel at different cross sections at t=1300 in scenario 10 a) velocity components b) mean TKE c) mean vorticity (the cross sections are based on Figure 9.4 (b))

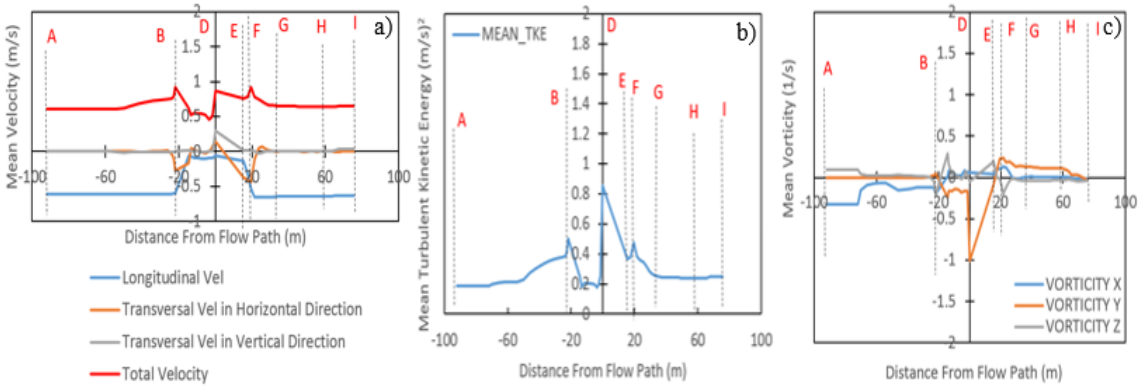

Figure 9.30. The mean velocity components, mean TKE and the mean vorticity along the height of the tunnel at different cross sections at t=1300 in scenario 11 a) velocity components b) mean TKE c) mean vorticity (the cross sections are based on Figure 9.4 (b))

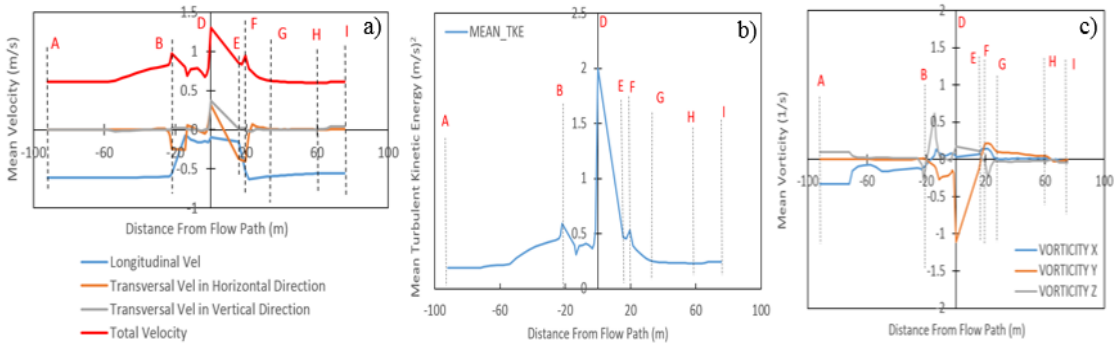

Figure 9.31. The mean velocity components, mean TKE and the mean vorticity along the height of the tunnel at different cross sections at t=1300 in scenario 12 a) velocity components b) mean TKE c) mean vorticity (the cross sections are based on Figure 9.4 (b))

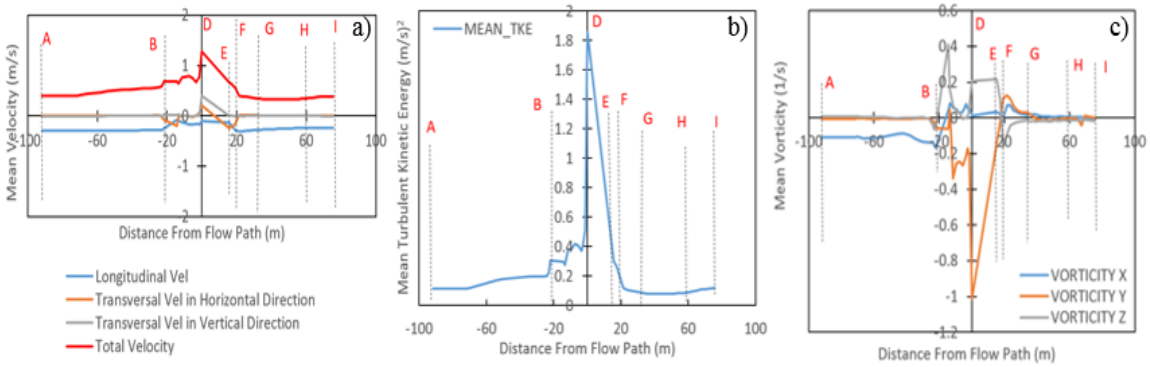

Figure 9.32. The mean velocity components, mean TKE and the mean vorticity along the height of the tunnel at different cross sections at t=1300 in scenario 13 a) velocity components b) mean TKE c) mean vorticity (the cross sections are based on Figure 9.4 (b))

Appendix I: Chapter 9 Supplemental Data

The mean temperature and the mean velocity results along the height of the tunnel at different cross sections in the tunnels for CFD, 1D, and the coupled simulations in scenarios 4 to 13 are shown in Figures 9.33 to 9.35.

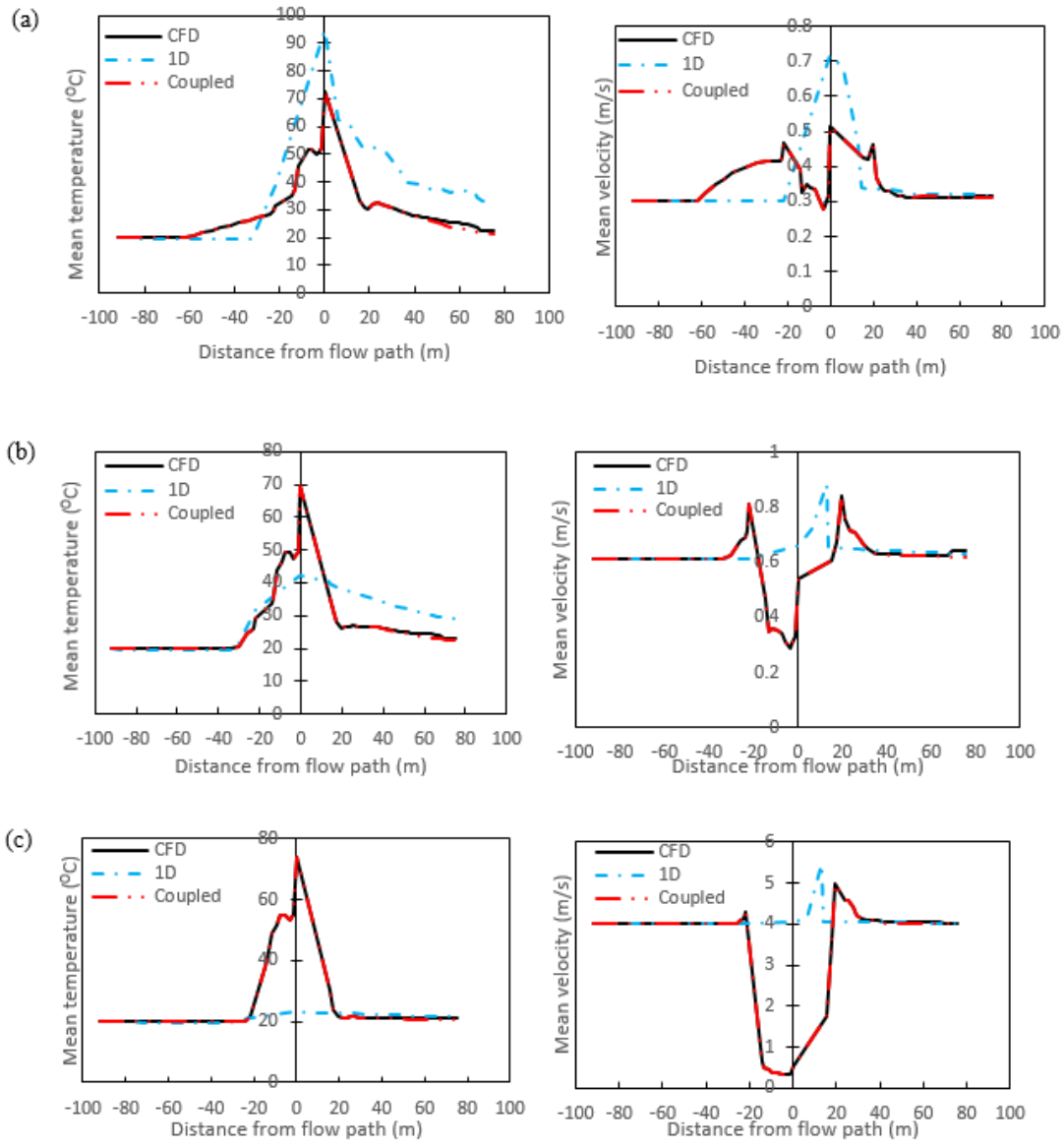

Figure 9.33. Mean temperature and mean velocity comparison between CFD, 1D, and the coupled models at different cross sections of the tunnel for all scenarios (a) scenario 4 (b) scenario 5 (c) scenario 6

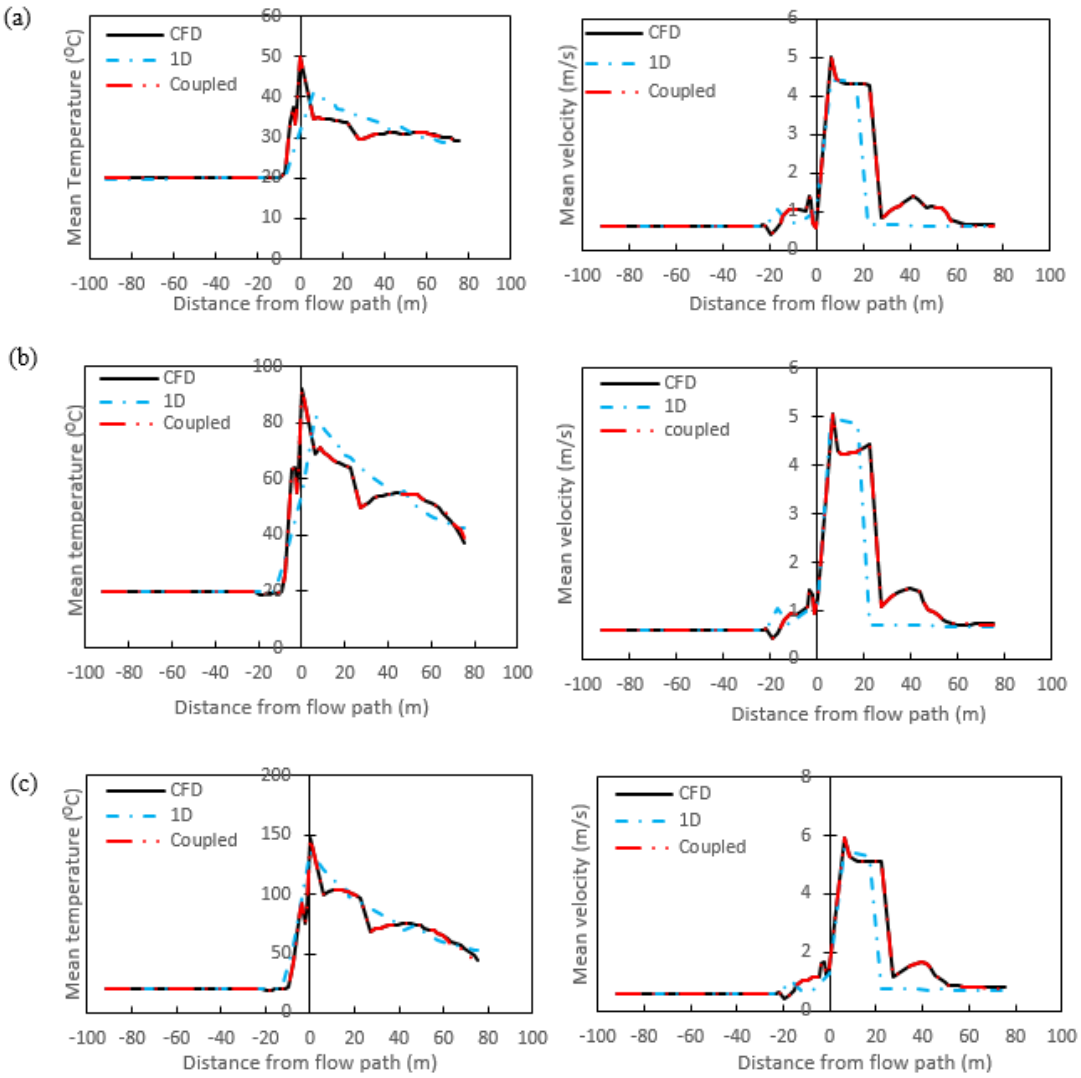

Figure 9.34. Mean temperature and mean velocity comparison between CFD, 1D, and the coupled models at different cross sections of the tunnel for all scenarios (a) scenario 7 (b) scenario 8 (c) scenario 9

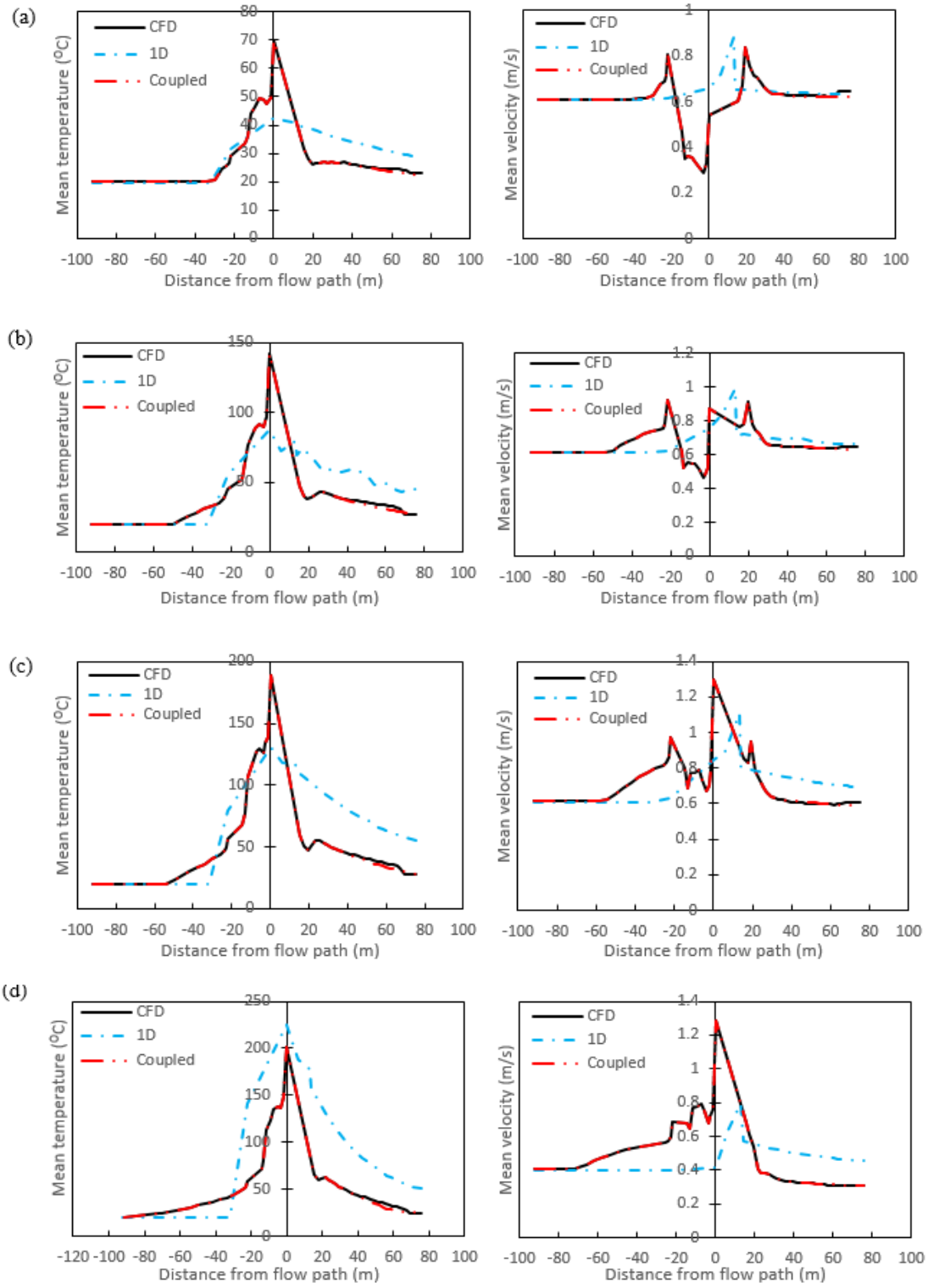

Figure 9.35. Mean temperature and mean velocity comparison between CFD, 1D, and the coupled models at different cross sections of the tunnel for all scenarios (a) scenario 10 (b) scenario 11 (c) scenario 12 (d) scenario 13

10. Conclusion and Future Work

10.1. Conclusions and Research Highlights

The research study presented in this dissertation sought to develop a novel approach to reduce the fire simulation and airflow simulation costs in order to improve the health and safety in the underground space environments.

Therefore, a review study was conducted to provide an overview of fire research achievements in the mining industry and also tunnel fires research studies in the United States and all around the world. It is noteworthy that with the rapid advancement of technology, the mine fire knowledge has progressed significantly. The experimental equipment has been improved; the numerical analysis has been expedited with the usage of supercomputers; and more regulations and standards have been set to improve health and safety of miners. In spite of all advancements in these areas, fire hazards remain omnipresent in mines all around the world. In addition, CFD numerical analysis is shown a useful tool for precise studies near fire field. However, for the huge domains such as underground mine environments, because of low computational requirements, network modeling software (1D models) can be an efficient tool for fire analysis at the far field. However, network modeling approach (1D) cannot capture the characteristics of complex three-dimensional (3D) flow regions typically encountered close to the fire. Hence, the multiscale model can be utilized to couples a CFD model with a network model, with the intention of decreasing the simulation cost without losing the accuracy. Model reduction strategies such as Reduced Order Models (ROM's) can be the other helpful approach to circumvent the simulation cost problem. Therfore, fire numerical simulation, in concert with reasonable health and safety guidelines, can be utilized to train miners and rescue teams for the fire events. These simulations, applied to training will result in more efficient evacuations (e.g., the decision to leave can be made quickly and with less delay), as well as safe and effective firefighting under certain situations.

So, due to this, a risk analysis study was conducted on mine fires for all U.S. underground coal mines from 2000–2012 in order to identify locations that have a high risk

for fire incidents. The fire incident risk assessment of the MSHA incident database identified four general locations, the active face, belt areas, gob and sealed areas, and electrical installations as the most significant risk areas for fire events during 2000 to 2012. After identifying fire incidents from this database, a risk matrix was developed for underground locations that showed a significant propensity for fire incidents. This investigation shows that the fire incidents at the "Active Face" happened more frequently during this time period relative to the remaining locations. In contrast, the "Belt Area" had the highest average severity in comparison with the remaining locations and a moderate frequency. This higher relative severity resulted from a number of incidents in which a belt fire resulted in either significant injuries or long periods of mine inactivity. The "Active Face" was selected to be the focus of further studies regarding development of the tenability analysis for rescue teams or miners, and the airflow simulations and the fire simulations cost reduction.

For tenability analysis, there is a need to determine the smoke layer depth in the methane fire events at a coal mine working face. Therefore, a numerical study was conducted to accomplish three main objectives. First, to assess visibility and temperature in the entry for anyone approaching the fire. Second, to develop an understanding of conditions that result from several ventilation damage scenarios, and third, to use this knowledge to determine the smoke layer depth through interface and fresh air heights study. The computational fluid dynamics software Fire Dynamics Simulator (FDS) Version 6.0 was utilized to predict the conditions that develop due to a 200-kW fire in the face following a methane ignition with different levels of assumed ventilation curtain damage. It was noteworthy that the smoke propagation in an entry is dependent on different parameters, such as the location of the fire, the physical size and intensity of fire, air velocity and direction. In examining interface height and simulations of visibility throughout the entry, it is clear that as damage to the ventilation curtain approaches the last open crosscut it will become increasingly difficult for miners to approach the fire in order to observe conditions or fight the fire, due to limited visibility and high temperature. The five simulations presented underscore the importance of maintaining or immediately reestablishing face ventilation immediately after damage in order to maintain visibility and

keep smoke moving to the return. The maintenance or reestablishment of ventilation allows personnel to approach the fire in order to extinguish it or observe involvement for emergency response.

Next, a study was conducted to develop an approach to analyze the tenable limits in a fire event in an underground coal mine for bare-faced miners, mine rescue teams, and fire brigade teams in order to improve safety and training of personnel trained to fight fires. The source of the combustion products analysis and the exposure effect were considered to assess the potential for harm to mine personnel, mine rescue teams, or fire brigades during a firefighting operation, taking into account their training and personal protective equipment during 5 and 15 minutes exposure. This study illustrates that the status of ventilation controls has a substantial effect on tenability for personnel engaged in firefighting. The findings were utilized to recommend the tenable limits for bare-faced miners, mine rescue team, and fire brigade teams during 5 and 15 minutes exposure to the methane fire at a coal mine working face. This work applies to the training of mine personnel in responding to face fires: it is reasonable to miners that they can consider barefaced firefighting when ventilation controls are intact and they are actively monitoring the atmosphere, but evacuation or reventilation is necessary if ventilation controls are destroyed. This scenario is best left to mine rescue or fire brigade teams. Fire simulation, in concert with reasonable tenability guidelines, can be utilized to train miners as to when approaching fire barefaced is appropriate and when evacuation is the best option. Unfortunately, underground mine ventilation system design and hazard assessments require numerous simulations to support evaluating the risk and overall safety of the system. These simulations have domains that span kilometers and require higher resolution in areas with increased hazards. These simulations are costly, and even with high performance workstations, complex domains may require days to solve. Therefore, the cost of numerical simulations is one of the most important issues.

So, due to this a study was conducted to explore the use of computationally efficient reduced-order models (ROMs) for the reduction of airflow simulation cost at the high resolution area (active working face). A ROM was produced to predict the flow field of a

complex tunnel geometry (Continuous Miner (CM) working face) using proper orthogonal decomposition (POD) to reduce the simulation cost in the nonlinear model. The ROM resulted in significant increases in computational efficiency (more than 3 orders of magnitude). ROMs were then used to predict conditions with different input conditions, resulting predictions with error of less than 5%. It is evident that ROM is an effective tool for approximating several possible solutions near a known solution, resulting in significant time savings over calculating full solutions and suitable for ensemble calculations. The inlet velocity was not varied substantially here, but we have demonstrated that ROM can be used to effectively study the effect of varying input parameters on an initial model, with relatively few computational resources. It is noteworthy that the quality and quantity of the snapshots played a key role on the creation of the POD modes. Due to the large size of transportation tunnels, this technique is applicable for reduction of underground space environments airflow simulation cost such as simulation of the airflow in the subways, metro stations, road tunnels, train tunnels, and parking lots. This approach may also be applicable to a broad range of mining simulations, such as fire dynamics simulations in underground environments, underground mine fires or transportation tunnel fires, with lower cost compared to common CFD practice.

For the reduction of fire simulation cost, there was a need to investigate the influential parameters can affect the fluid characteristic in underground space environments. Therefore, a study was conducted to develop a statistical analysis on the computational fluid dynamics (CFD) data of the road tunnel fire simulations in order to quantify the significance of tunnel dimension, inlet air velocity, HRR, and the physical fire size (fire perimeter) on the fluid characteristics downstream of the fire source. The developed statistical analysis was applied to the tunnels with 73.73 m^2 and 119.8 m^2 cross sections and 960 m in length. Based on the prediction of the designed statistical models, the linear models were found to provide statistically good prediction. The effect of computational domain length on the selection of the significant parameters downstream of the fire source was analyzed. It is noteworthy that by getting further from the fire source, the number of significant parameters on the response variable changes downstream of the fire decreased. This study has shown that the changes of the physical size of the fire did

not influence the average temperature, average velocity, average density, and average viscosity downstream of the fire source. In addition, it was observed that the interactive effect of the parameters was inconsequential on the changes of the average temperature, average density, average velocity, and the average viscosity downstream of the fire source. The proposed statistical analysis was demonstrated to be a useful technique for screening the significant parameters on the fluid characteristics downstream of the fire source. Robust emergency response layout design and fire safety plan require numerous simulations to support evaluating the safety of the underground environment. Understanding and screening the key parameters on the fluid characteristics downstream of the fire is required for decreasing the number of fire simulations for future studies and for improving the tunnel fire safety plan of the occupants. The two main parameters which influenced the fluid characteristics in general were HRR and the inlet velocity. Hence, these two parameters were selected to be the focus of further studies regarding the reduction of fire simulation cost in underground space environments.

Therefore, a study was conducted to develop a novel iterative methodology based on the physics of the fluid structure, Turbulent Kinetic Energy (TKE), and the vortex dynamics to determine the interface boundary region upstream and downstream of a fire source in the transportation tunnels to decompose the domain into 3D and 1D domains for reduction of the simulation cost. The effect of changes in heat release rate (HRR) and the air velocity on the selection of an interface boundary was also investigated. The selected downstream interface boundary was $12D_h$ m downstream of the fire for the simulations. The upstream interface boundary selection depends on the utilized velocity in the model. The upstream interface boundary was selected at 0.5 D_h upstream the tip of the object when the velocity was greater than equal to the V_{cr}. In the simulations with backlayering ($V < V_{cr}$), the interface boundary was selected 1.2 D_h m further from the tip of the rollback. Although, the downstream interface boundary was HRR independent and velocity independent, the upstream interface boundary was velocity dependent. It was observed that the upstream interface boundary was not changed by changing the HRR. The indirect coupling strategy was utilized to couple 3D sub-domain to 1D sub-domains. The calculated temperature and velocity errors between multiscale models and the full CFD models were

less than 5%. In addition, it was evident that the longitudinal velocity was temperature dependent in the whole computational domain while the transversal velocity components (lateral and vertical) were temperature dependent just at the near field.

The developed novel methodology for selection of interface boundary in multiscale fire simulations was applied on more complex fluid structure such as fluid structure at a working face in an underground mine in order to determine the interface boundary for multiscale mine fire simulations. Different working face methane fire scenarios ranging 200 kW to 1000 kW were investigated with various inlet velocities. The impact of velocity changes, HRR changes, and the ventilation curtain position on the selection of interface boundary to decompose the model into 3D and 1D subdomains were investigated. This study has shown that the longitudinal velocity component was affected by the temperature in the whole computational domain while the transversal velocity components were temperature depended just close to the fire. It was noteworthy that the temperature impact on the transversal velocities was inconsequential away from the fire source. Moreover, it was evident that the downstream interface boundaries did not depend on the fire size (HRR) and the velocity in all scenarios. However, the upstream interface boundary depends on different parameters such as the size of the fire (HRR), velocity, and the used objects in the computational domain. The selected downstream interface boundary was at least $12D_h$ away from the fire source or the used object (ex: exhausting line curtain) in the numerical domain for all simulations. Due to the effects of the size of the fire (HRR), velocity, and the objects on the rollback (backlayering) phenomenon, the upstream interface boundary varied. In the simulations with backlayering ($V < V_{cr}$), the upstream interface boundary was selected at least $1.2D_h$ further from the tip of the rollback. The upstream interface boundary for scenarios without backlayering ($V \geq V_{cr}$) was calculated at least $0.5D_h$ from the upwind the end of the cross cut or the used object at the upstream of the fire source in the computational domain. The indirect coupling strategy was utilized to couple 3D sub-domain to 1D sub-domains. The calculated mean temperature and the mean velocity errors between multiscale models and the full CFD models were less than 6%. A novel algorithm was developed to be applied for selection of interface boundary for all different types of

the fire in underground mines such as multiscale fire simulations at different areas such as longwall, gob areas, or belt areas (neutral airways).

10.2. Limitations and Future Work

Although my Ph.D. research includes investigating and developing the tenability criteria for barefaced miners, fire brigade and mine rescue teams for approaching a mine fire in an active coal mine face for 200 kW methane fire, future work must account for explosibility by further examining combustion of methane and the effect of various strata emission levels. In addition, the developed methodology for tenability analysis can be applied for different range of fire and the scenarios should be studied over a longer period of time than 15 minutes to further inform mine rescue and fire brigade approach. The tenability criteria should be further examined and formalized for various mine fire scenarios, as this approach can lead to more effective decision making for personnel faced with fire and supervisory personnel during emergencies, ultimately improving safety by mitigating fire early. Also, it is clear that while US regulation provides for firefighting training and equipment for all mine personnel, provision of basic firefighting PPE and a limited number of SCBAs could allow for immediate control of fires that could not otherwise be approached by barefaced personnel. Broadly, this study can inform further work in the ways miners are trained in firefighting, and be utilized to further develop tenability criteria for various personnel in underground coal mines. First, we recognize that mine personnel is extensively trained in firefighting and have access to firefighting equipment, so their preparation differs from that of the average structure occupant on the surface. Fire simulation, in concert with reasonable tenability guidelines, can be used to train miners as to when approaching fire barefaced is appropriate and when evacuation is the best option. Also, the numerical simulations need to be validated in order to determine how well the developed mathematical models predict the actual physics of interest. Although there are various codes and standards in terms of tenability criteria for fires in road tunnels (NFPA® 502), there are no codes for tenability study in underground mines. Therefore, this study can make a great contribution to improving the NFPA® 120, 122, 123 and health and safety in mining industry.

In addition, the work that I have completed for my dissertation has generated evidence that the simulation and control of large complex dynamical systems such as a fire in underground spaces can make unmanageably large demands on computational resources, creating a crucial need for efficient model utilization. Coupling of Computational Fluid Dynamics (CFD) models and network modeling simulations (multiscale method) of fire event can be a useful tool to increase the computational efficiency and accuracy. Although I applied the reduce order model (ROM POD) for reduction of airflow simulation, the reduced order model could be applied for cost reduction of underground space environments fire simulations. This technique can be integrated to the multiscale mine fire simulations (ROM-Multiscale methodology) to increase the efficiency of fire simulations. With the implementation of ROM-Multiscale methodology the significant time savings can be achieved over calculating full solutions and suitable for ensemble calculations. Fire modeling has a critical role to play in planning for emergency response, evacuation and the rescue service studies, reacting to fires, and forensic analysis, ultimately leading to safer mines.